Quantifying Drivers of Mercury Bioaccumulation

Modeling Biological Controls of Inorganic and Organic Mercury Cycling and Their Link to Seafood Contamination

Dissertation
with the aim of achieving a doctoral degree
at the Faculty of Mathematics, Informatics and Natural Sciences
Department of Earth System Sciences
at University of Hamburg

Submitted by:
David Johannes Amptmeijer

Hamburg, 2025

Department of Earth Sciences

Date of Oral Defense:

16.01.2026

Reviewers:

- Prof. Dr. Corinna Schrum
- Dr. Johannes Bieser

Members of the Examination Commission:

- Prof. Dr. Corinna Schrum
- Dr. Johannes Bieser
- Dr. Joël Knœry
- Prof. Dr. Christian Möllmann
- Prof. Dr. Tatiana Ilyina

Chair of the Subject Doctoral Committee
Earth System Sciences: Prof. Dr. Hermann Held
Dean of Faculty MIN: Prof. Dr.-Ing. Norbert Ritter

Contents

Terminology and abbreviations

It is important to mention the usage of MeHg, $MMHg^{+}$, and iHg and Hg^{2+}. DMHg is believed to not bioaccumulate but is understudied. In this thesis, I only model the bioaccumulation of $MMHg^{+}$ and Hg^{2+}, as they are known to bioaccumulate. However, measurements typically do not distinguish between $MMHg^{+}$ and MeHg, or between Hg^{2+} and iHg. Therefore, to ensure absolute correctness, I refer to Hg^{2+} and $MMHg^{+}$ when discussing my model and mention MeHg and iHg when discussing field measurements. I compare these under the assumption that bioaccumulated Hg^{2+} is equal to bioaccumulated iHg and bioaccumulated $MMHg^{+}$ equals bioaccumulated MeHg.

Abbr.	Long name	Toxicity	Bio-acc.	Description
Hg	Mercury	–	–	Mercury in general, unspecified which form
Hg^{0}	Elemental Hg	Highly toxic	No	Volatile, undergoes long range transport
Hg^{2+}	Dissolved Hg	Highly toxic	Yes	Most common in the marine environment
HgS	Cinnabar	Mildly toxic	No	Stable, important sink of Hg from the biosphere
iHg	Inorganic Hg	–	–	All inorganic forms of Hg
$MMHg^{+}$	Monomethyl mercury	Extremely toxic	Yes	Hg species of most concern
DMHg	Dimethylmercury	Extremely toxic	No	Common in deep water, uncommon in shelf seas.
MeHg	Methylmercury	Extremely toxic	–	$MMHg^{+}$ + DMHg
tHg	Total Hg	–	–	All Hg

Table 1: Overvieuw of Mercury (Hg) forms, their abbreviation (Abbr.), their toxicity, if they bioaccumulate (Bio-Acc.), and descriptions.

Models	Long names	Usage
GOTM	Generalized Ocean Turbulence Model	Model 1D water column setups
FABM	Framework for Aquatic Biogeochemical Modeling	Couple different models
HAMSOM	HAMburg Shelf Ocean Model	Model the physics of the North and Baltic Seas
MERCY	Marine mERcury CYcling model	Models the marine cycling of Hg
ECOSMO	ECOSystem MOdel	Model nutrient fluxes and the ecosystem in which Hg bioaccumulates

Table 2: Summary of oceanographic and biogeochemical models.

Term	Abbreviation	Description
Detritus	–	Organic matter with particles large enough to be filtered by filter feeders
Dissolved Organic Matter	DOM	Organic material with particles too small to be filtered by filter feeders
Labile DOM	–	DOM which is broken down by bacteria faster than detritus
Semi-labile DOM	sDOM	DOM that is broken down by bacteria at the same rate as detritus
Refractory DOM	rDOM	DOM that is extremely resistant to bacterial breakdown
Producers	–	Biota that transform inorganic nutrients into organic matter
Consumer	–	Animals that are dependent on the consumption of organic material for survival
Low Microbial Assemblage Sponge	LMA	Sponges with low microbial abundance
High Microbial Assemblage Sponge	HMA	Sponges with high microbial abundance, specialized in eating DOM

Table 3: Biological terms related to marine ecosystems and organic matter.

Figure 1: Dendronatus Robustus. Picture taken by David Amptmeijer in Adventfjorden.

Abstract

English

Mercury (Hg) contamination poses a serious risk to human health and ecosystems, particularly through the bioaccumulation of the neurotoxin methylmercury (MeHg). This thesis develops and applies a series of models to quantify the biological drivers of Hg bioaccumulation. First, the MERCY v2.0 model is introduced. This is the first multi-compartment model that links atmospheric Hg deposition to MeHg concentrations in seafood. After this, feedback between the ecosystem and Hg cycling is quantified to estimate the influence of bioaccumulation on the Hg balance of the North and Baltic Seas. The model shows that bioaccumulation can increase total MeHg concentrations by up to 44% and increase the export of Hg from the North Sea to the Atlantic Ocean by 14 kg y^{-1}. The relative importance of bioconcentration by phytoplankton and subsequent biomagnification versus direct bioconcentration at the consumer level is then investigated. While MeHg uptake by phytoplankton and consequent biomagnification is the dominant uptake pathway of MeHg, direct bioconcentration becomes more important with increasing trophic level, and it can increase bioaccumulation by 15% per trophic level. Then, an expansion of the benthic food web of the ECOSMO E2E model is presented. The one macrobenthos functional group in ECOSMO E2E is split into 6 megabenthos functional groups. This model is used to analyze the role of the feeding strategy of benthos on bioaccumulation and shows that the feeding strategy has a significant influence on MeHg concentrations in megabenthos and that the feeding strategy is the main determinant of total Hg content in low-trophic level biota. Finally, these findings are integrated to explain the unusually low MeHg concentrations observed in Mediterranean Sea sponges. Sponges can have high amounts of microbial symbionts that assist with their metabolic demands (High Microbial Abundance or HMA sponges), or a concentration of microbes similar to that in seawater (Low Microbial Abundance or LMA sponges). The models show that the consumption of dissolved organic matter (DOM) by LMA sponges can account for the observed low MeHg content. The even lower concentrations in HMA sponges can be explained by the additional consumption of refractory DOM. Demethylation is not required to explain the MeHg concentrations in HMA sponges, but if it occurs, it is likely at a rate of 1% d^{-1}. This model also shows that the dominance of HMA sponges at the base of the food web can reduce MeHg concentrations in top predators by up to 45%. Overall, these models improve our ability to predict how ecosystem structure and feeding ecology influence MeHg bioaccumulation.

Deutsch

Quecksilber (Hg)-Kontamination stellt ein ernsthaftes Risiko für die menschliche Gesundheit und Ökosysteme dar, insbesondere durch die Bioakkumulation des neurotoxischen Methylquecksilbers (MeHg). Diese Dissertation entwickelt und wendet eine Reihe von Modellen an, um die biologischen Treiber der Hg-Bioakkumulation zu quantifizieren.Zunächst wird das MERCY v2.0-Modell vorgestellt. Es handelt sich um das erste Mehrkompartimentmodell, das atmosphärische Hg-Ablagerung mit MeHg-Konzentration in Meeresfrüchten und Fisch quantifiziert, um den Einfluss der Bioakkumulation auf die Quecksilberbilanz der Nord- und Ostsee abzuschätzen. Das Modell zeigt, dass die Primärproduktion die gesamten MeHg-Konzentration um bis zu 44% erhöhen kann und dass Bioakkumulation den Hg-Export aus der Nordsee in den Atlantik um 14 kg a^{-1} steigern kann. Anschließend wird die relative Bedeutung von Biokonzen-

tration durch Phytoplankton und anschließender Biomagnifikation gegenüber der direkten Biokonzentration auf Konsumentenebene untersucht. Während die Aufnahme von MeHg durch Phytoplankton mit anschließender Biomagnifikation der dominierende Aufnahmeweg ist, wird die direkte Biokonzentration von größerer Bedeutung mit steigender trophischer Stufe. Daraufhin wird eine Erweiterung des benthischen Nahrungsnetzes des ECOSMO E2E-Modells vorgestellt, mit der die Rolle der Ernährungsstrategie von Benthosorganismen bei der Bioakkumulation analysiert wird. Dieses Modell zeigt, dass die Ernährungsstrategie einen signifikanten Einfluss auf die MeHg-Konzentration im Megabenthos hat und dass sie der Hauptfaktor für den Gesamt-Hg-Gehalt in niedertrophischen Organismen ist. Abschließend werden diese Erkenntnisse integriert, um die ungewöhnlich niedrigen MeHg-Konzentration in Schwämmen des Mittelmeers zu erklären. Schwämme können entweder hohe Mengen an mikrobiellen Symbionten aufweisen, die ihren Stoffwechselbedarf unterstützen (Schwämme mit hoher mikrobieller Abundanz oder HMA-Schwämme), oder eine Konzentration von Mikroben, die der im Meerwasser ähnlich ist (Schwämme mit niedriger mikrobieller Abundanz oder LMA-Schwämme). Die Modelle zeigen, dass der Konsum von gelöster organischer Substanz (DOM) durch LMA Schwämme die beobachteten niedrigen MeHg-Gehalte erklären kann. Die noch niedrigeren Konzentration in HMA Schwämmen lassen sich durch zusätzlichen Konsum von refraktärem DOM erklären. Eine Demethylierung ist nicht erforderlich, um die MeHg-Konzentration in HMA-Schwämmen zu erklären, aber falls sie auftritt, geschieht dies wahrscheinlich mit einer Rate von 1% d^{-1}. Das Modell zeigt außerdem, dass die Dominanz von HMA-Schwämmen an der Basis des Nahrungsnetzes die MeHg-Konzentration in Fischen um bis zu 45 % senken kann. Insgesamt verbessern diese Modelle unsere Fähigkeit, vorherzusagen, wie die Struktur von Ökosystemen und Ernährungstaktiken die Bioakkumulation von MeHg beeinflussen.

Nederlands

Kwik (Hg) verontreiniging vormt een ernstig risico voor de menselijke gezondheid en voor ecosystemen, met name door de bioaccumulatie van het neurotoxische methylkwik (MeHg). Dit proefschrift ontwikkelt en past een reeks modellen toe om de biologische oorzaken van Hg-bioaccumulatie te kwantificeren. Allereerst wordt het MERCY v2.0-model geïntroduceerd. Dit is het eerste multi-compartimentmodel dat atmosferische kwikdepositie koppelt aan MeHg-concentraties in zeevruchten en vis. Vervolgens wordt de terugkoppeling tussen het ecosysteem en de kwikcyclus gekwantificeerd om de invloed van bioaccumulatie op de kwikbalans van de Noordzee en de Baltische Zee te schatten. Het model toont aan dat bioaccumulatie de totale MeHg-concentraties tot 44% kan verhogen, en de export van kwik uit de Noordzee naar de Atlantische Oceaan met 14 kg j^{-1} kan verhogen. Daarna wordt het relatieve belang onderzocht van bioconcentratie door fytoplankton gevolgd door biomagnificatie, versus directe bioconcentratie op consumenten. Hoewel opname van MeHg door fytoplankton en daaropvolgende biomagnificatie de dominante opnameweg is, wordt directe bioconcentratie belangrijker naarmate het trofisch niveau toeneemt. Vervolgens wordt een uitbreiding van het benthische voedselweb van het ECOSMO E2E-model gepresenteerd, waarmee de rol van de eetstrategie van benthos in bioaccumulatie wordt geanalyseerd. Dit model toont aan dat de eetstrategie een significante invloed heeft op MeHg-concentraties in megabenthos, en dat deze strategie de belangrijkste drijfveer is van het totale kwikgehalte in organismen op lage trofische niveaus. Ten slotte worden deze bevindingen geïntegreerd om de ongewoon lage MeHg-concentraties in sponzen uit de Middellandse Zee te verklaren. Sponzen kunnen ofwel grote hoeveelheden microbiële symbionten bevatten die helpen bij hun metabolische behoeften (sponzen met hoge microbiële abundantie of HMA-sponzen), ofwel een concentratie van microben die vergelijkbaar is met die in zeewater (sponzen met lage microbiële abundantie of LMA-sponzen). Het model laat zien dat de consumptie van opgeloste organische stof (DOM) door LMA-sponzen de waargenomen lage MeHg-gehalten kan verklaren. De nog lagere concentraties in HMA-sponzen kunnen worden verklaard door extra consumptie van refractair DOM. Demethylering is niet noodzakelijk om de MeHg-concentraties in HMA-sponzen te verklaren, maar als dit proces optreedt, gebeurt dit waarschijnlijk met een snelheid van 1% d^{-1}. Dit model toont ook aan dat de dominantie van HMA-sponzen aan de basis van het voedselweb de MeHg-concentraties in toppredatoren met wel 45% kan verlagen. Al met al verbeteren deze modellen ons vermogen om te voorspellen hoe ecosysteemstructuur en voedseldynamiek de bioaccumulatie van MeHg beïnvloeden.

CHAPTER 1
Introduction

This thesis focuses on quantifying the drivers of mercury (Hg) bioaccumulation. This chapter provides an introduction to the topic. It begins with a discussion of the historical use of Hg, including its applications and pathways of emission into the environment. The characteristics of Hg as a pollutant are then examined, focussing on the properties that make it such a unique pollutant and particularly challenging to manage. After establishing the basis for its classification as a pollutant of concern, this chapter reviews the current environmental status of Hg pollution and considers the associated economic costs. With this context, attention shifts to understanding Hg behavior in the environment, with a particular focus on bioaccumulation, as this is a critical link between environmental Hg concentrations and human exposure. Then a historical review of the scientific understanding of bioaccumulation is performed. This is followed by an analyses of how bioaccumulation can be studied using models, including their relevance and application in environmental assessments. The chapter concludes with a review of existing bioaccumulation models and outlines the key research gaps that are addressed in this thesis.

1.1 Hg as a pollutant

1.1.1 Mercury in the Anthropocene

Historical usage of Hg

Humans have used Hg for millennia. The first known use of Hg by humans was cinnabar (HgS) as pigments, better known as vermilion. The oldest Hg mines in the world are believed to have been in Turkey in the northwest in Konya and are 8000 years old, while the earliest known mining of Hg in Europe is suggested to have taken place at Mount Avala in present-day Serbia, where HgS was extracted during the Eneolithic period (Durman, 1988, as cited in Bogosavljević Petrović et al. (2017)). The usage of Hg in the ancient world is recorded in Roman, Chinese, and Persian sources. Hg was seen by the Romans as such an essential good that the Roman government fixed the price by law. In those days, Hg was mostly used as a red pigment in the form of HgS, for medication, and for amalgamation with gold. The usage of Hg in medication was described in De Medicina by Celsus, where HgS was recommended as a purgative and incorporated in several salves. A century later, however, the Greek-Roman physician Galen described Hg as so toxic that he could not even sanction its external application. The first industrial-scale use of Hg was the patio process, which uses Hg to extract silver from ore and was developed by Bartolomé de Medina in Pachuca, Mexico, in 1554 (Nriagu 1994). Later, the unique properties of Hg were discovered to be of use for scientific instruments, and in 1643, the Hg barometer was discovered by Torricelli and in 1720, the Hg thermometer by Fahrenheit. In the late industrial era, the usage of Hg in medication also reemerged. A common medication for a variety of diseases in the 17th and 18th centuries, including syphilis, tuberculosis, or toothaches, was blue mass, or pilula hydrargyri. This compound was composed of Hg for 33%

by mass. Hg-based medication was common, especially for hard-to-cure bacterial diseases, but its usage quickly disappeared after 1940 when penicillin was discovered as it proved to be more effective with considerably fewer side effects (Norn et al. 2008). The final large increase in anthropogenic use of Hg originates from its ability to amalgamate with gold. While this process was known since ancient times, it led to a notable increase in Hg usage when mining techniques further developed and deep mining became possible. Hg became a key component of the Californian gold rush between 1850 and 1900 and during the Brazilian gold rush of 1970. While the usage of Hg in gold mining in Western countries like the US is currently limited, Hg remains in use in small-scale artisanal gold mining in developing countries.

Unintended consequences of Hg uses

Despite its many use cases, Hg also has a dark side. Human activities have increased Hg levels threefold in the upper ocean since pre-anthropogenic times (Lamborg et al. 2014). The main historical anthropogenic sources of Hg emissions include direct Hg production and use, the burning of fossil fuels, the production of cement and ferrous metals, and small-scale artisanal gold mining (Nriagu 1994; Pirrone et al. 2010; Mason et al. 2012). Although reducing Hg emissions from some sectors, such as direct use of Hg, may be relatively straightforward, mitigating emissions from industries such as fossil fuel burning and the production of cement and ferrous metals presents greater challenges and costs (Streets et al. 2019). This trend is evident in the reduction of Hg emissions by developed economies in the EU and North America, compared to the continued increase in global Hg emissions due to the increased emissions from Asia, Africa, and South America (Streets et al. 2019). Hg mitigation is possible; it comes with significant costs.

1.1.2 Hg as an ubiquitous pollutant

In addition to its toxic legacy, Hg persistence in the environment is a key concern. Since Hg is toxic in its elemental form, it cannot be created or eliminated. The emitted Hg is taken merely from outside the biosphere and emitted into the biosphere. Here, it remains toxic until it is removed from the biosphere. Because of this, sites that were polluted decades or centuries ago are still contaminated. The soil around the historic Hg mining town of Idrija in Slovenia has soil Hg levels up to 300 times higher than the surrounding towns, despite the fact that Hg mining stopped decades ago (Asare and Afriyie 2021). The removal of Hg from the biosphere revolves around processes that bury Hg where it cannot be reemitted naturally and is stored out of the biosphere for geological time scales. These processes are minimal, and the majority of Hg deposited from the atmosphere on land is either reemitted or transported to the world's oceans. In the oceans, Hg can be deposited into deep-sea sediments where it is stored for geological time scales and effectively removed from the biosphere. The problem is that the residence time of Hg in the environment is around 10,000 years (Kawarazuka and Béné 2011). We can compare Hg to other "forever chemicals" such as PCBs; even though it is a slow process, these chemicals can be broken down into less toxic compounds, and natural remediation of pollution typically has a half-life period in the decades. Since Hg, on the other hand, cannot be broken down but merely buried, the natural remediation relies exclusively on geological processes that can take millennia. In addition to the extremely long residence time of Hg in the biosphere,

A common misconception is that the abbreviation for mercury, *Hg*, derives from the Roman word for Mercury. The Romans referred to the element as *mercurium*, which is the origin of the English word mercury. However, the abbreviation *Hg* actually comes from the Latin word *hydrargyrum*, which itself is derived from the Greek *hydrárgyros* (ὑδράργυρος), meaning water-silver (*hydor* = water, *argyros* = silver), due to its liquid, silvery appearance.
The Dutch word for mercury, *kwik*, originates from Middle Dutch *quic*, meaning alive, a reference to the metal's fluid, moving nature. Similarly, the German term *Quecksilber* (literally quick silver) combines *Queck*, an old word for alive, with *Silber*, meaning silver. These terms are etymologically related to the English quicksilver.

it is also omnipresent and can be found everywhere on the planet. While Hg is naturally occurring, and it is therefore expected to be found everywhere, elevated levels of Hg due to anthropogenic emissions are measured in extremely remote areas, such as the stratosphere (Slemr et al. 2018), deep-sea biota (Sisma-Ventura et al. 2024), and Antarctica (Dommergue et al. 2010). To understand the widespread distribution of Hg, it is essential to understand the properties that make Hg such a unique element.

1.2 Hg as a unique pollutant

1.2.1 Atomic properties of Hg

To understand why Hg is so mobile and persistent, we must first understand its atomic structure. Hg is a metal with unique chemical and physical properties. As the 80th element in the periodic table, it has a mean molar mass of 200.59 g mol^{-1} (Prohaska et al. 2022). It is the only metal that can be liquid at room temperature. This is due to its electron shell structure, which is shown in Fig. 1.1a. Hg is a unique element, and its chemical properties can best be described by comparing it to a very similar element, gold (Au). As shown in Fig. 1.1b, Au and Hg vary only in 1 proton and electron, yet Au has a density of 19.32 g cm^{-1} while Hg is 5.81 g cm^{-1} lighter with a density of 13.6 g cm^{-1}. This difference of 5.81 g cm^{-1} is the largest difference between 2 neighboring elements in the periodic table. Furthermore, the melting point between the elements varies by 1101 °C, which is more than any neighboring element, except lithium-beryllium (Norrby 1991). The unique properties of Hg are caused by having a second electron in the 6^{th} shell. Electron shells have a fixed number of electrons, and this means that for Hg all spots are taken (Bohr 1913). The 2 electrons in the outer shell of Hg move fast. These 2 electrons move at 58% of the speed of light. At this speed, the mass of the electrons is increased by relativistic effects by 23%, which leads to an orbital contraction of 23%. Since all electron shells must be orthogonal to one another, this means that the entire electron orbit of Hg is 23% smaller. This has several consequences. Firstly, the electrons and the core of the Hg atom are relatively close, increasing the strength of the bond between the negative electrons and the positive protons in the core. In addition, this prevents Hg molecules from sharing electrons from their outer shell with other Hg molecules, which means that the Hg-Hg bonds are solely based on weak van der Waals interactions, rather than a true metallic bond (Calvo et al. 2013).

Hg as a sulfur-loving metal

The relativistic effects of Hg make it a chalcophilic (sulfur-loving) metal. As we will discuss later, under certain conditions—typically in halogen-rich environments, Hg^0 can lose its two 6s electrons and be oxidized to Hg^{2+} Qu et al. (2009). Even after losing both 6s electrons, relativistic effects cause a contraction of the 5d orbitals, increasing the effective nuclear charge and polarizability of Hg^{2+}. This results in Hg^{2+} acting as a soft Lewis acid with a strong preference for soft bases such as sulfur ligands (Chaudret et al. 2014). As a result, Hg^{2+} forms stable covalent bonds in sulfur-rich environments. This chalcophilic behavior is a key reason why mercury is enriched in the sulfur-rich Earth's crust and mantle, whereas it is relatively scarce in the Earth's deeper interior (Christy 1879; Akçay et al. 2006).

The low boiling point of Hg

To go back to the comparison with Au, in Au these relativistic effects are not present. The outer electron in Au atoms moves at a speed similar to that in Hg atoms, which causes a similar relativistic effect, driving the shrinkage of the electron orbit. When Au elements are together, they can share the electrons in the outer bond, which creates metallic bonds, and they form a solid metal; additionally, they can form aurophilic bonds that further strengthen the metal (Schmidbaur et al. 1988). This means that when Hg is heated, the van der Waals bonds easily break, and Hg has a boiling point of only 356.7 ° C, while this is 2807 °C for Au. Because of this, it is often stated that Hg behaves as a pseudo-noble gas. This means that Hg can be gaseous at room temperature and elemental Hg (Hg^0) has a very long residence time in the atmosphere (3-6 months), which means that it can be transported to remote regions by long-range atmospheric transport (Jackson and Jackson 1997).

1.2.2 Atmospheric chemistry and Long-range transport

When Hg becomes atmospheric, it can be transported all over the world due to its long atmospheric residence time. For example, it is estimated that only 30% of the Hg deposition in the continental US originates from anthropogenic emissions of the US, while natural remission accounts for 33% and the remaining 37% originates from other countries, particularly 21% from Asia. At the same time, US emissions are deposited on other continents as well (Seigneur et al. 2004). This shows the extremely high potential for long-range Hg transport and demonstrates that Hg should be seen as a global pollutant. Although Hg^0 has a very long atmospheric residence time, it can be oxidized to Hg^{2+} due to gas-phase atmospheric reactions involving ozone or hydroxyl radicals (Bergan and Rodhe 2001). This oxidized Hg^{2+} is soluble and can be deposited through wet and dry deposition in the world's oceans and in remote regions such as the Antarctic and Arctic lakes (Lindqvist and Rodhe 2017; Schroeder et al. 1998; Vandal et al. 1993). The processes that control the atmospheric oxidation state of Hg are essential to understand, as they determine where Hg is deposited. Unfortunately, they are also complex and diverse. Schroeder et al. (1998) reported that Hg was depleted in the spring in the Arctic area during moments of ozone depletion. Later, it was discovered that Hg depletion was caused by bromine (Br). During Arctic winter, Br_2 is stable and accumulates in snow, ice, and sea ice. During spring, the light intensity increases and Br_2 is photodegraded to volatile Br (Fan and Jacob 1992). Atmospheric Br can react with ozone forming BrO and oxygen. BrO and Br are in dynamic equilibrium, so during the Arctic spring, there is an abundance of atmospheric Br that can react with Hg (Simpson et al. 2007). The oxidation of Hg^0 by Br occurs in 2 steps, as shown by Dibble et al. (2012) and discussed by Si and Ariya (2018).

$$Hg^0 + Br \rightarrow HgBr$$

and,

$$HgBr + Y \rightarrow HgBrY$$

In which Y is NO^2, HO^2, ClO, or BrO. HgBrY, which is soluble, can be associated with atmospheric droplets and removed from the atmosphere during rain. This mechanism demonstrates how atmospheric Hg chemistry can control the global distribution of Hg (Ebinghaus et al. 2004). Over time more such interactions are discovered and the modern atmospheric Hg model GEOS-Chem takes 14 Hg chemical reactions into account; an overview of this modern understanding of atmospheric Hg speciation is shown in Fig. 1.2 (Shah et al. 2021). The importance of understanding atmospheric oxidation is further shown in Fig. 1.3 by Zhang et al. (2023b). Although Hg^{2+} is only 2% of atmospheric Hg, it constitutes 60% of atmospheric flux into the oceans. If we take a closer look at the 2023 Hg budget, as presented by (Zhang et al. 2023b), they predicted global emissions to the atmosphere of 12,000 Mg $year^1$, of which 1,670 Mg $year^1$ are direct anthropogenic emissions. Based on this model, 1,670 Mg $year^1$ of these anthropogenic emissions are sequestered on land and 910 Mg $year^1$ in the ocean. Other models have very different estimations and, for example, Shah et al. (2021) predicts anthropogenic Hg sequestering of 1,400 Mg $year^1$ and 1,100 Mg $year^1$ for land and ocean respectively, while Horowitz et al. (2017) predicts anthropogenic Hg emission sequestering of 780 Mg $year^1$ for land and 1,700 Mg $year^1$ for oceans. To put these numbers in context, the pre-industrial sequestering of Hg of geothermic emissions is estimated to be 40 Mg $year^1$ and 460 Mg

The relativistic effects of Hg also influences Hg in ways that are not relevant in this thesis. For example the silver shine of liquid Hg is also caused by this. Due to relativistic contraction, the 6s orbital in Hg is stabilized (lowered in energy), which increases the energy gap between the 6s and 6p orbitals to 10.4 eV. As a result, the energy required for an electron to transition from 6s to 6p is higher than the energy of most visible photons (1.6–3.1 eV). Therefore, Hg does not efficiently absorb visible light and instead reflects it, giving it its metallic luster. Without this relativistic effect, mercury would likely appear duller and less metallic. In gold the gap is smaller (2.38 eV), which means that gold can absorb light in the blue and ultra violet range, giving gold its colour

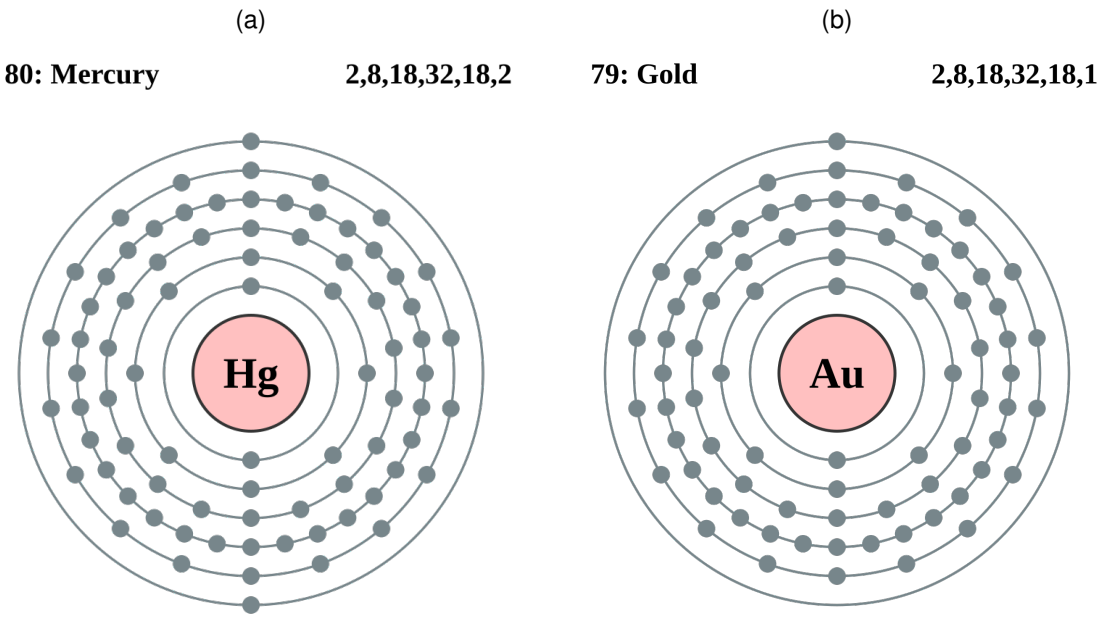

Figure 1.1: 1.1a) shows the electron configuration of a Hg atom while 1.1b) shows the electron configuration of a gold atom. Note that the only difference between the 2 atoms is that Hg has 2 electrons in the 6th electron shell whereas gold only has 1. Both images are taken from Wikipedia and distributed under the Creative Commons license (Robson 2005; Robson and Pumbaa 2006)

year^{1} for land and ocean, respectively (Selin et al. 2008). The differences between these models are driven mainly by differences in the Hg^0:Hg^{2+} ratio (Zhang et al. 2023b). The difference in Hg fluxes between the land, ocean, and atmosphere can have a dramatic effect on the global Hg budget.

1.2.3 Biological Hg uptake on land

Although interactions within the atmosphere determine the speciation and mobility of Hg, vegetation contributes to the removal of Hg from the air (Feinberg et al. 2022). The annual uptake of Hg by plants is estimated at approximately 2491 ± 551 Mg Hg y^{-1}, which is crucial for the seasonal variations observed in atmospheric Hg levels (Jiskra et al. 2018). It is estimated that Hg uptake by plants accounts for 60-90% of atmospheric Hg deposition and that it reduces global atmospheric Hg by 660 Mg and reduces Hg input into the oceans by 960 Mg y^{-1} (Zhou and Obrist 2021). Plants can absorb Hg through their stomata, similar to how they absorb CO_2 (Laacouri et al. 2013), and through other non-stomatal pathways (Stamenkovic and

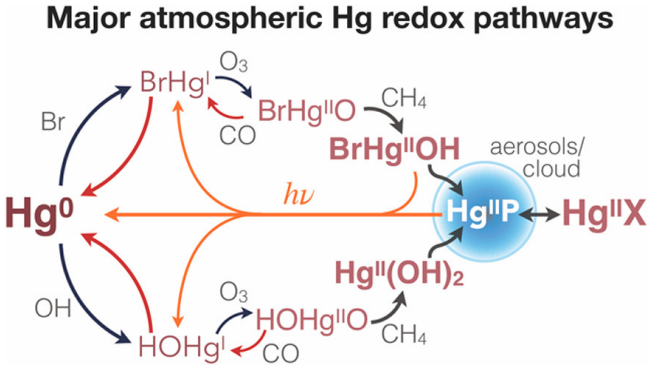

Figure 1.2: Known atmospheric Hg reaction pathways. Reprinted from Shah et al. (2021), licensed under CC BY 4.0 (http://creativecommons.org/licenses/by/4.0)

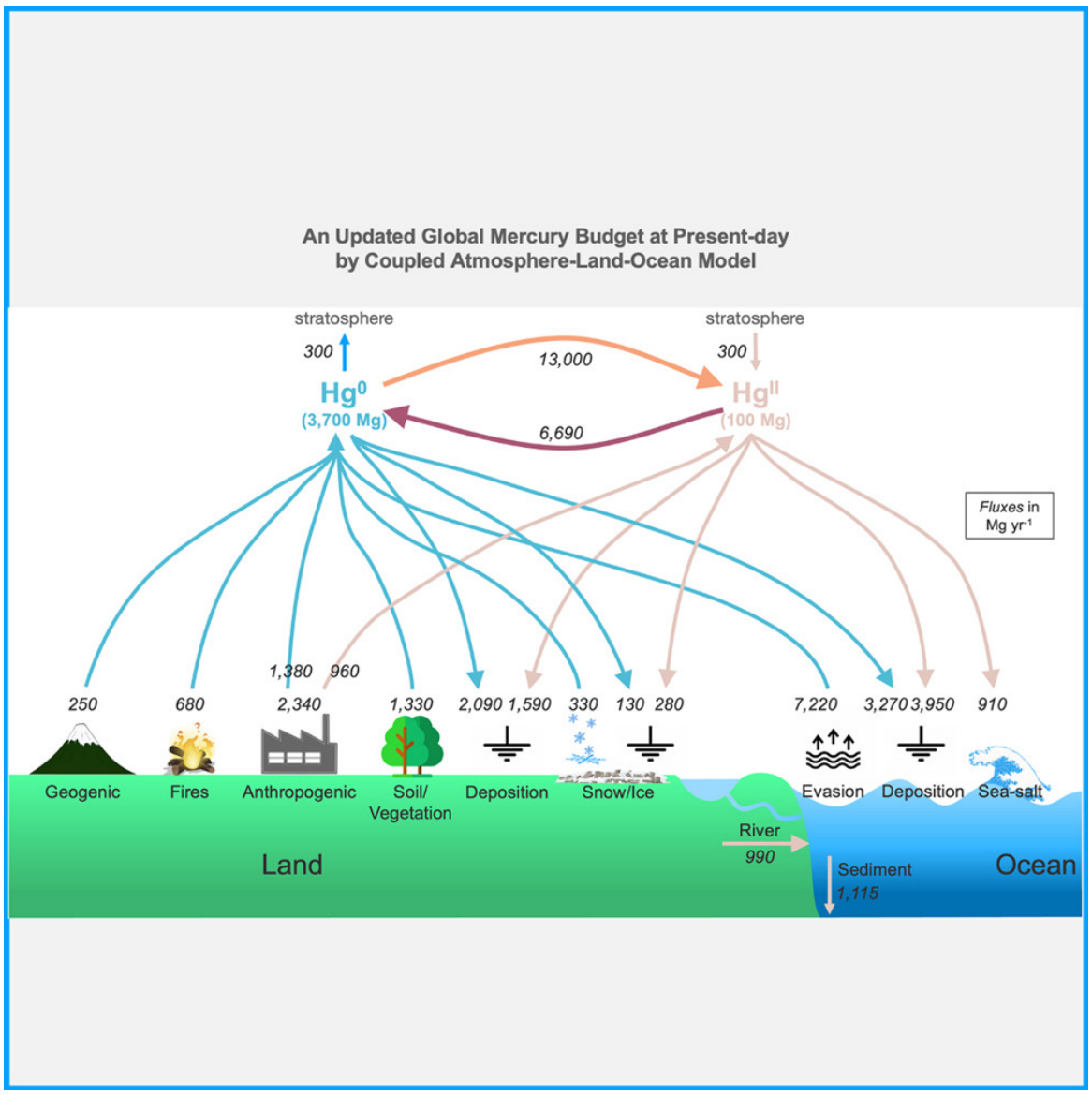

Figure 1.3: The global Hg fluxes. The largest main fluxes into the ocean are the deposition of Hg^{2+} (4,860 Mg y^{-1}) and Hg^0. Hg^0 7,220 Mg y^{-1} is rereleased into the atmosphere. Smaller yet essential fluxes are the riverine input of Hg into the oceans (990 Mg y^{-1}) and sedimentation (1,115 Mg y^{-1}). Reprinted from Zhang et al. (2023a), licensed under CC BY 4.0 (http://creativecommons.org/licenses/by/4.0)

Gustin 2009). The reason why Hg absorption on land plants is an essential link between anthropogenic Hg emissions and Hg bioaccumulation in seafood is twofold. First, Hg that is taken up by plants can be deposited by litterfall. Litterfall is a large flux of Hg and accounts for the deposition of 1180 ± 710 Mg Hg y^{-1}, and the transport of litterfall through rivers can be a source of Hg for coastal oceans (Wang et al. 2016; Outridge et al. 2018). Secondly, some organic plant material is buried and fossilized, and when the plant material is buried so is its associated Hg. This means that buried plant material has a high Hg content and fossil fuel formed from fossilized organic carbon has high Hg levels as a consequence. This is the reason why burning dried plant material, in the form of coal, is currently the largest global anthropogenic source of Hg. This process of Hg burial via plant fossilization resulted in 2/3^{rds} of the global Hg being buried and stored in the northern permafrost regions. These regions have 1,656 ± 962 Gg Hg, of which 793 ± 461 Gg Hg are frozen in the permafrost, demonstrating that land plants are very important for the global Hg budget (Obrist et al. 2018; Schuster et al. 2018).

1.3 State of Hg pollution

1.3.1 The Global Hg budget

The global Hg inventory refers to the Hg standing stock while the Hg budget refers to the inventory and Hg fluxes. Because Hg is a stable element, it is neither created nor destroyed by natural processes on Earth, and the total Hg inventory of the planet does not change. However, it matters a lot where and in what form this Hg is. There is much more Hg in the northern permafrost regions than there was in Minamata Bay. However, in Minamata Bay, the high concentration of Hg caused the tragic events of the Minamata disease, whereas the Hg stored in the permafrost is only of concern when it is remobilized. Therefore, we are worried by how much Hg is available in the biosphere, and we consider processes such as the burning of fossil fuels as emissions, as even though they do not increase the total amount of Hg on Earth, they do increase Hg in the biosphere. To help policymakers, scientists, and stakeholders, the state of the art global Hg budget and inventory are presented in UN's periodic publication entitled Global Mercury Assessments. In this assessment, the major global fluxes and pools of Hg are estimated based on the most up-to-date research available. The last Global Mercury Assessments was presented in 2018. The graphical abstract of this publication is shown in Fig. 1.4. This is where we start to see the whole picture of Hg as a global pollutant. An important observation here is that the anthropogenic flux appears to be relatively small; only 31% of the total input of Hg into the atmosphere is direct anthropogenic emissions. However, this misses the crucial point of Hg pollution. It is an element and does not degrade. Therefore, Hg emissions from previous years become part of the global Hg cycle and are remitted as part of the next year's Hg budget. If we include reemissions, anthropogenic Hg emissions suddenly become 94% of global Hg emissions. This shows that Hg is not only a pollutant of global concern, but also of generational concern, since current emissions will remain in the environment for 3000 years (Selin 2009). The budget estimated that atmospheric Hg depositions are currently 300% higher than pre-industrial quantities, while Hg in the world's surface oceans increased by 230% compared to pre-industrial times. The key reason why we are interested is that it allows us to estimate how anthropogenic Hg emissions today can influence the Hg concentrations in the world's oceans in the future.

1.3.2 The importance of the world's oceans

The world's oceans are an essential resource for human civilization. Aquaculture alone generates annual revenues of more than € 500 billion (FAO 2020). In addition to the quantifiable financial benefits of the ocean, many people depend on the oceans for their livelihood or cultural way of life (Khakzad et al. 2015). Three billion people around the world depend on seafood as their main source of animal protein; many of these people live in poor areas where alternative sources of protein are not available (Tacon and Metian 2009).

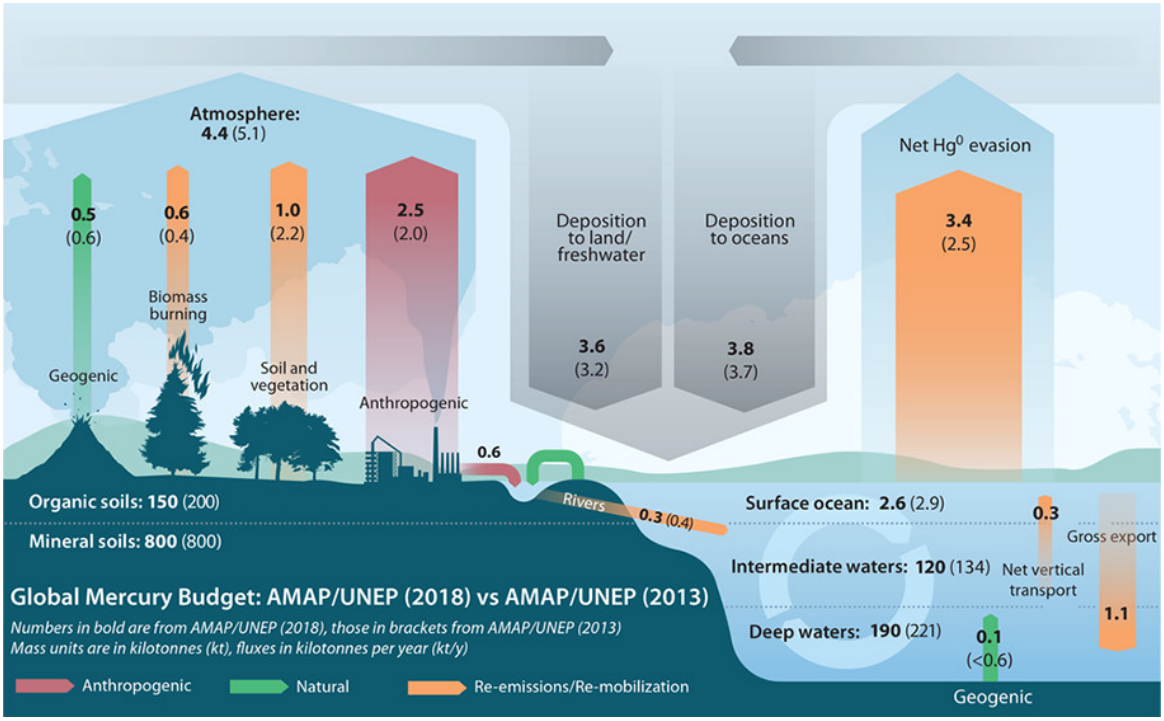

Figure 1.4: Estimations of the global Hg budget. Reprinted (adapted) with permission from (Outridge et al. 2018). The fat numbers are the newest 2018 global Hg budget, while the numbers between brackets represent the previous estimated budget from 2013. Copyright 2018 American Chemical Society.

1.3.3 Hg in the marine environment

When Hg enters the ocean, it usually enters in the form of Hg^{2+}, due to wet deposition and riverine input, or as Hg^0 due to atmospheric exchange (Outridge et al. 2018). In the same way that occurs in the atmosphere, in the marine environment, the oxidation state and particle partitioning of Hg are critical to understanding its behavior. Hg^0 and Hg^{2+} are in a dynamic equilibrium. Both oxidation of Hg^0 to Hg^{2+}, and reduction of Hg^{2+} to Hg^0 can occur under dark conditions, but both reactions are increased in surface water due to photochemical mediation (Whalin et al. 2007). Unlike atmospheric Hg, which is dominated by Hg^0, the percentage of Hg^0 of total Hg is lower. It is typically higher in surface water (9-47%) than in deep water (6-39%), but there is great regional variation (Bowman et al. 2020; Bowman et al. 2015). This is because, as mentioned before, halogens drive the oxidation of Hg^0 and in the marine environment, there is an abundance of Cl^-. Also, the earlier described Calcophilic nature of Hg becomes relevant again, as Hg^{2+} can, in turn, react with sulfate to form HgS or be methylated by bacteria into methylmercury (CH_3Hg^+) or dimethylmercury ($(CH_3)_2Hg$), referred to as $MMHg^+$ and DMHg respectively (Fitzgerald et al. 2007; Compeau and Bartha 1985; Jensen and Jernelov 1969). $MMHg^+$ and DMHg are together called methylmercury (MeHg). Both DMHg and Hg^0 are dissolved gaseous compounds and can evaporate from the water, and are therefore together referred to as Dissolved Gaseous Hg (DGM). MeHg is a small but significant Hg fraction. The percentage of MeHg from total Hg is typically between 7 and 22% in surface water (<150m deep). The contribution of MeHg to the total Hg pool can be greater in deeper water (Fitzgerald et al. 2007). Hg^{2+} and $MMHg^+$ associate with organic material, such as dissolved and particulate organic carbon as well as living organisms (Mason et al. 1995; Morel et al. 1998). This interaction acts as an important mechanism for the transfer of Hg to deep-sea sediments, where it becomes a substantial repository (Sanei et al. 2021). On the other hand, the binding of Hg^{2+} and $MMHg^+$ to living material facilitates their buildup in living organisms, a process known as bioaccumulation (Mason et al. 1995). The bioaccumulation of MeHg in marine environments can lead to MeHg concentrations that are unsafe for human consumption, impacting both public health and economic resources. Consequently, this thesis concentrates on Hg bioaccumulation, with a particular emphasis on MeHg.

1.4 The cost of Hg pollution

1.4.1 The toxicity of MeHg

While MeHg refers to both $MMHg^+$ and MeHg, the consumption of $MMHg^+$ causes the main health risk associated with the consumption of Hg. The mechanism of $MMHg^+$ toxicity is not fully understood, but the basic concepts are known. $MMHg^+$ toxicity has to do with the electrophilic properties of the pollutant. This allows it to strongly bind to thiol (R-SH) and selenol (R-SeH) groups. However, thiol groups are quite common in the human body and present in micromolar amounts, while the toxicity of $MMHg^+$ can be observed in the nanomolar range. This means that $MMHg^+$ toxicity cannot simply be caused by the depletion of the thiol groups. When $MMHg^+$ binds to a thiol or selenol group, it forms a very strong $RSHgCH_3$ or $RSeHgCH_3$ type complex, respectively (Farina et al. 2011). The main mechanism of toxicity appears to be the strong binding of $MMHg^+$ to the antioxidant seleno-enzyme glutathione peroxidase and thioredoxin reductase (Carvalho et al. 2008). These enzymes are responsible for the balance of redox cells, and their permanent inhibition by $MMHg^+$ can cause cell oxidative stress. This oxidative stress can cause irreparable neurological damage, especially in developing children (Farina et al. 2011; Johansson et al. 2007). DMHg is also extremely toxic, but its mechanisms are less understood for two reasons. First of all, because of its volatility, it is harder to work with. Second, and most importantly, it is currently not assumed that DMHg bioaccumulates in significant amounts (Morel et al. 1998). This means that extreme care must be taken while working with DMHg as a purified chemical, but there is no evidence that it poses a threat to people in their regular lives.

1.4.2 The first major outbreak of MeHg intoxication; The Minamata disease

The toxicity of MeHg made international headlines when, between 1932 and 1968 a Hg chemical factory contaminated the sea near the city of Minamata in Japan. The Hg released into the water was methylated in MeHg and bioaccumulated in seafood at concentrations that were very toxic to humans and animals. The first victims of this outbreak were local cats that ate fish. Due to their small size, MeHg quickly reached dangerous levels, and the cats started to move erratically; this phenomenon got nicknamed the *dancing cat syndrome*. When humans started to have similar symptoms, the government of Japan launched an investigation in 1956 into the cause of what is now called Minamata disease. The investigation successfully identified MeHg as the source of the pollutant in 1959. The factory was aware that they were the prime suspect of this outbreak, and to circumvent scrutiny, they decided to reroute their wastewater away from the bay that was under investigation, directly into the Minamata River. The factory was ordered by the Ministry of International Trade and Industry to redirect its wastewater back to the bay and install water purification systems to reduce the amount of Hg in the wastewater. However, the factory pretended to comply and installed a water purification system; later testimony revealed that this was only for show and that nothing was installed that could filter Hg from the wastewater. This led to 9 more years of Hg polluted wastewater dumping until, in 1968 the factory stopped using Hg. This pollution affected many. The government of Japan introduced a program to compensate the victims, and currently, 48,000 people have applied for government compensation, but only 2,995 have been recognized as victims (Ministry of the Environment-Government of Japan 2002; Yamaguchi 2023). This results in ongoing legal battles between victims, stakeholders, and the government that are still in progress, with more than 1,700 plaintiffs involved in lawsuits in four district courts (Ekino et al. 2007; Kyodo news 2024; The Mainichi 2023; Ministry

When referring to observations, I refer to MeHg, as both DMHg and $MMHg^+$ are known to be highly toxic, but are usually not separated in measurements. DMHg is not assumed to bioaccumulate in significant quantities, so bioaccumulated MeHg and $MMHg^+$ are assumed to be equal. Furthermore, I would refer to observed Hg^{2+} as iHg, as measurements separating between individual iHg fractions are extremely rare.

of the Environment-Government of Japan 2002).

1.4.3 The response to Hg pollution; The Minamata Convention on Mercury

This outbreak stimulated the need for global control of Hg pollution and in 2009 at a United Nations Environmental Governing Council meeting, it was decided to hold five meetings to discuss the form of a global treaty on Hg as a pollutant. The first meeting was held in Stockholm in 2010, during which hair samples of participants from 40 countries were measured for Hg. All samples were positive and more than 1/3 of the samples had Hg levels higher than the reference dose of 1 ppm (Kessler 2013). This showcased the scope of the problem to the delegates and on 19th January 2013, the Minamata Convention on Mercury was proposed. 140 parties signed this international treaty that aims to protect both humans and the environment from anthropogenic emissions of Hg and Hg compounds. As of March 14th 2024, the convention had 148 parties. Although the convention does not forbid Hg emissions, it aims to reduce them to levels as low as reasonably possible while sharing the cost of the reduction of Hg emissions between different countries in a fair way. For this, the bioaccumulation of Hg needed to be investigated so that the emission of Hg could be linked to MeHg concentration in seafood.

1.4.4 The current cost of Hg pollution

The preservation of seafood as a safe and healthy source of nutrition is essential to feed an increasing world population, and bioaccumulation of MeHg is currently threatening this. The resolution 48/13 of the UN declared that having a clean environment is a human right, and the WHO has set the environmental quality standard for MeHg in fish at 0.5 mg kg^{-1} for low trophic and 1.0 mg kg^{-1} for high trophic level fish per wet weight (Kehris 2022; FAO/WHO 2012). This human right is threatened by marine Hg pollution, as studies show that currently about one-third of all commercial fish have Hg levels that pose a risk to humans when consumed regularly (Burger and Gochfeld 2011).

Because of the continued emission of Hg, the long residence time, and its toxicity, Hg remains a pollutant of major concern, with major costs associated with its pollution. It is estimated by Chen et al. (2019) that in 2010 Hg pollution resulted in 7,360 deaths in China due to MeHg-related heart attacks; additionally, it is estimated that there is a cost of 16$ billion per year in the EU and US due to the loss of intelligence in children (Bellanger et al. 2013). An attempt to quantify the total cost of Hg pollution was made by Zhang et al. (2021) by propagating the estimated cost of all forms of Hg pollution. They estimated that the total global cost of Hg pollution would be 16$ trillion between 2010 and 2050, with a 95% confidence interval that is between 4.7$–54$ trillion if we keep the current policy scenario. This is an enormous cost in a financial sense, but it cannot be forgotten that this cost is driven by human suffering and the opportunity loss of lost intelligence in children. Additionally, the risk of MeHg toxicity is highest in children in communities in developing countries that rely on fishing for sustenance, while especially these people need the intelligence of future generations to increase their economic prospects (Li et al. 2024). As discussed earlier, the emission of Hg is incredibly hard to directly tackle, and historic emissions will remain relevant in the foreseeable future. Because of this, it is important to fully understand what happens to Hg that is emitted and what cost it incurs. An invaluable tool for this is the use of models that can estimate the total cycle of Hg and can link Hg emission to the MeHg exposure in people.

1.5 Towards the end-to-end modeling of Hg cycling

1.5.1 Bioaccumulation; the end station of Hg emissions.

As discussed in the previous segment, significant progress has been made in the modeling of Hg cycling. While all models can always be improved, we have a general understanding of atmospheric Hg cycling. Our ability to model Hg in the marine environment is, however, less advanced. This is partially because, in the marine environment, Hg reacts with the ecosystem and bioaccumulates, and the modeling of the marine ecosystems is still in its infancy compared to our ability to model atmospheric fluxes. In this thesis,

I focus on modeling the bioaccumulation of Hg and on identifying key drivers of the link between marine MeHg concentrations and the concentration of MeHg in seafood.

1.5.2 Defining the bioaccumulation of Hg

When discussing the implementation of a process, such as bioaccumulation, in a model, it is first essential to clarify the terminology, especially since terms are sometimes used with slightly different meanings in different sources. In this thesis, bioaccumulation refers to the net uptake, transformation, and elimination of Hg from all sources. It is commonly expressed as a bioaccumulation factor (BAF), which is the ratio of the concentration of Hg in an organism and the concentrations in its surroundings (Neely 1980). The BAF for marine biota can be measured by measuring both the concentration of Hg in marine biota and in the surrounding water and then calculating the ratio between the two (Hamelink 1977). The most important step in bioaccumulation is bioconcentration. Bioconcentration refers to the uptake of Hg directly from the water column. Similarly to bioaccumulation, bioconcentration is often presented as the bioconcentration factor (BCF), which is the ratio of Hg in the biota that originates from direct uptake from the water, and the concentration in the water in steady state (Hamelink 1977). As mentioned above, an equilibrium between pollutants in the marine biota and seawater is dynamic, rather than passive (Mackay 1991). This means that BCF and BAF are the ratios between a bioconcentration and a bioaccumulation rate, respectively, and a release rate. In primary producers, the only bioaccumulation method is bioconcentration, and thus the bioaccumulation and bioconcentration rates are equal. This rate depends on the chemical form of Hg and the surface of the contact area between the organism and the water (Mason et al. 1995). This means that smaller primary producers, which have a higher surface-to-volume ratio, have a higher bioaccumulation rate. Although both iHg and MeHg can bioaccumulate, they do not do this in the same way. MeHg has a stronger affinity for proteins within the cytoplasm, while iHg has a higher affinity for the cell wall (Mason et al. 1996). Although Mason et al. (1996) shows that the bioconcentration rates of iHg and MeHg are similar and both depend on cell size, the release rates of iHg and MeHg do not. This is demonstrated by Pickhardt and Fisher (2007), who shows that there is no correlation between the BCF of iHg and cell size ($r^2 = 0.021$, $p > 0.73$), while the BCF of MeHg has a strong significant correlation ($r^2 = 0.922$, $p < 0.001$) between cell size and the BCF, in which smaller cells have a higher BCF.

Although BAF and BCF are the same for primary producers, this is not the case for consumers. In addition to direct uptake of Hg from the environment, consumers can also take up Hg from their food. The increase in Hg with higher trophic levels is called biomagnification and is often presented as the biomagnification factor (BMF). The BMF is the relative increase in Hg between one trophic level and the next. An example is the feeding of the carnivorous beltfish (*Trichiurus lepturus*) and herbivorous Lebranche mullet (*Mugil liza*) measured by Seixas et al. (2014). They found that the predator had a MeHg concentration that was 10 times higher than that of the prey, while the predator only had 30% of the iHg concentration of the prey. In this case, the trophic interaction would have a BMF of 10 for MeHg and 0.3 for iHg. As demonstrated by Seixas et al. (2014), the BMF of MeHg is generally higher than that of iHg. This phenomenon is also noted when examining lower trophic levels and is explained by Mason et al. (1996). Their study shows that MeHg predominantly binds to cytoplasmic proteins, while iHg mostly binds to the cell wall. This distribution reflects the differential assimilation efficiency of iHg and MeHg during the predation of consumers on phytoplankton. Given that consumers more effectively absorb cytoplasmic proteins than the lipid bilayer, MeHg associated with these proteins is transferred into higher trophic levels more efficiently than iHg, which is bound to the cell wall. Having established that MeHg is a toxic pollutant which bioaccumulates, leading to significant costs, the importance of efforts to comprehend this process becomes apparent. However, prior to discussing model design, it is crucial to understand the current knowledge on the bioaccumulation of Hg.

1.5.3 History of bioaccumulation research

To understand how Hg bioaccumulation can be modeled today, it is helpful to reflect on how the concepts of both bioaccumulation and modeling emerged historically, and what role they have played both scientifically and culturally.

While it is debated where and when humans started metallurgy, this was likely around 6000-7000 BC and might have been developed in different locations in parallel (Radivojević et al. 2010). The first humans were likely oblivious to the potential harmful effects of heavy metals, or the benefits could have outweighed the possible downsides. The first mention of the negative effect of heavy metals on human health is currently attributed to the Greek physician Nicander of Colophon, who described acute paralysis and colic after high-dose lead exposure (Riva et al. 2012). The cornerstones of what would become bioaccumulation research were arguably first presented by Pliny the Elder in *Naturalis Historia*. He described that the food of animals influences the quality of the meat and that lead can have negative health effects on humans and animals (Bartnik 2023; Pliny the Elder 0077). While Pliny the Elder described that the quality of the food of animals depended on their diet, this was concerning the flavor, and the link between pollutants in the diet of animals affecting the predator consuming those animals was not made until early modern times.

1.5.4 Towards our modern understanding of bioaccumulation

During the industrial revolution, arsenic became a commonly used fertilizer to assist in the agriculture of wine and wheat (Hughes et al. 2011). Although this was very effective as a pesticide, crops readily absorbed arsenic, which could cause arsenic intoxication when the produce was consumed. This started to attract attention as several lethal outbreaks of arsenic toxicity occurred, notably an outbreak of arsenic toxicity in beer in England that affected 6,000 people and killed 70 (Dyer 2009; Copping 2009). It can be argued that our modern understanding of bioaccumulation started when Rachel Carson published the book *Silent Spring* in 1962 (Carson 1962). In this book, she outlined that pesticides can accumulate in the natural environment, where they can disrupt natural ecosystems and cause cancer and nervous diseases in humans. A major further step in our understanding of bioaccumulation occurred when Donald Mackay applied the concept of fugacity to the environmental system. Fugacity, first mentioned by Newton Lewis and Gilbert Newton Lewis (1901), describes substances' escaping tendency between phases. Mackay demonstrated that pollutants in nature are distributed between compartments according to the principles of fugacity. This framework showed that pollutant distribution between compartments under equilibrium conditions is dynamic and that apparent steady-state represents the net flux of a continuous bidirectional flux (Mackay 1991).

1.5.5 Modeling: A Tool for Enhancing Understanding of Bioaccumulation

One sector that is fast growing in capabilities is the use of models for pollution and bioaccumulation research. Moore's law, which states that the transistor density on chips doubles every two years, has been accurate over the last 6 decades, and computational power increased significantly (Zhu et al. 2023; Moore 1965). Most importantly, this resulted in a dramatic reduction in computing costs, making high-performance computing more accessible across a wide range of research fields (Nordhaus et al. 2006). This allows researchers to make increasingly complex models to simulate complex interactions. At its core, a model is a simplified representation of a more complex system. In this way, models help us understand complex systems (Box 1976). Another benefit of using models is that we can use them to perform in silico experiments. A model allows us to simulate a complex system, such as the world oceans, and analyze how changes to the system, such as increased Hg emissions, global warming or the building of wind parks, influence the MeHg concentration in fish.

The referenced Historia Naturalis by Pliny the Elder is widely considered the first encyclopedia ever written. It consists of 37 books grouped into 10 volumes, each of which could be referenced individually. This was an innovative approach for its time, as it allowed for systematic referencing and validation of information. Pliny compiled over 20,000 facts from more than 100 different authors. The work remained so influential that it became a model for later encyclopedias and was one of the first books printed after the invention of the printing press.

The core motivation for writing this thesis is the risk posed by the high concentration of MeHg in fish. To address this challenge, we can build a model that links Hg concentrations in the ocean to MeHg bioaccumulation in fish to understand the processes governing Hg bioaccumulation. There are several ways in which we can approach this.

Non-mechanistic models

Non-mechanistic models are those that do not directly represent the underlying processes. Statistical approaches provide a framework to place measurements and transform data into general, quantifiable assertions (Judd et al. 2014). Tools such as frequentist, Bayesian statistics and machine learning can be utilized in non-mechanistic models to estimate probabilities and make predictions (Clark 2005; Jermilova et al. 2025). These approaches perform best when large datasets are available (Dou et al. 2023). However, due to the high cost of sampling Hg in the marine environment and logistical challenges, data availability is often limited (Cossa et al. 2022). This low amount of data makes it difficult to train complex models, such as neural networks, to estimate MeHg concentrations in fish based on anthropogenic emissions. Moreover, data-driven models have limited usability outside of their training regime, which makes the limited data even more problematic (Reichstein et al. 2019). An example of a non-mechanistic model producing an unlikely outcome is a study linking atmospheric Hg concentrations to Hg concentration in fish by Zhang et al. (2022). They found that over a 35-year period, there was an inverse relationship between Hg emission and Hg concentrations in fish in China. It is unlikely that increased Hg emission would drive a reduction in fish Hg concentration; thus, it is likely that there are other drivers influencing the fish Hg concentration that are not accounted for in this non-mechanistic model, such as marine MeHg methylation or changes in the ecosystem. To better understand these drivers, it is often necessary to use mechanistic models that explicitly resolve Hg cycling and bioaccumulation. This way, these drivers can be accounted for, identified, and quantified. These mechanistic models typically take one of two approaches: modeling the movement of substances (Lagrangian models) or modeling their distribution in space (Eulerian models).

Lagrangian models

Lagrangian models focus on tracking where something goes or where it originates from. The pollutant is tracked through space and time. For pollution research, this is interesting as it allows us to estimate where pollution ends up, or what is causing observed pollution. Research questions that can use a Lagrangian model are, for example: when a Hg spill occurs, where does this Hg go, and how will it increase the MeHg concentration in what seafood? Examples of Lagrangian models used in Hg pollution research are the Regional Lagrangian Model of Air Pollution (RELMAP) by Bullock et al. (1998), which simulates the atmospheric emission, transport, diffusion, transformation, and deposition of several Hg species using a Lagrangian modeling approach, a special version of the NOAA HYSPLIT4 model.

Eulerian models and their core components

Eulerian models do not track the pollutant, but instead focus on modeling the concentration on a grid within a defined area. As Eulerian models are extensively used in this thesis, I will go over them in more detail and describe the essential components of a Eulerian model in more depth. Since the main focus of this thesis is to quantify biological drivers of MeHg bioaccumulation, I will also discuss here why a Eulerian model is useful in this context.

Setup; Grid and initial conditions

As a Eulerian bioaccumulation model estimates bioaccumulation in a certain area over time, it is essential to define this area and its dimensions first. The model can, for example, be a 3D model of all global oceans for Hg air-sea exchange (Soerensen et al. 2010), or MeHg bioaccumulation (Zhang et al. 2020), a 2D model of Hg cycling in the Xiaxi river (Zhu et al. 2017), or a 1D model to resolve Hg dynamics in the Black Sea (Rosati et al. 2018). Eulerian models are based on a structure made up of discrete grid cells. Most Eulerian models typically rely on structured cubic grids, but modern models allow for variable resolution grids. This enables high spatial resolution in areas where this is important, such as coastal zones,

while maintaining computational efficiency in less variable zones such as the open ocean (Logemann et al. 2021).

External drivers and boundary conditions

For marine models, it is essential to establish external forcing from outside the model. Key physical drivers include tides and light, more specifically, Photosynthetic Active Radiation (PAR) (Zhao et al. 2019; Thewes et al. 2022). Additional nutrient deposition plays a key role in the ecosystem dynamics of the North Sea (Troost et al. 2013). A related essential component is the boundary conditions, which specify processes at the model domain's boundaries, for instance, during horizontal advection, sedimentation, or evaporation. These boundary conditions also outline external inputs like riverine inflows or lateral advection, which can significantly influence the behavior of the model (Mikolajewicz and Maier-Reimer 1994).

For Hg cycling, there are several essential drivers, such as Hg fluxes from atmospheric deposition and exchange, riverine input, or Hg dry deposition via the deposition of dust particles that would be defined as boundary conditions (Bieser and Schrum 2016; Liu et al. 2021; Cossa et al. 2023).

Advection and diffusion

In marine systems, the concentration of a pollutant such as MeHg is dependent on the water movement. This happens through two processes: advection, which refers to large-scale transport by currents and tides, and turbulent diffusion, which captures the small-scale mixing driven by turbulence. These physical processes are governed by the Navier-Stokes equations, which describe how water moves in response to forces such as gravity, pressure, and viscosity. In order for us to estimate the MeHg concentration, we therefore need to take this into account (Griffies 2003).

To estimate the change of the concentration of something, such as MeHg in a grid cell in biogeochemical-hydrodynamic models, we can use a tracer transport equation, which calculates the change in concentration under the effect of advection, diffusion and biogeochemical reactions (Fennel and Neumann 2015). This means that the concentration change of state variable C in an ocean model can be calculated as:

$$\frac{\partial C}{\partial t} = \underbrace{-u\frac{\partial C}{\partial x} - v\frac{\partial C}{\partial y}}_{\text{horizontal advection}} + \underbrace{-(w + w_s)\frac{\partial C}{\partial z}}_{\text{vertical advection and sinking}} + \underbrace{D_h\left(\frac{\partial^2 C}{\partial x^2} + \frac{\partial^2 C}{\partial y^2}\right)}_{\text{horizontal diffusion}} + \underbrace{\frac{\partial}{\partial z}\left(A_v(z)\frac{\partial C}{\partial z}\right)}_{\text{vertical diffusion}} + \underbrace{S}_{\text{source/sink}} \quad (1.1)$$

C = Tracer concentration [e.g. ng Hg m^{-3}]
u, v, w = Velocity components in x, y, z [$m\,s^{-1}$]
w_s = Sinking velocity (vertical) [$m\,s^{-1}$]
D_h = Horizontal diffusivity [$m^2\,s^{-1}$]
$A_v(z)$ = Vertical diffusivity, function of depth [$m^2\,s^{-1}$]
S = Grid cell specific source or sink terms [e.g. ng Hg $m^{-3}s^{-1}$]
t = Time [s]

Biogeochemical reactions per grid cell

S in equation 1.1 represents all source and sink terms, which occur solely within grid cells. These terms might include riverine inflow of MeHg at a model domain boundary grid cell, sedimentation in a bottom grid cell, or MeHg production and degradation driven by biogeochemical reactions. Each grid cell undergoes biogeochemical reactions, which are the core of the bioaccumulation processes modeled in this thesis. These reactions would involve, among other things, the growth of phytoplankton based on available light and nutrients, the recycling of nutrients, the speciation of Hg, and, of course, bioaccumulation. Here, it is important to clarify some terminology. The biogeochemical components of the model are declared as **state variables**. State variables can react in chemistry and are moved by currents. Most of the equations that drive changes in state variables are dependent on constant rates; these are called **parameters** (Soetaert

and Herman 2009). A final type are **diagnostic variables**; these variables are calculated from state variables but not transported or influenced directly by hydrodynamics. We can, for example, use this for the estimation of how MeHg is broken down by PAR in a process called photodemethylation (Sellers et al. 1996). This process is calculated as:

$$\frac{dC_{\text{MeHg}}}{dt} = -K_{\text{PD}} \cdot PAR \cdot C_{\text{MeHg}} \tag{1.2}$$

where:

$$C_{\text{MeHg}} = \text{MeHg concentration} \quad [\text{ng Hg m}^{-3}]$$
$$K_{\text{PD}} = \text{Photodemethylation rate constant} \quad [\text{s}^{-1}]$$
$$\text{PAR} = \text{Photosynthetically active radiation} \quad [\text{W m}^{-2}]$$

Here, the C_{MeHg} is a state variable, K_{PD} is a parameter, and PAR is an external driver. This represents a sink term for MeHg. If the demethylation rate is saved as a separate output variable, this would be a diagnostic variable.

If we assume that PAR is constant, we can analytically solve this as a linear first order differential equation, and use this to calculate the MeHg concentration at time step t as follows:

$$C_{\text{MeHg}}(t) = C_{\text{MeHg}}(0) \cdot e^{-K_{\text{PD}} \cdot \text{PAR} \cdot t} \tag{1.3}$$

where:

$$C_{\text{MeHg}}(t) = \text{MeHg concentration at time step t} \quad [\text{ng Hg m}^{-3}]$$
$$C_{\text{MeHg}}(0) = \text{MeHg concentration at time step 0} \quad [\text{ng Hg m}^{-3}]$$

This way, most processes can be described as a pseudo-first order reaction. However, there is a limitation to this approach. Many biogeochemical reactions are dependent on the concentration of the reactants themselves; in this case, the process would need to be implemented as a higher order reaction. In the case of photodemethylation, the MeHg concentration at a given time depends on its prior concentration and its loss rate (Black et al. 2012). This results in first-order exponential decay. If we estimate the change in MeHg concentration during peak daylight by applying an exponential decay over a 1-hour interval, we may underestimate or overestimate the actual concentration due to variability in PAR during that hour. Similarly, growth processes, such as phytoplankton growth, can show exponential increases during periods of optimal conditions (Geider et al. 1998). Assuming a constant rate over an hour in such cases could lead to model-breaking overestimation of biomass. This can be mitigated by reducing the time length, but while reducing the time step size improves accuracy, it increases computational cost (Singh et al. 2022). Because of this, the Ordinary Differential Equations (ODEs) are solved numerically, using solvers that account for time-dependent rates and nonlinear feedbacks. This allows the time step to remain larger while preserving model stability.

Ordinary Differential Equation solver

As discussed, one of the main issues in analytically solving the ODE is exponential growth; as such, the easiest method to circumvent this is the forward Euler ODE solver, which was presented by Leonhard Euler and dates back to 1768 (Euler 1768). To approximate the MeHg concentration as a result of photo demethylation using the Forward Euler approximation, the rate of change of MeHg at time step n first needs to be calculated. This can be done by solving equation 1.2 with the value for PAR at timestep n:

$$f(C^n_{MeHg}, t^n) = \left.\frac{dC_{MeHg}}{dt}\right|_{t=t^n} \tag{1.4}$$

where,

$$n = \text{indexed time step} \quad [-]$$
$$f(C^n_{MeHg}, t^n) = \text{Is the change in MeHg at time step } n \text{ [ng Hg m}^{-3}\text{ s}^{-1}]$$

This approximates the solution to the ODE as follows:

$$C^{n+1}_{MeHg} = C^{n}_{MeHg} + Dt \cdot f(C^{n}_{MeHg}, t^{n}) \tag{1.5}$$

Rather than assuming that the exponential behavior persists throughout the full time step, the forward Euler method takes the tangent (the rate of change) at the beginning of the time step and assumes it remains constant over the time step. This linear approximation can introduce errors, but it is computationally efficient and significantly increases the stability of the model compared to assuming exponential growth by analytically solving the ODE.
Other ODE solvers offer improved accuracy and stability over the forward Euler method. One commonly used alternative in modern numerical modeling is the fourth-order Runge–Kutta method. This was developed in 1901 by Carl Runge and Martin Kutta (Kutta 1901).

$$\begin{aligned}
k_1 &= Dt \cdot f^n_c(t_n,\ C^n_{MeHg}) \\
k_2 &= Dt \cdot f^n_c\left(t_n + \frac{Dt}{2},\ C^n_{MeHg} + \frac{k_1}{2}\right) \\
k_3 &= Dt \cdot f^n_c\left(t_n + \frac{Dt}{2},\ C^n_{MeHg} + \frac{k_2}{2}\right) \\
k_4 &= Dt \cdot f^n_c(t_n + Dt,\ C^n_{MeHg} + k_3) \\
C_{n+1} &= C_n + \frac{1}{6}(k_1 + 2k_2 + 2k_3 + k_4)
\end{aligned}$$

This method evaluates the rate of change at four points within the time step, then combines them to produce a weighted average estimate. Although the fourth-order Runge–Kutta method is computationally more expensive than the forward Euler method, its higher accuracy and improved stability often allow for larger time steps, making it more efficient in practice for many systems. As a result, it is widely adopted in environmental and biogeochemical models (Schippmann and Burchard 2011).

Using models to link rates to reality
Eulerian models are used in this thesis because they provide a robust framework for simulating the spatial and temporal dynamics of Hg species in the marine environment. A laboratory experiment can estimate K_{pd} but we need to take the environment, in which the rates occur, into account. Modeling allows us to estimate C_{MeHg}, based on K_{pd} in a realistic scenario. In doing so, we can link experimentally obtained reaction rates to MeHg bioaccumulation in biota. The central objective is to identify which biological processes significantly influence the bioaccumulation of MeHg in fish and quantify this. This approach allows us to go beyond correlational studies and estimate how changes in biological activity translate into differences in MeHg exposure at higher trophic levels. Further models allow us to isolate individual processes and perform process studies that are not possible in a laboratory setting.

1.5.6 Recent modeling efforts facilitate bioaccumulation modeling

To make a model that is actually useful, we first need to identify which role the model should fulfill and how it is different from existing models. Models currently have the capabilities to simulate atmospheric transport

The Navier-Stokes equations originated when Claude-Louis Navier and George Gabriel Stokes independently derived the equations to describe the motion of fluids. This approach was revolutionary as it applied Newton's second law of motion ($force = mass * acceleration$) to fluids, which allowed a fluid to be treated as a continuous medium rather than discrete particles. The solving of this equation, does, however, not mean we fully understand turbulence. The Navier-Stokes equation is one of the seven "million-dollar price problems"; if anyone can prove that the Navier-Stokes equation can be solved for all initial conditions, they receive one million USD, a challenge that remains unsolved.

and oceanic deposition in models such as GEOS-Chem (Selin et al. 2008), ECHMERIT (Jung et al. 2009), GEM-MACH-Hg (Dastoor et al. 2015), MITgcm-ECCO2-Hg (Zhu et al. 2023) WRF-Chem (Hedgecock et al. 2024), and the CMAQ (Bullock and Brehme 2002). New advancements in hydrodynamics models such as the ocean compartment of the ICOsahedral Nonhydrostatic weather- and climate model (ICON-O) (Korn 2017), Semi-implicit Cross-scale Hydroscience Integrated System Model (SCHISM) (Zhang et al. 2023a), Generalised Ocean Turbulence Model (GOTM) (Burchard et al. 1999a), Finite-volume Sea ice-Ocean Model (FESOM2.0) (Scholz et al. 2019) enable the estimation of how this deposited Hg is transported. The currently fast-developing field of ecosystem models allows for the estimation of carbon fluxes in ecosystem models such as the ECOsystem MOdel End to End (ECOSMO E2E) (Daewel et al. 2019) and the European Regional Seas Ecosystem Model (ERSEM) (Butenschön et al. 2016). This means that we can now model where Hg is deposited in the oceans, how it is cycled, and what carbon fluxes are there. These recent advancements in other modeling fields mean that bioaccumulation can now be incorporated explicitly in these complex Eulerian models, for example in a 3D Hg cycling and bioaccumulation model in the Mediterranean Sea (Rosati et al. 2022).

1.5.7 The role of modeling in Hg management

There are several compelling reasons for using models in Hg management, each incorporating two fundamental elements that enhance their usefulness. At times, the use of models is not just beneficial but essential. Since we have only one Earth, when estimating the future impact of specific Hg emissions, we face two choices: either we release the estimated quantity of Hg and observe the outcomes or we develop a model to forecast these effects. The first option is limited by the inability to repeat or alter scenarios if they prove detrimental. Consequently, modeling becomes a means to anticipate future outcomes. While nobody can predict the future, least of all modelers, a model can help to guide an educated guess under certain constraints. The second reason is that models are generally cost-effective to design and deploy. Despite the notable computational expenses, employing models to interpolate between measurements typically proves more practical than expanding research fleets. These theoretical benefits allow models to support the Minamata Convention in several practical ways.

Support the evaluation

The first way in which models can be used to support the Minamata Convention on Mercury is to support its evaluation. As mentioned in the segment about the global Hg budget, new anthropogenic emissions are only a small fraction of global Hg fluxes, but the Hg emissions today can remain in the biosphere for millennia. Models can be used to contextualize measurements of environmental Hg concentrations and compare these to emission data reported by countries. Models help evaluate if countries accurately estimate their Hg emissions.

While Moore's Law is a relatively well-known phenomenon, many people don't fully grasp its scale. Computational power is often quantified by how many Floating-Point Operations Per Second (FLOPS) a processor can calculate. If a computer can calculate 1 billion floating-point calculations per second, it has 1 GIGA-FLOP, or GFLOPS. The first supercomputer used by the German Climate Computing Centre (DKRZ), the Cray-2S, had a peak performance of about 1.9 GFLOPS and cost the equivalent of around €46 million in today's money (adjusted for inflation). In contrast, a modern Samsung smart fridge, such as the Samsung Family Hub (3.0 and later), has a built-in processor with a raw performance in the range of 10–15 GFLOPS, nearly an order of magnitude more. While actual performance depends heavily on code optimization and architecture, this highlights a remarkable trend: global climate models from the early 2000s can, in principle, now be run and tested on a modern personal computer. What once required access to a supercomputing facility can today be explored from a desktop, thanks to decades of exponential growth in computing power.

Improve monitoring

Erroneous Hg reporting does not mean malevolent reporting. A complication with Hg emissions is that Hg is released in extremely low quantities, and it might be hard to assess, especially for developing countries. This is especially true for small-scale artisanal gold mining. As this is generally performed illegally, countries would not have reliable data to report regarding their Hg emissions. Models can be used to reconstruct emissions based on measurements. The point of this is not to blame a specific country for its Hg emissions, but efforts to mitigate emissions can only effectively be deployed if there is a good understanding of the origin of these measurements.

Cost benefit analyses

Once it is understood how and where Hg is emitted, it can be estimated why this Hg is emitted and what the cost of preventing this emission would be. The ideal scenario for policymakers is to use the predictive capacity of models to estimate the costs and benefits of policies before they are implemented. When models can accurately predict the outcome of policies, they can be used to ensure an efficient and beneficial policy is implemented with reasonable costs and trade-offs. Although models are never perfect, some models have already been used to this end in Hg management. Examples are the use of atmospheric models by UNEP in evaluating the Minamata Convention (UNEP 2021). The problem with this, in regard to Hg, is that due to the combination of Hg's ability to engage in long-range atmospheric transport, its complex cycling in the marine environment, and its ability to bioaccumulate, it moves through different areas of the biosphere that are typically captured in different models. To this extent, a framework that models and analyzes Hg through different compartments is needed. To this extent, the Multi-Compartment Hg Modeling and Analysis Project was started to assist the Minamata Convention Dastoor et al. (2024).

Multi-Compartment Hg Modeling and Analysis Project (MCHgMAP)

The MCHgMAP is a global initiative designed to enhance our comprehension of worldwide Hg dynamics, to support the Minamata Convention on Mercury. This initiative focuses on developing a system of atmospheric, terrestrial, and oceanic models. By unifying these models under a standardized framework, a comprehensive model can be created, connecting Hg emissions to MeHg concentrations in marine life. This integrated model across various domains enables us to first assess our knowledge of mercury cycling. When the model accurately reproduces historical patterns, it can be used to predict baseline future trends of MeHg levels in seafood, based on existing policy scenarios. With this improved model, policymakers can then use the model to predict the impacts of different policy options and cost-benefit analyses. It is important to acknowledge, however, that as models become increasingly complex, it is critical to ensure they function correctly, as uncertainties in individual models can propagate. Especially in the modeling of bioaccumulation, there are several limitations that can drive uncertainty and reduce the quality of the model.

Of course, when estimating costs, the answer is always "it depends." But it can be informative to do a simple back-of-the-envelope estimation to visualize the scale of investment in modeling versus empirical science. The German Climate Computing Centre (DKRZ) had an annual budget of €15 million in 2024, while the operating cost of the German research icebreaker Polarstern is estimated at €21.4 million per year. This means that a single research icebreaker costs more to operate than the entire German national climate modeling effort. Naturally, this is just an illustration, there would be no good models without empirical data to validate and improve them, and both approaches are essential to advancing climate science.

1.5.8 Limitations of the modeling of marine Hg bioaccumulation

Complexity of measuring marine Hg

The first complication in marine Hg modeling compared to atmospheric Hg modeling is caused by the complexity of Hg measurements in the environment. Although several instruments exist that can continuously measure atmospheric Hg, including speciation, such devices do not exist for marine Hg. Most marine Hg measurements are still made via ship-based research, and older datasets often do not include speciation. Especially, DMHg is rarely measured in historic datasets. Since it is gaseous, it would have been identified by sampling campaigns such as the ones performed in (Kuss et al. 2015; Fitzgerald et al. 2007) as DGM. Although this is technically correct, there is a considerable difference between the way DMHg and Hg^0 speciate and the potential risk they pose to food safety. This is because DMHg can be photo-demethylated under conditions found in the euphotic zone to the bioaccumulative $MMHg^+$. In Germany specifically, an additional complication is that Hg pollution used to be much higher. Because of this, measurement campaigns focus on measuring if Hg is within a detection limit that is much higher than the current expected values. Although Hg values are often below the detection limit in seawater or sediment, MeHg concentrations in seafood are often still above acceptable limits. The inability to reliably understand how Hg is transported and speciated in the marine environment complicates the modeling of the source-receptor relationship between Hg emissions and MeHg in seafood.

Measuring and modeling different Hg species

As mentioned earlier, while only MeHg is assumed to biomagnify to very high levels in the marine food chain, iHg has a similar bioconcentration rate at the base of the food web. When measurements only report tHg, the ratio of tHg to MeHg adds additional uncertainty to the validation process. Although at the top of the food web, MeHg is likely the majority of all tHg, this might not be the case at the base of the food web. This makes estimating important drivers, such as the biomagnification factor, harder, as reliable measurements of different Hg species at the base of the food web are rare.

Uncertainty propagation

The second complication comes from the propagation of uncertainty. Modeling MeHg levels in high-trophic-level animals is the tip of the modeling iceberg. The bioaccumulation of MeHg is dependent on several drivers that are understood to varying degrees. This complication is related to the modest amount of data available that can be used to evaluate the model at different stages. The MeHg, and especially MeHg, content of high-trophic-level fish is relatively well known because it is so high that we can measure it. However, to use predictive models, we must understand every step leading up to these high concentrations. Any uncertainty in Hg emissions, Hg transport to the marine system, hydrodynamics, Hg speciation, bioconcentration, ecosystem dynamics, and biomagnification leads to uncertainty in MeHg levels in high-trophic-level animals. If one driver is underestimated, another driver might be overestimated when evaluating which parameterization leads to realistic Hg values, leading to a reduced ability to predict the bioaccumulation of MeHg under varying circumstances.

1.6 Previous Hg bioaccumulation models

A variety of models have been developed to study MeHg bioaccumulation, ranging from simple frameworks based on single studies to sophisticated 3D models capable of simulating detailed processes across space and time. In this section, I review some of the most influential models and their contributions to our understanding of MeHg bioaccumulation, before describing how this thesis expands upon them.

Using 0D models towards a basic understanding of Hg bioaccumulation

To gain an initial understanding of bioaccumulation based on measurements, several zero-dimensional (0D) models were developed. These models estimate bioaccumulation using constrained drivers and are

essential for understanding the reaction rates applied in coupled models.

Trophic transfer model of iHg and MeHg by Mason et al. (1995)
Mason et al. (1995) carried out experiments analyzing the bioaccumulation of iHg and MeHg in diatoms. They discovered that the assimilation efficiency for iHg and MeHg of 15% and 62%, respectively, strongly overlaps with the distribution of Hg in the cytoplasm of 9% for iHg and 63% for MeHg. They presented their "eat-the-grapes-and-spit-the-skins" model for the difference in the assimilation efficiency of iHg and MeHg, in which they explain that the assimilation efficiency of different Hg species is related to the fraction that associates with the cytoplasm rather than with the cell membrane. They proposed that since the protein-rich cytoplasm is digested more efficiently upon consumption, MeHg, which is strongly associated with this cytoplasm, is transferred more efficiently upon consumption.
This model was instrumental in its initial understanding of Hg bioaccumulation, especially by providing a framework that explained the high bioaccumulation potential of MeHg and the lower bioaccumulation potential of iHg. This model led to the development of later models looking at the bioaccumulation of MeHg in higher trophic levels.

A kinetic bioaccumulation of Hg and MeHg in water flies (Daphnea pulex) by Tsui and Wang (2004)
The study by Tsui and Wang (2004) expands on the work of Mason et al. (1995) by investigating the differences between the bioaccumulation of iHg and MeHg in invertebrates, in this case, the water flea. They demonstrate that, unlike in phytoplankton, the efflux rate constant of iHg and MeHg in zooplankton are comparable. While they confirm the observations by Mason et al. (1995) that MeHg has a much higher assimilation efficiency than iHg, which drives the high MeHg bioaccumulation in zooplankton.
By combining these models, a clearer picture emerged of the key factors driving bioaccumulation in zooplankton. Phytoplankton exhibits a very high BCF for MeHg, while the BCF for inorganic iHg is lower, primarily due to the low efflux rate of MeHg from phytoplankton. This elevated MeHg concentration is then transferred to zooplankton, due to the high assimilation efficiency of MeHg. From there, MeHg can be transferred further up the food chain to fish and ultimately to humans.
While 0D kinetic models are valuable for revealing theoretical mechanisms, they lack representation of environmental complexity and therefore are limited in their predictive capacity for real-world systems.

Including environmental drivers to estimate bioaccumulation in nature

Building upon basic models, researchers introduced environmental factors to more realistically estimate bioaccumulation in natural systems. These models used measured environmental Hg concentrations or dynamic drivers such as temperature to improve predictions.

A trace metal bioaccumulation model that includes Hg in the Mediterranean mussel (Mytilus galloprovincialis) by Casas and Bacher (2006)
Casas and Bacher (2006) combines a bioaccumulation model and a dynamic energy budget model for the Mediterranean mussel. This allows them to investigate the kinetics of the uptake and elimination rates of Hg and lead. The model quantified the contributions of physiological variables such as body and tissue composition to the bioaccumulation of Hg.

Non-spatial MeHg bioaccumulation model linking the concentration of marine MeHg and the consumption of seafood with MeHg in humans by Gizem Bacaksızlar and Önsel (2013)
The study by Gizem Bacaksızlar and Önsel (2013) was published in a conference proceeding of the International Conference on System Dynamics, but I could not find a peer-reviewed version of the study. They used a non-partially resolved dynamic simulation model to link MeHg concentration in seawater and fish consumption to MeHg exposure in humans. They concluded that an increase in aquatic MeHg directly increases MeHg concentrations at all levels of the trophic scale, including humans, and that increased fish consumption increases the MeHg burden on humans.

A source receptor relationship of the drivers of MeHg bioaccumulation using STORM by Kim et al. (2008)

A study of the controlling factors of MeHg bioaccumulation was carried out in Kim et al. (2008). In this study, a model investigating the drivers of bioaccumulation of MeHg was designed using high-bottom Shear realistic water column Turbulence Resuspension Mesocosms (STORM). Their results showed that the introduction of hard clams (*Mercenaria mercenaria*) resulted in higher phytoplankton and zooplankton biomass and MeHg bioaccumulation. They also showed that sediment resuspension plays a critical role in the transfer of MeHg from the sediment to the pelagic and benthic biota.

Non-spatial MeHg bioaccumulation by Schartup et al. (2018)
Schartup et al. (2018) models the bioaccumulation of MeHg at the base of the food web. This model is not spatially resolved, but rather relies on field measurements of several important drivers, such as DOC, nutrients, and MeHg concentration, to feed model data so that they could evaluate the output. This study provides valuable information on the drivers of MeHg bioaccumulation by, among other things, the trade-off between growth dilution and high consumption in Hg-containing foods. The results of this study highlight that growth dilution in the marine environment does not always reduce MeHg in zooplankton, as increased food consumption offsets this. In addition, they investigated the role of bioconcentration in consumers at low trophic levels and concluded that this contributes to 10-20% of MeHg bioaccumulation.

These models advanced our understanding by identifying environmental factors that modulate bioaccumulation, though they remained limited by their reliance on measured field data and lack of full ecosystem integration.

Coupling 3D models to evaluate source receptor relationships

To address the limitations of simpler models, researchers began to develop spatially explicit coupled 3D models. These models are capable of simulating MeHg dynamics under more realistic environmental conditions and can therefore be used to analyse complex interactions using in silico experiments.

Global phytoplankton uptake model by Zhang et al. (2020)
In Zhang et al. (2020), a global model is used to model MeHg bioaccumulation at the base of the food web. This study models MeHg formation and bioaccumulation of $MMHg^{+}$ at the second level on a global scale. This allows it to be used to analyze the global pattern of MeHg bioaccumulation. Although it has two different groups of zooplankton, they feed on different groups of phytoplankton and not on each other. So, there is no modeled trophic cascade after the second trophic level.

Kinetic toxicology bioaccumulation model by Li et al. (2022)
Li et al. (2022) incorporates the bioaccumulation of MeHg in the Beaufort Sea shelf food web using the Ecotracer module of Ecopath with Ecosim. This comprehensive module incorporates both passive uptake of MeHg by low trophic level consumers and the demethylation of MeHg in high marine mammals. They show that a complex food web with a relatively simple parameterization of MeHg bioaccumulation can accurately predict the bioaccumulation of MeHg in benthos. Furthermore, they demonstrate that uptake in macrobenthos is the main driver of MeHg variability in high-trophic-level fish. Finally, they show that there are no experimentally obtained *in vivo* demethylation rates for MeHg available in marine mammals, but that the MeHg concentration would be highly sensitive to *in vivo* demethylation.

Coupled 3D Mediterranean uptake by Rosati et al. (2022)
A second recent modeling effort focused on modeling MeHg bioaccumulation in the Mediterranean Sea by Rosati et al. (2022). They used a fully coupled 3D model for bioaccumulation in the marine food web of the Mediterranean Sea. They used their model to investigate the bioaccumulation drivers and used this to identify regions at increased risk of high MeHg bioaccumulation.

Bridging this gap is essential for improving our understanding of Hg as a pollutant and refining the source-receptor framework linking emissions to seafood safety. With this understanding of the current state of the art, we can identify what is needed to improve future models.

1.6.1 The current knowledge gap

As described above, the causal link between Hg emissions and MeHg toxicity in seafood is identified. Human activities emit Hg, which is transported to the oceans through rivers and the atmosphere, where it can be methylated to MeHg and bioaccumulate. The details of this process are, however, much less understood, and despite substantial progress in understanding the chemistry, toxicity, and global distribution of Hg, major gaps remain in our ability to link marine Hg concentration to the concentration of MeHg in seafood. This is partially because of a limited ability to model the bioaccumulation. Existing models often consider the ecosystem as an optional addition to the model, rather than an integrated part of the marine systems. In addition to this, the ecosystem complexity is underestimated due to real-world limitations in models, such as competitive power and limited observations to evaluate the models. Addressing this knowledge gap is an essential step towards a better understanding of Hg as a pollutant and the source-receptor relationship between Hg emissions and seafood safety.

1.7 The research goals of this thesis

The central aim of this thesis is to quantify the biological drivers of Hg bioaccumulation in marine food webs. This includes both biological drivers of iHg and MeHg cycling. While MeHg poses the largest threat to human health, iHg is an essential component of the marine Hg cycling, and the bioaccumulation of MeHg can only be understood as a component of a large complex biogeochemical cycle, rather than a stand-alone interaction.
Because marine bioaccumulation modeling is still relatively underdeveloped compared to other forms of pollution modeling, such as the atmospheric Hg cycling, bioaccumulation is potentially a weak spot in Hg pollution modeling initiatives such as the MCHgMAP. In more developed modeling fields, extensive knowledge is available, not only for what works in models but also what interactions are insignificant. For bioaccumulation, this is not sufficiently explored. Therefore, I focus my thesis on contributing to the main research question:

"What are the key biological drivers of MeHg bioaccumulation in the marine food web?"

Completely resolving the role of the ecosystem is beyond the scope of a single PhD project. But here I try to support our understanding of this main research question by answering the 5 following sub-research questions. These questions are all focused on identifying biological drivers of MeHg bioaccumulation that should be incorporated in global models.

1. How can the bioaccumulation of inorganic mercury (iHg) and methylmercury (MeHg) be parameterized in a biogeochemical model?
2. How does ecosystem structure and function influence mercury cycling in marine environments?
3. What are the dominant drivers of MeHg bioaccumulation in high-trophic-level fish?
4. How does the feeding strategy of low-trophic-level biota affect the bioaccumulation of iHg and MeHg?
5. What explains the low MeHg concentrations observed in high microbial abundance (HMA) sponges, and how does this influence MeHg exposure in higher trophic levels?

In modeling work, previous questions often build upon the previous answers as the model is expanded, evaluated, and improved. The different research questions and how they support each other to address the main research question are shown in Fig. 1.5.

Chapter 2; Incorporating bioaccumulation into the Mercy v2.0 model

First, I needed to design, implement, and validate the model. This led to the first sub-research question:

"How can the bioaccumulation of iHg and MeHg be parameterized in a biogeochemical model?"

The first step in bridging the knowledge gap is incorporating bioaccumulation in an up-to-date, fully coupled model. This is explained in detail in Chapter 2. I contributed to the development of the 3D Mercy v2.0 model that links atmospheric Hg concentrations to the bioaccumulation of MeHg in fish by designing the bioaccumulation module of this model, thus linking marine Hg cycling to the bioaccumulation of MeHg in fish. This, of course, is not as much a scientific hypothesis as a model technical question. Nonetheless, it is important to critically evaluate if the implementation is correct and if the model provides results that are in line with observations. Only if this question is answered can we focus on more fundamental research questions.

Chapter 3; Bioaccumulation as a driver of high MeHg in coastal seas

Afterwards, I used the MERCY v2.0 model to evaluate three sub-research questions. For the first question, I wanted to know if bioaccumulation is only of concern because it leads to high concentrations of MeHg in seafood, or if it also has a significant effect on marine Hg cycling.

> *"How does ecosystem structure and function influence mercury cycling in marine environments?"*

In chapter 3, I used both the 3D MERCY v2.0 ECOSMO Hamson setup, and I present a new 1D MERCY v2.0 GOTM setup to evaluate the role of ecosystem drivers on Hg cycling. I use this model to quantify the feedback between the ecosystem and the Hg cycle in the North and Baltic Seas. Here we will investigate how ecosystem interactions, notably bioaccumulation, biogenic reduction, and partitioning of iHg and MeHg into detritus and DOM originating from the ECOSMO E2E model, affect marine Hg speciation and the Hg budget of the North and Baltic Seas. This is one of the key research questions of my thesis. If the ecosystem proves to be insignificant in Hg cycling, global Hg cycling models do not necessarily require a coupled ecosystem component, and bioaccumulation can be estimated either using reanalyses data or potentially a proxy based on basic assumptions of the animals of interest, such as the trophic levels and marine MeHg concentrations. If, on the other hand, the ecosystem proves to be an integral part of the global Hg cycle, models must have a coupled ecosystem component, as it will not be possible to reliably replicate the observed marine MeHg concentration without one of its key drivers.

Chapter 4; Bioconcentration in consumers: a key driver of MeHg in fish

The 1D MERCY v2.0 model is also used to investigate drivers of MeHg bioaccumulation in high-trophic-level fish. In Chapter 4 I evaluate the 3rd sub-research questions:

> *"What are the dominant drivers of MeHg bioaccumulation in high-trophic-level fish?"*

Here, I evaluate how the inclusion of the bioconcentration of MeHg and the bioaccumulation of iHg affects the bioaccumulation of MeHg in fish. The 1D model used in this study is computationally relatively cheap to run with extra state variables. Because of that, we can use this 1D setup to include several potential drivers of MeHg bioaccumulation before running the model again while excluding these drivers. This enables me to examine which bioaccumulation interactions should be included in models and which can be excluded to enhance model efficiency. Although this improvement is not essential for the 1D setups employed in this study, it becomes crucial when executing global 3D Hg bioaccumulation models. Consequently, I contribute to future developments by determining which variables should be incorporated or omitted in these more complex models.

Chapter 5; Feeding strategies and their role in Hg bioaccumulation

In Chapter 5, I further update the 1D MERCY v2.0 GOTM setup. Here, I replace the high trophic levels of the original ECOSMO E2E model by including 6 megabenthos functional groups. I only changed their feeding strategy and left all other rates equal. This allows me to isolate the effect of the feeding strategy, and I can use this model to investigate which feeding strategies can result in especially high or low values of the iHg and MeHg values. Which allows me to answer the following sub-research question:

"How does the feeding strategy of low-trophic-level biota affect the bioaccumulation of iHg and MeHg?"

This is important to understand, since the bioaccumulation into low trophic level animals determines the concentration of MeHg in the food of high trophic level animals, and can therefore influence the MeHg bioaccumulation in high trophic level fish. A key reason why this is an important research question is that it addresses a second important question: Should the bioaccumulation model incorporate multiple animals that occupy similar trophic levels, or is it adequate to simulate general ecosystem dynamics? If the feeding strategy significantly influences MeHg bioaccumulation, it clearly suggests that the modeled ecosystem's complexity should reflect differences among organisms beyond mere trophic interactions.

Chapter 6; DOM uptake and Demethylation in HMA Sponges: Drivers of Low MeHg in Benthic Food Webs

The final sub-research question is evaluated in Chapter 6. This is a case study where I bring the lessons learned from the previous chapters together to analyze a real-world ecosystem. Here, I investigate the potential *in vivo* demethylation rate in sponges by modeling sponges in the Mediterranean Sea in the well-studied bay of Villefranche. By comparing bioaccumulation in the modeled sponges with field observations, I can estimate the likely demethylation rates of MeHg in these sponges. Finally, I used this model to analyze how the different amounts of sponge biomass will influence the MeHg content of higher trophic levels. I do this by updating the model presented in Chapter 5 by giving the 6 megabenthos functional groups realistic feeding, mortality, and respiration rates. Then I include a 7th megabenthos functional group, the high Microbial Assemblage Sponge. This allows me to answer the final sub-research question:

"What explains the low MeHg concentrations observed in high microbial abundance (HMA) sponges, and how does this influence MeHg exposure in higher trophic levels?"

By answering this final research question, I can contextualise my findings, and transform my results from a model technical outcome to a prediction of how certain ecosystem dynamics that are influenced by anthropogenic factors can influence Hg bioaccumulation. The answers to this research question go beyond recommendations for modelers, but can be used to answer an important question concerning policy making: do vulnerable ecosystems, such as sponge grounds, influence Hg cycling, and does their preservation or destruction influence the MeHg loading on commercial fish?

Discussion & future work

After addressing each chapter and resolving the sub-research questions, all elements will converge in Chapter 7. Here, I have summarized all the answers to the sub-research questions and evaluated how this thesis contributes to the main research question. These findings are integrated in Chapter 8. In this section, I discussed what I think are the main constraints of the model. The discussion serves as a basis for identifying key areas for further work. This is expanded upon in Chapter 9, wherein I will review the crucial research questions that remain unaddressed and outline what should be prioritized in forthcoming Hg research, both for modeling, laboratories, and field studies.

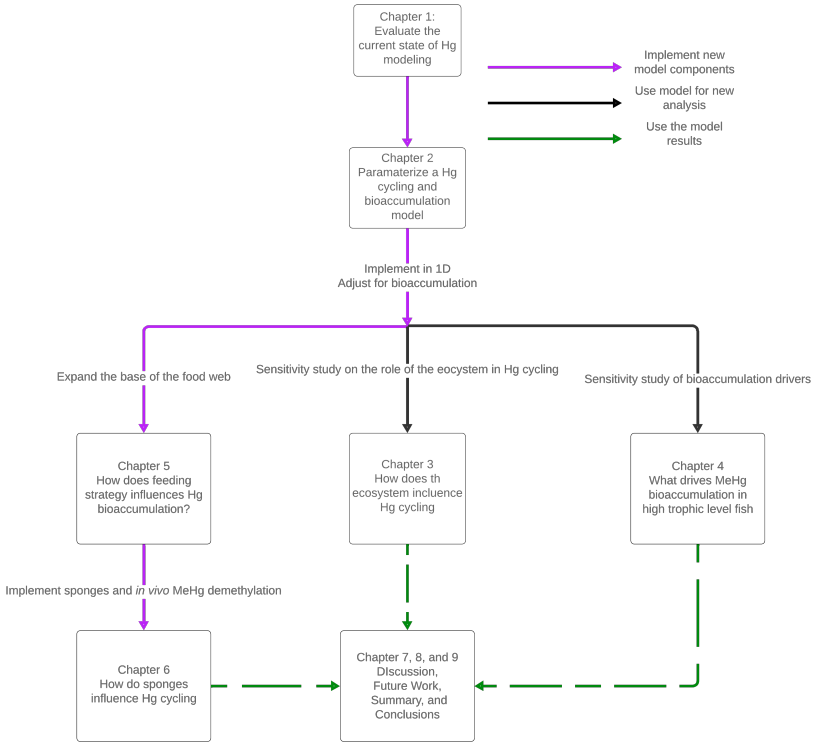

Figure 1.5: The basic thesis outline. The MERCY v2.0 design is discussed in Chapter 2. This model is used and extended upon in Chapter 3 to estimate the role of the ecosystem in Hg cycling. The 1D version of the model is used in Chapter 4 to identify drivers of MeHg bioaccumulation in high trophic level fish, and expanded upon in Chapter 5 to include more megabenthic functional groups and identify the role of feeding strategies at the base of the foodweb. Finally, the expanded megabenthic model used in Chapter 5 is expanded upon further by estimating realistic carbon fluxes and including both LMA and HMA sponges in Chapter 6, so that we can estimate the role of *in vivo* MeHg demethylation.

Figure 1.6: Sea vase (*Ciona intestinalis*), a tunicate. Picture taken by Dr. Eric Wurtz.

CHAPTER 2

Incorporating bioaccumulation into the MERCY v2.0 model

Publication Status

This chapter is based on the following publication:

Bieser, J., Amptmeijer, D., Daewel, U., Kuss, J., Soerensen, A. L., & Schrum, C. (2022). *The 3D biogeochemical marine mercury cycling model MERCY v2.0 – Linking atmospheric Hg to methyl mercury in fish*. *Geoscientific Model Development Discussions*, **2022**, 1–59. https://doi.org/10.5194/gmd-2022-35

2.1 Introduction

My first contribution to reducing the knowledge gap in MeHg bioaccumulation is through my work on the MERCY v2.0 Hg speciation model Bieser et al. 2023. This model is the first coupled model that links atmospheric and riverine Hg input into the marine system to MeHg concentrations in fish, as is shown in Fig. 2.1. My supervisor, Dr. Johannes Bieser, developed most of this model; I contributed by designing the bioaccumulation routine, assisting in the validation of the bioaccumulation, and authored a chapter in the manuscript dedicated to this. So, Dr. Bieser modeled the link between atmospheric Hg and marine MeHg; I expanded the model by linking the marine MeHg to MeHg in fish.

The MERCY v2.0 model is driven by the ECOSMO-HAMSOM coupled system (Daewel et al. 2019). The ECOSMO E2E model simulates carbon fluxes and the ecosystem in the North and Baltic Seas. It simulates 3 groups of phytoplankton, 2 groups of zooplankton, 1 group of fish, and macrobenthos. The ECOSMO E2E model is coupled to the 3D HAMSOM (Hamburg Shelf Ocean Model) which simulates the hydrodynamics of the North and Baltic Seas. ECOSMO is fully coupled to HAMSOM, creating the ECOSMO-HAMSOM coupled system, which allows feedback between the ecosystem and the physical system. This is important, in, for example, correctly estimating light, as biota influence light absorption. Hg cycling, however, is not expected to have significant feedback with either the physical or biogeochemical system. Because of this, hourly output data from the ECOSMO-HAMSOM modeled system is used to drive the MERCY v2.0 model. This makes the ECOSMO-HAMSOM-MERCY effectively an offline coupled system. This setup enables us to estimate Hg cycling on a temporal and spatial scale while accounting for physical and biogeophysical drivers.

This chapter summarizes my contributions to this model. Additional analyses and visualizations of mechanisms and results were primarily conducted by Dr. Johannes Bieser. A detailed breakdown of the contributions per author is presented in the published manuscript and displayed in table 2.1. For a detailed examination of the linking of atmospheric Hg concentration to MeHg concentration in fish, please refer to the original manuscript.

2.2 Methods

2.2.1 Bioaccumulation in the MERCY v2.0 model

To create a comprehensive understanding of the bioaccumulation of Hg, and evaluate its feedback on Hg speciation, I incorporate both the bioconcentration and biomagnification of both Hg^{2+} and $MMHg^{+}$ at every trophic level. A schematic overview of the difference between bioconcentration and biomagnification is shown in Fig. 2.2a. A schematic overview of the bioaccumulation in the full model is shown in Fig. 2.2b.

2.2.2 Bioaccumulation of Hg^{2+}

The bioaccumulation of Hg^{2+} was also included in this model. This is often omitted as the bioaccumulation of Hg^{2+} does not have the same health concerns as the bioaccumulation of $MMHg^{+}$. While Hg^{2+} does not bioaccumulate to the extremely high levels in fish, it can be a major component of the total bioaccumulated Hg in lower trophic levels (Nfon et al. 2009). The inclusion of the bioaccumulation of Hg^{2} allows us to see to which degree the uptake of Hg^{2+} influences Hg cycling.

2.2.3 Species dependent bioconcentration in phytoplankton

Bioconcentration at the base of the food web is the most important step in bioaccumulation. The uptake into phytoplankton is controlled by the cell size (Mason et al. 1996). I estimated the most typical phytoplankton species in the North and Baltic Seas and estimated their cell-surface-to-biomass ratio based on the size and shape of the phytoplankton. I chose the *T. Baltica* for diatoms, *E. Haxleyi* for flagellates and *A. flos-aqua* for cyanobacteria. It must be noted that most flagellates and diatoms had roughly similar sizes, but for cyanobacteria, the size estimation for different species could be very variable. Which would influence the derived uptake and release rates. Based on Olenina et al. 2003, I estimated the size and shape as a cylinder with a radius of 12 and a height of 25 μm for diatoms, a hemisphere with a radius of 6 and a sphere with a radius of 4 μm respectively for flagellates and cyanobacteria. This was then converted to a surface-to-biomass ratio of 49.38, 50.42, and 86.04 cm^3 mg C^{-1} for diatoms, flagellates, and cyanobacteria respectively based on (Menden-Deuer et al. 2000).

2.2.4 Bioconcentration in higher trophic levels

We also included the bioconcentration of both Hg^{2+} and $MMHg^{+}$ in higher trophic levels. This interaction is often omitted as it only accounts for 10-20% of the total bioaccumulated MeHg (Schartup et al. 2018). This is included because there are no fully coupled models that model the total effect of bioconcentration in higher trophic levels, and this allows us to quantify the importance of this driver.

2.3 Results

2.3.1 Bioaccumulation of tHg

Since the ECOSMO E2E model is a Redfield ratio-based model, we needed to convert the bioaccumulation of Hg from being normalized per carbon to biomass in dry weight. For this, we assumed a ratio of 0.2 for diatoms, 0.33 for flagellates and cyanobacteria, and 0.5 for zooplankton and fish (Sicko-Goad et al. 1984; Walve and Larsson 1999). This dry weight is then converted to wet weight, assuming a ratio of 0.2 for phytoplankton, 0.16 for zooplankton, and 0.2 for fish Cushing 1958; Ricciardi and Bourget 1998. tHg concentrations in plankton are observed to be 0.002 ± 0.001 for phytoplankton and 0.006 ± 0.005 for zooplankton in the Baltic Sea. The yearly average modeled rates are shown in Fig. 2.3. While there is not enough data to validate the bioaccumulation on a spatial or temporal scale, the modeled values for both tHg are well within the range of observations for both Hg and MeHg.

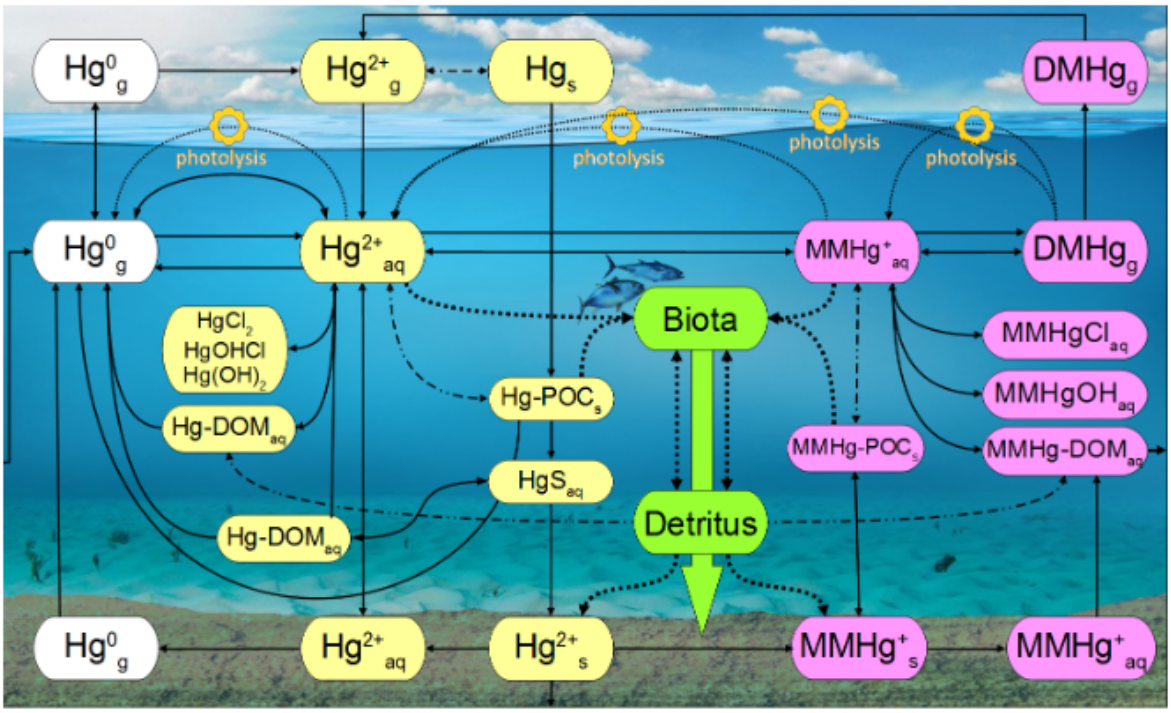

Figure 2.1: Schematic overview of Hg speciation as incorporated in the MERCY v2.0 Hg speciation model. This graph is from Bieser et al. 2023. More details on the biogeochemical mechanism are described in this paper.

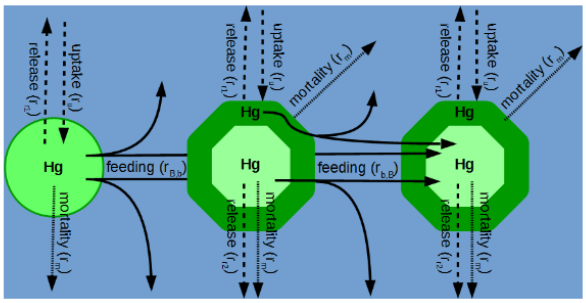

(a) Schematic representation of the bioaccumulation mechanism implemented and the distinctions between Hg uptake from the water column (bioconcentration) and Hg bioaccumulation via trophic interactions (biomagnification).

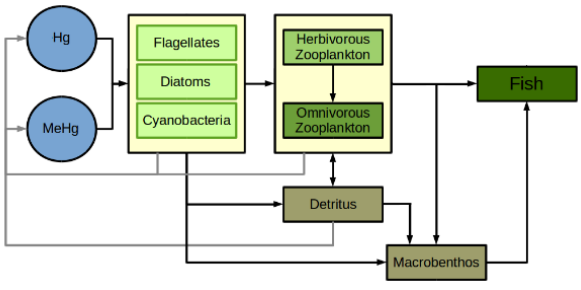

(b) Flowchart of the MERCY v2.0 model. This shows how Hg and MeHg are bioconcentrated on all trophic levels and how they can be further biomagnified via trophic interactions.

Figure 2.2: Side-by-side overview of the Hg cycling and flowchart of the MERCY v2.0 model. Both graphs are from Bieser et al. 2023.

2.3.2 Bioaccumulation of MeHg in fish

The bioaccumulation of MeHg in fish was also validated. This was mostly done by Dr. Anne Soerenson, but since this is based on the rates that I provided, I will show the results to visualize the model's performance. The fish in the model were parameterized to resemble herring (*Clupea harengus*) and compared to observed MeHg concentrations in herring in the North and Baltic Seas. The model reproduces the observed average concentrations in herring (28 ng Hg g^{-1}) with a -9% systematic error (25 ng Hg g^{-1}). While observations of bioaccumulation in captured fish cannot be linked to individual grid cells, there is a lot more data on MeHg concentrations in fish than for dissolved MeHg and MeHg bioaccumulation in plankton. To utilize this, the model is separated into 5 regions, and the observed MeHg concentrations in herring in these regions are compared to modeled vertically integrated yearly average values of MeHg concentration in fish in the same region. The regions are:

- The Swedish coast
- The southern Baltic Proper
- The northern Baltic Proper
- The Bothnian Sea
- The Bothnian Bay

The results of this are shown in Fig. 2.4. The model is evaluated by evaluating the Normalised Mean Standard Deviation (NMSD) per region. Over the whole Baltic Sea, the model captures the observed variability (NMSD=9%). The only notable mismatch between the model and observations is the Swedish West Coast. Here the average modeled fish MeHg concentration is less than half the observed concentration. This is likely caused by the regular resuspension of Hg from the sediment, which could create locallised clusters of high tHg and MeHg concentrations. Fish in the ECOSMO E2E model are static and don't migrate, which might result in such an interaction not being properly captured in the model. However, because overall the modeled and measured concentrations in the Baltic Sea overlap well with a normalized bias of 3%, we conclude that the models accurately capture the bioaccumulation of MeHg, while certain specific regional drivers could be improved upon.

2.4 Summary and conclusion

In this paper, we linked atmospheric Hg concentration to MeHg concentration in fish. We demonstrate good agreement between the model and observations at every trophic level. While certain regional differences in the bioaccumulation of MeHg in fish are not fully captured in the model, the overall performance of the model in the Baltic Sea is good, with a normalized bias of 3% and a normalized mean standard deviation of 9%. Because of this, we conclude that the MERCY v2.0 model successfully couples atmospheric Hg concentrations to MeHg concentrations in fish.
I contributed to this study by parameterizing the bioaccumulation, validating the bioaccumulation in the phyto- and zooplankton, and helping with the validation of bioaccumulation in fish by estimating the conversion ratios of carbon to wet weight, which was needed to validate the data. The table with author contributions for the publications is shown in 2.1.

Contributor role	Role definition	Authors
Conceptualization	Ideas and formulation or evolution of overarching research goals and aims	
	– for the mercury model	JB
	– for the bioaccumulation model	DA, UD, JB
Methodology	Development or design of methodology and creation of models	
	– Hg chemical mechanism	JB, JK, ALS
	– Hg and MeHg bioaccumulation	DA, JB
Software	Programming and software development, designing computer programs, implementation of the computer code and supporting algorithms, and testing of existing code components	
	– for HAMSOM and ECOSMO	UD
	– for MERCY	JB
Validation	Verification, whether as a part of the activity or separate, of the overall replication/reproducibility of results/experiments and other research outputs	JB
Formal analysis	Application of statistical, mathematical, computational, or other formal techniques to analyze or synthesize study data	
	– for HgT and MeHg concentrations	JB
	– for Hg0 concentrations and air–sea exchange	JB, JK
	– for Hg and MeHg bioaccumulation at lower and higher trophic levels	DA, ALS
Investigation	Conducting a research and investigation process, specifically performing the experiments, or data/evidence collection	JB, JK, ALS
Resources	– Provision of study materials, reagents, materials, patients, laboratory samples, animals, instrumentation, computing resources, or other analysis tools	CS
	– Hg and MeHg observational data	JK, ALS
Data curation	Management activities to annotate (produce metadata), scrub data, and maintain research data (including software code, where it is necessary for interpreting the data themselves) for initial use and later reuse	ALS, JK, UD
Writing – original draft	Creation and/or presentation of the published work, specifically writing the initial draft (including substantive translation)	JB, ALS, DA
Writing – review and editing	Preparation, creation, and/or presentation of the published work by those from the original research group, specifically critical review, commentary, or revision – including pre- and post-publication stages	ALS, CS, DA, JK
Visualization	Preparation, creation, and/or presentation of the published work, specifically visualization/data presentation	JB
Supervision	Oversight and leadership responsibility for the research activity planning and execution, including mentorship external to the core team	JB, CS
Project administration	Management and coordination responsibility for the research activity planning and execution	JB, CS
Funding acquisition	Acquisition of the financial support for the project leading to this publication	CS, JB

Table 2.1: Author contributions for the published MERCY v2.0 model by Johannes Bieser (JB), Anne L. Soerensen (ALS), David Amptmeijer (DA), Joachim Kuss (JK), and Corinna Schrum (CS).

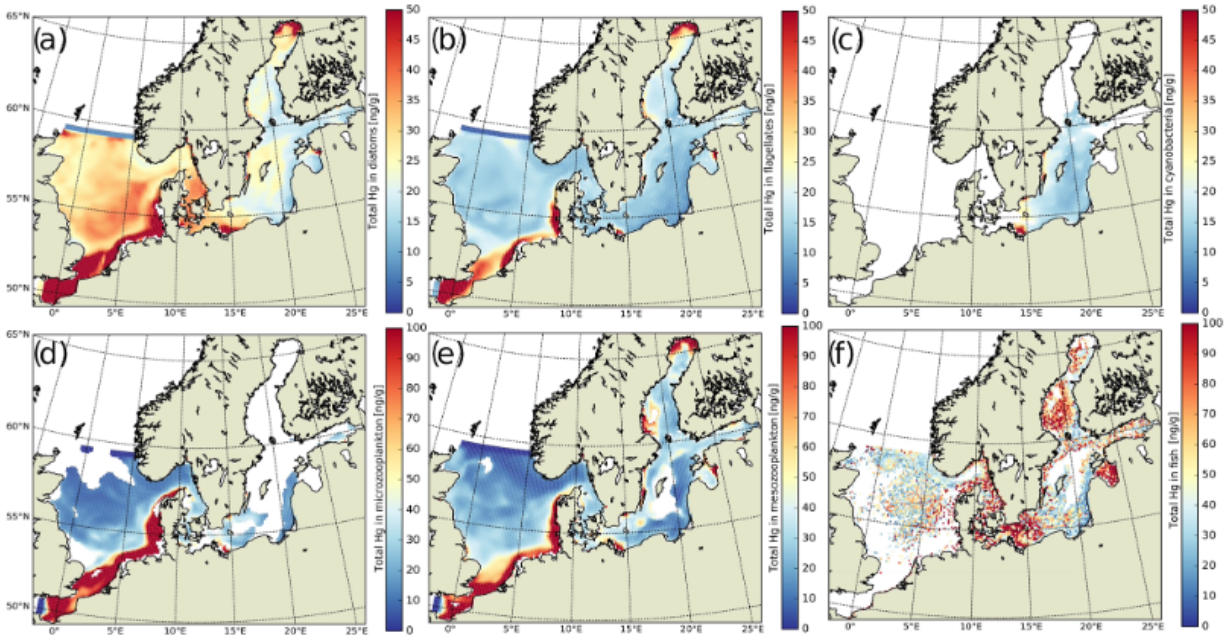

Figure 2.3: The tHg in biota as modeled by the MERCY v2.0 model. The concentrations are in ng Hg g^{-1}. The figures show the concentrations in Fig. a: diatoms, b: flagellates, c:cyanobacteria, d:microzooplankton, e:mesozooplankton, f:fish.

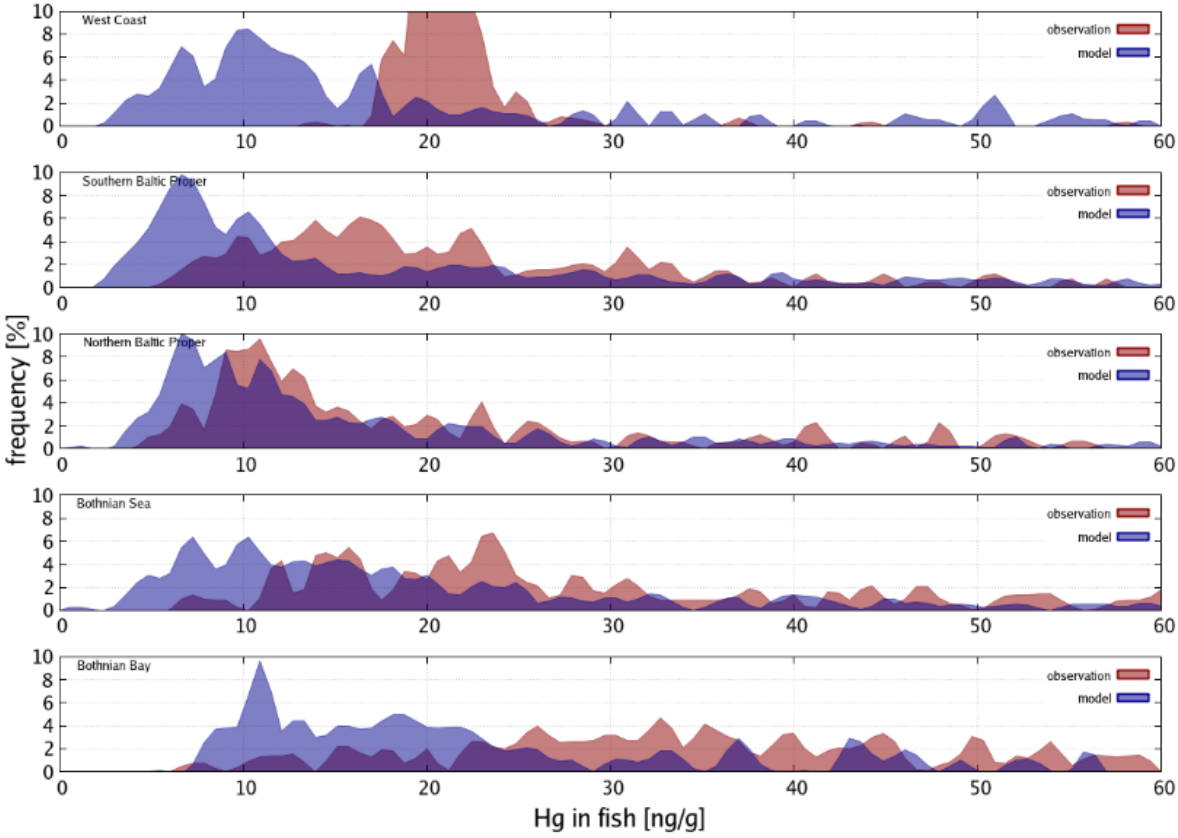

Figure 2.4: The relationship between MeHg concentration in the MERCY v2.0 model and the observed concentrations in fish. The graph is from Bieser et al. 2023.

Bridging chapter

As described in Chapter 2, the model I used in this thesis is unique in several aspects. Notably, it is the first fully coupled and models both the bioaccumulation of Hg^{2+} and $MMHg^{+}$. This means that it can be used to evaluate the feedback of the ecosystem on Hg cycling. Before we use this model to investigate what drives bioaccumulation, I wanted to investigate whether there are notable feedback mechanisms of marine bioaccumulation on marine Hg cycling (e.g. speciation, concentration levels, air-sea exchange, spatio-temporal distribution). To this extent, I ran the MERCY v2.0 model in its 3D configuration as described in Bieser et al. 2023 with and without bioaccumulation and without the biogenic reduction of cyanobacteria in the Baltic Sea. Additionally, Dr. Mikheeva helped me by providing her setups for three 1D water column models in the North and Baltic Seas that resembled a variety of hydrodynamic conditions typical for shelf oceans.This approach allowed me to visualize and quantify the extent to which the ecosystem influences Hg cycling, helping to determine whether including ecosystem dynamics in marine Hg speciation models is essential. This means that while Chapter 2 focuses on the implementation of bioaccumulation to couple atmospheric Hg concentration to MeHg concentrations in fish, the next chapter expands on this by evaluating the total effect of bioaccumulation on Hg cycling. I would also like to mention the difference in terminology here. Since the chapters are designed as standalone papers, the terms Hg^{2+} and tHg and $MMHg^{+}$ and tMeHg are used in the following chapter. This is done because this chapter focuses heavily on the chemistry and the difference between the different Hg fractions. Because of this, the difference between Hg^{2+} and Hg^{0} and $MMHg^{+}$ and DMHg is important. However, in most publications, the more general terms of iHg, Hg and MeHg are used. This is a deliberate choice to ensure correctness in the chapter where it matters while sticking to commonly used terminology where it doesn't.

Figure 2.5: Nudibranche (*Aeolidiella sp.*). Picture taken by Dr. Eric Wurtz.

CHAPTER 3

Bioaccumulation as a driver of high MeHg in coastal Seas

David J. Amptmeijer[1], Johannes Bieser[1], Elena Mikheeva[1], Ute Daewel[1], Corinna Schrum[1,2]
[1]Matter Transport and Ecosystem Dynamics, Helmholtz-Zentrum Hereon, Geesthacht, Germany
[2]Universität Hamburg, Institute for Marine Sciences, Mittelweg 177, 20146 Hamburg, Germany

Mercury (Hg) is a toxic pollutant that poses significant risks to marine ecosystems and human health as a result of bioaccumulation. Despite its known hazards, the processes that govern Hg bioaccumulation within the marine food web are poorly understood. This study examines the role of the marine ecosystem in Hg cycling in highly productive coastal seas. We integrate Hg biotic uptake, release and transformation into the ECOSMO E2E marine ecosystem model, coupled with the MERCY v2.0 marine Hg cycling model. Our results show that bioaccumulation can increase total methylmercury (tMeHg) in coastal pelagic waters from 0.059 to 0.092pM, an increase 44%. The bioaccumulation and binding of Hg to organic matter contribute to elevated Hg levels in surface waters. Furthermore, cyanobacteria-driven reduction of Hg^{2+} to Hg^0 reduces average marine Hg concentrations by up to 9% above the mixed layer depth in the Gotland Deep and 20% in shallow Baltic Sea regions, and increases Hg^0 evaporation in the Baltic Sea, reducing Hg inflow into the North Sea. We quantify a 1% increase in tMeHg per 4.5 mgC m^{-3} biota biomass. Finally, we show that bioaccumulation decreases the burial of Hg by 13 kg y^{-1} increasing Hg export to the Atlantic Ocean and the English Channel. These findings highlight the importance of ecosystem feedback on marine Hg cycling and demonstrate the need to integrate biological processes into Hg cycling models.

Keywords: Mercury (Hg), Methylmercury (MeHg), Bioaccumulation, Ecosystem modeling (ECOSMO), marine biogeochemical modeling (MERCY)

Publication Status

This chapter is based on the following preprint:

Amptmeijer, D. J., Mikheeva, E., Daewel, U., Bieser, J., & Schrum, C. (2025). *Bioaccumulation as a driver of high MeHg in the North and Baltic Seas*. *EGUsphere*, **2025**, 1–46. *Preprint*. https://doi.org/10.5194/egusphere-2025-1486

Graphical abstract

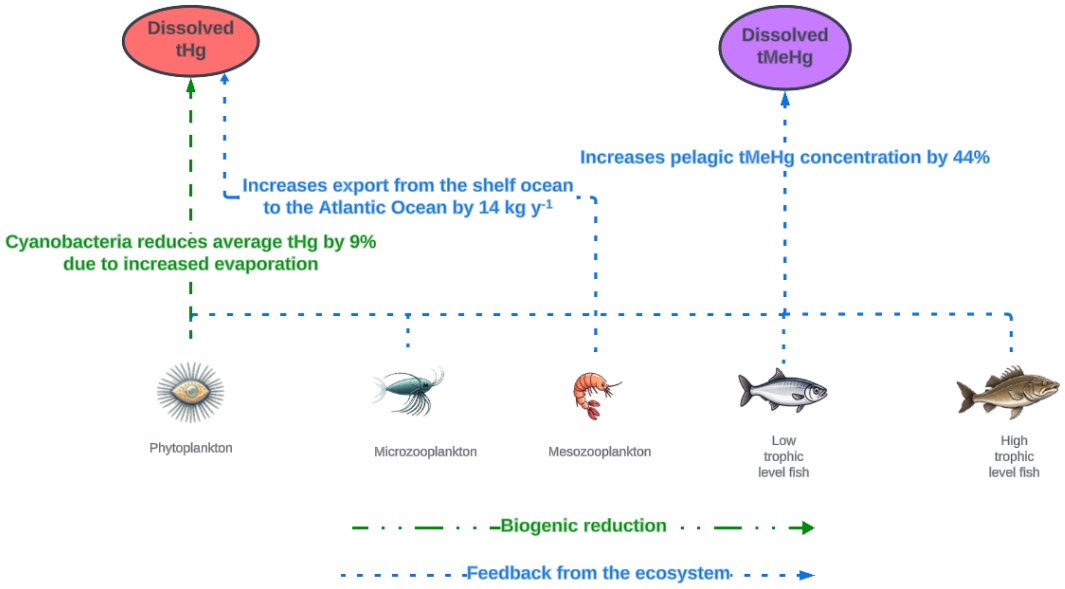

Figure 3.1: There is important feedback between the ecosystem and Hg cycling. Cyanobacteria can reduce the tHg content in the Baltic Sea by 9% by increasing evaporation. Additionally bioaccumulation can increase the pelagic tMeHg content by 44% and increase the export of tHg from the North and Baltic Seas to the North Atlantic by 14 kg y^{-1}. The image is made of several sub-images that are generated using openArt.

3.1 Introduction

Mercury (Hg) is a naturally occurring toxic element that is extremely persistent in the environment (Driscoll et al. 2013). It can be methylated to methylmercury (MeHg) by marine microorganisms, a dangerous neurotoxin that can bioaccumulate in the marine food chain (Trevors 1986; Mason et al. 1995). Hg can reach levels 10^6 times higher in fish than in the surrounding water and can reach levels in seafood that are unsafe for human consumption, especially during pregnancy or for developing children (Hsi et al. 2016; Counter and Buchanan 2004; Outridge et al. 2018). The toxicity and emission of Hg received worldwide attention in 1956 when Minamata Bay in Japan was polluted with large amounts of Hg. This Hg was methylated by microorganisms and bioaccumulated in the marine ecosystem. Due to the consumption of polluted marine wildlife, more than 1000 people died and more were permanently disabled (Harada 1995). Efforts to control Hg emissions culminated in the Minamata Convention on Mercury, which is a pledge to reduce Hg emissions and is currently signed by 128 countries (Outridge et al. 2018).

To ensure the effectiveness of the Minamata Convention in controlling the level of Hg pollution, the status of Hg emissions is periodically reviewed in the effectiveness evaluations of the Minamata Convention. In the first draft of the 2023 effectiveness evaluation, it is stated that Hg measurements in the air, biota, and humans are the key parameters to monitor the current risk of Hg (UNEP 2021). Because samples of high-trophic-level animals are easily available in the form of commercial fish and their Hg levels are comparatively high and thus easier to measure accurately, Hg biomonitoring is often focused on assessing the Hg levels in high trophic levels. In the effectiveness evaluation, it is stated that Hg levels in water can be insightful, but because of the complexity of sampling and the variability in the data, it does not receive the same recommendation for sampling as fish and wildlife receive. This can lead to insufficient data to understand the cycling and bioaccumulation of marine Hg at the base of the food web, although these processes are essential in linking Hg emissions to (Me)Hg concentrations in seafood. Modeling studies are a perfect tool to improve our understanding of these complex interactions and can help evaluate the effectiveness of Hg reduction strategies.

3.1.1 Bioaccumulation of Hg

Because MeHg formation and subsequent bioaccumulation in seafood are the dominant source of Hg exposure to humans, Hg levels in the world's oceans are of special concern. Oceanic Hg levels are influenced by a variety of sources. Hg can enter the ocean from the atmosphere through atmospheric exchange of Hg^0 or wet deposition of oxidized Hg^{2+}. Along with the atmosphere, Hg can enter the global ocean; it can enter through rivers, sea ice melt, coastal erosion, and hydrothermal vents (Zagar et al. 2006). Hg can be released from the ocean by the evaporation of volatile Hg^0 and dimethylmercury (DMHg), or it can be buried in the sediment, removing it from the biosphere (Van Veen et al. 2002; Zagar et al. 2006; Outridge et al. 2018). The dominant species of Hg in surface water is inorganic Hg^{2+}. Hg^{2+} and Hg^0 are in a dynamic equilibrium, but in water, this equilibrium favors Hg^{2+}. Although Hg^0 can evaporate, Hg^{2+} can be methylated into two forms of organic Hg, monomethyl mercury ($MMHg^+$) and double-methylated DMHg. Both forms are highly toxic, but only DMHg is volatile and can evaporate from surface water, while $MMHg^+$ can bioaccumulate (Morel et al. 1998). The role DMHg in bioaccumulation is unknown. The sum of $MMHg^+$ and DMHg is referred to as MeHg. Since only $MMHg^+$ bioaccumulates, the term MeHg, in this paper, refers to the total methylated fraction of Hg in seawater. Under anoxic conditions, Hg^{2+} can be bound to S^{2-} to form cinnabar (HgS), which is considered a sink due to its low solubility (Oliveri et al. 2016). In seawater, due to an abundance of chloride, Hg^{2+} and $MMHg^+$ exist primarily in the form of inorganic chlorine complexes. The neutral forms of these complexes, $HgCl_2$ and MMHgCl compounds, can diffuse through cell membranes due to their lipophilic nature or bind to organic matter (Zhong and Wang 2009). The speciation of Hg with organic carbon in the marine ecosystem, such as detritus and DOM, is a complex interaction that can influence the speciation, solubility, mobility, membrane permeability, and toxicity of Hg (Ravichandran 2004). In summary, there are three fractions of Hg^{2+} and $MMHg^+$ in our model. HgCl and MMHgCl, referred to as Hg^{2+} and $MMHg^+$ in this paper, Hg-DOM and MMHg-DOM and Hg-detritus and MMHg-detritus. An overview of all Hg abbreviations used in this paper is shown in Table 3.1.

Bioaccumulation of Hg occurs when species take up Hg at a rate higher than that at which it is excreted (Bryan 1979). The most important step in bioaccumulation is the uptake of Hg directly from the water through respiration, absorption, or swallowing (Lee and Fisher 2016). This can lead to a concentration of Hg inside organisms up to 100,000 times higher than in surrounding water. This process is called bioconcentration and is especially important at the base of the food web. The second process is the increase of Hg with increasing trophic position, which is called biomagnification. As a result of biomagnification, already high bioconcentrated Hg values in phytoplankton can be amplified to extremely high values in high trophic animals, such as predatory fish, marine mammals, and seabirds (Lavoie et al. 2013).

Bioconcentration can be measured in laboratory studies as it is the equilibrium between dissolved Hg and Hg concentrated in biota. In the case of Hg, several chemical forms of Hg, such as Hg^{2+} and $MMHg^+$ can bioconcentrate at the same time and have different bioconcentration rates (Mason et al. 1996). Biomagnification is more variable because it depends on the trophic transfer efficiency of both biomass and Hg and their excretion rates, which can be influenced by various factors such as life cycle, water temperature, and diet (Borgå et al. 2004). Biomagnification can be estimated in nature by sampling stable carbon and nitrogen isotopes with Hg to assess both the Hg content and the trophic position of a series of species (Lavoie et al. 2013). The biomagnification factor can then be calculated based on the increase in Hg per increase in the trophic position (Mackay and Fraser 2000). The bioconcentration of Hg^{2+} and $MMHg^+$ can occur at every trophic level. However, it is mainly dependent on the surface area of organic membranes that are in contact with water and therefore dominated by microorganisms such as phytoplankton (Mason et al. 1996).

3.1.2 Bioaccumulation into phytoplankton

The uptake of Hg^{2+} and $MMHg^+$ into phytoplankton is a complex 2-step process in which Hg binds first to the phytosphere before it is absorbed into the cell. Recent data suggest that MMHg uptake$^+$ is influenced by cell-dependent factors such as phytosphere thickness and availability of transmembrane channels for $MMHg^+$ transport, while this is not the case for Hg^{2+} (Garcia-Arevalo et al. 2024). When phytoplankton is grazed, protein-bound $MMHg^+$ uptake is much more efficient than lipid-bound Hg^{2+}. This leads to an

increased biomagnification factor for $MMHg^+$ compared to Hg^{2+} (Mason et al. 1996). This results in much higher levels of $MMHg^+$ in high trophic animals compared to Hg^{2+}, although the dissolved concentration of Hg^{2+} is generally higher than the concentration of $MMHg^+$ by an order of magnitude (Bieser et al. 2023).

In addition to Hg^{2+} and $MMHg^+$ uptake, another role for phytoplankton in Hg cycling is demonstrated by Kuss et al. (2015). Their research showed that certain species of cyanobacteria in the Baltic Sea (notable Synechococcus and Aphanizomenon) can also react with Hg by reducing dissolved Hg^{2+} to dissolved gaseous Hg^0. Since Hg^0 is volatile and can evaporate, increasing the fraction of Hg^0 can reduce the Hg. This process is referred to as biogenic reduction.

3.1.3 Previous marine Hg bioaccumulation models

Marine Hg cycling and bioaccumulation modeling have received attention in the past, with a strong focus on $MMHg^+$ bioaccumulation modeling. A model using the Shear realistic water column Turbulence Resuspension Mesocosms in the Beaufort Sea was presented by Kim et al. (2008); they incorporated the bioaccumulation and trophic transfer of $MMHg^+$ in a pelagic food web and the bentho-pelagic coupling to study the effect of sediment resuspension on $MMHg^+$ bioaccumulation. Schartup et al. (2018) made a non-spatial model of $MMHg^+$ uptake and trophic transfer; they model bioaccumulation and trophic transfer of $MMHg^+$ at the base of the food web. Their non-spatial model is driven by observations of aquatic $MMHg^+$ and successfully reproduces observed bioaccumulated $MMHg^+$ concentrations in mesozooplankton. Zhang et al. (2020) developed a global model for $MMHg^+$ uptake in plankton; they modeled bioaccumulation by assuming an instant equilibrium between marine $MMHg^+$ and phytoplankton, and consequently modeled bioaccumulation into two functional groups of primary consumer zooplankton that were differentiated by their size. Bioaccumulation in these zooplankton species was estimated based on the concentration of $MMHg^+$ in the phytoplankton they consume and a size-specific $MMHg^+$ elimination rate. Rosati et al. (2022) published a model for the cycling and bioaccumulation of $MMHg^+$ in plankton in the Mediterranean Sea; they developed a coupled 3D Hg biogeochemical transport model to assess the cycling of Hg^{2+}, Hg^0, $MMHg^+$ and DMHg. Bioaccumulation was incorporated by modeling the bioconcentration of $MMHg^+$ in phytoplankton and the consequent biomagnification to zooplankton when they consume phytoplankton. Together, these models create a strong base for understanding the coupling of $MMHg^+$ in the marine environment to bioaccumulation at the base of the food web. This is expanded on by Bieser et al. (2023), which couples atmospheric Hg concentrations and deposition with $MMHg^+$ bioaccumulation in the mid-trophic level fish herring (*Clupea harengus*), while taking into account the bioconcentration of Hg^{2+} and $MMHg^+$ for all biota. This is done by integrating the MERCY v2.0 model to the output of the 3D ECOSMO-HAMSOM coupled system, which models biogeochemistry and hydrodynamics in the North and Baltic Seas on a spatial and temporal scale. In this way, the bioaccumulation of $MMHg^+$ could be coupled to atmospheric Hg cycling without having the models interact at run-time.

In the expansion of these approaches, we implemented the bioaccumulation of Hg^{2+} and $MMHg^+$ in a fully coupled model, which includes 2 trophic levels of fish. In addition to being fully coupled, it expands on previous models by including high-trophic-level fish while explicitly tracking the trophic level of all biota. Similarly as in Bieser et al. (2023), we incorporate the Hg cycle and active and passive uptake of both Hg^{2+} and $MMHg^+$ at every trophic level. We analyze bioaccumulation in the North and Baltic Seas in idealized 1D water columns, as this region provides varied hydrodynamical environments that we can use to test our model. Then we evaluate the importance of our findings in the same offline coupled 3D ECOSMO-HAMSOM-MERCY system presented in Bieser et al. (2023) to estimate the effect of bioaccumulation on the Hg cycle and the Hg and MeHg budget.

The North and Baltic Seas are shelf seas in North-Western Europe. The Baltic Sea is a brackish sea of approximately 377,000 km^2, which is connected to the 575,000 km^2 large North Sea via the Danish straits. Both seas are important sources of seafood and 2 million tonnes of metric tonnes are landed annually (ICES 2022). Hg input into the North and Baltic Seas is dominated by riverine input and atmospheric deposition (Kwasigroch et al. 2021).

Table 3.1: Definitions of Hg abbreviations.

Abbreviation	Meaning
Hg	Refers to Hg in general
Hg^{2+}	Dissolved Hg (Bioaccumulates)
Hg^{0}	Elemental Hg (Volatile)
$MMHg^{+}$	Monomethylmercury (Bioaccumulates, extremely toxic)
DMHg	Dimethylmercury (Volatile, extremely toxic)
MeHg	$MMHg^{+}$ + DMHg
tHg	All Hg, including what is bioaccumulated
tMeHg	All MeHg, including what is bioaccumulated
Bioaccumulated Hg^{+}	All Hg^{2+} that is bioaccumulation
Bioaccumulated $MMHg^{+}$	All $MMHg^{+}$ that is bioaccumulation
Aquatic Hg	All Hg excluding what is bioaccumulated
Aquatic MeHg	All MeHg excluding what is bioaccumulated

3.1.4 The hypothesis

In this study, we hypothesize that the ecosystem can influence Hg cycling in several ways, and our aim is to quantify its effect on Hg cycling. To support this goal, we quantify the feedback of the ecosystem on marine Hg cycling by modeling a fully coupled Hg speciation and bioaccumulation model with and without bioaccumulation, the complexation of Hg with detritus and labile DOM, and the biogenic reduction of Hg^{2+} to Hg^{0} facilitated by cyanobacteria. Then we analyze the difference between the scenarios. In this article, we present the results of model runs in the North and Baltic Seas, using three idealized 1D water column setups that represent permanently mixed, seasonally mixed, and permanently stratified water column conditions. Furthermore, we run the model in a 3D configuration of the North and Baltic Seas to analyze the spatial variation of the impact of the ecosystem on Hg cycling and quantify the overall effect of these interactions on the Hg budget of these seas. We investigated the role of the ecosystem on both the total Hg budget and the aquatic Hg fraction. The total Hg (tHg) and total MeHg (tMeHg) refer to all Hg and MeHg, including what is bioaccumulated. The aquatic Hg and aquatic MeHg refer to all Hg species that are in water but are not bioaccumulated. This is shown in Table 3.1 for clarity.

The 3D configuration used in this study is based on the model of (Bieser et al. 2023), which is modified to investigate scenarios in which we change the ecosystem drivers of Hg speciation to assess their impact.

3.2 Methodology

To evaluate the role of the ecosystem, we quantify the impact of several processes on total and aquatic Hg concentrations. In the first part of this section, we specify how these processes are implemented in the different scenarios that are simulated. The second part focuses on the models, setups, and parameterizations used in this study.

3.2.1 Processes

To quantify the impact of ecosystem interactions on marine Hg cycling, we evaluated three processes:

- Bioaccumulation
- Biogenic reduction
- Partitioning to detritus and labile-DOM

Bioaccumulation is the uptake of Hg^{2+} or $MMHg^{+}$ from the water. When Hg is bioaccumulated, it cannot evaporate or undergo speciation and photolysis, but it will be transported with the organism that bioaccumulated the Hg. We are interested in this, as the bioaccumulation of Hg removes aquatic Hg^{2+} and $MMHg^{+}$, which undergoes speciation. Aquatic Hg^{2+} and $MMHg^{+}$ is removed during the phytoplankton bloom, and it is released when the bloom period is over. This seasonal removal and release has the potential to influence Hg cycling. Moreover, Hg accumulated in the biota is protected from photolysis, making the accumulated Hg species more stable than that in the surrounding water.

Biogenic reduction is the reduction of Hg^{2+} to volatile Hg^{0} by cyanobacteria. It has been shown to be an important interaction during cyanobacterial blooms in the Baltic Sea (Kuss et al. 2015). Here, we attempt to quantify the impact that cyanobacterial blooms have on Hg cycling in the Baltic Sea. Biogenic reduction does not play a role in our North Sea setups, as there are no cyanobacteria in the North Sea in the ECOSMO E2E model (Daewel and Schrum 2013). That agrees with the research of Kuss et al. (2015), where cyanobacteria-induced biogenic reduction was found in cyanobacteria that are specific to the Baltic Sea.

Partitioning to organic carbon is represented in the model by the binding of Hg^{2+} and $MMHg^{+}$ to detritus and labile-DOM. Hg associated with organic carbon can be ingested by scavengers, contributing to the bioaccumulation process. Alternatively, when the detritus sinks, the Hg bound to it is transported to deeper water layers. In this way, the binding of Hg to organic carbon not only facilitates a flux of Hg to deeper water but also can deliver Hg from the upper water layers directly to scavenging animals. The only organic carbon particles for which the 1D setups account are detritus and labile-DOM originating from the ECOSMO E2E model.

The simulation scenarios of our research model are visualized in Fig. 3.2. Here we run the model with the following interactions enabled: (base case) without bioaccumulation but all other interactions (scenario A), without bioaccumulation and biogenic reduction (scenario B), without partitioning to detritus and labile-DOM (scenario C), and without any of the previously described interactions (scenario D). Since there is no biogenic reduction in the North Sea, the base case is only compared to scenarios B and C in the North Sea setups.

3.2.2 Models

In this study, we used two model systems with different purposes. The first system are idealized 1D water column setups, which are used to generalize our findings. The second is a 3D setup, which is used to analyze the spatial patterns and estimate the budgets of the North and Baltic Sea.

1D water column model

For the 1D system, the model design is shown in Fig. 3.2. We use the Generalized Ocean Turbulence Model (GOTM) to simulate the hydrodynamics of the 1D water column setups, the ECOSMO E2E ecosystem model to simulate the marine ecosystem, and the MERCY v2.0 model to simulate Hg cycling. (Daewel et al. 2019; Bieser et al. 2023; Burchard et al. 1999b). The models are coupled using the Framework for Aquatic Biogeochemical Modeling (FABM) (Bruggeman and Bolding 2014). ECOSMO E2E, MERCY v2.0, and bioaccumulation models are implemented through FABM and coupled to GOTM using this framework. This coupling allows us to simulate the effect of the marine ecosystem from the ECOSMO E2E model, on the Hg cycling in the MERCY v2.0 model under the influence of the hydrodynamics from the GOTM model.

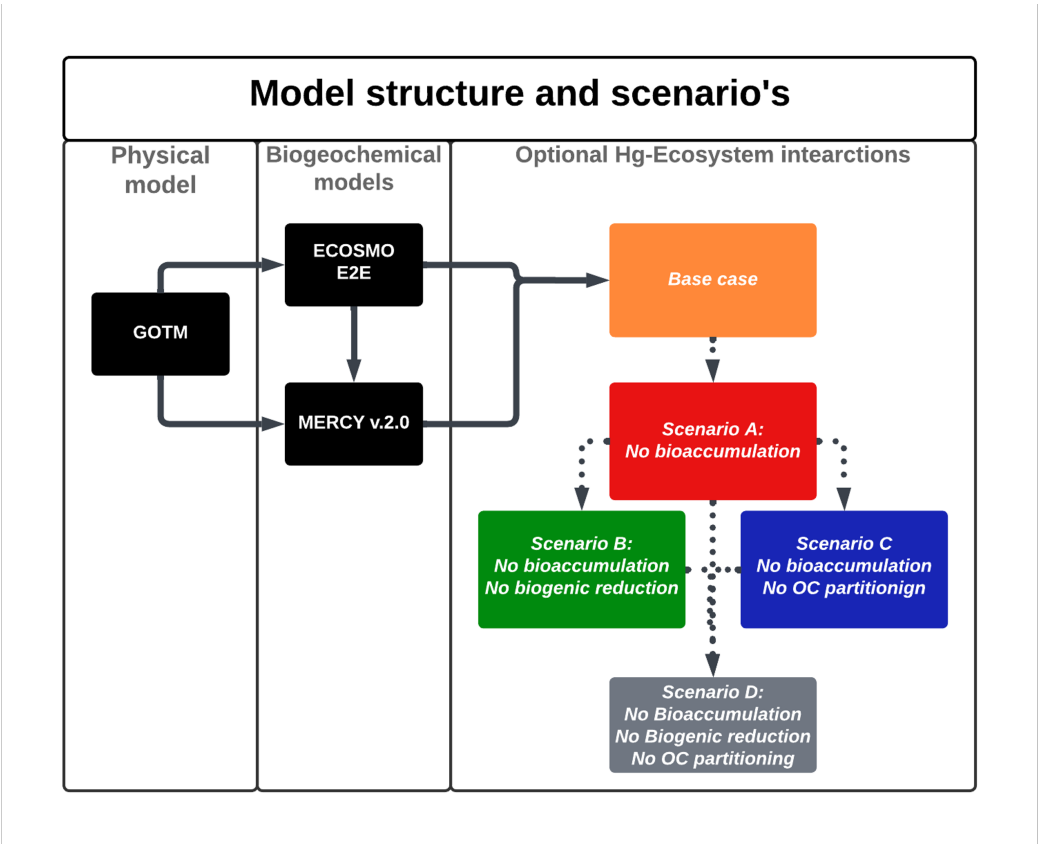

Figure 3.2: Model setup diagram. The GOTM model drives the ECOSMO E2E Ecosystem model and MERCY v2.0 Hg speciations model. These models drive different setups with optional Hg-Ecosystem interactions. The impact of the ecosystem is evaluated by comparing the base case to a scenario without; bioaccumulation (scenario A), bioaccumulation and biogenic reduction (scenario B), bioaccumulation and partitioning to detritus and DOM (scenario C), and all mentioned ecosystem interactions (scenario D).

GOTM

The GOTM model is a 1D model that calculates the turbulence of a vertical 1D water column setup by computing the solutions to the one-dimensional version of the transport equation of momentum, salinity and temperature, while being nudged to observational datasets. Therefore, our model has only a vertical resolution and no horizontal resolution. GOTM calculates variables of the physical state (temperature, salinity and density), vertical transport (advection, diffusion, turbulence, and sinking) and surface processes (surface elevation, friction, and velocity). GOTM communicates these state variables to the biochemical models using the FABM interface.

MERCY

The MERCY v2.0 model is a comprehensive Hg cycling model. It includes the speciation of Hg^0, Hg^{2+}, HgS, $MMHg^+$, and DMHg in water, sediment, and biota. With this model, we implement the partitioning of Hg^{2+} and $MMHg^+$ to organic carbon and its speciation between the dissolved, particulate and colloidal phases. In addition, atmospheric deposition of Hg, its air-sea and sediment-water exchanges are also resolved in this model. In 1D setups, the MERCY v2.0 model is fully coupled with the ECOSMO E2E-GOTM system.

The ECOSMO E2E ecosystem model

The ECOSMO E2E (ECOSystem Model End-to-End) ecosystem model (Daewel et al. 2019) is an extended version of the ECOSMO II model. ECOSMO E2E includes higher trophic levels, such as macrobenthos and fish. In the 3D setups, this model includes the following 7 biological functional groups: cyanobacteria, flagellates, diatoms, microzooplankton, mesozooplankton, fish, and macrobenthos. In the 1D setup, there are two functional groups of fish, 1 representing lower trophic level pelagic fish such as herring or sprat, and 1 representing a benthic top predator, such as cod. The model simulates nutrient cycles (nitrogen, phosphorus, and silicon), oxygen dynamics, and sedimentation processes.

3.2.3 Modeled regions

To generalize our findings, the scenarios are tested using the 1D GOTM model in 3 setups with hydrodynamics common for coastal areas. They are designed around physical and biogeochemical regimes representing specific locations in the North and Baltic Seas. For this, we use a 1D ocean water column model to simulate a permanently mixed, a seasonally stratified, and a permanently stratified water column. This allows us to compare our findings across different physical and biogeochemical regimes.

Permanently mixed - Southern North Sea

The first North Sea setup is located in the Southern North Sea (54°15′00.0″ *N* 3°34′12.0″ *E*) with a depth of 41.5 m. This area is characterized by strong tidal mixing, resulting in high dissolved oxygen concentrations and temperatures throughout the water column. Remineralized nutrients are quickly available for phytoplankton production as they can be mixed with surface water throughout the year. The constant mixing of the water column results in the temperature fluctuating between 5 and 15 $^\circ C$ for the whole water column depending on the season (Van Leeuwen et al. 2015). The setup location is 170 km away from the mainland, so despite being in the Southern North Sea it does have characteristics of the open North Sea. This region is characterized by high primary production between 60 and 80 g C m^{-2} y^{-1} (Daewel and Schrum 2013). The constant mixing allows macrobenthos to feed directly from the phytoplankton bloom, leading to a high macrobenthos stock (Heip et al. 1992). 41.5 m is also deep enough to support larger species of fish, such as herring and cod.
The available concentrations of dissolved silicate limit the growth of diatoms in the North Sea. Diatoms can dominate at the start of the bloom, but other phytoplankton species will take over the bloom after the silicate is depleted. The second flagellate bloom in the North Sea typically exceeds the first and can continue until light, nitrogen, or phosphorus becomes limiting (Peeters et al. 1991).

Seasonally mixed - Northern North Sea

The second setup is in the Northern North Sea (57°42′00.0″ *N* 2°42′00.0″ *E*) with a depth of 110 m. This setup has seasonal stratification in summer and complete mixing of the water column in winter (Van Leeuwen et al. 2015). This results in good growth conditions for phytoplankton in spring on the surface and a subsurface bloom in summer, when nutrients become depleted on the surface. In fall and winter, nutrients from the deeper water layers are mixed back into the surface. During summer, the temperatures in the Northern North Sea setup increase at the surface to 15-20 $^\circ C$ but remain at 6 $^\circ C$ in deeper water.

Primary production in the Northern North Sea is typically lower than in the Southern North Sea and ranges from 40 to 60 g C m^{-2} y^{-1} (Daewel and Schrum 2013). Furthermore, seasonal stratification means that macrobenthos cannot feed directly from the phytoplankton bloom. This leads to smaller macrobenthos communities than in the Southern North Sea. Fish are better adapted to the Northern North Sea environment, which results in high stocks of fish. The Northern North Sea has a similar nutrient regime as the Southern North Sea, in which silicate limits diatom growth, and flagellates can be limited by light, nitrogen, or phosphorus (Peeters et al. 1991).

Permanently stratified - Gotland Deep

The third setup is the Gotland Deep (57°18′00.0″ *N* 20°00′00.0″ *E*) located in the central Baltic Sea. It is 249 m deep and is characterized by a permanent halo and oxycline. During spring and summer, an additional thermal stratification is established. This causes temperatures of 6 °*C* and preserves anoxia in deep water. The surface water of the Gotland Deep setup remains oxic throughout the year and has temperatures fluctuating between 5 and 20 °*C*. The Gotland Deep setup is also considerably less saline than the North Sea and has a salinity of 12 and 7 g Kg^{-1} in the deep and surface water, respectively (Nausch et al. 2003). This is caused by major freshwater riverine input combined with sporadic and limited inflow from the North Sea (Lehmann et al. 2021). Phytoplankton growth in the Baltic Sea is typically dominated by diatoms, but flagellates can form a large portion of the biomass in open-water areas, such as the Gotland Deep. The autumn bloom is usually dominated by cyanobacteria. Primary production is estimated to be between 20 and 40 g C m^{-2} y^{-1} in this region (Daewel and Schrum 2013). The open Baltic Sea is a productive fishing region with a fish biomass density as the North Sea; however, due to the anoxic bottom water, macrobenthos in the Gotland Deep is extremely limited. Studies in the Gdansk Deep found no macrobenthos with a population density significant for the benthopelagic coupling under anoxic conditions, and similar conditions can be expected in the Gotland Deep (Kendzierska and Janas 2024).
The Gotland Deep has silicate concentrations similar to those of the North Sea but with less nitrogen and phosphorus. Because of this, the available silicate is enough to support diatoms as the most abundant phytoplankton group in the Baltic Sea. The heavily stratified nitrogen-limited surface layer forms an ideal growth environment for cyanobacteria, which can fix nitrogen from the atmosphere. In this way, they can use the available phosphorus, until either phosphorus becomes limiting or the end of the bloom seasons causes light to become limiting (Savage et al. 2010).

3.2.4 3D spatial model

In addition to the idealized 1D setups of the different regimes, the total effect of the ecosystem on Hg cycling in the North and Baltic Seas is quantified using a 3D model of the entire region. Both 1D and 3D models are used because the 1D models allow us to analyze different ecosystem interactions in idealized circumstances, while the 3D models allow us to evaluate the total effect of the ecosystem on Hg cycling, sedimentation, and evaporation in the model domain while assessing the effect on the ecosystem on the total Hg budget of the North and Baltic Seas. The effect of the ecosystem on the Hg budget is analyzed by running the MERCY v2.0 3D Hg bioaccumulation and speciation model described in Bieser et al. (2023) in the North and Baltic Seas with and without bioaccumulation and biogenic reduction. MERCY v2.0 model uses the 3D hydrodynamic model HAMSOM (Hamburg Shelf Ocean Model) as a physical model. In this setup, the HAMSOM-ECOSMO hourly output is used to drive the MERCY v2.0 model, making it effectively an offline coupled system. The model is run from the beginning of 2011 to the end of 2015. The first 4 years are used as spin-up and the final year is used for the analyses. The model is run in its default setup, without bioaccumulation or biogenic reduction. The effect of bioaccumulation on both tHg and tMeHg is visualized by plotting the relative difference in tHg and tMeHg caused by the ecosystem. The data is visualized using the cartopy package in Python version 3.11.2.0.

3.2.5 HAMSOM

The HAMSOM (Hamburg Shelf Ocean Model) is a physical hydrodynamic ice-ocean model (Backhaus 1983; Schrum and Backhaus 1999). It is directly coupled to the ECOSMO (ECOSystem MOdel) to form HAMSOM-ECOSMO (Schrum et al. 2006). This coupling allows the ecosystem to directly influence the physical system, for example, through light absorption by the biota. The HAMSOM-ECOSMO system is used to model the North and Baltic Seas. It is a comprehensive simulation of both physical and biogeochemical drivers in the North and Baltic Seas and simulates key drivers such as riverine and atmospheric nutrient input, horizontal advection and sedimentation, and burial of organic matter. This system provides the physical, chemical, and ecosystem data that drive the MERCY v2.0 model.

3.2.6 Model development

The ECOSMO E2E ecosystem model is originally designed to represent organic matter based on macronutrient fluxes, such as nitrogen, phosphate, and silicate fluxes. This means that certain interactions of the marine ecosystem that could biomagnify Hg, such as predation of species within the same functional group or even cannibalism, which do not alter nutrient fluxes or organic matter stocks, are not explicitly specified in the model (Montagnes and Fenton 2012; Arrhenius and Hansson 1996; Schrum et al. 2006). Because of this, the carbon assimilation efficiency of consumers is reduced, compared to the previously published ECOSMO E2E parameterization, so biota needs to take up more carbon for growth and can accumulate more Hg. To compensate for the reduction in carbon intake, the mortality and respiration rate of zooplankton is reduced to a value that is lower than in Daewel et al. (2019), but still within the range used in previously published models (Cruz et al. 2021). This is verified by modeling the trophic level of all biota. This allows us to compare the modeled biomagifnication factor to observations and evaluate if our model simulate bioaccumulation in line with observations of animals with the same trohic level. The phytoplankton is parameterized as shown in Table 3.2. To compensate for the increased zooplankton grazing, the growth rate is increased compared to the previously published ECOSMO E2E version, but remains within the experimentally observed range (Stelmakh and Kovrigina 2021). All other values are the same as in (Daewel et al. 2019). One notable difference between the ECOSMO E2E model in Daewel et al. (2019) and used in (Bieser et al. 2023) and the version used in this study is the inclusion of a second fish functional group. The fish functional groups are referred to as fish 1 and fish 2. Both are parameterized by the same set of equations as described in the published ECOSMO E2E model, but differ in feeding preferences and rates (Daewel et al. (2019)). Fish 1 preferably feeds on mesoplankton and microzooplankton and feeds on detritus and macrobenthos with lower preference. Fish 1 in the model represents a variety of smaller, mainly pelagic, fish such as herring (*Clupea harengus*) and European sprat (*Sprattus sprattus*). The fish 2 group is modeled as a benthic top predator and prefers to eat macrobenthos, but can also feed on mesozooplankton, fish 1, and detritus. It is mainly representative of large demersal species, such as cod (*Gadus spp.*), but would as a functional group also include other large benthic species such as whiting (*Micromesistius poutassou*) or haddock (*Melanogrammus aeglefinus*). Fish 2 is at the head of the food chain and therefore is not pre-dated in the model. Instead, all loss terms are implicitly included in the mortality term. Table 3.3 shows the parameterization of the ECOSMO E2E model setup used in this study.

Table 3.2: Dimensions, shape, and maximum growth and mortality rates of most common phytoplankton species in the North and Baltic Seas, to resemble ECOSMO E2E functional groups and the conversion ratio of mg C to cm^2 cell membrane and dm^3 cell volume. The dimensions and shapes are based on Olenina et al. (2003). For the Cylinder they are radius and height, for the sphere and hemisphere - the radius. The maximum growth rate and the mortality are based on Daewel et al. (2019).

Group	Species	Shape	Dimensions (μm)	μ_{max} (d^{-1})	Mortality (d^{-1})
Diatoms	*T. baltica*	Cylinder	12.5 x 25	1.4	0.04
Flagellate	*P. Catanata*	Hemisphere	6	1.2	0.04
Cyanobacteria	*A. flos-aquae*	Sphere	4	1.0	0.08

Table 3.3: The parameterization of consumers. The preference and consumption rate (r_{cons}) determine how much of each prey is consumed, the assimilation efficiency (AE) how much of the consumed carbon is assimilated into the predator; the mortality (r_{mort}) and respiration (r_{resp}) rate determine the total loss. Adjustments were made for higher trophic levels compared to Daewel et al. (2019) to enhance the model's suitability for bioaccumulation. Specifically, the AE and grazing rate were lowered. Additionally, fish 2 was introduced as a top predator with modified parameters. It has a higher preference for macrobenthos and consumes fish 1 rather than microzooplankton. As a top predator, fish 2 has a lower AE and consumption rate compared to fish 1. All other rates and equations remain consistent with the ECOSMO E2E model (Daewel et al. 2019).

Group	Prey	Preference (1)	r_{cons} (d^{-1})	AE (1)	r_{mort} (d^{-1})	r_{resp} (d^{-1})
Microzooplankton	Diatom	0.25	0.8	0.75	0.05	0.02
	Flagellates	0.70	0.8	0.75		
	Cyanobacteria	0.30	0.3	0.75		
	Detritus	0.10	0.8	0.8		
Mesozooplankton	Diatom	0.85	0.7	0.6	0.025	0.015
	Flagellates	0.10	0.7	0.6		
	Cyanobacteria	0.30	0.3	0.6		
	Microzooplankton	0.15	0.8	0.6		
	Detritus	0.10	0.7	0.6		
Macrobenthos	Phytoplankton	0.2	0.1	0.6	0.01	0.001
	Zooplankton	0.2	0.2	0.6		
	Sediment	0.15	0.15	0.6		
	Detritus	0.15	0.15	0.6		
	DOM	0.15	0.1	0.6		
Fish 1	Microzooplankton	0.45	0.015	0.5	0.001	0.002
	Mesozooplankton	0.45	0.015	0.5		
	Macrobenthos	0.05	0.015	0.5		
	Detritus	0.05	0.0125	0.5		
Fish 2	Mesozooplankton	0.25	0.012	0.45	0.001	0.002
	Fish 1	0.25	0.012	0.45		
	Macrobenthos	0.45	0.013	0.45		
	Detritus	0.05	0.001	0.45		

Trophic interactions play a crucial role in our model; therefore, the trophic positions of the biota are also explicitly modeled. We modeled the trophic level in two different ways.

- **Trace organic carbon origin form biota** - Initially, we assumed that the trophic level of pelagic detritus and DOM is the same as that of the organisms from which it originates.

- **Standardize organic carbon trophic level as 1** - Afterward, we defined the trophic level of detritus and DOM as 1.0. This is done because Hg associated with detritus and DOM is assumed to have an instantaneous equilibration with Hg, rather than storing it as other state variables do.

Tracking the trophic level through the detritus and DOM provides the actual trophic level of biota, which can be compared with observations. The assignment of a fixed trophic level of 1.0 to the detritus and DOM emphasizes the number of trophic interactions that contribute to the biomagnification of Hg. Since Hg in sediment is tracked through organic carbon in our model, the trophic level of sediment detritus remains consistently modeled.

The modeled trophic levels are shown in Table 3.4. In the Gotland, Deep macrobenthos is absent because of the anoxic conditions. Except for fish 2 in the Northern North Sea, all functional groups have trophic levels that are lower than observed in the North and Baltic Seas. To compensate for this, the carbon uptake efficiency of all zooplankton that feed on detritus and mesozooplankton feeding on plankton was lowered from 0.75 to 0.6, the carbon uptake efficiency for fish 1 from 0.7 to 0.5 and for fish 2 from 0.7 to 0.45, as mentioned in the model development section and shown in Table 3.3.

Table 3.4: Observed and modeled trophic level of functional groups. Observed values for microzooplankton, mesozooplankton, and fish 1 are based on Nfon et al. (2009), the trophic level for fish 2 is based on Jennings and Van Der Molen (2015), and for macrobenthos on Steger et al. (2019).

Setup	Gotland Deep		Northern North Sea		Southern North Sea		Observed
OC Trophic Level	modeled	1	modeled	1	modeled	1	-
Microzooplankton	2.1	2.0	2.2	2.0	2.1	2.0	2.00
Mesozooplankton	2.2	2.2	2.8	2.5	2.6	2.5	2.87
Fish 1	2.8	2.6	3.4	2.9	3.5	3.2	3.98
Fish 2	3.7	3.5	4.2	3.7	3.8	3.5	4-4.2
Macrobenthos	-	-	2.8	2.3	2.6	2.3	2-4
Detritus	1.4	1.0	1.5	1.0	1.3	1.0	-
DOM	1.3	1.0	1.6	1.0	1.4	1.0	-
Sediment	1.4	1.3	1.4	1.3	1.4	1.3	-

Bioconcentration

All biota in our model take up Hg^{2+} and $MMHg^{+}$ from the water column due to bioconcentration. The bioconcentration rate for phytoplankton depends on the cell surface area and the diffusivity rate of Hg^{2+} and $MMHg^{+}$ through the cell membrane (Mason et al. 1996). The surface area is estimated from the most common phytoplankton species in the three phytoplankton functional groups for the North and Baltic Seas. The species and dimensions are shown in Table 3.2. The dimensions and shapes of phytoplankton are based on Olenina et al. (2003). The carbon content per cell was estimated from the calculated cell volume for diatoms as $pgC = 0.288\mu l^{0.811}$ and for flagellates and cyanobacteria as $pgC = 0.216\mu l^{0.939}$ (Menden-Deuer et al. 2000).
Due to limited information on phytoplankton release rates, they are estimated based on uptake rates and observed concentrations ((Hg^{Aq} * uptake rate)/ $Hg^{Observed}$ = release rate) of Hg^{2+} and $MMHg^{+}$.
Based on this, we implemented the change of bioconcentrated pollutant per day for a functional group (Hg^{2+} or $MMHg^{+}$) via the following equation:

$$\frac{dC^{BC}_{(p,g)}}{dt} = b_g * C_p * r_{bc(g,p)} - (r_{rel(p,g)} + r_{bl(g)}) * C^{BC}_{(p,g)} - \sum_{z=1}^{n_z} r_{pred(z,g)} * b_z * \frac{C^{BC}_{(p,g)}}{b_g} \quad (3.1)$$

$C^{BC}_{(p,g)}$ – concentration of pollutant p that is in the functional group g originating from bioconcentration [ng Hg m^{-3}];
b_g – the biomass concentration of the functional group g [mgC m^{-3}];
C_p – concentration of pollutant p [ng Hg m^{-3}];
$r_{bc(g,p)}$ – bioconcentration rate of group g of pollutant p [m^3 mgC^{-1} d^{-1}];
$r_{rel(p,g)}$ – release rate of pollutant p by the functional group g [d^{-1}];
$r_{bl(g)}$ – biological loss rate due to mortality and respiration of group g [d^{-1}];
n_z – total number of consumers that feed on group g;
z – consumers that feed on group g;
b_z - biomass concentration of consumer group z [mgC m^{-3}];
$r_{pred(z,g)}$ – the rate at which predator z feeds on group g [d^{-1}];
t - time [day];

Note that this calculates the change in the concentration of the pollutant per volume of water. So by dividing this by the biomass in this volume of water in mgC $^{-3}$ we can calculate the concentration of the pollutant in biota in ng Hg mgC^{-1}. The bioconcentration, release, and turnover rates are shown in Table 3.5. In particular, Pickhardt and Fisher (2007) observes that Hg^{2+} accumulates at similar levels in all phytoplankton, while the accumulation of $MMHg^{+}$ exhibits an inverse relationship with cell size. Due to this, the uptake / loss rate ratio is the same for all phytoplankton groups for Hg^{2+}, however, only the loss rate is the same for all phytoplankton groups for $MMHg^{+}$. The groups representing phytoplankton

species with a smaller size and therefore a higher uptake rate also have a high Hg^{2+} release rate. As a result, all phytoplankton groups reach equilibrium at similar Hg^{2+} concentrations. However, the equilibrium between uptake and release for $MMHg^{+}$ is inversely related to cell size. This means that smaller cells will accumulate more $MMHg^{+}$ per biomass while accumulating a similar amount of Hg^{2+}, compared to larger cells. The difference in the excretion rates of Hg^{2+} and $MMHg^{+}$ can be explained by the different binding behaviors of Hg^{2+} and $MMHg^{+}$ in the cell. While Hg^{2+} binds to smaller compounds and adheres to the cell wall, $MMHg^{+}$ binds to larger cytoplastmic proteins. This means that to excrete $MMHg^{+}$, it needs to be demethylated to Hg^{2+}, or excreted using dedicated peptide membrane channels (Bridges and Zalups 2010; Takanezawa et al. 2023).

Biomagnification in consumers

The bioaccumulation in consumers depends on both bioconcentration and biomagnification. The release of bioconcentrated Hg is referred to as the release rate, and the release of biomagnified Hg is the turnover rate. This difference is caused by a different way of accumulation: bioconcentrated Hg can adsorb on the gills of fish where it can be released at different rates, compared to Hg, absorbed in the gut tissues (Pickhardt and Fisher 2007; Wang and Wong 2003). In zooplankton, the same release and turnover rate is assumed. This is because zooplankton is so small that the bioconcentrated and biomagnified Hg can more easily homogenize throughout the animal (Tsui and Wang 2004). The functional group-specific release and turnover rates are shown in Table 3.5.

The formulation for biomagnification is based on the consumption rates calculated by the ECOSMO E2E model, multiplied by an assimilation efficiency based on observations. The assimilation efficiency depends on the type of prey and is for Hg^{2+} 0.2 when phytoplankton, 0.27 when consumers, and 0.13 when detritus or DOM is consumed. For $MMHg^{+}$, when phytoplankton, detritus, or DOM is consumed, assimilation efficiency is set for 0.80, and it is set to 0.96 when consumers are consumed (Mason et al. 1995; Tsui and Wang 2004; Wang and Wong 2003). The increase in Hg for consumer g per day is implemented into the model by the following equation:

$$\frac{dC^{BM}_{(p,g)}}{dt} = \sum_{s=1}^{n_s}(r_{pred(g,s)} * b_g * a_{(s,p)} * \frac{C_{(s,p)}}{b_s}) - (r_{to(p,g)} + r_{bl(g)}) * C^{BM}_{(p,g)} - \sum_{z=1}^{n_z} r_{pred(z,g)} * b_z * \frac{C^{BM}_{(p,g)}}{b_g} \quad (3.2)$$

n_s – total number of prey that group g feeds on;
$C^{BM}_{(p,g)}$ – concentration of pollutant p that is in the functional group g originating from biomagnification [ng Hg m^{-3}];
$r_{pred(g,s)}$ – consumption rate of group g on group s [d^{-1}];
s – prey groups that are consumed by g;
$a_{s,p}$ – assimilation efficiency of pollutant p when group s is consumed [unitless];
$C_{(s,p)}$ - the total concentration (from both biomagnification and bioconcentration) of pollutant p in group s [ng Hg m^{-3}];
b_s - the biomass concentration of prey s [mgC m^{-3}];
$r_{to(p,g)}$ – turnover rate [d^{-1}];
Biomagnification follows the same loss process as bioconcentration, except that the turnover rate ($r_{to(p,g)}$) replaces the release rate ($r_{rel(p,g)}$)

Biomagnification follows the same loss process as bioconcentration, except that the turnover rate ($r_{to(p,g)}$) replaces the release rate ($r_{rel(p,g)}$).

It is important to note that extensive studies that separate the effects of bioconcentration and biomagnification are rare. Due to this, the estimated bioconcentration, turnover, and release rate of microzooplankton, mesozooplankton, and macrobenthos are all based on studies performed on pelagic water flea *Daphnia pulex*. This species is abundant in the Baltic Sea, but not in the North Sea. Salinity does not appear to have a direct effect on the bioconcentration of Hg in zooplankton and since Daphnia can have a size of 1-5 mm it is average in size for zooplankton (Reinhart et al. 2018). The fish rates are based on a study investigating the uptake, release, and turnover rates in the Indo-Pacific species Harry hotlips *Plectorhinchus gibbosus* (Wang and Wong 2003).

Table 3.5: The estimated bioconcentration (r_{bc}), release rates (r_{rel}), and turnover rates (r_{to}) for phytoplankton (Mason et al. 1996), zooplankton (Tsui and Wang 2004) and fish (Wang and Wong 2003; Trudel and Rasmussen 1997). Bioconcentration rates are in m^3 mgC^{-1} d^{-1} and release and turnover rates are d^{-1} (Trudel and Rasmussen 1997; Pickhardt et al. 2006; Mason et al. 1996; Tsui and Wang 2004). The bioconcentration rates for phytoplankton are based on the cell size, for zooplankton and macrobenthos on *Dapnia pulex*, and for fish on *Plectorhinchus gibbosus*.

	Hg^{2+}			$MMHg^{+}$		
Functional group	$r_{bc}(m^3\ mg\ C^{-1}\ d^{-1})$	$r_{rel}(d^{-1})$	$r_{to}(d^{-1})$	$r_{bc}(m^3\ mg\ C^{-1}\ d^{-1})$	$r_{rel}(d^{-1})$	$r_{to}(d^{-1})$
Diatoms	3.2E-3	63.1	(-)	3.1E-3	0.75	(-)
Flagellates	3.2E-3	65.5	(-)	3.1E-3	0.75	(-)
Cyanobacteria	5.5E-3	109.7	(-)	5.4E-3	0.75	(-)
Microzooplankton	1.68E-5	3.0E-2	3.0E-2	2.22E-05	1.50E-02	1.50E-05
Mesozooplankton	1.68E-5	3.1E-3	3.1E-3	2.22E-05	1.50E-02	1.50E-02
Macrobenthos	1.68E-5	4.0E-2	4.0E-2	2.22E-05	2.50E-02	2.50E-02
Fish 1	3.90E-7	2.16E-2	4.47E-2	9.07E-6	2.90E-03	3.00E-04
Fish 2	3.90E-7	2.16E-2	4.47E-2	9.07E-6	2.90E-03	3.00E-04

3.2.7 Model setup

1D setups

The 1D setups are run using the GOTM model mentioned earlier. The GOTM setups are based on observational data that is used to generate setups using iGOTM (https://igotm.bolding-bruggeman.com). All GOTM simulations run for the period 01-01-1989 12:00:00 until 01-01-2011 12:00:00, of which the first 10 years are considered a spin-up period and the period from 01-01-2000 12:00:00 to 01-01-2011 12:00:00 is the actual simulation period and is used for analyses. These setups are based on gridded bathymetry data for water depth (1/240° resolution) (GEBCO Bathymetric Compilation Group 2020), ECMWF ERA5 data set for meteorological data (0.25°/hourly resolution) (Wouters et al. 2021), World Ocean Atlas for salinity and temperature profiles (0.25° resolution) (Garcia H.E. et al. 2019), and the TPOX-9 atlas for tides (1/30° resolution) (Egbert and Erofeeva 2002). The setups have 1 grid cell m^{-1}, and the model is run using a forward Euler time-step ordinary differential equation that solves the state every 60 seconds. The variables are exported as daily mean values before being processed using R v4.4.1. Plots are generated using ggplot v3.5.0.; linear regression and statistics are calculated using ggpubr v0.6.0.

Horizontal boundary exchange of Hg

In GOTM, sediment and atmosphere are considered a horizontal surface that interacts with 1 cell of the surface grid. Therefore, we assume that burial will take place in 2 steps. The first step is sedimentation to the shallow sediment layer. From this layer, there is a fixed burial rate of 1.0E-5 d^{-1} to deeper sediment that cannot be resuspended. These processes and rates are the same for Hg, nutrients and organic carbon in the sediment. Sedimentation and resuspension of Hg are coupled with detritus in the ECOSMO E2E model. Hg bound to detritus will sink, sediment, and resuspend at the same rate as the organic matter it is associated with. Macrobenthos can also take up Hg bound to organic carbon when it consumes detritus or DOM. When macrobenthos lose Hg due to respiration or mortality, it is released into the sediment. Hg in the sediment has the same burial and resuspension rates as sediment carbon in the ECOSMO E2E model, as it is assumed to remain bound to organic carbon in the sediment.

Due to its chemical properties, Hg^0 in the surface water layer is constantly exchanged with the atmosphere. This exchange is modeled the same as in Bieser et al. (2023) and modeled after Kuss (2014), which is based on the Henry's law constant determined by Andersson et al. (2008) to estimate the equilibrium between Hg^0 in the air and surface water. This method is extensively evaluated in Bieser et al. (2023) against measurements by Kuss et al. (2018). From all Hg speciations in aquatic environments, two species are volatile - Hg^0 and DMHg. The direction of atmospheric exchange depends on both the aquatic and

atmospheric concentrations of those forms of Hg. Furthermore, the atmosphere can be a source of Hg^0 and Hg^{2+}, through direct wet deposition. To simulate the interactions of Hg with the atmosphere in this study, we used the approach previously used in the MERCY v2.0 model (Bieser et al. 2023). Hg^0 is constantly exchanged between the surface layer and the atmosphere. When DMHg is present in the surface layer, it can evaporate from the marine system. In addition, there is the deposition of Hg^0 and Hg^{2+}. Both atmospheric concentration and Hg deposition are provided by the CMAQ model, and the values are the same as in the 3D MERCY v2.0 (Bullock and Brehme 2002; Bieser et al. 2023).

Atmospheric deposition of nutrients

Horizontal advection of nutrients plays an important role in the North and Baltic Seas. Nutrients are transported into the seas by rivers and are buried in sediment or transported to the Atlantic Ocean, and these processes are different for the three set-up locations (Vermaat et al. 2008). Horizontal transport cannot be accurately captured in a 1D setup and is beyond the scope of this model. To mimic realistic wintertime nutrient concentrations of nitrate, phosphate, and silicate of 3.7, 0.3, and 5.0 μM in the Gotland Deep setup and 7.5, 0.5, and 5.0 μM in the North Sea setups, respectively (Burson et al. 2016). Both regions are characterized by strong horizontal influxes of nutrients that are not present in our 1D setups. To compensate for this limitation of our model, we chose atmospheric deposition so that it would create realistic nutrient conditions during winter in the surface ocean throughout the simulation.

Partitioning to DOM and detritus

The only marine organic carbon particles in the water that interact with Hg in the 1D setups are detritus and DOM, which originate from the ECOSMO E2E model. The partitioning between Hg and detritus and DOM is assumed to be instantaneous, and equilibrium is forced on every model time step. This is based on K_{ow} which is log(6.4) and log(6.6) for the partition of Hg^{2+} into detritus and DOM responsibility and log(5.9) and log(6.0) for the binding of $MMHg^+$ to detritus and DOM responsibility. These values are based on Allison et al. (2005) and Tesán Onrubia et al. (2020) and evaluated in Bieser et al. (2023). This mechanism and rates are taken from the MERCY v2.0 model and are described in more detail in Bieser et al. (2023). Hg associated with organic carbon is taken up by organisms when they consume the detritus or DOM to which it is bound.

Organic carbon to dry and wet weight conversion

The biomass in our model is resolved in nutrients according to the Redfield ratio. In contrast, the uptake and release estimations are based on studies relying on weighing the samples and are therefore given in wet or dry weight. We assumed the ratio of milligram carbon to dry weight as: 0.2 for diatoms, 0.33 for flagellates and cyanobacteria and 0.5 for zooplankton and fish (Walve and Larsson 1999; Sicko-Goad et al. 1984). The weight values in this paper are always given in dry weight unless otherwise specified. Bioaccumulation can also be stated per wet weight in the literature (Nfon et al. 2009). The dry weight to wet weight conversion factor of 0.2 is then used for phytoplankton, 0.3 for fish, and 0.16 for zooplankton and macrobenthos (Cushing 1958; Ricciardi and Bourget 1998; Cresson et al. 2017).

3.3 Model evaluation

Since this is the first publication to use specific 1D GOTM setups in combination with ECOSMO E2E and MERCY v2.0 coupled via FABM, and we made changes to the ECOSMO E2E model, we evaluated whether the 1D setups perform as expected and if the biological carbon and Hg species relevant for bioaccumulation are within the range of published 3D models. Data for higher trophic levels and bioaccumulation is much rarer and therefore this data is evaluated by a quantitative analysis if the modeled values are 1 standard deviation (SD) of observations. The 3D HAMSOM-ECOSMO-MERCY setup is extensively evaluated and shows good agreement with observations for Hg cycling as is discussed in more detail in Bieser et al. (2023), and therefore it was not further evaluated in this study.

3.3.1 1D Model and Observational Data

For ECOSMO E2E we compared the biomass of the 1D model with the biomass predictions in the published 3D model. This is done because the ECOSMO E2E model is extensively validated in Daewel et al. (2019) and we want to ensure that our 1D setup is consistent with the 3D model setup. The 3D ECOSMO E2E model reports a total primary production of 50 to 90 grams of carbon m^{-2} y^{-1} in the open North Sea and between 30 and 50 grams of carbon m^{-2} y^{-1} in the open Baltic Sea. In the North Sea, the phytoplankton bloom is initiated by diatoms and is then taken over and exceeded by flagellates. In the Baltic Sea, the bloom is initiated by a large diatom bloom followed by a bloom in flagellates and cyanobacteria. Secondary production ranges between 20 and 40 grams of carbon m^{-2} y^{-1} in the open North Sea and 10 to 30 grams of carbon m^{-2} y^{-1} in the open Baltic Sea (Daewel et al. 2019). Macrobenthos total biomass estimates range from 1.5 to 40 grams of carbon for the open North Sea, with the higher values closer to the coast (Daan and Mulder 2001; Heip et al. 1992). The Gotland Deep has anoxic deep water, so there is no macrobenthos (Kendzierska and Janas 2024). The open Baltic Sea phytoplankton bloom is dominated by diatoms and is followed by flagellates and cyanobacteria (Hjerne et al. 2019). During the autumn, cyanobacteria can become the dominant species with a biomass of up to 50 mg C m^{-3}, but there is a large variety in the intensity of the bloom and the relative importance of different species (Hjerne et al. 2019).

The results of the simulations of ecosystem biomass are presented in Fig. 3.3. The total yearly primary production in our model is 50, 62, and 61 gC m^{-2} y^{-1}, the pelagic secondary production is 24, 42, and 29 gC m^{-2} y^{-1}, and the average fish stocks are 3.6, 2.6, and 2.2 gC m^{-2} in the Gotland Deep, Northern North Sea and Southern North Sea respectively. The peak macrobenthos population is 12.3 gC m^{-2} in the Southern North Sea, 3.4 gC m^{-2} in the Northern North Sea, and there are no macrobenthos in the Gotland Deep.
Therefore, we conclude that the primary production and biomass of the functional group in the 1D setups align well with observations and remain in line with the 3D ECOSMO-HAMSOM model Daewel et al. (2019). Additionally, the biomass falls within the range of observed ranges for all higher trophic-level functional groups. Because of this, we conclude that the general dynamic of biomass production in 1D setups provides similar results as the 3D ECOSMO and captures the key ecosystem dynamics in all setups.

Hg cycling; 1D Hg model results

Table 3.6 shows the observed concentration of aquatic Hg and MeHg in the Baltic Sea measured by Kuss et al. (2017), while Fig. 3.4 shows total and aquatic Hg and MeHg in our 1D model. As shown in Table 3.1, tHg and tMeHg include bioaccumulated Hg and MeHg, while aquatic Hg and MeHg do not. The aquatic Hg includes Hg^{2+}, Hg^{0}, HgS, $MMHg^{+}$, DMHg and all Hg bound to detritus and DOM, as shown in Table 3.1. The modeled tHg in the surface water of the Gotland Deep is 22% lower than the observations but will be within 1 standard deviation of the observed mean. For MeHg our modeled concentration is 50% below the observed mean and 17% below 1 standard deviation of the observed mean. This is hard to evaluate, as the measurement protocol does not lyse phytoplankton cells; we assume that no MeHg associated with biota is measured. However, if we assume that MeHg associated with phytoplankton is measured, our modeled concentration will be above the observed mean with 0.12 ± 0.08 pmol. Because of this uncertainty, we also evaluated the MeHg content indirectly through bioaccumulation. To this extent, Table 3.6 shows the modeled and observed concentration in diatoms and the observed volume concentration factor (VCF). Since the concentration of MeHg in diatoms in the Gotland Deep (14.4 ± 1.05) is within 1 standard deviation (SD) of the observed mean (10.0 ± 5.0), and the modeled VCF in Gotland Deep (1.22E5 ± 3.8E4) is within the observed range (2.0E4 - 6.4E6), and the observed concentration of MeHg (0.10 ± 0.04) is between our modeled concentration with (0.12 ± 0.08) and without (0.05 ± 0.09) MeHg in phytoplankton, we conclude that our model produces aquatic Hg and MeHg values that are in line with observations, with the caveat that the evaluation of the aquatic MeHg content is based on limited amount of data with a high measurement uncertainty. Figure 3.4 shows the aquatic and total Hg and MeHg values modeled and demonstrates the difference between the total and aquatic Hg fraction in both depth and time.

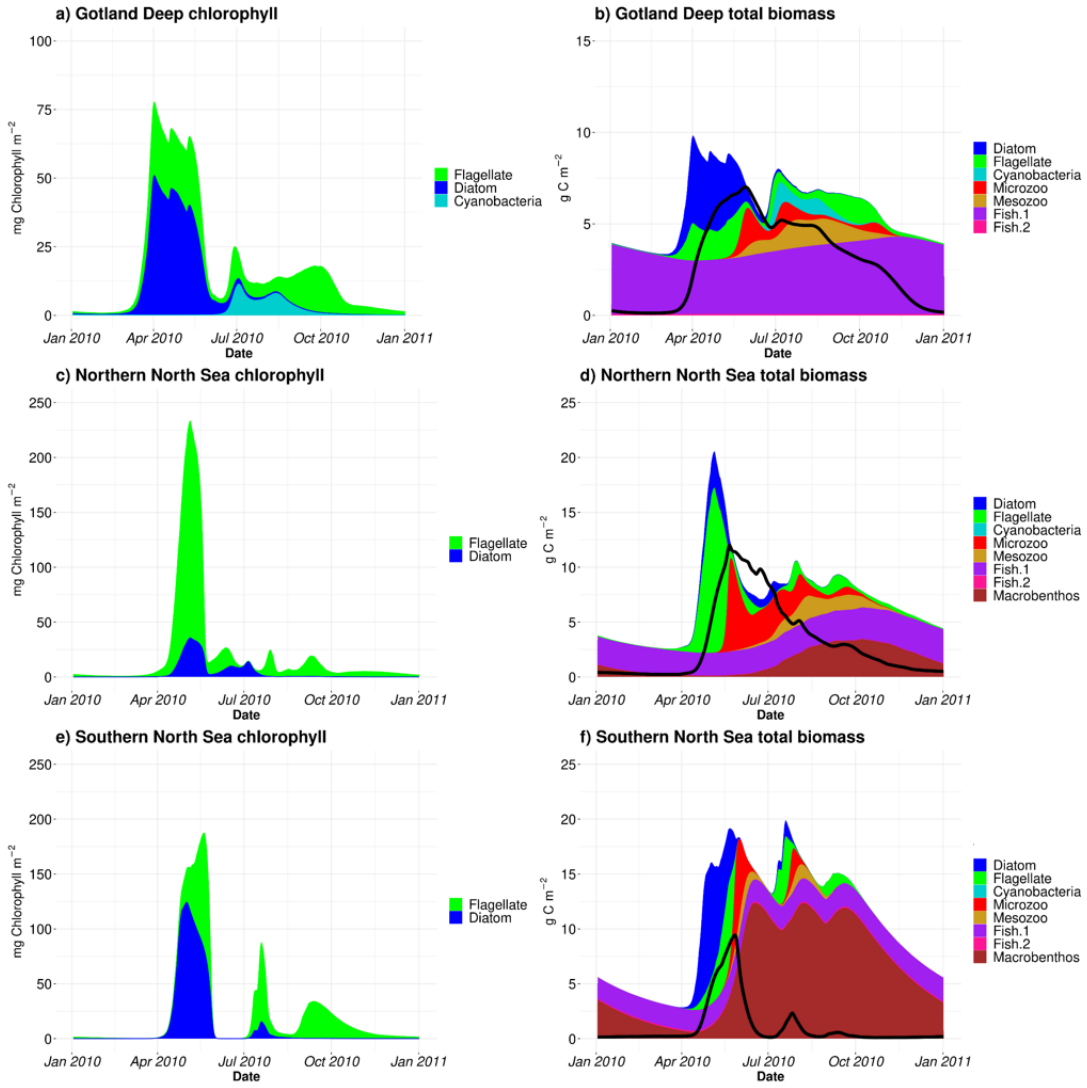

Figure 3.3: Modeled chlorophyll concentration (left) and organic matter concentration (right). In the last year of the simulation (Jan 2010 to Jan 2011). All living organic material is stacked, and detritus and DOM are plotted in the black line on top. Peak spring bloom chlorophyll concentration varies with location. Gotland Deep (a) has 77.8 mg m^{-2} chlorophyll with succession from diatoms to flagellates to cyanobacteria. The Northern North Sea (c) has 223.5 mg m^{-2} chlorophyll and is dominated by flagellates while the Southern North Sea (e) has 187.3 mg m^{-2} chlorophyll and is initially dominated by diatoms and later succeeded by flagellates. All locations have a succession of zooplankton after phytoplankton which microzooplankton and is taken over by mesozooplankton. Fish biomass ranges Northern North Sea (fish 1: 2.0-3.1, fish 2: 0.033-0.038 g C m^{-2}), Southern North Sea (fish 1: 1.7-2.2, fish 2: 0.10-0.12 g C m^{-2}). Macrobenthos biomass fluctuates seasonally: Northern North Sea (0.080-3.4 g C m^{-2}), Southern North Sea (0.56-12.3 g C m^{-2}), absent in Gotland Deep due to anoxic bottom water.

Notable is the small difference in the total and aquatic fractions of Hg compared to the large difference for MeHg in all three setups. In surface water during the bloom period, phytoplankton take up MeHg, which reduces aquatic MeHg. The removal of MeHg from the water prevents its (photo)demethylation, and the dissolved MeHg fraction is replenished by the methylation of Hg^{2+}. This increases the tMeHg content, while this is not the case for tHg. An additional noteworthy observation is in the shallow well-mixed Southern North Sea. The mixing allows macrobenthos to feed directly off the spring bloom and thus removes both organic material and Hg from the water column. This leads to a drop in tMeHg during the bloom. In winter, the $MMHg^{+}$ bioaccumulated by macrobenthos is resuspended, leading to a very high wintertime concentration of both aquatic and total MeHg in winter in the Southern North Sea.

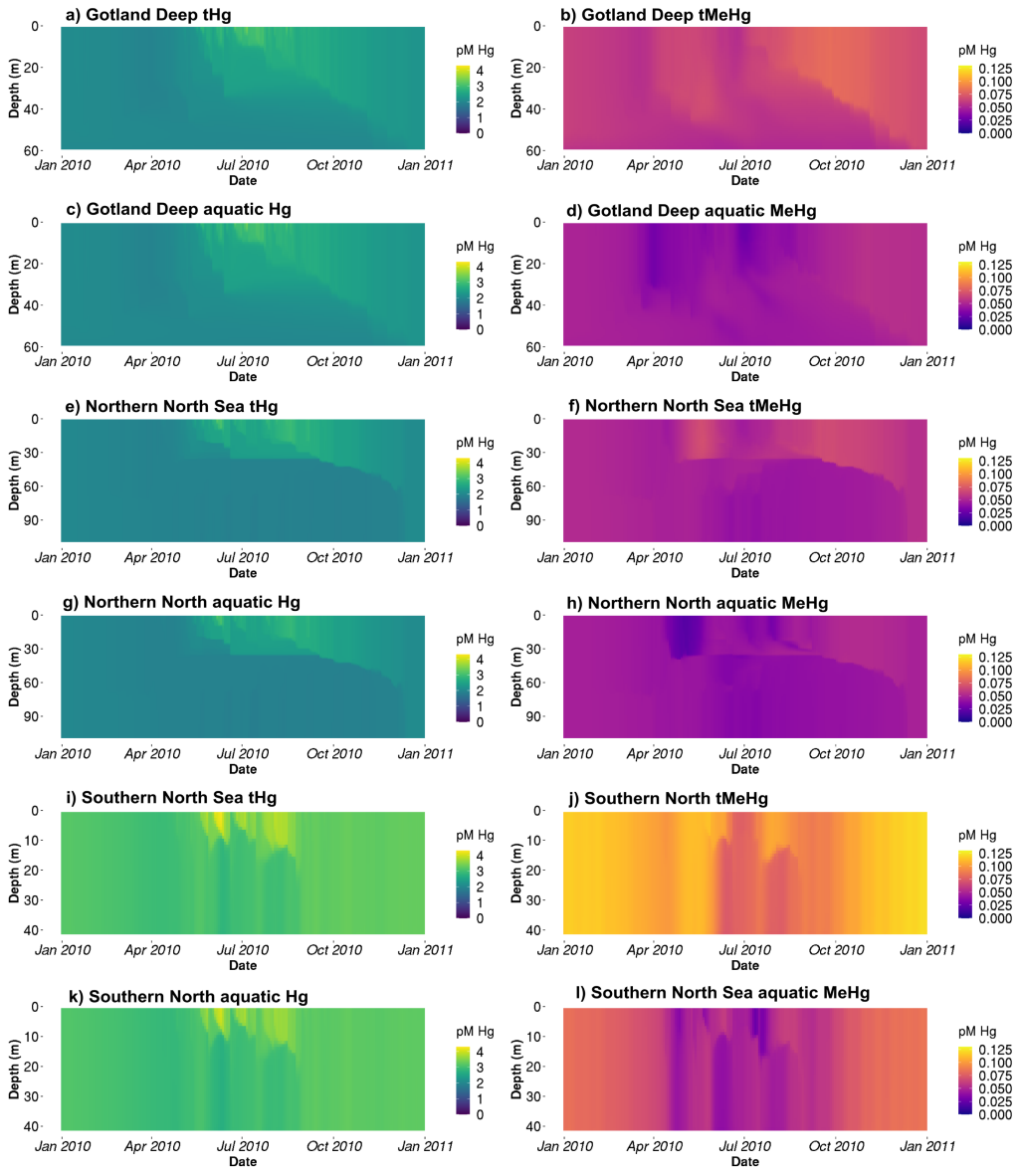

Figure 3.4: The tHg and tMeHg and the aquatic Hg (Hg^{2+}, Hg^{0}, HgS, $MMHg^{+}$, and DMHg) and MeHg ($MMHg^{+}$ and DMHg) concentrations in the last year of the simulation (Jan 2010-Jan2011) in all setups. The Gotland Deep and the Northern North Sea have a similar total Hg concentration of 2-3 pM, with an increase in Hg of up to 3.5 pM in the Northern North Sea. The concentration of Hg in the Southern North Sea is 2.5-3.5 pM during most of the year and reaches 4 pM during the spring bloom. The tMeHg content is 0.04-0.06 pM in the surface of the Gotland Deep and Northern North Sea and up to 0.08 pM in the Southern North Sea during winter. A clear reduction in all setups in aquatic MeHg during the bloom period can be seen, while the total concentration remains more stable.

Bioaccumulation model results

In Fig. 3.5 we show the bioaccumulation of Hg^{2+} and $MMHg^{+}$ in the Gotland Deep, in Fig. 3.6 of the Northern North Sea and in Fig. 3.7 for the Southern North Sea. We compare the modeled Hg bioaccumulation for biota in the Gotland Deep. We only compare when the total water column biomass>100 mg carbon m^2 and take the modeled values of the <5m for phytoplankton and <20 m for other biota to ensure that our bioaccumulation values resemble the modeled values in surface water where biota is active. A comparison between our modeled and observed bioaccumulation is shown in Table 3.6.

Table 3.6: Evaluation of the modeled bioaccumulation. Modeled and observed aquatic Hg and MeHg concentrations are shown first based on Kuss et al. (2017), then the observed range of the VCF in diatoms is shown based on Lee and Fisher (2016) and the mean and standard deviation of the modeled VCFs for MeHg into diatoms are shown. The observations for pelagic invertebrates are based on Nfon et al. (2009), the observations for fish on Kwaśniak et al. (2012) and Polak-Juszczak (2018) and the observations for macrobenthos on measurements of *Macoma Baltic* in the Baltic Sea (ICES 25 region) by Polak-Juszczak (2012). Of both model and observations the mean, standard deviation (SD) and coefficient of variation (CV) is shown. The concentration of aquatic tHg and MeHg are shown in pM, the VCF is unitless and the mean and SD of both bioaccumulated Hg^{2+} and $MMHg^{+}$ is shown in ng g^{-1} d.w. while the CV is unitless.

Variable	Observed	Model; Gotland Deep	Model; Northern North Sea	Model; Southern North Sea
Aquatic Hg	1.65 ± 2.1	2.37 ± 0.61	2.26 ± 0.22	2.97 ± 0.16
Aquatic MeHg	0.10 ± 0.04	0.05 ± 0.09	0.06 ± 0.01	0.04 ± 0.01
VCF MeHg in diatoms	2.0E4-6.4E6	1.22E5 ± 3.8E4	1.0E5 ± 4.58E4	1.1E5 ± 2.5E4
Diatoms (tHg)	10.0 ± 5.0 (0.50)	14.4 ± 1.05 (0.07)	12.9 ± 2.11 (0.16)	16.1 ± 1.62 (0.10)
Microzooplankton (tHg)	37.5 ± 31.3 (0.83)	47.0 ± 12.1 (0.26)	50.3 ± 10.8 (0.22)	54.4 ± 19.7 (0.36)
Mesozooplankton (tHg)	62.5 ± 12.5 (0.20)	66.1 ± 13.5 (0.20)	68.8 ± 10.8 (0.16)	68.3 ± 17.7 (0.26)
Fish 1 (Hg^{2+})	12.7 ± 7.0 (0.55)	7.17 ± 1.72 (0.24)	7.95 ± 0.82 (0.10)	11.8 ± 1.38 (0.12)
Fish 1 ($MMHg^{+}$)	49.3 ± 30.7 (0.62)	31.8 ± 1.90 (0.06)	21.2 ± 0.92 (0.04)	44.4 ± 3.62 (0.08)
Fish 2 (Hg^{2+})	34.3 ± 23.7 (0.69)	4.20 ± 0.82 (0.20)	4.81 ± 0.65 (0.14)	10.0 ± 1.84 (0.18)
Fish 2 ($MMHg^{+}$)	180 ± 72.3 (0.40)	65.0 ± 2.17 (0.03)	37.0 ± 0.95 (0.03)	64.5 ± 3.43 (0.05)
Macrobenthos (tHg)	25.0 ± 21.4 (0.84)	–	20.0 ± 6.6 (0.22)	30.1.5 ± 3.2 (0.16)

Evaluation of modeled bioaccumulation

Table 3.6 shows the modeled and observed means, the standard deviation (SD), the coefficient of variation (CV) and the VCF for MeHg in diatoms. The modeled bioaccumulation values from surface water (0-5 m) for diatoms and (0-20 m) for consumers are used for the evaluation. Because there are high-quality observations for the Baltic Sea, but not for the North Sea, we focused the evaluation efforts on the Baltic Sea. The observations are for tHg in invertebrates, while we have separate observations of Hg^{2+} and $MMHg^{+}$ in fish. Fish 1 in our model is compared to the observations of herring and fish 2, and to observations in Atlantic Cod. With the exception of the bioaccumulation into fish 2, all bioaccumulation values are within one observed SD of the observed mean. This, combined with the high CV of the observations, shows that our modeled values are well within the plausible range based on observations, except for the bioaccumulation in fish 2, which is lower than observed. It should be noted that the bioaccumulation modeled in fish 2 is not out of the observed range. Observations for tHg bioaccumulation in Atlantic Cod in the Baltic Sea range between 3 and 1567 ng g^{-1} d.w. (ICES 2020). However, the observed mean $MMHg^{+}$ content of all datasets is more than 1 observed SD higher than our modeled mean, leading us to believe that our model underestimates bioaccumulation in fish 2.

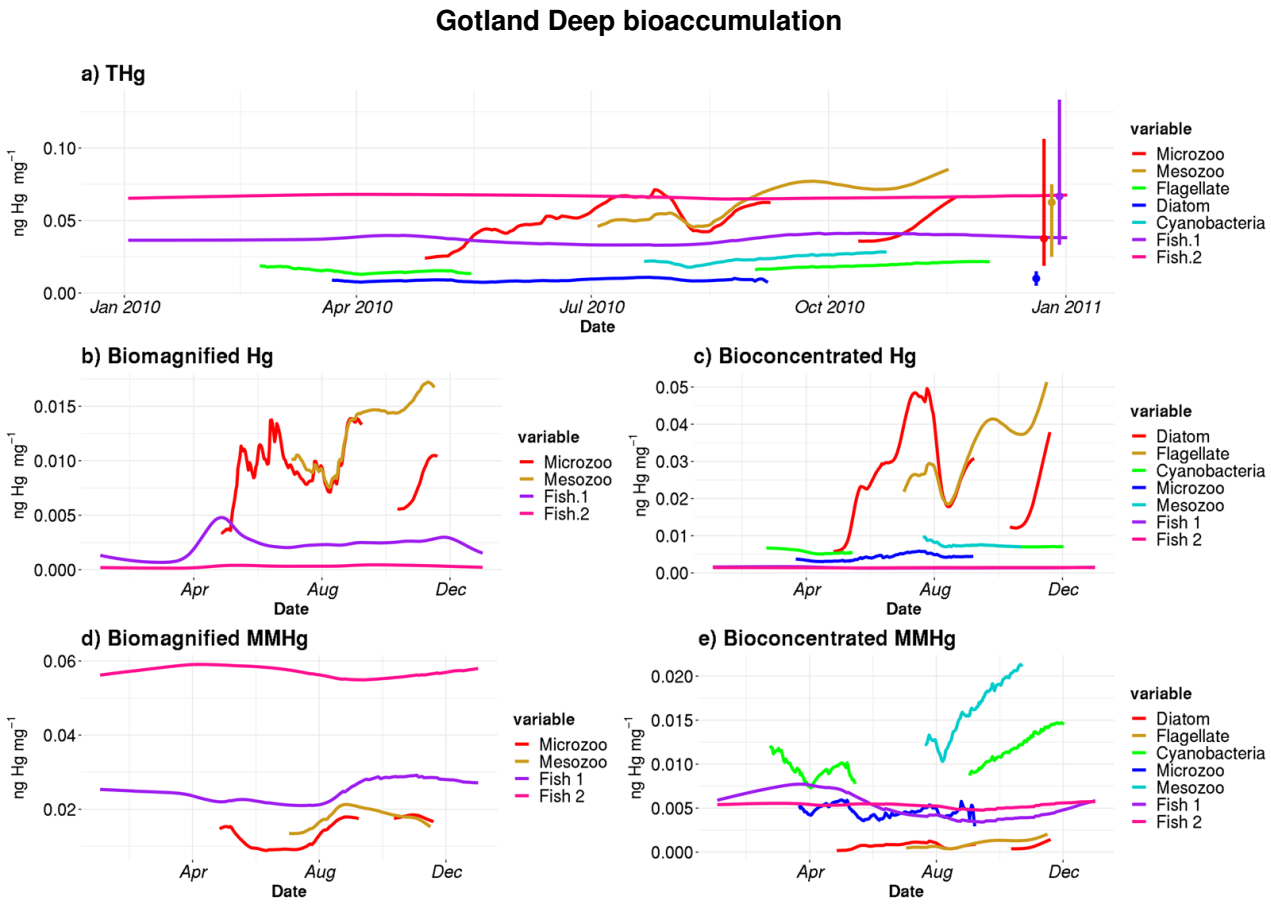

Figure 3.5: Hg accumulation in the Gotland Deep during the last simulation year (Jan 2010-Jan 2011). Plot 3.5a shows tHg bioaccumulation with mean and range of observations from Nfon et al. (2009) represented by the point and vertical bar on the right side of the plot. Bioaccumulation is displayed when biomass of the respecitive funtional group exceeds 0.1 gC m^{-2}. tHg bioaccumulation is highest in fish 2, followed by fish 1, microzooplankton, mesozooplankton, cyanobacteria, flagellates, and diatoms with tHg concentrations in observed ranges. The consecutive Fig. show the bioamagnification (3.5b, 3.5d) and bioconcentration (3.5c, 3.5e) of Hg^{2+} (3.5b, 3.5c) and $MMHg^{+}$ (3.5d, 3.5e). Biomagnified Hg^{2+} is highest in microzooplankton, followed by mesozooplankton and fish, while biomagnified $MMHg^{+}$ increases notable in fish 1 and fish 2. Bioconcentrated Hg^{2+} is very low in fish and highest in zooplankton. Bioconcentrated $MMHg^{+}$ is notable higher in cyanobacteria than in all biota and lowest zooplankton.

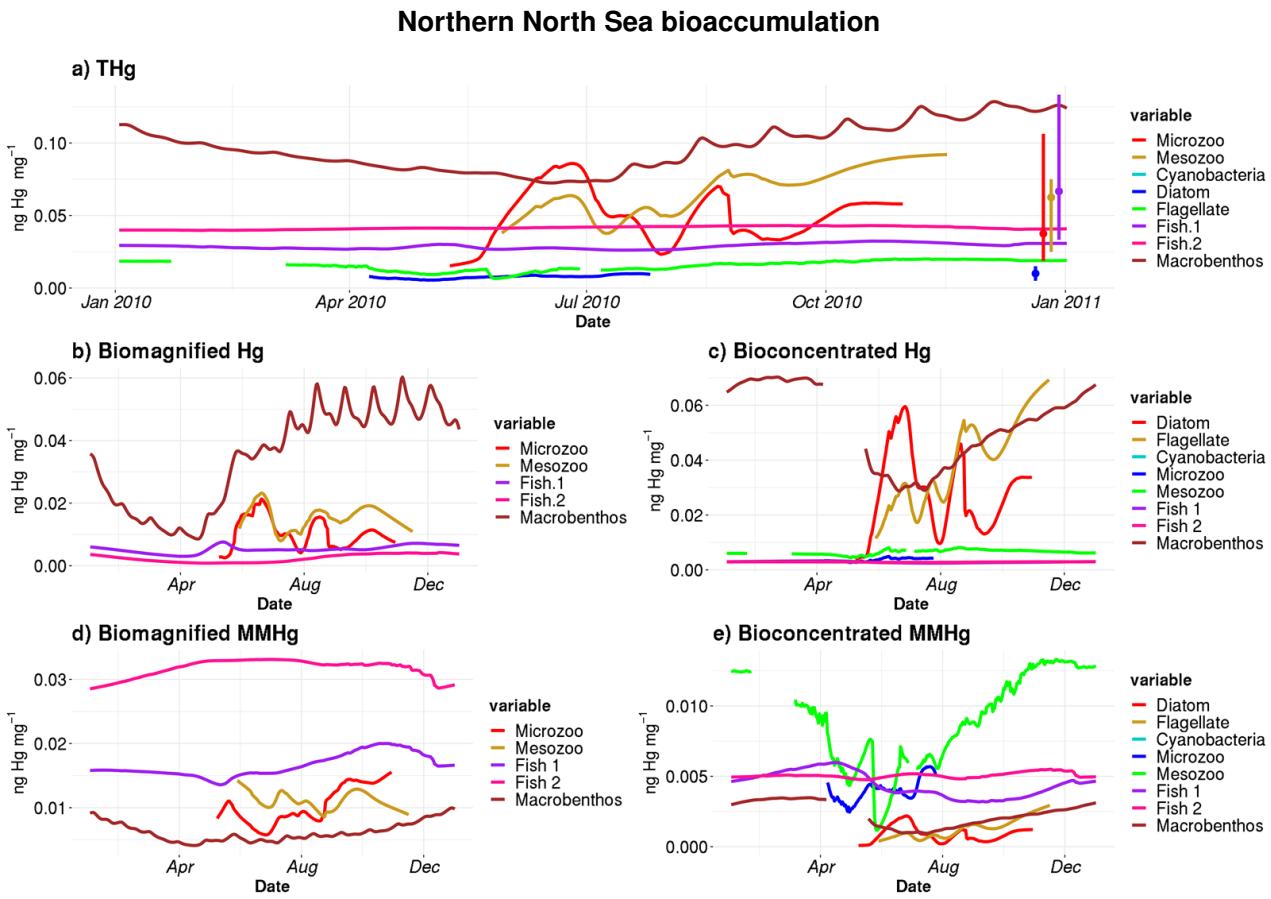

Figure 3.6: Hg bioaccumulation in the Northern North Sea. Plot 3.6a shows the tHg bioaccumulation in the Northern North Sea. Phytoplankton and zooplankton are shown if their average biomass is more than 0.1 gC m^{-2}. Phytoplankton has the lowest tHg, which is followed by fish 1, fish 2, mesozooplankton and macrobenthos. Plots 3.6 b-e show the origin (Biomagnification or Bioconcentration) and species (Hg^{2+} or $MMHg^{+}$) of the bioaccumulated tHg. Figure 3.6b and 3.6c show that the high tHg in microzooplankton, mesozooplankton and macrobenthos is due to high levels of Hg^{2+} bioconcentration and biomagnification. $MMHg^{+}$ Biomagnification follows a pattern in which it is lower in zooplankton and macrobenthos, higher in fish 1, and highest in fish 2. This means that while fish 2 has a lower Hg content than macrobenthos and zooplankton for part of the year, $MMHg^{+}$ is higher in fish than in zooplankton and macrobenthos. Figure 3.6e shows the bioconcentration of $MMHg^{+}$ and shows that this is highest in phytoplankton, followed by fish 1 and 2, macrobenthos, and zooplankton.

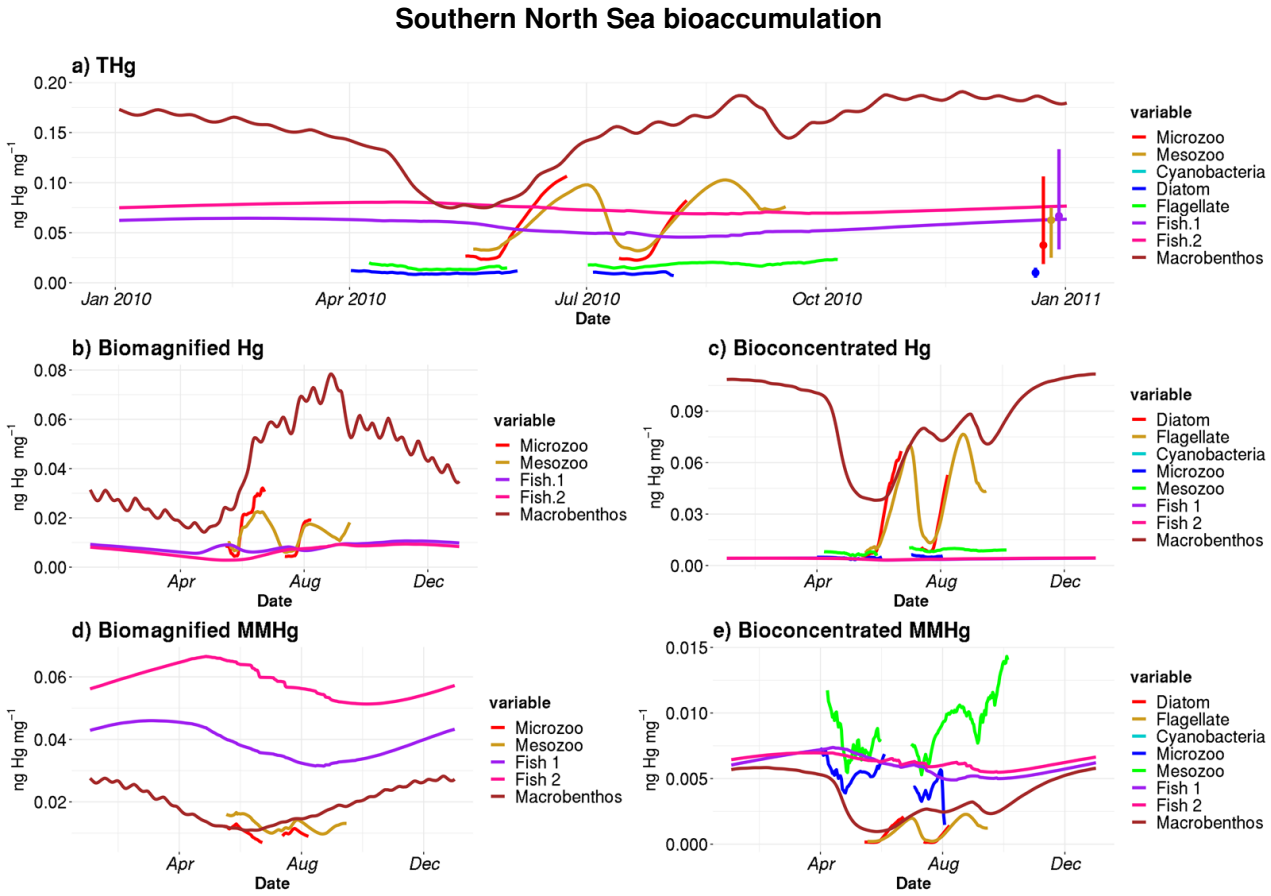

Figure 3.7: Bioaccumulation of Hg^{2+} and $MMHg^{+}$ in the Southern North Sea in the last year of the simulation (Jan 2010-Jan 2011). Figure 3.7a shows the accumulation of tHg per functional group over an annual cycle. Figures 3.7b-e display Hg^{2+} and $MMHg^{+}$ concentrations, while distinguishing between bioconcentration and biomagnification processes for each species. Phytoplankton and zooplankton are shown if their average biomass is more than 0.1 gC m^{-2}. tHg values for microzooplankton, mesozooplankton, and macrobenthos reach 0.10 and 0.10 ng and 0.19 ng Hg mg^{-1}. This is higher than fish 1 and fish 2 tHg which is 0.068 and 0.080 ng Hg mg^{-1}. Comparing Fig. 3.7b-e we see high tHg in microzooplankton, mesozooplankton, and macrobenthos is caused by high Hg^{2+} bioconcentration and biomagnification, while tHg content of fish 1 and fish 2 predominately originates from biomagnification of $MMHg^{+}$.

Modeled biomagnification

In Fig. 3.8 we plotted the correlation between the trophic level and the accumulated Hg^{2+} and $MMHg^{+}$. To assess biomagnification in bioaccumulated $MMHg^{+}$, we assumed an exponential trend between the bioaccumulation of $MMHg^{+}$ and the trophic level, which is forced through the first consumer (microzooplankton). In this way, the exponent is the biomagnification factor. Observed BMF are between 2.0 and 3.4 in the North Sea for $MMHg^{+}$ (Baeyens et al. 2003). For Hg^{2+} an exponential relationship between trophic level and bioaccumulation was neither expected nor present; therefore, we correlated this using a second degree polynomial. The modeled biomagnification factor is between 2.1 and 3.1 for $MMHg^{+}$. This means that our modeled biomagnification factor for $MMHg^{+}$ is within the range of observations in the North Sea.

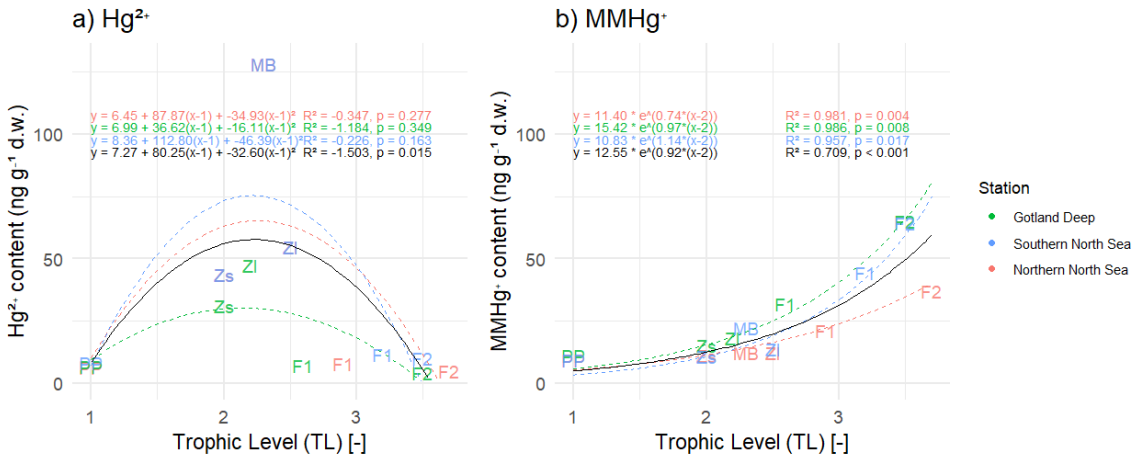

Figure 3.8: Figure 3.8 a) shows the correlation between trophic level and Hg^{2+} and Fig. 3.8 b) shows the correlation between trophic level and bioaccumulation of $MMHg^{+}$ in all three setups, the black indicates the average. PP stands for primary producers, Zs for microzooplankton, Zl for mesozooplankton, F1 for fish 1, F2 for fish 2, and MB for macrobenthos. The correlation is fitted that is forced through micrzooplankton. The R^2 of the correlation between trophic level and Hg^{2+} shows that there is a weak anti-correlation in the Gotland Deep (R^2=0.54) and no correlation ($R^2<0.01$) in the Northern North Sea and Southern North Sea. In all setups, there is a strong correlation between trophic level and $MMHg^{+}$ bioaccumulation ($R^2>0.8$). Interestingly, the correlation between bioaccumulation $MMHg^{+}$ and trophic level for all setups averages is considerably lower (R^2=0.51 for $MMHg^{+}$) than for the setups separate.

Summary of the model evaluation

Based on the evaluation of the bioaccumulation, we conclude that the general trend of high bioaccumulation of $MMHg^{+}$ and low Hg^{+} is well reproduced in our model. However, the performance of the model is lower in higher trophic levels and underestimates bioaccumulation into Atlantic Cod. The underestimation in modeled $MMHg^{+}$ values in cod can be attributed to the ecosystem model that understimates the trophic level of cod by 0.5-0.7. If we extrapolate the equation for biomagnification in the Gotland Deep shown in Fig. 3.8 ($15.42e^{TL-2}$), in which TL is the trophic level, and estimate bioaccumulation at the observed trophic level Atlantic Cod (4.2), we would expect a $MMHg^{+}$ content of 139 ng Hg g^{-1} d.w., which would be well within 1 observed SD of the observed mean. Because our model accurately predicts the tHg content of plankton, the content of Hg^{2+} and $MMHg^{+}$ in fish 1, and the $MMHg^{+}$ content at high trophic levels according to their trophic level, it appears that the bioaccumulation model accurately models $MMHg^{+}$ bioaccumulation based on trophic interactions, but that our fish 2 better resembles a mid level trophic predator both in trophic position and $MMHg^{+}$ than a high trophic level predator such as Atlantic Cod.

3.4 Results & Discussion

3.4.1 The effect of bioaccumulation on tHg and tMeHg concentrations

The 10-year average difference in the daily mean tHg and tMeHg between the base case and the setups without bioaccumulation and biogenic reduction in the Gotland Deep is shown in Fig. 3.9. Additionally, Table 3.7 shows the mean difference of tHg and tMeHg, the mean and range of the bioaccumulated Hg fraction in the bioaccumulation setup, and the average annual amplitude of the difference in tHg and tMeHg, calculated as half the total range of values. This is shown because, while the average differences provide information on the net effect of bioaccumulation, the amplitude highlights seasonal variations. If the ecosystem causes a large average difference, but this difference is consistent throughout the year, the amplitude will be 0%, but if the ecosystem causes an increase of a 100% and consequently a decrease of a 100% with no average effect, the amplitude will be 100%.

The effect of bioaccumulation on tHg

Bioaccumulation has only a small effect on tHg with a maximum increase of 3% while the average percentage of tHg that is bioaccumulated is 1% in every setup. This increase is caused because the biota takes up Hg, which is consequently protected against reduction to Hg^0. Since Hg^0 in the water is in exchange with atmospheric Hg^0, a reduction in Hg^0 will result in a reduction in evaporation until the concentration of Hg^0 in the water is re-equilibrated with the atmospheric concentration. At this point, the atmospheric exchange and the aquatic Hg concentration in the scenarios with and without bioaccumulation are similar, while the tHg concentration is up to 3% higher and in the scenario with bioaccumulation. This is further shown in Fig. 3.9. which shows the seasonal difference for both aquatic and total Hg and MeHg. Figure 3.9 shows that even though the difference is small, there is always more tHg in the base case than in scenario B without biaoccumulation. The only exception is in the permanently mixed shallow Southern North Sea in summer and autumn, which has a large amplitude in the difference in tHg with an increase of 11% at the beginning of the bloom period and a decrease of 6% later in the bloom. This reduction in tHg is caused by macrobenthos. which feeds directly of the plankton bloom and transports Hg from the water column to the benthic via the consumption of organic material. This is corraborated by Fig. 3.3 which shows that macrobenthos in the Southern North Sea have high biomass (up to 12.3 gC m^{-2}) and by Table 3.6 which shows a high tHg content in this macrobenthos of 30.1.5 ± 3.2 ng g^{-1} d.w. During late autumn,winter, and early spring, this tHg is released back into the water resulting in the above-mentioned high increase in tHg of 11% at the onset of the phytoplanktom bloom. This causes bioaccumulation to cause a similar mean increase of 3% in the Southern North Sea compared to the other setups, while the amplitude of the difference is 9% compared to 1% in other setups, demonstrating a strong seasonal effect.

The effect of bioaccumulation on tMeHg

tMeHg increases by 41, 23, and 46% for the Gotland Deep, Northern North Sea, and Southern North Sea respectively. This is very similar to the percentage of tMeHg that is bioaccumulated, which is 41, 29 and 43% respectively. Bioaccumulation increases tMeHg, as bioaccumulated $MMHg^+$ cannot be photodegraded, and aquatic MeHg is replenished by additional methylation. During autumn and winter, the biomass is reduced and bioaccumulated $MMHg^+$ is released back into the water column. During this period, the light intensity and therefore photodegredation are lower, and detritus and DOM concentrations are higher, which leads to additional shading. This causes the aquatic tMeHg concentration to be higher outside of the bloom period. This means that an increase in bioaccumulated $MMHg^+$ equals a smaller decrease in aquatic MeHg causing an increase in tMeHg. Additionally, bioaccumulation can increase aquatic MeHg by removing dissolved MeHg when photodegredation is high and re-releasing this MeHg when photodegredation is low.

This increase in tMeHg is driven by organic material and shows a linear relationship with biomass. The correlation of the daily 10-year average values for the increase in tMeHg and tHg with biomass in the surface (0-20 m) is shown in Table 3.8. If we combine the three setups, we find an increase in tMeHg of 0.028 ng Hg mgC^{-1} ($r=0.47, p<0.001$) or a relative increase of 1% per 4.5 mgC m^{-3} ($r=0.59$, $p<0.001$) and an

Table 3.7: The percentage difference in tHg, and tMeHg average concentrations caused by the ecosystem, and the average seasonal amplitude in surface water (0-20m). Additionally the mean and range of the percentage of tHg and tMeHg that is bioaccumulated (Hg(Bio) and MeHg(Bio)) in the scenario with bioaccumulation is shown. The percentage is calculated as the (scenario - base case)/((base case + scenario)/2)*100. Positive values indicate that the ecosystems increases Hg while negative values means the ecosystem reduces Hg.

Setup	tHg	tHg_{Amp}	tHg(Bio)	tMeHg	$tMeHg_{Amp}$	MeHg(Bio
Gotland Deep (no bioaccumulation)	3%	1%	1(0-2)%	**41%**	16%	41 (26-45)%
Northern North Sea (no bioaccumulation)	1%	1%	1(0-5)%	**23%**	24%	29 (13-59)%
Southern North Sea (no bioaccumulation)	3%	9%	1(0-4)%	**46%**	28%	43 (31–64)%
Gotland Deep (no biogenic reduction)	-8%	5%	1(0-2)%	**29%**	16%	41 (26-45)%

increase in tHg of 0.068 ng Hg mgC^{-1} (r=0.07,p<0.001) or a relative increase of 1% tHg per 71 mgC m^{-3} (r=0.07, p<0.001). Although both correlations are significant at the 99% confidence level, the relationship between the difference in tMeHg and biomass is notably stronger (r=0.47) than for the difference in tHg (r=0.07). Although bioaccumulation is a large amount of tMeHg, it does not constitute a large amount (< 5%) of tHg; therefore, the formation of MeHg due to methylation is not reduced and the bioaccumulated MeHg is replenished due to its rapid equilibrium with other Hg species.

Macrobenthos in the Southern North Sea have a similar, although stronger, effect on tMeHg concentrations to that of tHg. However, this effect is partially altered by the strong increase in tMeHg as a result of the high biomass in this setup. In spring in the Southern North Sea, there is a 77% increase in tMeHg due to bioaccumulation, which is the highest of all setups. However, this rapidly drops as the bloom progresses, and macrobenthos feed on the plankton bloom, causing the increase in tMeHg due to bioaccumulation to briefly be the lowest in the Southern North Sea at the end of the bloom. During winter, the macrobenthos population decreases and tMeHg is re-released, causing a large increase in wintertime tMeHg making the increase in tMeHg due to bioaccumulation in the Southern North Sea the largest in all setups.

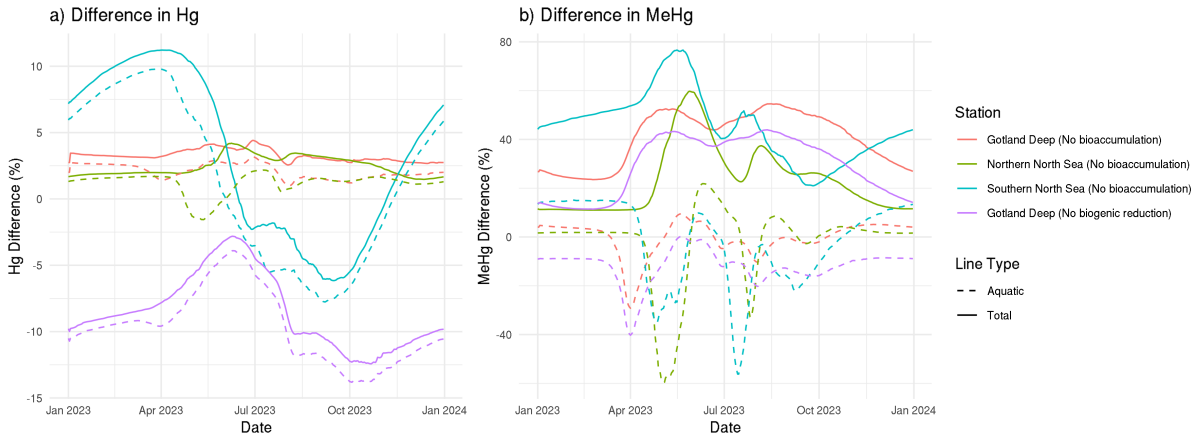

Figure 3.9: The difference in tHg, aquatic Hg, tMeHg, and aquatic MeHg the base case and the scenario without bioaccumulation and the scenario without biogenic reduction in the Gotland Deep in the top surface 20 meters of the watercolumn. For tHg there is a strong seasonal effect where it is decreased during summer and autumn and increased during spring. This is caused by the consumption of Hg-containing organic material during spring and summer and the release during winter. There is no notable effect (> 5%) in the tHg in the Northern North Sea and Gotland Deep due to bioaccumulation. In the Gotland Deep, however, biogenic reduction causes a strong decrease of up to 12%. There is no large difference (>5%) between the difference in aquatic Hg and tHg). The difference in tMeHg is much more pronounced. There is a consistent increase in tHg which peaks during spring and summer. These peaks in an increase in tMeHg coincide with a smaller decrease in aquatic MeHg.

Table 3.8: Correlation, slope, and p-value for the difference in tMeHg and tHg vs the total biomass per setup. There is a much stronger correlation (r=0.547-0.809) between the increase in tMeHg then the increase in tHg (r=0.114-0.149). The slope for tMeHg ranges from 0.134 and 0.25 and for tHg between -0.0631 and 0.0279 mgC^{-1} m^3

	tMeHg			tHg		
Setup	Correlation (r)	Slope	p-value	Correlation	Slope	p-value
Gotland Deep	0.809	0.252	<0.001	0.149	-0.0631	<0.001
Northern North Sea	0.739	0.134	<0.001	0.218	0.00691	<0.001
Southern North Sea	0.547	0.226	<0.001	0.114	0.0279	<0.001

The effect of bioaccumulation on the Hg budget and horizontal transport

In Fig. 3.10, the difference in the content of tHg and tMeHg and the export by sedimentation and evaporation from the North and Baltic Seas caused by bioaccumulation is evaluated using the 3D the MERCY-HAMSOM-ECOSMO setup. There is a decrease in the evaporation of 9% (Fig. 3.10b) and a decrease in the burial of 19% (Fig. 3.10i) caused by bioaccumulation. Figures 3.10e and Fig. 3.10f show tMeHg and the difference caused by bioaccumulation. While there is an average increase caused by the bioaccumulation of 10% in tMeHg, this is not uniform. There is a decrease in the Baltic Sea, an increase in the North Sea, and a very strong increase in the Danish Straits. This, combined with the reduction of both evaporation and burial, indicates that bioaccumulation facilitates a flux of Hg out of the Baltic Sea toward the North Sea and the Atlantic Ocean. We see an average reduction of 2.3 and 57 pmol m^{-2} y^{-1} in evaporation and burial, respectively. Our model shows that the bioaccumulation into plankton keeps Hg pelagic, which facilitates transport to the North Sea and consequently the Atlantic Ocean. Without bioaccumulation, a fraction of this Hg will evaporate or be bound to POC and be buried. The reduction in tHg due to bioaccumulation is strongest in areas such as the Wadden Sea and the Bay of Bothnia, where there are both large riverine inputs of Hg and high primary production. However, this local effect is relatively small and we see a total increase in export of 14 kg Hg y^{-1} to the Atlantic Ocean due to bioaccumulation. Of this 14 kg, 13 kg would be buried in sediment, and 1 kg would be evaporated into the atmosphere without bioaccumulation. To put this into perspective, this is 1% of the total modeled river influx into the North Sea, and thus does not significantly alter the the long range transport of Hg.

The effect of the ecosystem on the Hg budget under idealized circumstances

The 1D setup budget is shown in Fig. 3.11. This shows the modeled mean tHg and tMeHg concentrations, the difference in the run without an ecosystem compared to the setup with an ecosystem and the differences caused by biogenic reduction in the Gotland Deep.

The Southern North Sea setup is permanently mixed. Because of this, Hg can continuously reach the surface area where it can evaporate, and all aquatic MeHg is subject to photodegradation. At the same time, this constant mixing brings the plankton biomass and its bioaccumulated Hg to the benthic boundary layer, where it can be consumed by macrobenthos. This results in a large flux of Hg^{2+} and $MMHg^{+}$ from the pelagic to the benthic during the phytoplankton bloom, which is re-released during winter. This leads to high benthic Hg (11.1 pmol m^{-2}) and MeHg (1.6 pmol m^{-2}), but a relatively low burial rate (1.1 pmol tHg m^{-2} y^{-1}) as the Hg is bioaccumulated in macrobenthos rather than associated with organic carbon of sediment. The increase in tMeHg in the Southern North Sea is highest in the 3 settings, due to the high biomass, and the ecosystem increases tMeHg by 44%.

The Northern North Sea setup is only seasonally stratified. This means that during summer, macrobenthos cannot feed directly from the plankton bloom, but Hg-containing organic material can sink below the mixed layer, where it can settle as sediment, be consumed by macrobenthos, or remain until it is remixed to the surface during winter. This results in a low benthopelagic flux of Hg^{2+} and $MMHg^{+}$ throughout the year. However, the same average Hg burial as in the Southern North Sea of 1.1 pmol tHg m^{-2} y^{-1}. Due to the lower biomass, there is less tMeHg in this setup than in the Southern North Sea, and the effect of the

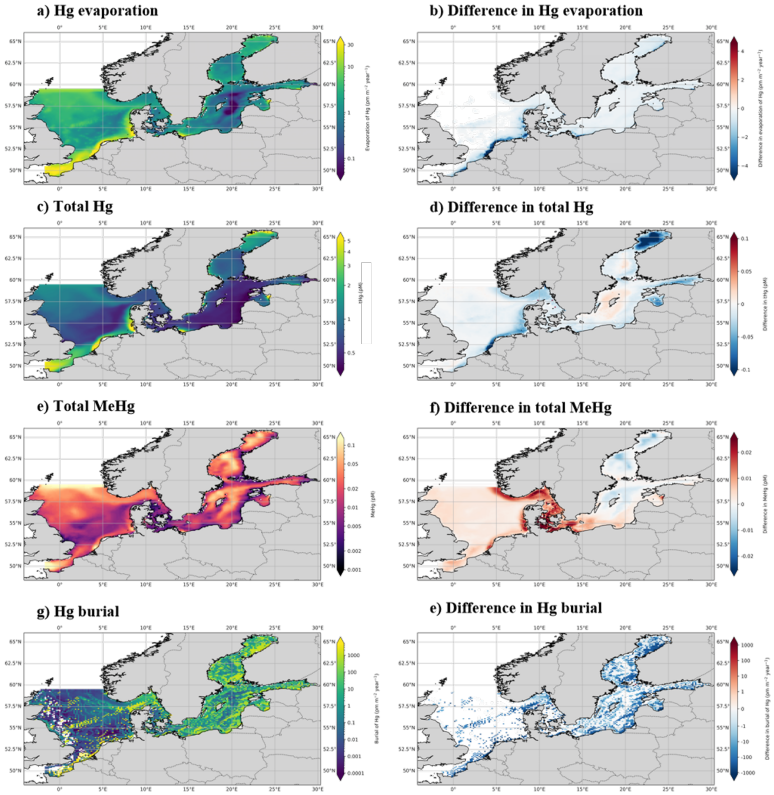

Figure 3.10: The yearly mean Hg budget of the North and Baltic Seas and the difference caused by the ecosystem, the concentrations and differences of tHg and tMeHg are the mean of the watercolumn. The difference is calculated as the Base case - Scenario A "No bioaccumulation". The average tHg is 0.5 pM, which is reduced by 0.02 pM without bioaccumulation. The average tMeHg is 0.03 pM, which is reduced by 0.003 pM without bioaccumulation. The decrease in dissolved tHg and tMeHg without bioaccumulation is coupled with a decrease in evaporation and burial. Evaporation decreases from 4.3 pm m^{-2} y^{-1} to 3.9 pm m^{-2} y^{-1} and burial from 323.5 pm m^{-2} y^{-1} to 263.2 pm m^{-2} y^{-1}.

ecosystem causes a smaller increase in tMeHg (13%) than in the Southern North Sea.

The Gotland Deep setup has permanent stratification. Hg can accumulate in the plankton in the surface layer or divide to detritus. When this detritus sinks, it will transport Hg to deeper water. As the Gotland Deep setup is permanently stratified, Hg eventually reaches the sediment and becomes buried. The flux of pelagic Hg^{2+} and $MMHg^{+}$ into the sediment is low, but since there is very low resuspension the burial rate is high (11.7 pmol tHg m^{-2} y^{-1}) compared to the lower burial rate (1.1 pmol tHg m^{-2} y^{-1}) for both North Sea setups. In the Gotland Deep setup, there is a big distinction between the effect of the ecosystem above and below the oxycline. Above the oxycline the ecosystem increases tMeHg by 13%, while below the oxycline this increase is replaced by a small decrease of 3%, as the binding of Hg^{2+} and $MMHg^{+}$ to the sinking detritus facilitates the flux of Hg to the sediment.

These differences led to the highest burial of tHg in the Gotland Deep, followed by the Northern North Sea, and the lowest in the Southern North Sea. This shows how ecosystem-induced Hg burial is influenced by local hydrodynamics.

3.4.2 The cyanobacterial reduction of Hg^{2+}

The model estimates that biogenic reduction can reduce average water column Hg above the mixed layer depth by 7% in the Gotland Deep, due to the transfer of soluble Hg^{2+} to volatile Hg^{0}, which increases

the evaporation of Hg out of the water to the atmosphere. In Fig. 3.11 we can see that there is still an increase in tMeHg (13%) above the oxycline without bioaccumulation and biogenic reduction, no increase (<0.5%) below the oxycline. This means that biogenic reduction reduces tMeHg, but the increase caused by bioaccumulation is higher above the mixed layer depth. Figure 3.12 shows the seasonal difference in the tHg and tMeHg in the 3D MERCY v2.0 model between runs with and without biogenic reduction and the cyanobacterial biomass in the surface layer. Note that we isolated the effect of biogenic reduction in these setups so bioaccumulation does still occur. The MERCY v2.0 model shows a similar reduction in the Gotland Deep as the 1D GOTM setups, but it shows a higher reduction in tHg in coastal areas of up to 0.8pM during autumn. Additionally, it shows that while cyanobacteria are most abundant during autumn (Fig. 3.12 g), they decrease the tHg content throughout the year (3.12 b, e, h, k), there is an average reduction of -0.2 pM, which is highest during the autumn bloom (-0.5 pM) and lowest in summer before the bloom (<-0.1pM) in the open Baltic Sea). Finally, cyanobacteria and biogenic reduction only occur in the Baltic Sea in the model, but we can see a decrease in tHg in the Southern North Sea of up to -0.6pM in summer and autumn and -0.5pM% in winter and spring. The difference in tMeHg is, follows a similar pattern with a reduction of up to -0.05pM in tMeHg during autumn and a smaller reduction of -0.02pM during the rest of the year in the Gotland Deep. There appears to be a small reduction in tMeHg in the Southern North Sea during summer and autumn of up to -0.03pM. This demonstrates that cyanobacteria can have a very large impact on the tHg budget of the Baltic Sea, even in areas where they are less abundant and this effect is relevant throughout the year. Kuss et al. (2017) finds that cyanobacterial-induced biogenic reduction causes approximately 30% of all Hg evaporation during summer, since we have cyanobacteria in our model for 3 months, a year-round average reduction of -9% of tHg above the mixed layer depth and a total reduction of up to -20% during summer and autumn is in line with these observations. Since Hg evaporation equilibrates the ocean with the atmosphere the annual average flux is not changed dramatically (-0.3%, or -0.42 nmol m^{-2} y^{-1}) as seen in the Fig. 3.11. Rather the aquatic Hg concentration that leads to this evaporation is lower, due to a higher Hg^0/Hg^{2+} ratio. In addition to the reduction of aquatic Hg, it also changes the seasonality of the evaporation of Hg^0. In Fig. 3.13 we show the 10-year average daily evaporation and 30-day running average of the relative difference between the 10-year average of the base case and scenario C (no bioaccumulation nor biogenic reduction). The cyanobacteria cause an increase in evaporation of Hg^0 during late summer and autumn facilitated by the cyanobacterial bloom, which is compensated by a small decrease in evaporation when the bloom is over, resulting in a similar yearly average evaporation of Hg^0. The cyanobacteria-facilitated reduction in tHg in our model does not mean that an abundance of cyanobacteria would automatically lead to a reduced Hg concentration in other regions. Cyanobacteria are a very diverse group, and not all cyanobacteria will reduce Hg^{2+} to Hg^0 (Kuss et al. 2015).

3.4.3 Partitioning to detritus and DOM

In Fig. 3.14, we show that the partition of Hg^{2+} and $MMHg^+$ into detritus and DOM causes an increase in tHg and tMeHg above the mixed layer depth in every setup. Since both North Sea setups are mixed during winter, this leads to a small increase in tHg (1-2%) in both North Sea setups. In the Gotland Deep, we observe the same increase in tHg caused by the partitioning of Hg to detritus and DOM above the mixed layer depth. However, simultaneously, we notice that partitioning to detritus and DOM decreases tHg below the mixed layer depth. This occurs because the detritus and the DOM can remove Hg from the water column since the Hg bound to the detritus can settle as sediment. Since atmospheric Hg wet deposition and atmospheric concentrations are consistent across all setups, evaporation and burial will equilibrate to the atmospheric influx. If the fraction of Hg^0 of tHg is lower, tHg will increase until Hg^0 is high enough that the evaporation of Hg^0 reaches equilibrium with atmospheric inputs. Below the mixed layer in Gotland Deep, partitioning to detritus and DOM reduces tHg. This indicates that below the mixed layer depth, the effect of the detritus and DOM partitioning on the increase in burial is stronger than its effect on the decrease in evaporation.

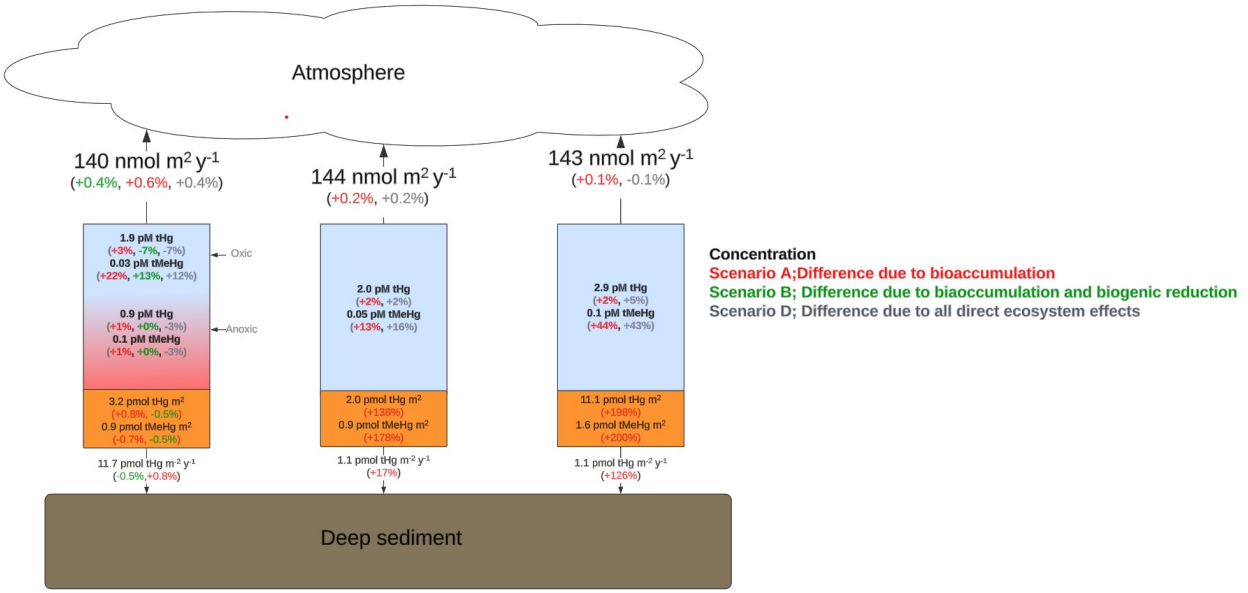

Figure 3.11: Hg Budget of the 3 Setups. All values are the average values for the final 10 years of the simulation. The blue area indicates oxic water, the red indicates anoxic water, and the brown area indicates sediment. The arrows indicate the direction of the flux. The black values are for the full model that includes all ecosystem effects, and the red indicates the percentage difference in the run without any ecosystem effects. The percentage differences are calculated by (Base case-scenario)/((Base case+scenario)/2). Thus negative numbers correspond to a decrease caused by the ecosystem while positive numbers indicate an increase caused by the ecosystem. In the Gotland Deep, dark green percentages show differences between the full model and setups without biogenic reduction and bioaccumulation. There is net evaporation in all setups of 140-143 nmol m^{-2} y^{-1}. In the North Sea, there is a decrease of both tHg and tMeHg when the ecosystem is not included. This decrease is larger for tMeHg (10-39%) than for tHg (9-2.2%). There is a decrease of 9% of tHg in the oxic layer of the Gotland Deep caused by cyanobacterial biogenic reduction. There is a lower increase in tMeHg (10%) in the oxic water column of the Gotland Deep compared to the northern (+12%) and southern (+39%) North Sea. The effect of biogenic reduction only causes a 0.6-0.5% decrease for tHg and tMeHg in anoxic water respectively in the Gotland Deep and a 0.92% decrease in sediment and burial. Sediment concentrations of both tHg and tMeHg are lowest in the Northern North Sea, followed by the Southern North Sea, and highest in the Gotland Deep.

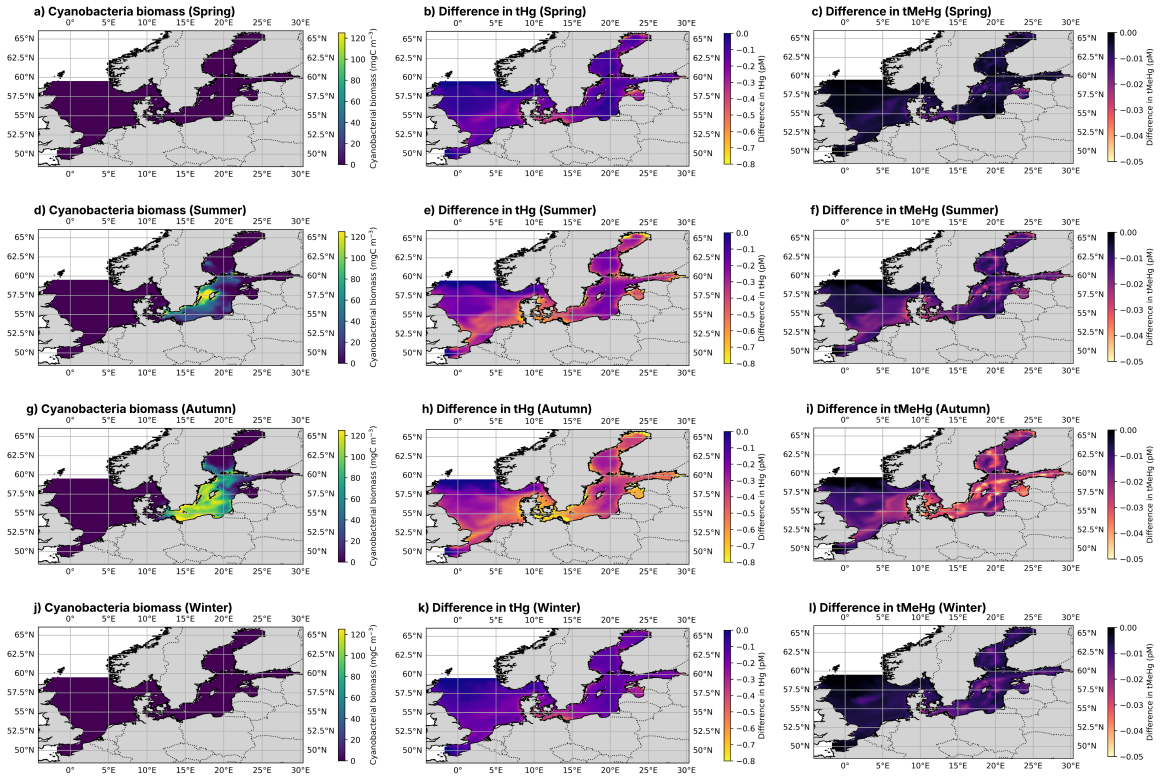

Figure 3.12: Cyanobacterial biomass and seasonal differences in tHg and tMeHg between the base case and the scenario without biogenic reduction.

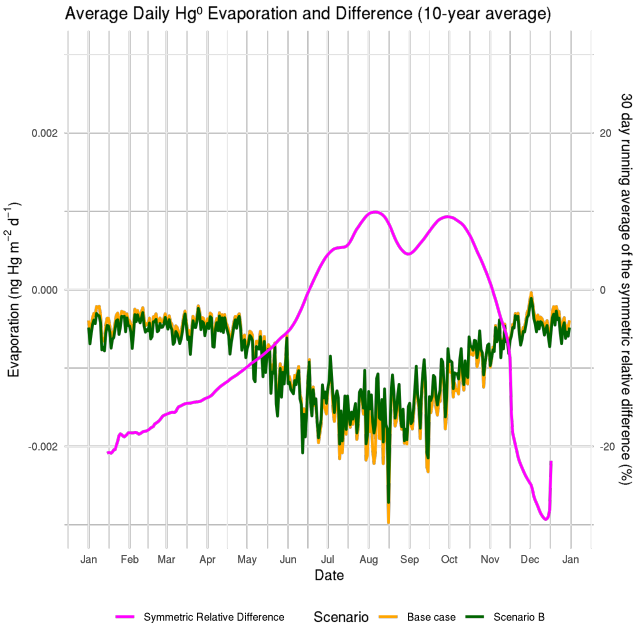

Figure 3.13: The 10-year average daily atmospheric exchange of Hg0 between the atmosphere and the sea surface in the base case and scenario c (no bioaccumulation nor biogenic reduction).

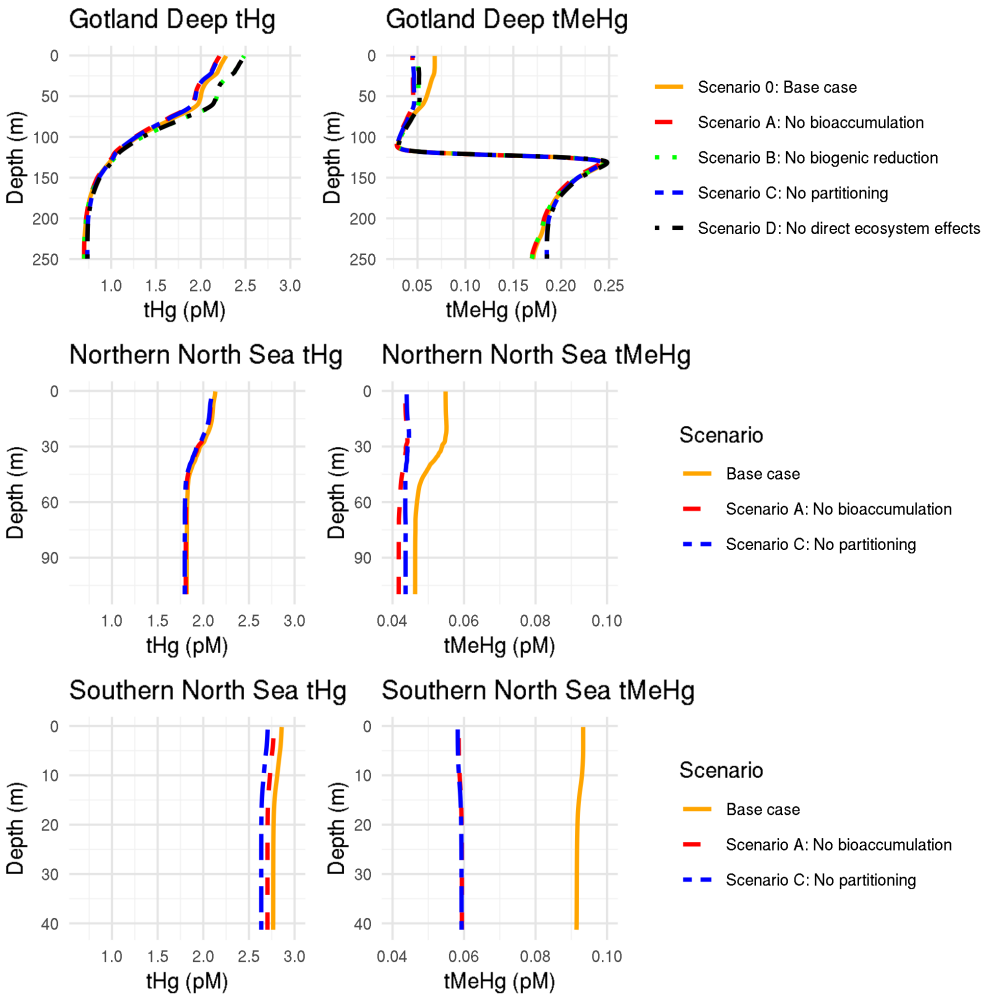

Figure 3.14: Depth profiles of tHg and tMeHg in the three setups with different model scenarios. In the Gotland Deep, the scenario without biogenic reduction (green) has an increased tHg content. This shows that biogenic reduction can reduce the yearly average water column Hg when cyanobacteria are present for part of the year. Setups without binding to detritus and DOM (blue) have lower tHg in the surface layer. This effect is strongest in the North Sea. Setups without binding to detritus and DOM (blue) also have reduced tMeHg in oxic water, but the effect is smaller than for tHg. In the Gotland Deep anoxic water, the only noticeable effect is caused by binding to detritus and DOM. In this setup, without this, there is both more tHg and tMeHg in the anoxic deep water. In all setups, runs with bioaccumulation (orange) have more tMeHg than without bioaccumulation (red). The Southern North Sea has a slightly lower amount of tHg than the Northern North Sea and Gotland Deep setups.

3.4.4 The unique properties of Hg as drivers of these results

These results are partially driven by the unique properties of Hg as a pollutant. Because Hg as an element is stable but can be present in both methylated and nonmethylated forms, it behaves radically differently than a pollutant that would have a constant total concentration. We find that this is the case for two reasons. First, the concentration of Hg^0 in the surface layer is in constant exchange with the atmosphere. If the fraction of Hg present as Hg^0 is reduced, because Hg^{2+} is bound to the biota, the evaporation of Hg^0 will be reduced until a new equilibrium with a higher tHg content is reached. Secondly, when $MMHg^+$ is removed from the water column due to bioaccumulation, only a small amount of tHg is removed ($< 3\%$), which means that methylation of Hg^{2+} into $MMHg^+$ is reduced by only a small amount. This would favor the net production of $MMHg^+$ which leads to an increase in tMeHg.

3.5 Summary

In this study, we hypothesized that the ecosystem is an essential part of the marine Hg cycle. We quantified the impact of the ecosystem on the marine Hg cycle by simulating a 1D water column with and without bioaccumulation, biogenic reduction, and partitioning into detritus and dissolved organic matter (DOM). Furthermore, we ran a 3D model for the North and Baltic Seas with and without bioaccumulation to analyze the spatial effects. Our analysis focused on the effects of these ecosystem interactions on total Hg (tHg) and total methylated Hg (tMeHg) concentrations in the water column and the intercompartmental fluxes.

Our model demonstrates the complex differences in bioaccumulation between different species of Hg. The model accurately reproduces bioaccumulation at the base of the food web as shown in Table 3.6 and models biomagnification to higher trophic levels according to observations for both Hg^{2+} and $MMHg^+$ as shown in Fig. 3.8. Although our model underrepresents $MMHg^+$ in cod compared to the observed mean, this underrepresentation is still within the observations and is explained by an underrepresentation of the trophic level as shown in Table 3.4. It is important to note that we wanted to implement realistic bioconcentration and trophic transfer rates to not over-tune the model. Several interactions, such as, for example, cannibalism within the functional groups or even the same species, can increase bioaccumulation in ways that are not captured by the model, which would result in both increased bioaccumulation and trophic levels.

The impact of the ecosystem on the MeHg cycling is very strong. In idealized 1D setups, bioaccumulation increases the average tMeHg content by 44% in the Southern North Sea, by 13% in the Northern North Sea, and in the Gotland Deep above the mixed layer depth by 22% as shown in Fig. 3.11. The surge in tMeHg attributed to bioaccumulation is most notable during plankton blooms, where phytoplankton absorbs a large portion of tMeHg, shielding bioaccumulated $MMHg^+$ from demethylation processes. This $MMHg^+$ is released to the water column towards the end of the year, where less solar radiation, more particles, more mixing, and more cloud coverage reduce photodemethylation. Our models show that the increase in tMeHg is strongly related to average biomass. And that an increase of 4.5 mgC m^{-3} in the average biomass content will result in a 1% increase in tMeHg due to bioaccumulation.

The model reveals regional and seasonal differences in how the ecosystem influences Hg cycling and bioaccumulation across the North and Baltic Seas. The ecosystem increases tHg and tMeHg mostly in highly productive shallow coastal regions, with a reduced effect in deeper, less productive zones. In the Baltic Sea, our findings quantify the average reduction in tHg due to bioaccumulation and cyanobacterial-induced biogenic reduction as a 7% reduction in tHg above the mixed layer depth.

The 3D simulation expands on this by visualizing the spatial pattern and allowing us to quantify the effect of bioaccumulation on the Hg budget of the North and Baltic Seas while taking into account spatial variability and horizontal transport. The average tMeHg content increases by 10%, but this increase is caused by an increase in the North Sea and the Danish straits, while there is a decrease in tMeHg in large parts of the Baltic Sea.

3.5.1 Conclusion

This study demonstrates and quantifies the complex role of the ecosystem in shaping Hg speciation and the influence of physical, biochemical, and ecological factors. In addition, it shows the sensitivity of parameterization in modeling and shows that evaluating ecosystem parameters such as the trophic level is essential to comprehend the results of bioaccumulation modeling. Here, we show that bioaccumulation does have notable feedback effects on Hg cycling and therefore should be included in any marine Hg model, even in cases where bioaccumulation is not of direct interest. We conclude that the ecosystem has a direct effect on Hg cycling by;

- The ecosystem increases marine tMeHg
  - Increase in tMeHg up to 77%
  - Increase of the 10-year average tMeHg up to 44%
  - An increase of 4.5 mgC $^{-3}$ average biomass leads to a 1% increase in tMeHg.
- Facilitate the burial of Hg by transporting Hg below the thermocline in deep unmixed water via the sinking of detritus
- Cause a wintertime increase in both aquatic and tMeHg permanently mixed productive coastal water

Because of this we conclude that the ecosystem has essential feedback on marine Hg cycling.

3.6 Future outlook

It is important to continue improving our models and to increase our understanding of the mechanisms that drive Hg bioaccumulation and cycling. More efforts should be directed toward understanding the nuanced interactions between Hg cycling and biogeochemical processes, trophic interactions, and ecosystem structure, all of which influence Hg speciation and fate in marine ecosystems. Typically, bioaccumulation is thought of as an add-on to model additional end members, and thus as non-essential when modeling global transport and air-sea exchange. We demonstrate that this is not the case and that bioaccumulation plays an important role in Hg cycling in coastal oceans.
To support the Minamata Convention, a solid understanding of the Hg cycle in marine environments is important for designing effective management strategies that aim to mitigate Hg contamination and minimize its impact on aquatic ecosystems and human health. By improving the models and by incorporating new advancements in field observations and experimental studies, we can increase our ability to predict and manage Hg pollution, safeguarding both the environment and human well-being.

Conflict of interest

None of the authors declare any competing interest.

Funding

This research has been funded by the European Union's Horizon 2020 research and innovation programme under the Marie Sklodowska-Curie grant agreement no. 860497.

3.7 Contribution per author

The author contributions are listed in Table 3.9.

Table 3.9: . Contributions per Author. Authors are: David Johannes Amptmeijer (DA), Dr. Johannes Bieser (JB), Dr. Ute Daewel (UD), Elena Mikheeva (EM), and Prof. Dr. Corinna Schrum (CS).

Contributor role	**Role definition**	**Authors**
Conceptualisation	Identified the need for bioaccumulation in the MERCY v2.0 model	JB, CS
	Conceptualised the study	DA, JB, CS
Methodology	Coupling of MERCY v2.0 to FABM	DA, JB
	Developing the physical setups	EM
	Developed ECOSMO E2E to better suit bioaccumulation	DA, UD
	Design and implement the different scenarios	DA
Validation	Validate if Hg cycling matches in the 1D MERCY v2.0 model	JB, DA
	Validate hydrodynamic conditions	EM, CS, DA
	Validate carbon cycling	DA, UD
Writing	Writing of the original draft	DA, JB
	Reviewing the original draft and quality control	JB, CS, UD, EM, DA
Supervision	Supervising the development of the work	CS, JB
Funding acquisition	Acquired funding via the GMOS-Train ITN	JB, CS

Bridging chapter

Initially, I designed the model to incorporate bioaccumulation into MERCY v2.0 as accurately as possible. The study performed in Chapter 3, in which I evaluated the feedback between bioaccumulation and Hg speciation, was a logical start as currently MERCY v2.0 is the most comprehensive marine Hg cycling and bioaccumulation model in use and, therefore, the only model that could attempt to quantify this feedback. As mentioned above, the bioaccumulation in the MERCY v2.0 model takes many more interactions into account than other bioaccumulation models, such as the bioaccumulation of Hg^{2+} and the direct uptake of Hg^{2+} and $MMHg^{+}$ from the water column at higher trophic levels. It is important to remain critical about what seemingly minor interactions should be omitted from the model, as small effects can compound into big effects. However, everything comes at a cost, in this case, computational resources and model complexity. The MERCY v2.0 model has 4 Hg state variables per biological functional group, namely both bioaccumulated and biomagnified Hg^{2+} and $MMHg^{+}$. This is a lot considering that most models, such as those by Rosati et al. 2022, Schartup et al. 2018, and Zhang et al. 2020, only have 1 state variable per functional group. Namely bioaccumulated $MMHg^{+}$. This means that for 2 zooplankton, 2 fish, and 1 macrobenthos group the MERCY V2.0 model has 15 potentially redundant state variables. Since I can run my model in 1D, and therefore computational resources are not as much of a constraint, I can evaluate the relevance of each of these state variables and evaluate which interactions are essential to account for. If the bioaccumulation is incorporated into larger models, such as the ICON-O 3D global earth system model, adding 15 redundant state variables is an indefensible misuse of resources. Therefore I decided to critically evaluate the design choices I made in the model by evaluating how much the bioaccumulation of Hg and bioconcentration of $MMHg^{+}$ in higher trophic levels contribute to bioaccumulation.

Figure 3.15: Hermit crab (*Pagurus bernhardus*). Picture taken by Dr. Eric Wurtz.

CHAPTER 4

Bioconcentration in consumers: a key driver of MeHg in fish

David J. Amptmeijer[1], Johannes Bieser[1]
[1]Matter Transport and Ecosystem Dynamics, Helmholtz-Zentrum Hereon, Geesthacht, Germany

The ability of monomethylmercury ($MMHg^+$) to bioaccumulate in seafood is of concern due to its neurotoxic properties. Understanding the bioaccumulation of $MMHg^+$ is challenging because the $MMHg^+$ content at higher trophic levels depends on both bioconcentration and biomagnification. Furthermore, Hg can occur in several chemical species, including Hg^{2+} and $MMHg^+$, which both bioaccumulate. Although the dominant pathway for $MMHg^+$ bioaccumulation into seafood is the bioconcentration of $MMHg^+$ in primary producers and the subsequent biomagnification to higher trophic levels, other pathways can contribute to $MMHg^+$ bioaccumulation. In this study, we quantify the importance of the bioaccumulation of Hg^{2+} and the bioconcentration of $MMHg^+$ in higher trophic levels in the bioaccumulation of $MMHg^+$ in high trophic level fish by running a fully coupled 1D water column Hg bioaccumulation model under 3 hydrodynamic regimes typical for the North and Baltic Seas. We find that Hg^{2+} bioaccumulation does not influence the bioaccumulation of $MMHg^+$ but the bioconcentration of $MMHg^+$ plays an important role. Although direct bioconcentration accounts for $< 15\%$ of $MMHg^+$ bioaccumulation in cod, the cumulative effect of bioconcentration on all trophic levels increases the $MMHg^+$ content of cod by 28-48%. We show that up to the highest trophic level modeled (TL = 3.7), the percentage of $MMHg^+$ that originates from consumer bioconcentration increases with an average of 15% per trophic level. These results demonstrate that bioconcentration in consumers is essential to accurately model the bioaccumulation of $MMHg^+$ at higher trophic levels.

Keywords: Mercury, Bioaccumulation, ECOSMO. Macrobenthos

Publication Status

This chapter is based on the following preprint:

Amptmeijer, D., & Bieser, J. (2025). *Bioconcentration as a key driver of Hg bioaccumulation in high trophic level fish*. *EGUsphere*, **2025**, 1–16. *Preprint*. https://doi.org/10.5194/egusphere-2025-312

Grahical abstract of chapter 4

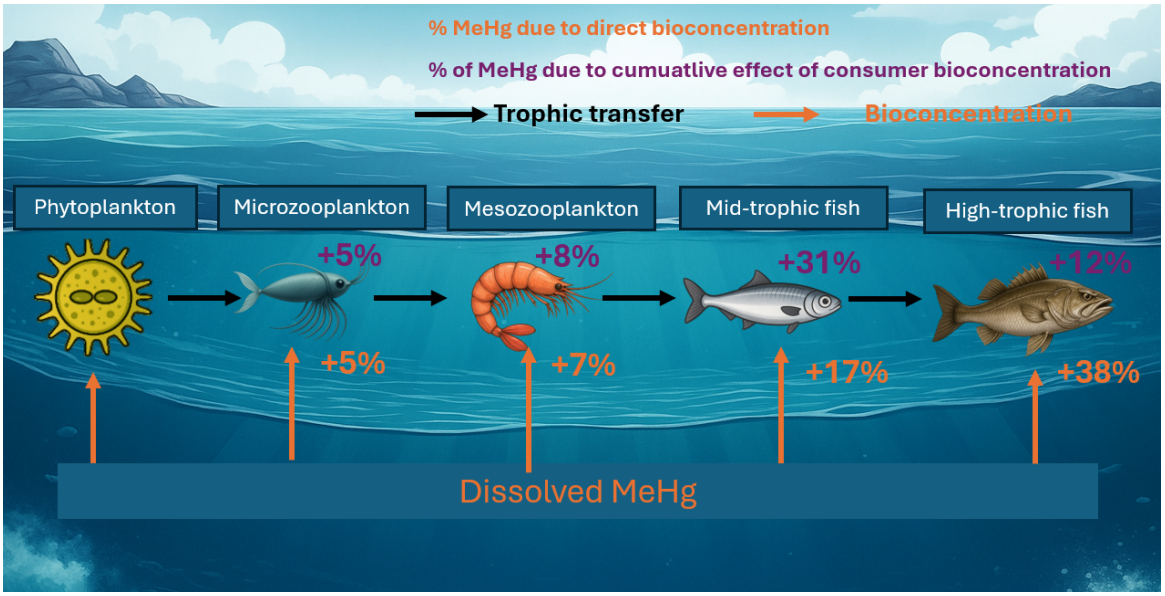

Figure 4.1: Eventhough the direct percentage of $MMHg^+$ bioaccumulated by high trophic level fish via bioconcentration (uptake direclty from the watercolumn) is low, the cumulative effect of bioconcentration in consumers is high. The image is made of several sub-images that are generated using openART and GPT 4.1.

4.1 Introduction

The natural element mercury (Hg) is currently on the list of 10 substances of most concern by the World Health Organization (WHO 2020). This is because Hg can be methylated into monomethyl mercury ($MMHg^+$). $MMHg^+$is a potent neurotoxin produced by microbial methylation of inorganic mercury. It biomagnifies through aquatic food webs, accumulating in predatory fish at levels that can impair human neurological development and function when consumed. Aquatic foods account for more than 15% of the world's protein consumption, and preserving this as a safe and reliable food source is essential to feed an increasing population (Boyd et al. 2022). Despite recent efforts, the bioaccumulation of $MMHg^+$ in the marine environment is a complex topic and is not yet fully understood. Part of the complexity of understanding $MMHg^+$ bioaccumulation and toxicity is that Hg can undergo speciation and occur in the environment in several chemical forms with distinct physical and chemical properties (Bieser et al. 2023). In particular, there are dissolved Hg (Hg^{2+}), dissolved elemental gaseous Hg (Hg^0), $MMHg^+$, and dissolved dimethylmercury (DMHg).

Often both $MMHg^+$ and DMHg are combined and are termed methylmercury (MeHg). The importance of DMHg is currently debated. Although DMHg is uncharged, which would give it higher permeability to migrate through cell membranes, it is assumed that it does not bioaccumulate to a significant degree (Morel et al. 1998). The higher bioaccumulation of $MMHg^+$ compared to DMHg can be attributed to several reasons; $MMHg^+$ can be absorbed by phytoplankton by cell-dependent factors, such as membrane channels (Garcia-Arevalo et al. 2024), volatile DMHg can more easily migrate out of cells and evaporate from the water column, and $MMHg^+$ can strongly bind to sulfhydryl (-SH) groups in organic material, notably cysteine, which traps toxic $MMHg^+$ in the cell. Although DMHg appears to be a common form of Hg in deeper water, there are no measurements in the North and Baltic Seas that would differentiate between DMHg and Hg^0, and its role can therefore not be assessed in the model (Fitzgerald et al. 2007). Since DMHg is susceptible to photodegradation, we can assume that it does not play an important role in the coastal water investigated in this study until better observational studies confirm or correct this assumption (West et al. 2022) .

Both Hg^{2+} and $MMHg^+$ bioaccumulate in the marine food web. However, due to the higher toxicity and bioaccumulation potential of $MMHg^+$, the bioaccumulation of $MMHg^+$ is the most important concern and

receives the most attention. There are 3 ways in which species bioaccumulate $MMHg^+$; bioconcentration, biomagnification, and in vivo methylation.

4.1.1 Used terminology: bioaccumulation, bioconcentration, and biomagnification

Bioaccumulation in the marine environment refers to the total increase in pollutants in biota compared to that in the water. This can be quantified in nature by measuring the concentration of pollutants in both water and biota and estimating the difference. This is typically expressed as the bioaccumulation factor, BAF. For example, the bioaccumulation of $MMHg^+$ in organisms *i* can be calculated based on observations as:

$$BAF_i^{MMHg^+} = \frac{C_i^{MMHg^+}}{C_w^{MMHg^+}} \tag{4.1}$$

In which,
$BAF_i^{MMHg^+}$ - The bioaccumulation factor of $MMHg^+$ for organism *i* [L kg^{-1}]
$C_i^{MMHg^+}$ - The concentration of $MMHg^+$ in organisms *i* [ng Hg kg^{-1}]
$C_w^{MMHg^+}$ - The free concentration of $MMHg^+$ in the water [ng Hg L^{-1}]

Since the BAF can be based on field measurements, it is a commonly used metric to estimate the link between the concentrations of pollutants in seawater and those in biota. In this study, we are interested in separating the bioaccumulation into separate pathways: the direct uptake from the water (bioconcentration) and the increase in pollutants due to trophic interactions (biomagnification).
Bioconcentration, is the increase in the concentration of Hg in biota directly due to uptake from the water. Because the process of bioconcentration relies on the exchange of Hg between the dissolved phase and an organism, it depends on the surface area of the organic material that is in contact with the water. Due to this, small organisms, such as bacteria and phytoplankton, have a greater ability to bioconcentrate Hg (Mason et al. 1996; Pickhardt et al. 2006). However, the bioconcentration process is complicated and recent studies show that the bioconcentration of $MMHg^+$ is influenced by cell-dependent factors, such as the thickness of the phycosphere and the availability of transmembrane channels, while this is not the case for Hg^{2+} Garcia-Arevalo et al. (2024). Bioconcentration is typically defined by the bioconcentration factor (BCF). The BCF for $MMHg^+$ in organism *i*, can for example be calculated as

$$BCF_i^{MMHg^+} = \frac{C_i^{MMHg^+}}{C_w^{MMHg^+}} \tag{4.2}$$

In which,
$BCF_i^{MMHg^+}$ - The bioconcentration factor of $MMHg^+$ for organism *i* [L kg^{-1}]
$C_i^{MMHg^+}$ - The concentration of $MMHg^+$ in organisms *i* due to direct uptake of $MMHg^+$ from the water [ng Hg kg^{-1}]
$C_w^{MMHg^+}$ - The free concentration of $MMHg^+$ in the water [ng Hg L^{-1}]

In this Hg could then either refer to Hg^{2+} or $MMHg^+$. Note that this defines the theoretical BCF. In nature it is typically impossible to directly measure the BCF, as it would be impossible to separate between $MMHg^+$ that is taken up directly from the water and $MMHg^+$ that is ingested via food. Bioconcentration is the most important step in bioaccumulation and phytoplankton can have a BCF of $MMHg^+$ between 2E4 $^{-1}$ and 6.4E6 L kg^{-1} higher than $MMHg^+$ in surrounding water (Gosnell and Mason 2015).
Biomagnification is when $MMHg^+$ reaches higher concentrations at progressively higher trophic levels. The biomagnification factor, the fractional increase in $MMHg^+$ with each trophic level, is estimated to be 7.0 $\pm$ 4.9 (Harding et al. 2018; Lavoie et al. 2013). This means that in addition to the high increase in $MMHg^+$ in phytoplankton, there is a large increase in $MMHg^+$ at every consecutive trophic level. Many seafoods consist of high-trophic animals, such as cod, tuna, or marlin, which can have trophic levels between 4 and 4.8 (Nilsen et al. 2008; Sarà and Sarà 2007). Biomagnification can increase the already high levels

of $MMHg^+$ in phytoplankton by up to another factor $11.9^{4.8} \approx 145420$. This is typically defined by the biomagnification factor, BMF, which can be calculated for organism i, preying on organism j for $MMHg^+$ as:

$$BMF_{i,j}^{MMHg^+} = \frac{C_i^{MMHg^+}}{C_j^{MMHg^+}} \tag{4.3}$$

In which,
$BCF_j^{MMHg^+}$ - The biomagnification factor for trophic consumption of *j* by *i* [unitless]
$C_j^{MMHg^+}$ - The concentration of $MMHg^+$ in the organism *j* [ng Hg kg $^{-1}$]

The biomagnification factor of $MMHg^+$ is extremely high, Lavoie et al. (2013) estimates the diet-weighted average BMF for $MMHg^+$ as 8.1 $\pm$ 7.2 while it is only 4.7 $\pm$ 4.7 for Hg^+. This combined with the higher toxicity of $MMHg^+$ is the reason why the bioaccumulation of $MMHg^+$ is of much higher concern than the bioaccumulation of Hg^{2+}. A final way in which organisms can bioaccumulate $MMHg^+$ is *in vivo* Hg methylation.

In vivo methylation occurs when animals take other forms of Hg and transform it into $MMHg^+$ in organisms. Although the existence of this process has been demonstrated in specific organisms such as cuttlefish, it is poorly understood and only recently gaining attention (Gentè et al. 2023). There is no direct evidence of in vivo methylation in the animals that we model, so it is not implemented in this model.
Overall the dominant pathway of bioaccumulation, the bioaccumulation of $MMHg^+$ is the bioconcentration of $MMHg^+$ in phytoplankton and consequent biomagnification. The important route is quantified by Wu et al. (2019) using a meta-analysis. They find that the concentration of MeHg at the base of the food web predicts 63% of the observed variability in high trophic level fish, while the remaining 37% is controlled by factors such as the dissolved organic matter content and oligotrophy.

4.1.2 Current models

Multiple models have been developed to explain $MMHg^+$ bioaccumulation in marine ecosystems. Key examples include trophic transfer (Schartup et al. 2018), base-level accumulation (Zhang et al. 2020), planktonic bioaccumulation in the Mediterranean Sea (Rosati et al. 2022), MeHg dynamics on the Beaufort Shelf (Li et al. 2022), and speciation plus accumulation in the North and Baltic Seas (Bieser et al. 2023).
In all of the previous models, bioconcentration of $MMHg^+$ is included as it is an essential driver. These models, however, do not include higher trophic level animals such as fish. It is concluded in Schartup et al. (2018) that the bioconcentration of $MMHg^+$ in zooplankton is not a major contributor and contributes less than 15% of total MeHg bioaccumulation. Consequently, in later models such as presented by Rosati et al. (2022) this interaction is not included because their model focuses on the base of the food web. The study performed by Li et al. (2022) includes the process of bioconcentration for invertebrates, but it is not included for vertebrates. This means that our model would be the first model to include bioconcentration at every trophic level.
The bioaccumulation of Hg^{2+} is much less studied and not incorporated in any of the above-mentioned models. This is because Hg^{2+} is much less toxic than $MMHg^+$ and therefore comparably understudied. While data is limited, this raises the speculative question if the link between the bioaccumulation Hg^{2+} and $MMHg^+$ is not underestimated as Hg^{2+} and $MMHg^+$ are in active equilibrium in the water.
The ECOSMO-MERCY coupled system, which is used by Bieser et al. (2023) and Chapter 3 is the only coupled model that models the bioaccumulation of Hg^{2+} and $MMHg^+$ at higher trophic levels such as fish, while incorporating bioconcentration at every trophic level.

4.1.3 The hypotheses

While $MMHg^+$ is more concerning than Hg^{2+} at higher trophic levels, Hg^{2+} can form up to 98% of the bioaccumulated Hg in phytoplankton (Pickhardt and Fisher 2007). This results in a large removal of Hg^{2+} during the phytoplankton bloom period (Soerensen et al. 2016). **Our first hypothesis in this study is that**

the bioaccumulation of Hg^{2+} can lower the bioaccumulation of $MMHg^{+}$ by removing Hg^{2+}, which in turn cannot be methylated and accumulated as $MMHg^{+}$.

A counterpoint is that Chapter 3 does not show an average change in tHg and aqueous Hg caused by bioaccumulation, including the bioaccumulation of Hg^{2+}. While this indicates that there is no likely effect of Hg^{2+} bioaccumulation on $MMHg^{+}$ bioaccumulation, it does not exclude this. Most of the bioaccumulation of Hg^{2+} and $MMHg^{+}$ takes place at the same time and space, in the surface layer during the phytoplankton bloom. While there is no change in the average tHg, the results of Chapter 3 show seasonal variation. This means that even if the average concentrations of tHg are not altered, there may still be an effect of Hg^{2+} bioaccumulation on $MMHg^{+}$ bioaccumulation. It could be theorized that as the ecosystem reduces tHg during the phytoplankton bloom it would reduce dissolved $MMHg^{+}$, as this is in active equilibrium with other Hg species and therefore reduce the availability of $MMHg^{+}$ for bioaccumulation.

Most $MMHg^{+}$ in high trophic levels originates from their diet (Lavoie et al. 2013). So it is often assumed that the bioconcentration of $MMHg^{+}$ does not play an essential role in high trophic level $MMHg^{+}$ bioaccumulation. However, this ignores the fact that bioconcentration plays a role at all trophic levels. If both micro and mesozooplankton, for example, have 5% of $MMHg^{+}$ originating from bioconcentration. Mesozooplankton will have 5% less $MMHg^{+}$ in their diet, composed of microzooplankton, and an additional 5% less from its lack of bioconcentration. This results in a total reduction of 10%. **The second hypothesis in this paper is that the bioconcentration of $MMHg^{+}$ in consumers leads to a large increase in $MMHg^{+}$ at higher trophic levels**.

Studies that have analyzed the relative contribution of bioconcentration in the bioaccumulation of $MMHg^{+}$ in fish found that in freshwater fine-scale dace *Phoxinus neogaeus*, the bioconcentration accounts for up to 15% of the total bioaccumulation of $MMHg^{+}$ (Hall et al. 1997). A study by Wang and Wong (2003) found that in marine sweetlips *Plectorhinchus gibbosus* bioconcentration in fish can dominate total $MMHg^{+}$ concentration, if they eat food with low $MMHg^{+}$ levels, while intake from food dominates total $MMHg^{+}$ uptake when fish eat food with higher $MMHg^{+}$ levels. This means that there will be an effect of $MMHg^{+}$ bioaccumulation in higher trophic levels as it is a direct flux of $MMHg^{+}$ into the organism. In this study, we want to expand this and quantify the cumulative effect of $MMHg^{+}$ bioconcentration in all consumers. This allows us to evaluate if consumer bioconcentration is indeed a small percentage of total $MMHg^{+}$, or if it is a major contributor to the total $MMHg^{+}$ concentrations.

It is important to analyze these interactions using models as they cannot be fully understood using field and laboratory studies. This is because Hg^{2+} and $MMHg^{+}$ are in active equilibrium and we cannot measure $MMHg^{+}$ in a system where phytoplankton would not absorb Hg^{2+}. The effect of bioconcentration of $MMHg^{+}$ can also not easily be measured. It is possible to measure the direct uptake and release of $MMHg^{+}$ by higher trophic levels from the water column. This is done, for example, to estimate the bioconcentration rates of Hg^{2+} and $MMHg^{+}$ in sweetlips by Wang and Wong (2003). The complexity is that the origin (bioconcentration or biomagnification) of $MMHg^{+}$ cannot be measured in observational studies, and part of the $MMHg^{+}$ that is consumed by higher trophic levels is bioconcentrated in consumers at the lower trophic level, making it impossible to measure the full importance of bioconcentration in consumers.

To test the 2 hypotheses that Hg^{2+} bioaccumulation decreases $MMHg^{+}$ bioaccumulation and that $MMHg^{+}$ bioconcentration increases it, we quantify the effect of bioaccumulation of Hg^{2+} and the bioconcentration of $MMHg^{+}$ on the bioaccumulation of $MMHg^{+}$. We do this by running the fully coupled GOTM-ECOSMO-MERCY coupled system used in Chapter 3 with and without the bioaccumulation of Hg^{2+} and bioconcentration of $MMHg^{+}$. Then we analyze the bioaccumulation of $MMHg^{+}$ at different trophic levels in these different scenarios and finally evaluate the importance of both interactions.

The model is run using 3 idealized 1D water column setups to represent different hydrological conditions. The setups represent the coastal hydrodynamics found in the North and Baltic Seas.

Modeled region

The first North Sea setup is the **permanetenly mixed- southern North Sea** at (54°15′00.0″ *N* 3°34′12.0″ *E*). The 41.5 m deep location of this setup is characterized by having constant water-column mixing. This remixing of nutrients within the euphoric zone creates good conditions for phytoplankton growth. Additionally, since the water column is mixed during the bloom period, macrobenthos can feed directly from the

phytoplankton bloom, which results in a late population of macrobenthos. This results in a high biomass turnover rate, and macrobenthos are an important food source for predatory fish (Heip et al. 1992). The southern North Sea is rich in nutrients, and the phytoplankton bloom is often light-limited. Diatoms typically dominate the phytoplankton bloom in spring until silicate limitations reduce their growth, and flagellates can become dominant (Emeis et al. 2015).

The second setup is the **seasonally mixed- Northern North Sea** at (57°42′00.0″ *N* 2°42′00.0″ *E*). This 110 m deep setup is only seasonally mixed. The northern North Sea is still rich in nutrients, resulting in similar high phytoplankton growth, which is dominated by diatoms in spring and succeeded by flagellates in summer, as is the case in the southern North Sea (Bresnan et al. 2009). A key difference between the southern and northern North Sea setups is that in the northern North Sea setup, macrobenthos cannot feed directly on the bloom but predominantly feed on sinking detritus. This results in lower macrobenthos biomass and lower importance of macrobenthos in the diet of top predators (Heip et al. 1992).

The final set is the **permanently stratified- Gotland Deep** (57°18′00.0″ *N* 20°00′00.0″ *E*). This setup is different from the 2 North Sea setups in a few ways. First, the Baltic Sea, in general, is not limited by silicate, resulting in a dominance of diatoms in the phytoplankton bloom. In the Gotland Deep specifically, silicate limitation can occur, but diatoms will still be more dominant. Gotland Deep has a very low salinity (7 g l^{-1}), is strongly stratified, and can be eutrophied in phosphate. This results in perfect growth conditions for nitrogen-fixing cyanobacteria that can form a major part of the total phytoplankton biomass in the autumn when nitrogen limitations limit the growth of other phytoplankton (Kahru and Elmgren 2014). The presence of cyanobacteria can alter bioaccumulation because they can reduce dissolved Hg^{2+} to volatile Hg^0, which increases Hg evaporation and therefore lowers the concentration (Kuss et al. 2015). This can reduce the average Hg content by up to 8% Chapter 3. At the same time, the small size of the cyanobacteria gives them an extremely high surface: biomass ratio, resulting in a very high bioconcentration factor of $MMHg^+$ (Pickhardt et al. 2006). Finally, the Gotland Deep has anoxic water below the thermocline; because of this, there is no macrobenthos (Conley et al. 2009).

The 1D setups are the same as those used in Chapter 3 and are described there in more detail. The physics of the setups is based on the Generalized Ocean Turbulence Model (GOTM) (Bolding et al. 2021), the biogeochemistry is based on the ECOSMO E2E (Daewel and Schrum 2013), and the Hg chemistry is based on the MERCY v2.0 model (Bieser et al. 2023).

Quantifying the importance of the bioaccumulation of Hg^{2+} and bioconcentration of $MMHg^+$ in consumers on $MMHg^+$ bioaccumulation into higher trophic levels under these idealized circumstances will provide a unique insight into the drivers of the bioaccumulation of $MMHg^+$ bioaccumulation and increase our fundamental understanding of this process. Additionally, it is important to quantify the importance of these interactions using lighter models because their inclusion in models comes at a cost. Especially, the implementation of the bioaccumulation of Hg^{2+} is done by adding 1 state variable to the model per biota functional group, or 2 state variables if the biomagnified and bioconcentrated Hg^{2+} is treated as separate variables, as is done in the model used in this study. While this is feasible without much concern in the 1D water column models that we use in this study, when running earth system models, adding insignificant state variables becomes an unnecessary waste of computational resources which results in the wasteful expenditure of research funds and energy.

4.2 Methodology

To quantify the importance of Hg^{2+} bioaccumulation and $MMHg^+$ bioconcentration on the bioaccumulation of $MMHg^+$ we modeled the bioaccumulation of $MMHg^+$ in three different scenarios using three idealized 1D water column models representing different hydrodynamic regimes typical for the North and Baltic Seas.

4.2.1 Model

Hypotheses are evaluated using the Generalized Ocean Turbulence Model (GOTM) (Bolding et al. 2021) that is coupled to the ECOSMO E2E ecosystem model (Daewel et al. 2019) and the MERCY v2.0 mercury speciation model (Bieser et al. 2023). The models are coupled using the Framework for Aquatic Biogeo-

chemical modeling (FABM) (Bruggeman and Bolding 2014). This setup is chosen because it has been used and evaluated in previous studies to analyze the bioaccumulation and cycling of Hg in the North and Baltic Seas and it is the only fully coupled model to incorporate the bioaccumulation of Hg^{2+} and the bioconcentration of $MMHg^{+}$ at higher trophic levels.

GOTM

GOTM is used to simulate the hydrodynamics of the 1D water column models. GOTM is a 1D turbulence model that computes the 1D version of the transport equation of temperature, momentum, and salinity. It does this while being nudged to observational datasets. GOTM simulations are designed using the iGOTM tool (https://igotm.bolding-bruggeman.com/). This tool compiles the observational datasets used for the GOTM simulation and estimates the water depth based on the gridded bathymetry data (1/240° resolution) (GEBCO Bathymetric Compilation Group 2020), the ECMWF ERA5 data for meteorological data, the TPOX-9 atlas for tides (1/30° resolution)(Egbert and Erofeeva 2002), and for salinity and temperature, it uses the wold ocean Atlas (0.25° resolution) (Garcia H.E. et al. 2019). The state is solved every 60 seconds using forward Euler differential equations. The setups have 1 grid cell per meter and the variables are exported as daily means for the post-processing analyses.

ECOSMO E2E

The ecosystem model used in this study is the ECOSMO E2E ecosystem model. The ECOSMO E2E ecosystem model is an intermediately complex ecosystem model that uses a functional group approach to estimate the biomass and carbon fluxes in the North and Baltic Seas. The version used here has 3 functional groups of phytoplankton; diatoms, flagellates, and cyanobacteria, 2 functional groups of zooplankton; microzooplankton, and mesozooplankton, 2 functional groups of fish, and 1 group of macrobenthos. The basic version of the model is published by Daewel et al. (2019), but the version used here has some modifications to make it more suitable for bioaccumulation. The modification included reducing carbon uptake efficiencies at higher trophic levels and the addition of 1 more fish functional group. This is described in detail in Chapter 3.

MERCY v2.0

The MERCY v2.0 model links atmospheric Hg to $MMHg^{+}$ in fish. It does this by estimating air-sea exchange and wet deposition of Hg based on the CMAQ-Hg model and calculating the marine cycling while taking into account marine speciation and bioaccumulation. It uses 35 state variables to estimate Hg speciation, transport, and bioaccumulation. Estimates the partitioning of Hg^{2+} and $MMHg^{+}$ into dissolved organic carbon, particulate, and bioaccumulation based on ecosystem parameters derived from the ecosystem model ECOSMO E2E (Bieser et al. 2023).

4.2.2 Bioaccumulation in the model

The bioaccumulation of Hg^{2+} and $MMHg^{+}$ is the same as in Chapter 3. All functional groups of the biota can bioconcentrate both Hg^{2+} and $MMHg^{+}$ by default. This is implemented in the form of an active equilibrium in which the bioconcentrated Hg^{2+} or $MMHg^{+}$ on each interaction is changed by the uptake rate m^3 mgC d^{-1} multiplied by the biomass in mgC of the functional group and the concentration of Hg in ng Hg $^{-3}$. The release of Hg from the functional group is based on the respiration, mortality, and Hg release rate in d^{-1}. In addition to the bioconcentration, all consumer functional groups can take up Hg from the consumption of contaminated food. The uptake of Hg^{2+} or $MMHg^{+}$ from food depends on the assimilation efficiency of the food and Hg species. After Hg has been assimilated from food, $MMHg^{+}$ is released based on the mortality and respiration rate within the functional group, while there is an additional release rate for Hg^{+}. Since fish have a temperature-dependent respiration rate in the ECOSMO E2E model, this means that fish lose Hg from both bioconcentration and biomagnification faster in warmer water as their respiration, and thus Hg release rate increases with temperature. The bioconcentration rates for zooplankton are based on Tsui and Wang (2004), and those for fish are based on Wang and Wong (2003).

Post-processing analysis

The post-processing analysis is performed in R v4.4.1. Plots are generated using ggplot v3.5.0. and linear regression and statistics are calculated using ggpubr v0.6.0. A Wilcoxon signed rank test is performed to test the significance of differences and similarities between treatments. This is done because we assume that the trophic level influences the difference between the scenarios, which would mean that the differences between the scenarios are not normally distributed. The results are interpreted as $p < 0.05$ means a significant difference and $p > 0.05$ does not indicate a significant difference. Additionally, a Bayesian t-test is run using the BayesFactor v0.9.12-4.7 packages in R to assess the likelihood that the scenarios are different from or the same as the base case.

4.2.3 Scenarios

The model is run in 3 different scenarios. The "Base case", "No Hg^{2+} bioaccumulation" and "No $MMHg^{+}$ bioconcentration". The base case scenario is the same as the base case used in Chapter 3. For the "No Hg bioaccumulation" setup, all uptake rates of Hg^{2+} are set to zero. For the "No $MMHg^{+}$ bioconcentration" scenario, all consumer bioconcentrations of $MMHg^{+}$ and all Hg^{2+} uptake rates are set to zero.

4.3 Results and discussion

4.3.1 Bioaccumulation of Hg^{2+}

The effect of Hg^{2+} bioaccumulation on the bioaccumulation of $MMHg^{+}$ is shown in Table 4.1. The differences are low (1-5%). This is statistically evaluated, and the results are shown in Table 4.2. Wilcoxen's signed rank test shows that bioaccumulation of Hg^{2+} has no significant impact on the bioaccumulation of $MMHg^{+}$ ($p > 0.99$). Furthermore, the Bayesian t-test shows that the data are 2.9 times more likely under the null hypothesis of no effect than under the alternative hypothesis. This shows that Hg^{2+} bioaccumulation does not have a significant effect on $MMHg^{+}$ bioaccumulation (BF=0.35).

4.3.2 Bioaccumulation of $MMHg^{+}$

The $MMHg^{+}$ bioaccumulation for all biota functional groups in the different setups and scenarios and the percentage of bioaccumulated $MMHg^{+}$ originating from bioconcentration are shown in Table 4.1. The % bioconcentrated is calculated as $\text{Bioconcentrated (\%)} = \frac{\text{Bioconcentrated}}{\text{Bioaccumulated}}$ and the difference (%) is calculated as $\text{Difference (\%)} = \frac{\text{Scenario}}{\text{Default}}$. The values in red in the difference category indicate when the scenario causes a change larger than 10%. The values are based on the last 10 years of the simulation and the shallow 20m of the water column, to create an average value that we can compare between the setups.
These results show that the relative contribution of bioconcentration on the $MMHg^{+}$ content is low in microzooplankton (4-6%) while it is higher in mesozooplankton (5-10%) higher in fish 1 (13- 22%) while lower in fish 2 (8- 14%) and higher in macrobenthos (14- 25%). The relative contribution of direct bioconcentration on the $MMHg^{+}$ bioaccumulation in zooplankton, especially microzooplankton, is lower than in higher trophic levels of animals. In our model, this occurs because of the extremely high turnover rate of zooplankton. This "grow fast, die young" approach results in less $MMHg^{+}$ bioconcentration with higher relative contributions due to feeding caused by the high feeding rate of zooplankton.
In longer-lived fish, we see higher contributions of bioconcentration. Although these contributions are higher, they align with the experiments of (Wang and Wong 2003) and the observations of 15% by Hall et al. (1997). Both fish 1 and fish 2 have the same bioconcentration and release rates, so it is in line with expectations that the relative contribution of direct bioconcentration in fish 2 is lower than in fish 1 since it gets more $MMHg^{+}$ from its higher trophic level diet.
There is a great difference in the importance of bioconcentration of $MMHg^{+}$ in macrobenthos between the Southern and Northern North Sea. This difference is especially notable in the direct bioconcentration in macrobenthos, which is 25% of the total bioaccumulated $MMHg^{+}$ in the Northern North Sea and only 14% in the Southern North Sea. This difference is caused by the low intake of $MMHg^{+}$ from food

Table 4.1: The bioaccumulated $MMHg^+$, the percentage of bioaccumulated $MMHg^+$ that originates from bioconcentraton, and the bioaccumulated $MMHg^+$ in the scenario without bioaccumulation of Hg^{2+} and the bioconcentration of $MMHg^+$ in consumers and the difference to the default scenario. The % bioconcentrated is calculated as $\text{Bioconcentrated (\%)} = \frac{\text{Bioconcentrated}}{\text{Bioaccumulated}}$ and the difference (%) is calculated as $\text{Difference (\%)} = \frac{\text{Scenario}}{\text{Default}}$.

Gotland Deep							
	Default		No Hg^{2+} bioaccumulation		No $MMHg^+$ bioconcentration		Trophic Level
	(ng Hg mg-1)	Bioconcentrated (%)	(ng Hg mg-1)	Difference (%)	(ng Hg mg-1)	Difference (%)	-
Diatom	0.0050	100%	0.0050	0.%	0.0050	-0%	1
Flagellate	0.0096	100%	0.0096	0%	0.0096	-0%	1
Cyanobacteria	0.0152	100%	0.0152	0%	0.0152	0%	1
Microzooplankton	0.0130	5%	0.0130	0%	0.0123	-5%	2.0
Mesozooplankton	0.0190	5%	0.0191	0%	0.0180	-5%	2.2
Fish 1	0.0314	**16%**	0.0314	0%	0.0250	**-20%**	2.6
Fish 2	0.0647	8%	0.0647	0%	0.0464	**-28%**	3.5

Southern North Sea							
	Default		No Hg^{2+} bioaccumulation		No $MMHg^+$ bioconcentration		Trophic Level
	(ng Hg mg-1)	Bioconcentrated (%)	(ng Hg mg-1)	Difference (%)	(ng Hg mg-1)	Difference (%)	-
Diatom	0.0052	100%	0.0049	-5%	0.0048	-6%	1
Flagellate	0.0078	100%	0.0077	-2%	0.0076	-2%	1
Microzooplankton	0.0110	4%	0.0108	-2%	0.0103	-6%	2.0
Mesozooplankton	0.0139	6%	0.0140	1%	0.0129	-7%	2.5
Fish 1	0.0474	**13%**	0.0472	0%	0.0297	**-37%**	3.2
Fish 2	0.0692	9%	0.0689	-1%	0.0423	**-39%**	3.5
Macrobenthos	0.0225	**14%**	0.0224	-1%	0.0168	**-26%**	2.3

Northern North Sea							
	Default		No Hg^{2+} bioaccumulation		No $MMHg^+$ bioconcentration		Trophic Level
	(ng Hg mg-1)	Bioconcentrated (%)	(ng Hg mg-1)	Difference (%)	(ng Hg mg-1)	Difference (%)	-
Diatom	0.0034	100%	0.0034	1%	0.0034	1%	1
Flagellate	0.0062	100%	0.0062	1%	0.0062	1%	1
Microzooplankton	0.0104	6%	0.0105	2%	0.0098	-5%	2.0
Mesozooplankton	0.0122	**10%**	0.0124	2%	0.0106	**-13%**	2.5
Fish 1	0.0209	**22%**	0.0210	1%	0.0135	**-35%**	2.9
Fish 2	0.0373	**14%**	0.0374	0%	0.0194	**-48%**	3.7
Macrobenthos	0.0085	**25%**	0.0083	-2%	0.0054	**-37%**	2.3

by macrobenthos in the Northern North Sea. Since the water column is stratified during spring and summer, macrobenthos cannot directly feed on the phyto- and zooplankton bloom. Because of this, they are dependent on sinking detritus. The detritus has a lower $MMHg^+$ content than living material and consequently, the $MMHg^+$ intake in Northern North Sea macrobenthos is lower, and thus the relative importance of bioconcentration is higher.

4.3.3 Bioaccumulation of $MMHg^+$ and trophic level

The relationship between trophic level and $MMHg^+$ bioaccumulation is plotted in Fig. 4.2a. Since we assume biomagnification to be an exponential effect per trophic level on top of bioconcentration, the model is fitted as an exponential function with the average $MMHg^+$ content of phytoplankton as the origin. Fig. 4.2b expands on this by showing the relationship between the trophic level and the effect of both investigated drivers on the bioaccumulation of $MMHg^+$. This shows that while there is no effect of the bioaccumulation of Hg^+ on the bioaccumulation of $MMHg^+$. The setup without bioconcentration in consumers has 15% less $MMHg^+$ bioaccumulation per trophic level than the setup which does includes this interactions.

4.3.4 Evaluation hypotheses 1; The effect of Hg^{2+} bioaccumulation on $MMHg^+$ bioaccumulation

Based on the results of the statistical analysis shown in Table 4.2 we can see that there is no significant difference (p = 0.99) caused by Hg^{2+} bioaccumulation on $MMHg^+$ bioaccumulation. Based on the Bayesian t test we estimate that the change is 1/0.35 = 2.86 times greater than the data, that is, there is a difference.

Table 4.2: The results of the statistical test performed to evaluate the difference between the scenarios and the base case. The high p-value ($p > 0.99$) and below 1 Bayes Factor (BF=0.35) indicate that there is no significant difference between the base case and the scenario without Hg^{2+} bioaccumulation and that the change that there is no difference is 2.86 times larger than the chance that there is a difference. The difference between the scenario without $MMHg^{+}$ bioconcentration is significant ($p < 0.001$) and the change that there is a difference is 6.81 times higher than the change that there is no difference caused by the bioconcentration of $MMHg^{+}$ in consumers on the bioaccumulation of $MMHg^{+}$.

	No Hg^{2+} bioaccumulation	No $MMHg^{+}$ consumer bioconcentration
Wilcoxen signed-rank test	$p > 0.99$	$p<0.001$
Bayesian t-test	BF=0.35	BF=6.81

Based on these results, we conclude that Hg bioaccumulation^{2+} does not play a major direct role in the bioaccumulation of $MMHg^{+}$. However, it should be noted that bioaccumulation of Hg^{2+} can still play a role in the $MMHg^{+}$ content in biota by in vivo methylation. However, there is no data suggestion that this is a major pathway, so based on the current state of knowledge of $MMHg^{2+}$ bioaccumulation we conclude that the first hypothesis is incorrect and Hg^{2+} does not play a role in the bioaccumulation of $MMHg^{+}$ in coastal food webs.

4.3.5 Evaluation hypotheses 2; The effect of $MMHg^{+}$ bioconcentration in consumers on $MMHg^{+}$ bioaccumulation

Based on the statistical results shown in Table 4.2 we conclude that there is a significant difference between the base case and the scenario without consumer bioconcentration ($P < 0.001$), we based on the Bayesian t-test that the chance that the data are different is 6.81 times larger than that no difference exists. Based on the results, we conclude that the bioconcentration of $MMHg^{+}$ in consumers is a significant contributor to the bioaccumulation of $MMHg^{+}$. We quantify this significant increase in the bioaccumulation of $MMHg^{+}$ at 15% per trophic level in our model.

4.3.6 Model limitations

There are some limitations to our model. First, estimates of the biomagnification factor or $MMHg^{+}$ range between 2-10. Our model represents the estimations of the lower end. The bioconcentration factor is probably more important in low biomagnification food webs. Another limitation is that our model stops at trophic level 3.7. This is a high trophic level that can represent piscivorous species, but many marine species that are consumed by humans such as tuna, Great Marlin, and cod can have higher trophic levels. These higher trophic levels might be influenced even more by consumers $MMHg^{+}$ bioconcentration. Additionally, it must be noted that fish 2 in our model is only trophic level 3.5-3.7. Typically, large cod can have a higher trophic level of 3.7-4.2 and high trophic levels such as bluefin tuna can reach trophic levels of up to 4.8 (Nilsen et al. 2008; Sarà and Sarà 2007).

When the absolute concentration of $MMHg^{+}$ increases at higher trophic levels, the relative increase in the importance of direct bioconcentration per trophic level likely decreases. Our modeled top predator with a trophic level of 3.7 has a high trophic level for a coastal ocean, but there is a marine biota with even higher trophic levels in our model domain, such as marine mammals. Without a dedicated modeling study to simulate the diet and bioconcentration of even higher trophic levels, we cannot simply extrapolate our findings to predict the importance of $MMHg^{+}$ bioconcentration in their $MMHg^{+}$ bioaccumulation.

Overall the most important driver of our model is the fraction of $MMHg^{+}$ that is bioaccumulated by bioconcentration for each trophic level, as this drives the relative importance of bioconcentration at the higher trophic levels. The contribution of bioconcentration in zooplankton of 3.97-10.07% is in line with the $< 20\%$ reported by Schartup et al. (2018), and the contribution of bioconcentration in fish between 8.14-21.82% is in line with the study by Wang and Wong (2003).

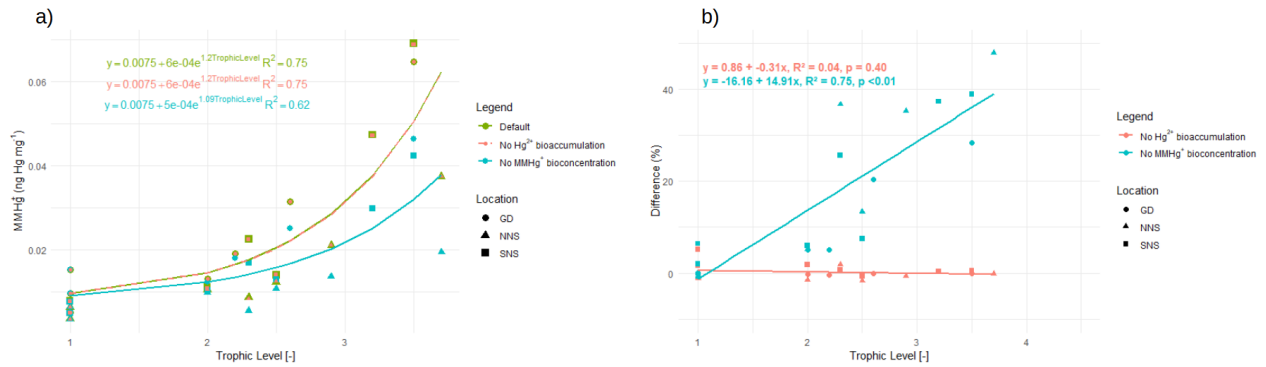

Figure 4.2: Figure a) shows the trophic level vs $MMHg^+$ bioaccumulation for the base case and the 2 scenarios. The base case and scenario "No Hg^{2+} bioaccumulation" have the relationship $0.0075+6E4*e^{1.2*TrophicLevel}$ and the scenario "No $MMHg^+$ bioconcentration" has $0.0075+5E4*e^{1.09*TrophicLevel}$. Figure b) shows that there is an exponential increase in $MMHg^+$ with trophic level, which is higher for the base case and the scenario without Hg bioaccumulation than for the scenario without $MMHg^+$ bioconcentration. Figure b) expands on this and demonstrates no significant effect on the importance of trophic level on the effect of the bioaccumulation of Hg^{2+} on $MMHg^+$ bioaccumulation. There is a reduction of 15% per trophic level caused by the bioconcentration of $MMHg^+$.

The main uncertainty for the fraction of $MMHg^+$ that originates from bioconcentration is the parameterization of bioconcentration and biomagnification. Both the bioconcentration and biomagnification of zooplankton are based on the work of Tsui and Wang (2004) on water fleas (*Daphia Pulex*) and for fish this is based on Wang and Wong (2003) and their work on the Indo-Pacific species Sweatlips. Although water fleas are common in the Baltic Sea, they are not in the North Sea, and sweetlips live neither in the North nor in the Baltic Sea. This means that the most important parameters in our model are not based on the animals they represent in our model. Although it is unfeasible to have dedicated bioaccumulation studies in every animal or functional group, there are currently not enough studies to verify whether these rates would differ between the circumstances in our model and those in the experiment. Drivers that might influence these factors are the size of the biota, physical circumstances such as temperature and salinity, or if there is a seasonal effect related to the activity of the animals. It would greatly improve our ability to model the bioaccumulation of $MMHg^+$ if more information on these different drivers were available.

It is a deliberate choice to perform this study in 1D idealized water column models, as it allows us to get a clear overview of the driving processes and generalize our findings. In this way, we can provide a general conclusion based on the biomagnification and bioconcentration rates of the biota that are presented in laboratory and field studies. However, it poses limitations compared to real fish by omitting spatial variability. Locally variable circumstances, such as the seasonally dependent flow of Hg from rivers to the ocean, could cause the importance of bioconcentration on $MMHg^+$ bioaccumulation to be regionally different.

Although the model can predict the importance of $MMHg^+$ bioconcentration, it can not evaluate the importance of the bioconcentration of gaseous Hg species, such as Hg^0 and DMHg. These gaseous Hg species are assumed not to biomagnify because they are not polar but could bioconcentrate. Because the gills of fish are optimized to facilitate the exchange of gases between water and fish blood, these gaseous Hg species can likely bioconcentrate in organisms. However, to model and evaluate the importance of this interaction, studies must be performed first, investigating both the bioconcentration and release rates of these gaseous species and their fate in the organism. In particular, the effect of the bioconcentration of DMHg on the concentration of MeHg at higher tropic levels will be very dependent on whether DMHg stays gaseous in the organism and is excreted quickly via the gills, or whether DMHg is demethylated in $MMHg^+$ and further biomagnified in the food chain. Since DMHg concentrations are low in the north and Baltic seas, this is unlikely to play a major role in our setups, but it could influence the importance of bioconcentration on the $MMHg^+$ content of higher trophic level fish in seas with higher DMHg concentrations, such as the open oceans and the Mediterranean sea.

4.4 Conclusion

In our paper, we used a 1D water column model to test two hypotheses. Our first hypothesis is that the bioaccumulation of $MMHg^{+}$ is influenced by the bioaccumulation of Hg^{2+}. We theorized that Hg bioaccumulation^{2+} removes a significant portion of Hg^{2+} from the water column, resulting in less Hg^{2+} that can be methylated in $MMHg^{+}$. As a result, we would expect that the bioaccumulation of Hg^{2+} can reduce the bioaccumulation of $MMHg^{+}$. Our second hypothesis is that the bioconcentration of $MMHg^{+}$ in consumers is a major contributor to the bioaccumulation of $MMHg^{+}$ at higher trophic levels. We theorized that while the direct effect of bioconcentration in high trophic level animals is low, the cumulative effect of bioaccumulation in all trophic levels below becomes a major source of $MMHg^{+}$

Our results show that the bioaccumulation of $MMHg^{+}$ in our model with and without the bioaccumulation of Hg^{2+} is the same, while this is not the case for the model with and without the bioconcentration of $MMHg^{+}$. We show that the bioconcentration of $MMHg^{+}$ in consumers becomes more important at higher trophic levels because it is an effect of the sum of all trophic levels before it. We show that while direct bioconcentration only accounts for 8-14% of $MMHg^{+}$ bioaccumulation in our highest trophic level fish, the total effect of bioconcentration in consumers accounts for 28-48%. This effect increases with the trophic level and the percentile contribution of the cumulative effect of $MMHg^{+}$ bioconcentration in consumers on $MMHg^{+}$ bioaccumulation is 15% per trophic level.

Because of this, we reject the first hypothesis that bioaccumulation of Hg^{2+} lowers $MMHg^{+}$ bioaccumulation and accept our second hypothesis that bioconcentration of $MMHg^{+}$ increases bioaccumulation of $MMHg^{+}$ in higher trophic levels fish. We supplement the second hypothesis by quantifying the effect as an average increase in bioaccumulated $MMHg^{+}$ of 15% per trophic level.

These results demonstrate that to model the bioaccumulation of $MMHg^{+}$, the bioaccumulation of Hg^{2+} can be ignored to save computational resources. However, the bioconcentration of $MMHg^{+}$ on the other hand is an essential interaction that should be taken into account. When modeling the bioaccumulation of $MMHg^{+}$ at higher trophic levels.

Funding

This research has been funded by the Horizon 2020 research and innovation program of the European Union under the Marie Sklodowska-Curie grant agreement no. 860497.

Author contribution

The work was performed by David J. Amptmeijer under the supervision of Dr. Johannes Bieser.

Competing interest

None of the authors declares any competing interest.

4.5 Acknowledgments

This paper's readability was refined using gAI tools like ChatGPT (OpenAI), and spelling corrections were made utilizing AI-driven applications, including Grammarly and Writefull. Moreover, AI tools optimized the R and Python scripts and offered coding suggestions, all of which were manually verified before implementation. For literature research, Google Scholar and Perplexity assisted in identifying sources, which were then manually verified and cited. Sub-images comprising the graphical abstract were crafted using openART and GPT-4.1.

Bridging chapter

While modeling the bioaccumulation in the North and Baltic seas, I noticed that the macrobenthos had extremely high iHg values, while their MeHg values were low. I tried to validate this by field observations. While data was minimal, the data did not consistently confirm high iHg values in macrobenthos; if anything, it was typically low. However, there were cases where macrobenthos had extremely high iHg values. Since in the MERCY v2.0 model, bioconcentrated and biomagnified Hg are stored as separate state variables, it could be seen that the macrobenthos diet caused the high iHg values. Because of that, I initially decided to trace in the model which food resulted in high Hg values in macrobenthos. This led me to discover that the consumption of DOM, even in small amounts, caused very high Hg levels in macrobenthos in the model. This sparked my attention, and I decided to split the macrobenthos group in the ECOSMO E2E model into 6 categories representing different feeding strategies so that I could see if different feeding strategies led to varying levels of MeHg bioaccumulation and if I saw similar patterns in field observations and the model. While trying to quantify this, I realized that there are not enough field observations on macrobenthos in the North and Baltic Sea to determine definitive patterns. I decided to gather all observations of iHg, MeHg, trophic level, and feeding strategy in macrobenthos and aggregate these to see if patterns emerged. Since this took a lot of manual work, I decided to cover it as a mini project for the Marine Biology MSc at the University of Hamburg, and I was happy to receive the excellent support of Andrea Padilla and Sofia Modesti with this work. I would also like to mention that since this paper is for a major part a majority of field studies that do not distinguish between different fractions of bioaccumulation, iHg I switched to using the terms iHg and MeHg for the following chapters. This is done because I neither wanted to confuse the reader while referring to the modeled and measured iHg and MeHg with different names, nor did I want to make assumptions about the measured data that all bioaccumulation iHg and MeHg is Hg^{2+} and $MMHg^{+}$. At the same time, since only Hg^{2+} and $MMHg^{+}$ bioaccumulate in my model, the concentration of bioaccumulated iHg and Hg^{2+} and MeHg and $MMHg^{+}$ is equal per definition. Additionally, I used the term megabenthos rather than macrobenthos. The term macrobenthos refers to animals between 1 mm and 1 cm in diameter, while megabenthos refers to benthic animals larger than 1 cm. Because of this, I used the term Megabenthos in the following paper, as all benthic animals in the model are larger than 1 cm.

Figure 4.3: common heart urchin (*Echinocardium cordatum*), a buried deposit feeder. Picture taken by Dr. Eric Wurtz.

CHAPTER 5

Feeding strategies and their role in Hg bioaccumulation

David J. Amptmeijer[1], Andrea Padilla[2], Sofia Modesti[2], Corinna Schrum[1,2], Johannes Bieser[1]
[1]Matter Transport and Ecosystem Dynamics, Helmholtz-Zentrum Hereon, Geesthacht, Germany
[2]Universität Hamburg, Institute for Marine Sciences, Mittelweg 177, 20146 Hamburg, Germany

Methylmercury (MeHg) bioaccumulation in the marine food chain poses a neurotoxic risk to human health, especially through seafood consumption. Although MeHg bioaccumulation at higher trophic levels is relatively well understood, MeHg bioaccumulation at the base of the food web remains underexplored. Given the neurotoxic effects of methylmercury on human health, it is essential to understand the drivers of bioaccumulation at every level of the food chain. In this study, we incorporate six macrobenthos functional groups into the ECOSMO marine end-to-end ecosystem model, coupled to the MERCY marine Hg cycling model. We investigated how various feeding strategies influence the bioaccumulation of both inorganic Hg (iHg) and MeHg in marine ecosystems. We show that the feeding strategy significantly influences bioaccumulation and correlates stronger with iHg than the trophic level and that suspension feeders have elevated iHg levels while filter feeders have higher MeHg values. Additionally, we show that the bioaccumulation of both iHg and MeHg can accurately be modeled solely based on feeding strategy in low trophic level macrobenthos. However, when modeling higher trophic levels, incorporating the allometric scaling law dramatically improves the model performance. These results demonstrate the need for a holistic approach in which iHg, MeHg, and trophic levels of organisms at both high and low trophic levels are all assessed to identify what food web structures drive high MeHg concentrations in seafood.

Keywords: Mercury, Bioaccumulation, ECOSMO. Macrobenthos

Publication Status

This chapter is based on the following preprint:

Amptmeijer, D. J., Padilla, A., Modesti, S., Schrum, C., & Bieser, J. (2025). *Feeding strategy as a key driver of the bioaccumulation of MeHg in megabenthos*. *EGUsphere*, **2025**, 1–26. *Preprint*. https://doi.org/10.5194/egusphere-2025-1494

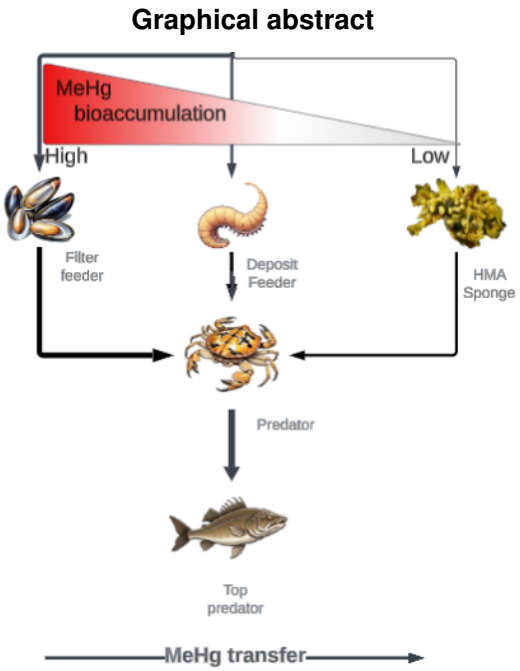

Figure 5.1: The bioaccumulation of MeHg depends on the feeding strategy of low trophic level megabenthos. In our model, filter feeders such as mussels (*Mytilus edulis*) bioaccumulate the highest amounts of MeHg, while deposit feeders such as lugworms (*Arenicola marina*) show lower levels. Suspension feeders such as High Microbial Abundance (HMA) sponges (e.g., *Chondrilla nucula*) exhibit exceptionally low MeHg bioaccumulation. This suggests that ecosystems dominated at the base by species like mussels, which are characterized by relatively high MeHg bioaccumulation, will have higher MeHg levels in higher trophic level fish compared to ecosystems where low-accumulating species such as HMA sponges dominate the base of the food web. The image is made of several sub-images that are generated using openART and GPT 4.1.

5.1 Introduction

Mercury (Hg) is a naturally occurring element. In addition to its natural occurrence, it is also emitted through various anthropogenic activities, such as the burning of fossil fuels, small-scale artisanal gold mining, and the production of cement and ferrous metals (Pacyna et al. 2006). These emissions have led to a threefold increase of Hg loading to the oceans compared to pre-anthropogenic levels (Lamborg et al. 2014; Driscoll et al. 2013).

When elemental Hg (Hg^0) is emitted, it can undergo long-range atmospheric transport. In this way, it can be transported on a global scale and deposited in the oceans, thus increasing Hg levels in the marine environment (Durnford et al. 2010). Marine Hg^0 is volatile and can return to the atmosphere or be oxidized into dissolved Hg (Hg^{2+}) (Sommar et al. 2020). This Hg^{2+} can be reduced back to volatile elemental Hg^0, or it can be methylated to dangerous neurotoxin methylmercury (MeHg), which occurs as monomethylmercury ($MMHg^+$) or dimethylmercury (DMHg) (Jensen and Jernelov 1969; Lin et al. 2021). In this paper, we will look at the bioaccumulation of three groups of Hg; total Hg (tHg) refers to all Hg, methylmercury (MeHg) refers to both $MMHg^+$ and DMHg, and inorganic Hg (iHg) refers to all Hg that is not MeHg.

5.1.1 Drivers of Hg bioaccumulation

There are two key processes involved in bioaccumulation: bioconcentration and biomagnification. Animals living in a polluted marine environment will absorb Hg directly from their environment; this is called bioconcentration. Both iHg and MeHg bioconcentrate. Since iHg is generally present in higher concentrations than MeHg, and its bioconcentration rate is higher, iHg is usually bioconcentrated faster than MeHg (Mason et al. 1996). The bioconcentration process can result in high Hg concentrations in organisms, and Hg

volume concentration factors of up to 6.4E6 have been found (Schartup et al. 2018).

These already high Hg concentrations can be increased even further by biomagnification. Biomagnification refers to the increase in Hg with each successive trophic level in the food chain. The trophic transfer efficiency of MeHg (66-80%) is higher than that of iHg (7-46%), where MeHg accumulates at much higher levels in the food chain (Metian et al. 2020; Wang and Wong 2003; Dutton and Fisher 2012). These concentrations can become harmful to humans when consumed, and the consumption of MeHg-polluted seafood is the main risk of exposure to Hg for the average person (Sheehan et al. 2014).

The danger posed by the consumption of MeHg-contaminated seafood received a great deal of attention when more than 1000 people died in Japan in 1956 due to the consumption of contaminated seafood caught in Minamata Bay(Harada 1995). In order to reduce the risk of further outbreaks of MeHg intoxications, the Minamata Convention on Mercury was founded. 151 countries have pledged to reduce their Hg emissions in support of the Minamata Convention, and 128 countries have signed and ratified the convention. The global state of Hg as a pollutant and the effect of the Minamata Convention is periodically reviewed in the Minamata Convention Effectiveness Evaluation (Outridge et al. 2018).

5.1.2 The knowledge gap; Hg bioaccumulation at the base of the food web

While there is considerable understanding of MeHg bioaccumulation in high trophic levels, less is known about the bioaccumulation drivers at the base of the food web. The lower concentration of Hg at the base of the food web reduces the risk for humans, which is why these animals do not receive the same monitoring recommendations from the effectiveness evaluation of the Minamata Convention as fish, humans and wildlife (Evers et al. 2016). Furthermore, the effectiveness evaluation noted that the concentrations of Hg and MeHg in water and sediment are poorly correlated with the concentrations in biota. Thus, Hg levels in water and sediment do not receive the same monitoring recommendations.

Once Hg is bioconcentrated in primary producers, a strong link appears between the trophic level and Hg bioaccumulation (Madgett et al. 2021). This indicates that our understanding of Hg bioaccumulation in high trophic levels is greatly limited by our understanding of Hg bioaccumulation at the base of the food web.

Improving our understanding of bioaccumulation at the base of the food web is challenging, as the base of the food web is very complex (Silberberger et al. 2018). There are several distinct groups of megabenthos with different feeding strategies, such as bivalves that filter feed, lugworms that feed on sediment carbon particles, active hunters and scavengers such as shrimps and crabs, and sponges that feed on suspended dissolved material. These different feeding strategies allow them to exploit a variety of food sources, but different food sources can have different Hg concentrations, and Hg originating from different food sources can have different assimilation efficiencies. In this study, we hypothesize that the low-trophic-level biota feeding strategy has a significant impact on their Hg content.

We focus this study on the benthic food web. Although primary production in the North Sea can be highly variable due to factors such as wind (Daewel and Schrum 2017), tidal mixing (Zhao et al. 2019) and nutrient availability (Richardson et al. 1998), primary production in coastal areas is generally dominated by pelagic phytoplankton, with the exception of extremely shallow areas that are dominated by benthic macroalgae (Krause-Jensen et al. 2012; Cibic et al. 2022). Especially in areas where pelagic phytoplankton dominate primary production, while the pelagic phytoplankton are available for consumption by megabenthos because of water column mixing, there is a strong coupling between the benthic and the pelagic, called the bentho-pelagic coupling. In these well-mixed areas, megabenthos can reach high biomass since food is abundant in several ways, resulting in megabenthos with different feeding strategies in the same ecosystem (Ghodrati Shojaei et al. 2016).

5.1.3 The hypothesis: Feeding strategy is key driver of Hg bioaccumulation in low trophic level biota

We hypothesize that the different feeding strategies of low-trophic-level megabenthos play an important role in creating the disconnect between Hg concentrations in the water and sediment and the concentrations at the base of the food web. We investigated whether the feeding strategy impacts bioaccumulation

and hypothesized that feeding strategies influence the bioaccumulation of iHg and MeHg differently, contributing to the high variation in Hg levels at the base of the benthic food web.

To test our hypotheses, we employed two methods. First, we performed literature research in which we collected field observations of the content of tHg, MeHg, and iHg, the trophic level, and the megabenthos feeding strategy. We performed statistical analyses on this literature to see if patterns between bioaccumulation and feeding strategies exist in nature. Afterward, we conducted an in silico experiment in which megabenthos with various feeding strategies compete under physical drivers in idealized scenarios that are typical of megabenthos-rich coastal oceans. The megabenthos groups are designed to differ only in their feeding strategies to isolate this effect. This was done to verify whether we can reproduce the observed effects from our literature study in a fully coupled model. Finally, we used the model to quantify the role of the feeding strategy in the bioaccumulation of Hg and investigated whether it fully explains the observed differences or if other drivers need to be incorporated.

5.2 Materials and methods

5.2.1 Literature research and statistics

To compare the findings with the literature, we collected field studies measuring Hg in megabenthos. The studies we used are shown in the Table 5.5 in annex 1. We categorized the megabenthos into the same feeding categories, ”deposit feeder”, ”filter feeder”, ”suspension feeder”, ”grazer” and ”predator”. To better look at the effect of the trophic level, we also added ”primary producers” as the base of the food web, ”predators” as benthic predators, and ”seabird” and ”benthic fish” as top predators. We analyze whether trophic level and feeding strategy influence megabenthos iHg, MeHg, and/or tHg content. The observations are analyzed by visualizing the data, performing a linear regression, and plotting a correlation matrix of the difference in bioaccumulation between different feeding strategies. The total and partial R^2 of the linear regression of the effect of the feeding strategy, the trophic level, and the feeding strategy are compared to analyze the effect of both drivers on bioaccumulated iHg, MeHg and tHg.

5.2.2 The models

To further assess the importance of the feeding strategy, we modeled bioaccumulation in megabenthos, with the feeding strategy being the only distinction between different groups of megabenthos. Then we compared our model to observations to evaluate whether this approach allows us to accurately model bioaccumulation or if additional drivers should be taken into account. We used a fully coupled 1D water column model that is run in 2 setups that resemble typical hydrological regimes found in coastal oceans. We coupled the Generalized Ocean Turbulence Model (GOTM) with the ECOSMO E2E ecosystem model and the MERCY v2.0 Hg speciation and bioaccumulation model.

5.2.3 The hydrodynamical model

The hydrodynamics of the model are estimated using the GOTM, which is a 1D hydrodynamic model (Bolding et al. 2021). GOTM calculates the turbulence of a vertical 1D water column set-up by computing the solutions to the one-dimensional version of the transport equation of momentum, salinity, and temperature. The model is nudged to observational data sets for temperature and salinity. The setups are based on gridded bathymetry data for water depth with 1/240° resolution (GEBCO Bathymetric Compilation Group 2020), ECMWF ERA5 dataset for meteorological data (Wouters et al. 2021), Ocean Atlas for salinity and temperature profiles (Garcia H.E. et al. 2019), and the TPOX-9 atlas for tides (Egbert and Erofeeva 2002), which is combined using the iGOTM tool (https://igotm.bolding-bruggeman.com). The GOTM model is coupled using the Framework for Aquatic Biogeochemical Modeling (FABM) (Bruggeman and Bolding 2014). The biogeochemical models are encoded in FABM. The FABM interfaces communicate the state variables between the GOTM model and the biogeochemical models.

5.2.4 The MERCY v2.0 model

Hg cycling and speciation is modeled using the MERCY v2.0 model (Bieser et al. 2023). The MERCY v2.0 model is a comprehensive Hg cycling model that includes speciation between 7 forms of Hg and partitioning to both dissolved organic matter (DOM) and detritus. It was originally developed as a 3D Hg cycling model of the North and Baltic Seas. However, in this study, we use the 1D version of this model, which is driven using the GOTM model. This configuration is used, described, and evaluated in more detail in Chapter 3.

5.2.5 ECOSMO E2E

The ecosystem model is based on the ECOSMO E2E (ECOSystem Model End-to-End) ecosystem model (Daewel et al. 2019). This model extends the ECOSMO II model to have higher trophic levels while preserving consistency at lower trophic levels (Daewel et al. 2019). The version used in this study is the same as the version used and evaluated in Chapter 3. In this version, small modifications have been made, such as lowering the mortality rate of zooplankton and decreasing the efficiency of carbon uptake to make the model more suitable for bioaccumulation compared to the version published by (Daewel et al. 2019). The model is evaluated and shown to reproduce the bioaccumulation of iHg and MeHg at the base of the food web within 1 standard deviation of observations for phytoplankton, microzooplankton, and mesozooplankton. Furthermore, the model accurately models the bioconcentration of both iHg and MeHg and the biomagnification of MeHg within the range of observations.

5.2.6 Model development

To use the model to study bioaccumulation in megabenthos, the higher trophic level of the ECOSMO E2E model is altered. We exchanged the functional group macrobenthos, fish 1, and fish 2 with 5 megabenthos functional groups, as shown in Fig. 5.2. The megabenthos groups are separated by their feeding strategy: filter feeder, deposit feeder, generalist feeder, suspension feeder, predator, and top predator.
Filter feeders filter suspended particles from the water column. In our model, they can eat phytoplankton, zooplankton, and detritus. Examples of filter feeders are mussels, tubeworms, and barnacles. The second group is **deposit feeders**. These animals consume organic carbon from the sediment; in our model, they exclusively feed on organic carbon deposited in the sediment. This group would include gastropods and polychaete worms, such as the lugworm (*Arenicula marina*). The **generalist feeder** resembles animals such as North Sea shrimp (*Crangon crangon*), which can utilize various feeding strategies. In our model, this group feeds on phytoplankton, zooplankton, detritus, and deposited material. We also include a **suspension feeder**. Suspension feeders, such as sponges, can consume detritus and DOM. The consumption of DOM, which is too small to be consumed by filter feeders, differentiates suspension and filter feeders. A common strategy to consume DOM as a food source is the utilization of symbiotic bacteria such as chemosymbiotic bivalves from the families Lucinidae, Solemyidae, and Thyasiridae and microbial biomes of high microbial assemblage sponges (Dufour 2018; Olinger et al. 2021). Finally, we included 2 predators. The first predator is referred to as **the predator**, it feeds on the 4 benthic groups mentioned above, and it has an equal preference and grazing rate in all groups, but it will prioritize abundant groups. This preference is caused by making the food available for predation by the predators not linearly related to the abundance of the prey, but calculated as:

$$b_{\text{available}} = \begin{cases} b_{\text{biomass}}, & \text{if } b_{\text{biomass}} \geq b_{\text{protected}}, \\ b_{\text{biomass}} \frac{b_{\text{biomass}}}{b_{\text{protected}}}, & \text{if } b_{\text{biomass}} < b_{\text{protected}}. \end{cases}$$

in which,

- $b_{\text{available}}$- Portion of prey biomass in accessible to predators [g C m^{-2}]
- $b_{\text{protected}}$- Prey biomass in below which hunting becomes less optimal[g C m^{-2}]
- b_{biomass}- Total prey biomass in in the environment [g C m^{-2}]

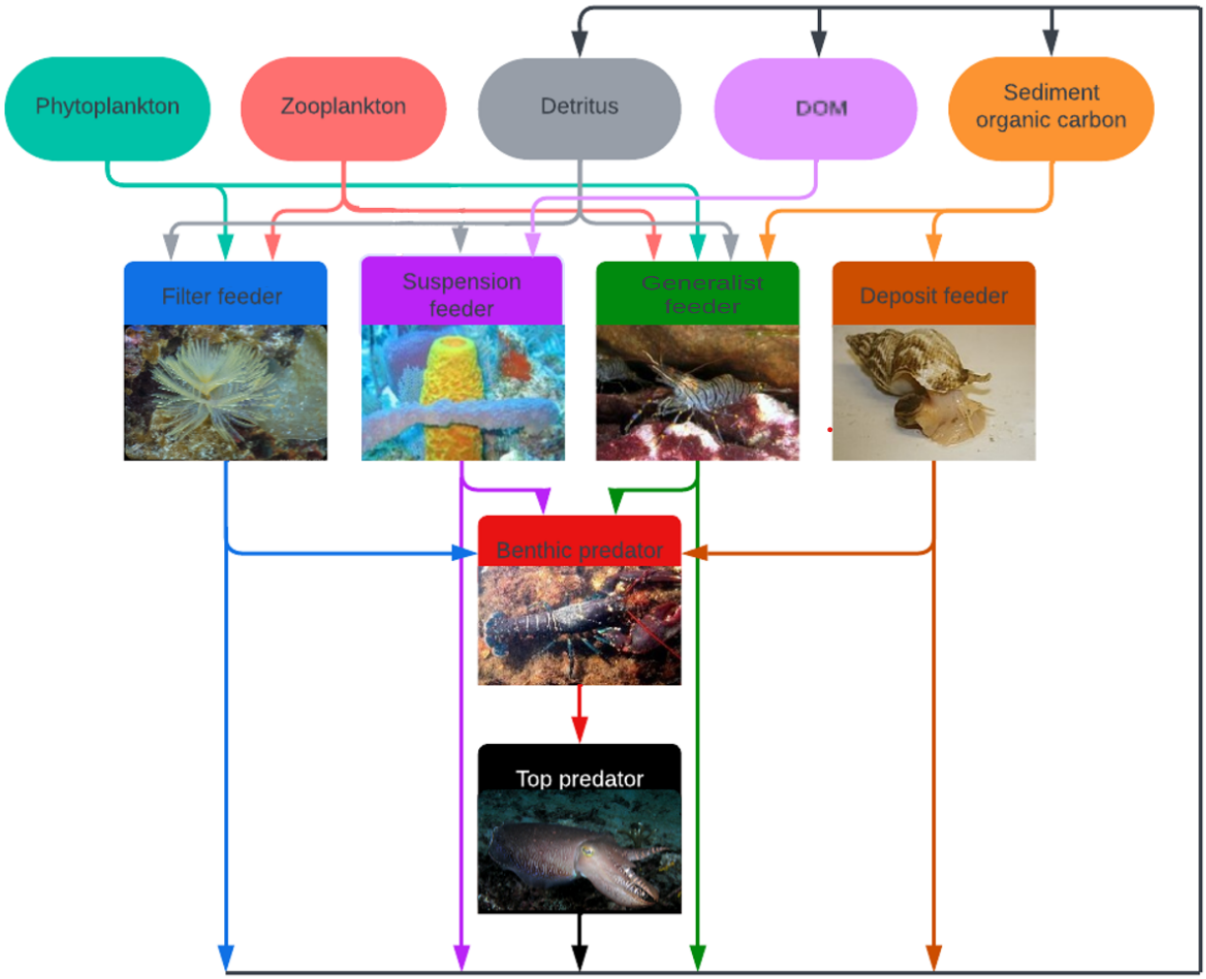

Figure 5.2: The overview of the modeled megabenthos functional groups and how they interact with each other and functional groups in the ECOSMO E2E model. There are 5 macrobenthic functional groups. The filter feeder feeds on pelagic detritus, zooplankton, and phytoplankton. The suspension feeders feeds on pelagic detritus, phytoplankton, zooplankton, and DOM. The generalist feeds on phytoplankton, zooplankton, pelagic detritus, and sediment organic carbon. The deposit feeder feeds on sediment organic carbon. The benthic predator feeds on the other 4 megabenthos functional groups and the top predator solely feeds on the benthic predator. Several sub-images have been used in this image. Sources of the images are: filter feeder: `https://en.wikipedia.org/wiki/Sabella_spallanzanii`, suspension feeder: `https://www.flickr.com/photos/noaaphotolib/5015046804/`, generalist feeder: `https://en.wikipedia.org/wiki/Shrimp`, deposit feeder: `https://nl.wikipedia.org/wiki/Buccinum_undatum`, benthic predator: `https://en.wikipedia.org/wiki/Lobster`, and top predator: `https://en.wikipedia.org/wiki/Cuttlefish`.

$b_{protected}$ is 1 g C m^2 for all megabenthos groups, and 0.5 g C m^2 for the benthic predator. This relationship models 2 real-world interactions. First, when the concentration of prey is low, the small number of individuals can more likely survive under ideal circumstances and, therefore, may be less exposed to predation (Campanella Id et al. 2019). Secondly, several predators, such as the shore crab, adapt their behaviors to the density of the prey and learn to be more efficient in the hunting of more common prey (Chakravarti and Cotton 2014).

5.2.7 Assimilation efficiency of iHg and MeHg

The assimilation efficiency (AE) of iHg and MeHg is a key parameter in correct biomagnification modeling. AE is based on laboratory experiments that analyze AE in phytoplankton (Metian et al. 2020; Wang and

Wong 2003). An assimilation efficiency of 0.95 for MeHg and 0.31 for iHg is chosen for everything except deposit feeding, which has a lower feeding efficiency of 0.07 for iHg and 0.43 for MeHg according to Dutton and Fisher (2012).

5.2.8 Semi-labile DOM

In the ECOSMO E2E model, only labile-DOM is resolved. This means that there is very little DOM. In our model, we want to incorporate a suspension feeder that would utilize DOM as a food source. Because of this, we added a DOM component referred to as semi-labile DOM. This semi-labile DOM has the same bacterial degradation rate as that of the detritus, and it has the same Hg partitioning behavior as labile DOM. 5% of the organic carbon (Detritus+labile-DOM+semi-labile-DOM) formed, is formed as semi-labile DOM, and there is a breakdown of the detritus into semi-labile DOM of 0.001 d^{-1}. Since the categorization of DOM is very complex, these rates are estimated to create a low maximum of 50 mg C m^{-3}. This is lower than the DOM concentrations typically found in the North Sea, but because it is unclear which fraction of DOM can be consumed by suspension feeders, this amount provides suspension feeders a unique food source that they can utilize while not outcompeting other megabenthos (Lønborg et al. 2024).

5.2.9 Allometric scaling model

Finally, we run the model while taking into account other drivers of MeHg bioaccumulation to see whether it improves the model. There are three interactions that we take into account for this second model. First, the allometric scaling law, which states that larger animals have a lower base metabolic rate when normalized to body weight (Silva et al. 2006). Secondly, we account for the observations that MeHg bioaccumulation in fish increases as the water temperature increases, indicating that increased activity does not increase MeHg excretion while it increases MeHg uptake due to a higher grazing rate (Dijkstra et al. 2013). Finally, we assume that predators need to spend more energy on active metabolism to hunt their prey. Because of this, we assumed that the total relative respiration rate of predators and top predators is not altered, so both models have the same carbon cycle. However, MeHg is excreted at a lower rate of 0.002 d^{-1}, rather than their respiration rate, which is the same base metabolic rate as the fish in the ECOSMO E2E model. This leads to a higher bioaccumulation of MeHg at higher trophic levels. The bioaccumulation of iHg is not altered between the two models. In the evaluation, the second model is referred to as the allometric scaling (AS) model.

5.2.10 The physical setups

The model runs in 2 setups, the first is a 41.5 m deep permanently mixed Southern North Sea set of 41.5 m deep and the second is a seasonally mixed 110 m Northern North Sea setup. These setups are described in more detail in Chapter 3. The Southern North Sea setup is located at (54°15′00.0″ *N* 3°34′12.0″ *E*). It is a shallow station that is permanently mixed, meaning that megabenthos can feed directly from the phytoplankton and zooplankton bloom. The setup is chosen because it resembles perfect growth conditions for megabenthos, and most megabenthos in the observations are sampled from similar circumstances. Because of this, samples are sampled from shallow well-mixed coastal areas, and we used this setup to evaluate the performance of the models.
The Northern North Sea setup is located at (57°42′00.0″ *N* 2°42′00.0″ *E*) and is only mixed in winter. This means that megabenthos cannot feed directly from the bloom, but are rather dependent on the sinking of detritus particles. In nature, these deeper areas typically have lower overall biomass. This setup is used to evaluate whether the models predict a difference in the bioaccumulation of iHg and MeHg under a different hydrodynamic regime.

5.2.11 Model evaluation

The goal of the model is to evaluate how well we can model the bioaccumulation of iHg and MeHg while only taking into account trophic interactions. To this extent, the model's result is its performance. If the model performs well, we can conclude that only taking into account trophic interactions explains a large

amount of the variability in Hg bioaccumulation. Initially we perform this comparison between observations and the modeled Southern North Sea setup. This is done because most samples are collected from shallow areas that are rich in macrobenthos. Our well mixed Southern North Sea setup would resemble the majority of the observations better than the seasonally mixed Northern North Sea. Afterward, the models are compared to the Northern North Sea models and the AS model to evaluate the effect of hydrodynamics and increased bioaccumulation in higher trophic level animals on our conclusions. The feeding strategy "grazer" was omitted, as the ECOSMO E2E model does not include benthic algae to graze on. The modeled generalist was compared to the deposit and filter feeder from the observations and the modeled top predator to the benthic fish and seabird feeding strategies from the observations. We first calculated the normalized bias as $(modeled - observed)/modeled$ for the average modeled and observed values. Then, we performed a Monte Carlo simulation in which we estimated the mean and standard deviation of the observed and yearly mean of the modeled data over the last 10 years of the simulation. Over 100,000 iterations, we estimated the probability that the modeled value is within 2 standard deviations of the observations, so it checks if the modeled mean is not outside 95% of the observations. After this, we evaluated the agreement between modeled and observed values by calculating a likelihood ratio (LR10). The likelihood ratio was estimated by calculating the likelihood of the modeled mean under a null hypothesis (H0), which assumes that the modeled and observed data share the same distribution centered on the observed value, and an alternative hypothesis (H1), which assumes a distribution derived from the modeled variability. The ratio between the likelihoods of H1 and H0 defines the LR10 value. Finally, the total model performance is evaluated by calculating the Root Mean Square Error (RMSE), the Normalised Root Mean Square Error (NRMSE), and the R^2 of the model for iHg and MeHg. In general, a normalized bias between <0.5 can be seen as low. The probability that the model values are not within 2 standard deviations is considered bad and indicates that the modeled mean is a considerable outlier compared to the data. A LR10 below 1 indicates that the modeled distribution is more likely the same as the observed distribution, and a LR10 <0.1 can be considered strong evidence and a LR10 <0.01 as very strong evidence in favor of the H0 hypotheses. A lower RMSE shows better model predictive capacity and an NRMSE below 0.5 is indicative of a good fit, while the R^2 is a value between 0 and 1, and closer to 1 shows a better fit.

5.3 Results and discussion

5.3.1 Literature study

The results of our literature study, depicted in Fig. 5.3, demonstrate that the feeding strategy affects the bioaccumulation of different benthic groups. If we only look at the groups that would represent the base of the benthic food web (filter feeder, suspension feeder, grazer, deposit feeder, and generalist) and perform an ANOVA, we see that there is greater significance of the effect of the feeding strategy ($p = 0.001$) on the bioaccumulation of iHg than on the bioaccumulation of MeHg ($p=0.09$). If we compare the median iHg and MeHg between organisms with different feeding strategies, we see that iHg is lowest in the benthic predator, followed by the deposit feeder, the top predator, the generalist, and the filter feeder, and the highest values are in the suspension feeders. Suspension feeders have by far the highest iHg concentrations and are more than double that of the second highest group, the filter feeders. At the same time, MeHg shows a very different pattern in which suspension feeders have low values, roughly half of that of filter, deposit, and generalist feeders, whereas the predators and top predators are higher.

Figure 5.4 illustrates the correlation between the bioaccumulation of iHg, MeHg, and tHg. We observe a strong correlation (R^2=0.49, $p<0.001$) between MeHg and trophic levels, while no correlation is found between iHg and trophic levels ($R^2<0.02$, P=0.474). The linear fit of the intercept of the equations for the iHg and MeHg intercept at trophic level 3.6, which means that below trophic level 3.6 the majority of tHg will on average be iHg.

In Table 5.1 we show the results of a linear regression taking into account both the trophic level and the feeding strategy, the relative fit of each model explains Hg bioaccumulation based on both factors. The trophic level and feeding strategy are adapted to the natural logarithms of iHg, tHg, and MeHg. This shows that we can explain the bioaccumulation of ln(MeHg) very well (R^2=0.72) with a linear model that

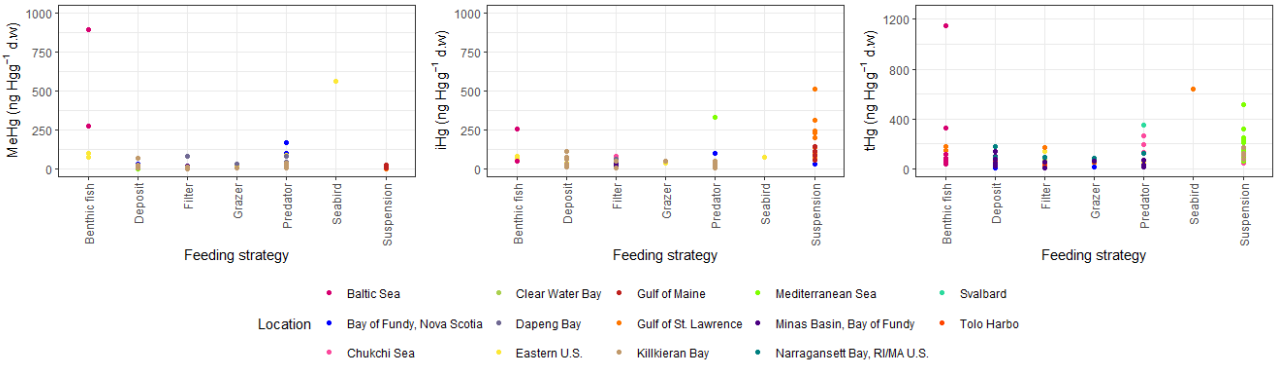

Figure 5.3: The effect of different feeding strategies on the measured MeHg and iHg in several benthic functional groups and groups of animals feeding on the benthos. The seabird is the common eider which feeds on benthos. Bioaccumulated MeHg is below 50 ng g^{-1} d.w. for all functional groups that are not predatorial (predators, benthic fish, and seabirds), but can reach up to 171, 565, and 895 ng g^{-1} d.w. for predators, seabirds, ad benthic fish respectively. This contrasts the iHg concentration below 100 ng g^{-1} d.w. for every animal. Except for starfish, Eel, and sponges. The tHg shows that the Hg can even be higher in suspension feeders (in this case sponges) than in fish.

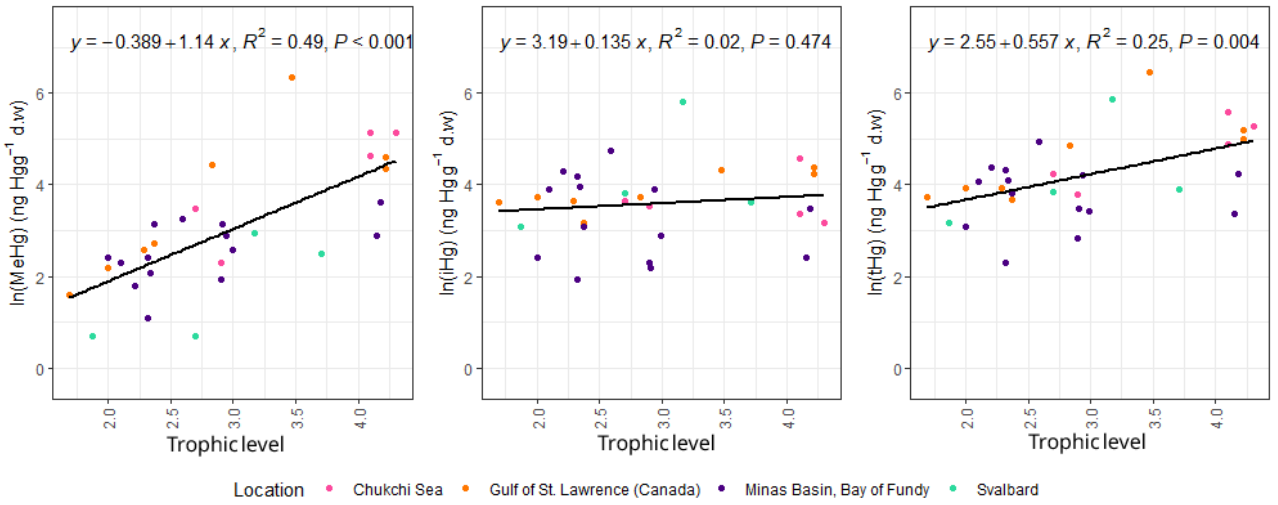

Figure 5.4: The correlation between the bioaccumulation of MeHg, iHg, and tHg. There is a strong correlation between MeHg and trophic level with a slope of 1.14 ln(ng Hg g^{-1} d.w.) trophic $level^{-1}$ with a R^2 of 0.49, while there is almost no correlation between iHg and trophic level (with a slope of 0.135 ln(ng Hg g^{-1} d.w.) trophic $level^{-1}$ with a R^2 of 0.02. The intercept is, however, much higher for iHg (3.3 at TL=1) than for MeHg (0.8 at TL=1). The tHg combines the 2 patterns with an intercept of 3.1 at TL=1 and a slope of 0.557.

Table 5.1: R-squared and Partial R-squared Results for ln(THg), ln(iHg), and ln(MeHg)

Model	ln(tHg)	ln(iHg)	ln(MeHg)
Full Model R-squared	0.46	0.11	0.72
Partial R-squared (Feeding Strategy)	0.22	0.089	0.32
Partial R-squared (Trophic Level)	0.10	0.012	0.31

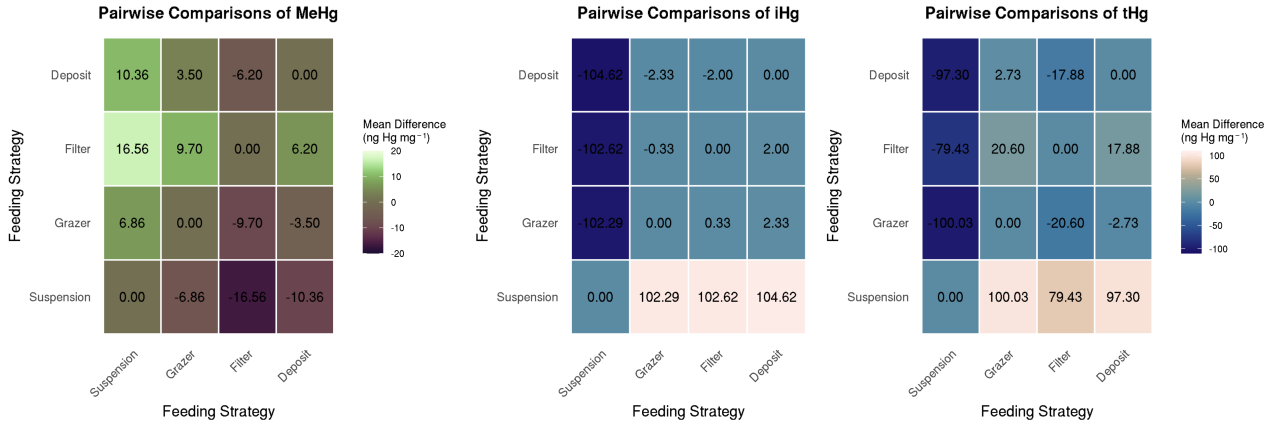

Figure 5.5: The pairwise comparison of the correlation between the bioaccumulation of MeHg, iHg and tHg and different feeding strategies. For clarity, MeHg has its own scale and iHg and tHg have the same scale. For the concentration of MeHg there is a pattern where suspension feeders $<$ grazers $<$ deposit feeders $<$ filter feeders. For iHg this is different and the main notable difference is much higher iHg in suspension feeders than in any other feeding strategy. tHg is the sum of MeHg and iHg and consequently shows very high tHg in suspension feeders due to the high iHg, and elevated tHg in filter feeders due to their high MeHg.

takes both drivers into account, while the bioaccumulation of iHg is poorly explained (R^2=0.11) and the bioaccumulation of tHg has an average fit (R^2=0.46). Furthermore, we show the unique contributions of the fit of each driver, the partial R^2. Note that feeding strategy and trophic level can sometimes co-correlate, especially in the case of high MeHg bioaccumulation in predators, benthic fish, and seabirds, as predators are naturally higher in trophic level than the prey they consume. The feeding strategy has an explanatory power larger than that of the trophic level for tHg and iHg, while it is similar for MeHg. Despite the limitations mentioned above, this still shows that the partial R^2 for the feeding strategy is double that of the trophic level, demonstrating the importance of the feeding strategy for the bioaccumulation of tHg at the base of the food web.

In Fig. 5.5 we show the pairwise comparison of the correlation between the bioaccumulation of iHg, MeHg, and tHg. This shows a clustering in which filter and deposit feeders have similar MeHg concentrations, but MeHg concentrations are lower in grazers and suspension feeders. The strong difference between suspension and filter feeders is especially notable as they both feed on pelagic organic carbon. Overall, this demonstrates that nuanced differences in MeHg bioaccumulation where the concentration in the suspension feeders $<$ grazers $<$ deposit feeders $<$ filter feeders. For iHg the pattern is different; deposit feeders, filter feeders, and grazers have similar iHg, while the iHg content of suspension feeders is much higher.

5.3.2 Model results

Biomass

Although our megabenthos groups only vary in feeding rate and, therefore, have no direct real-world counterpart to compare to, it is important to validate that they survive in the model. The yearly progression of megabenthos in the Southern North Sea setup is shown in Fig. 5.6. Filter feeders have the highest

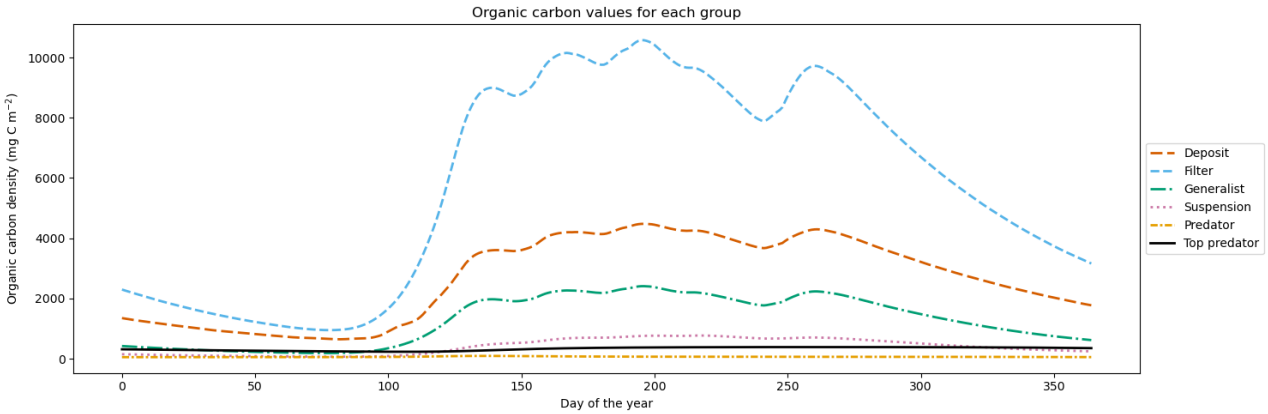

Figure 5.6: Megabenthos biomass in the modeled Southern North Sea, dominated by filter feeders, followed by deposit feeders, generalist feeders, suspension feeders, predators, and top predators. Biomass fluctuates between 10 and 15 gC m^{-2} and all functional groups have stable populations

biomass, which is up to 10 g C m^{-2} followed by deposit feeders with 5 up to g C m^{-2}, generalist feeders with up to 3 g C m^{-2}, and suspension feeders with up to 1 g C m^{-2}. Higher trophic levels have lower biomass, with up to 0.2 g C m^{-2} for the predator and 0.5 g C m^{-2} for the top predator. This shows that after a simulation period of 20 years, all megabenthos have a stable population, while biomass is highest at the base of the food web.

Bioaccumulation

The modeled bioaccumulation of iHg, MeHg, and tHg is shown in Table 5.2 and visualised in Fig. 5.7 and the evaluation is shown in Table 5.3. Note that the values are expressed in ng Hg mg C^{-1}, as this is the best proxy in our model to show the dietary uptake of Hg per energy and nutrients consumed. There is a very high concentration of iHg in the sediment, detritus, and DOM. These values are 0.22, 0.83, and 1.9 ng Hg mg C^{-1} for iHg and 0.038, 0.0046, and 0.0082 ng Hg mg C^{-1} for MeHg. The high amount of iHg in organic carbon is in line with observations that found values of up to 0.114-1.192 ng Hg mg d.w. in sediment in the Scheldt estuary and that DOM strongly binds up to 1.0 ng Hg mg^{-1} (Zaferani and Biester 2021; Haitzer et al. 2002; Muhaya et al. 1997), which would approximate our modeled 1.9 ng Hg mg C^{-1} if we assume a carbon to weight ratio of 1:2. These high iHg values in DOM lead to high values in suspension feeders in both setups. The bioaccumulation of MeHg is very different from that of iHg and has the highest bioaccumulation in the top predators and predators, followed by deposit feeders and suspension feeders. In Fig. 5.8 the relationship between the trophic level and the bioaccumulation of iHg and MeHg in megabenthos is shown. There is an increase in the MeHg content with trophic levels that are not present for iHg. For iHg, there is weak anti-correlation (R^2 = 0.20), which is mainly caused by the extremely high iHg content of the low-trophic-level suspension feeders. There is no positive relationship between the bioaccumulation of tHg and the trophic level, while this is present in the allometric scaling model; this indicates that our base model underestimates the bioaccumulation at higher trophic levels.

The effect of feeding strategy on bioaccumulation

The range and average of the annual average values of the bioaccumulation of iHg and MeHg in our model and the range and mean of measured iHg and MeHg are shown in Table 5.2. All values fall within the range of observations, except for the modeled top predator in the base model. In the allometric scaling model, the top predator has values for both iHg and MeHg in both the Southern North Sea and the Northern North Sea that are within the range of observations. Although the variation in measured iHg is considerable, suspension feeders consistently have high iHg values. MeHg is bioaccumulated more efficiently and has a higher assimilation efficiency. Because of this, MeHg content is not as dependent on the feeding strategy but is mostly dependent on the trophic level. The mean MeHg is lowest in suspension feeders (9 ng Hg

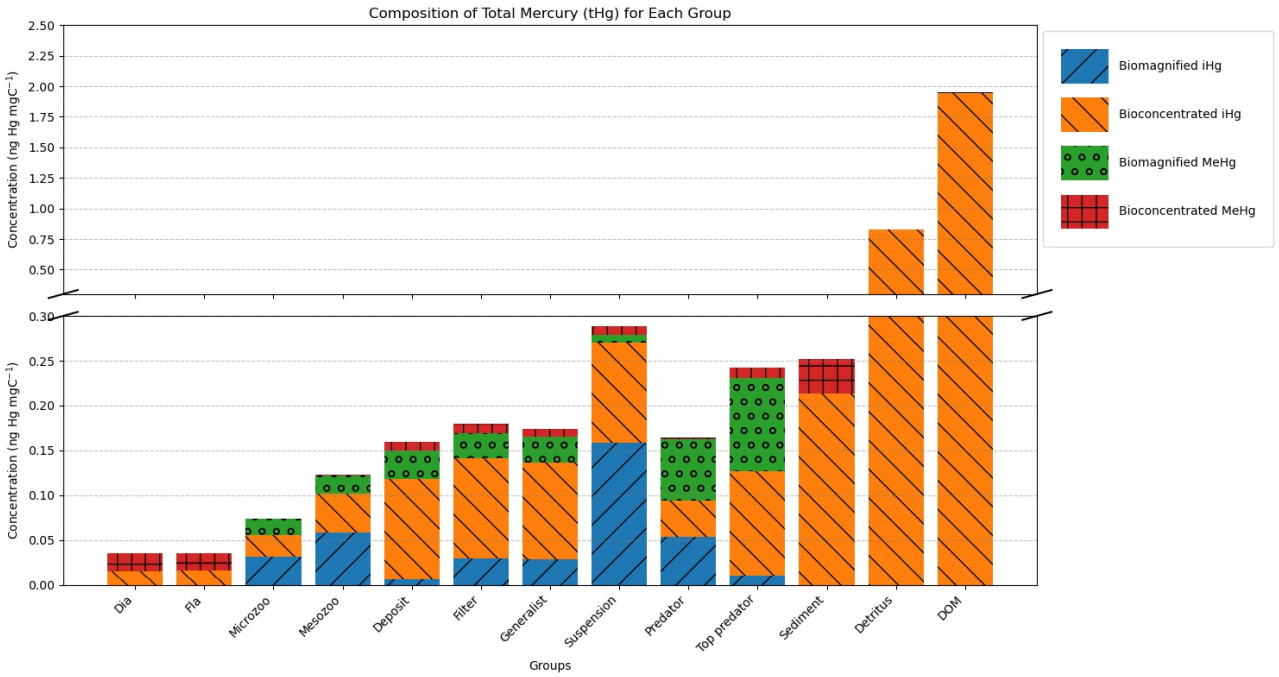

Figure 5.7: Modeled bioconcentration and biomagnification of iHg and MeHg. Partitioning to detritus and DOM is colored as bioconcentration. The y-axis is cut to show the high and low values. Notably is the high iHg to mgC ratio of detritus and DOM, leading to elevated iHg in suspension feeders. Additionally, higher trophic level animals have higher biomagnified MeHg.

g^{-1} d.w.) while it is very similar for deposit feeders (22 Hg g^{-1} d.w.), filter feeders (19 Hg g^{-1} d.w.) and generalist feeders (19 Hg g^{-1} d.w.). It is notably higher for predators and highest for top predators with a median value of 36 and 59 ng Hg g^{-1} d.w. respectively.

Trophic level vs bioaccumulation

The relationship between the trophic level and the bioaccumulation of iHg, MeHg, and tHg for the literature study is shown in Fig. 5.4, and for the model is shown in Fig. 5.8. In both the literature study and our model, there is no strong correlation between trophic level and iHg bioaccumulation. In the literature study, $R^2 < 0.01$ and in our model there is an anti-correlation of $R^2 = 0.20$. In both cases, there is a strong correlation between the bioaccumulation of MeHg and the trophic level. This is $R^2 = 0.49$ for the literature study and $R^2 = 0.81$ in our model. Our model does have a lower effect on the trophic level on MeHg bioaccumulation. Figure 5.9 shows the relationship between the trophic level and bioaccumulation in the allometric scaling model. There is a notable increase in the correlation between the bioaccumulation of

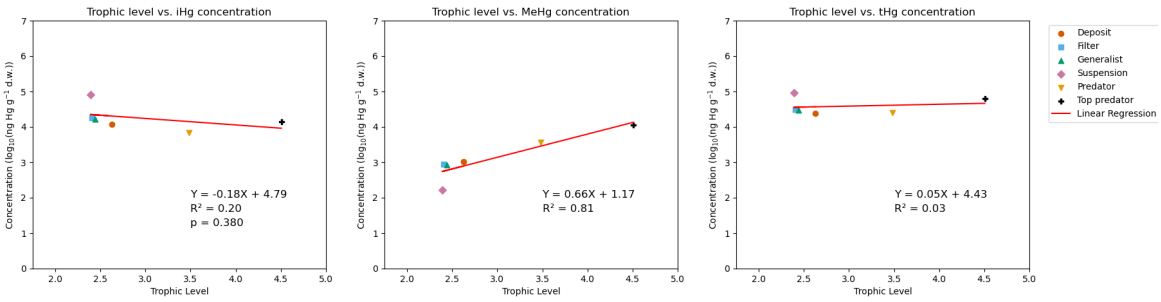

Figure 5.8: Relationship between the natural logarithm of bioaccumulated MeHg, iHg, and tHg with trophic level. There is a strong relationship between modeled MeHg and trophic level (R^2=0.81) but not for iHg (R^2=0.20) or tHg (R^2=0.03).

Table 5.2: Comparison of modeled and observed Hg and MeHg bioaccumulation in different feeding strategies for the Southern North Sea (SNS), Northern North Sea (NNS), and field observations. Values are presented as ranges with means in parentheses. Units are ng Hg g d.w. for iHg and MeHg, and % for MeHg percentage.

	Model (SNS)			Model (NNS)			Observations		
	iHg	**MeHg**	**% MeHg**	**iHg**	**MeHg**	**% MeHg**	**iHg**	**MeHg**	**% MeHg**
Suspension	104-155 (130)	8-11 (9)	7	60-148 (100)	5-11 (7)	7	34-515 (146)	1-26 (8)	5
Filter	63-77 (70)	16-21 (19)	20	66-96(77)	8-11 (9)	9	8-82 (44)	2-83 (25)	36
Deposit	53-66 (59)	19-26 (22)	16	34-56 (44)	8-12 (10)	13	12-113 (42)	2-70 (19)	31
Generalist	61-74 (68)	16-21 (19)	28	58-92(73)	7-11 (9)	9	8-113 (43)	2-83 (21)	33
Predator	45-49 (47)	35-37 (36)	39	38-42 (40)	15-17 (16)	25	1-329 (54)	7-171 (57)	51
Top predator	62-66 (64)	56-61 (59)	46	43-57 (50)	23-32 (27)	31	40-255 (47)	77-640 (158)	84
Predator (AS)	45-48 (47)	41-44 (42)	38	38-42 (40)	17-19 (18)	24	1-329 (54)	7-171 (57)	51
Top predator (AS)	62-66 (64)	249-264 (258)	80	43-57 (50)	101-131 (115)	39	40-255 (47)	77-640 (578)	84

Table 5.3: Statistical analysis of model performance for iHg and MeHg levels by feeding strategy for Southern North Sea (SNS) and Northern North Sea (NNS).

	SNS				NNS			
	iHg		MeHg		iHg		MeHg	
	N. Bias	**LR10**	**N. Bias**	**LR10**	**N. Bias**	**LR10**	**N. Bias**	**LR10**
Suspension	-0.11	0.11	0.16	0.0070	-0.37	0.12	-0.10	0.070
Filter	0.61	0.045	-0.25	0.031	0.77	0.069	-0.64	0.035
Deposit	0.43	0.035	0.18	0.019	0.052	0.029	-0.47	0.021
Generalist	0.60	0.042	-0.13	0.024	0.71	0.051	-0.60	0.028
Predator	-0.13	0.087	-0.37	0.061	-0.26	0.087	-0.71	0.074
Top predator	-0.44	0.10	-0.84	0.53	-0.56	0.11	-0.93	0.59
Predator (AS)	-0.13	0.087	-0.26	0.059	-0.26	0.087	-0.68	0.071
Top predator (AS)	-0.44	0.10	-0.32	0.37	-0.56	0.11	-0.70	0.47
Overall Model Performance								
RMSE	19		132		27		145	
NRMSE	0.19		0.35		0.26		0.39	
R-squared	0.84		0.86		**0.49**		0.91	
RMSE (AS)	19		51		27		110	
NRMSE (AS)	0.19		0.13		0.26		0.30	
R-squared (AS)	0.84		>0.99		**0.49**		>0.99	

MeHg and tHg with the trophic level compared to the base model.

5.3.3 The allometric scaling law in high trophic level animals

In Table 5.3 we show that if we take the allometric scaling law into account the model results for high-trophic level animals increase considerably. In Fig. 5.9 we show the relation between the natural logarithm of bioaccumulation and the trophic level of the allometric scaling model in the Southern North Sea setup. This increases the linear fit to 1.24x-0.26, which has a slope very similar to the observed 1.14x + 0.389. Additionally, the normalized bias in the predator and top predators decreased from -0.37 and -0.82 to -0.26 and -0.24, respectively. This is an improvement in the model and shows that while the feeding strategy is an essential driver of Hg bioaccumulation, other differences between high- and low-trophic-level animals should also be taken into account when modeling MeHg bioaccumulation.

5.3.4 The effect of water column mixing

Finally, if we compare our 2 setups, we find that our model predicts MeHg bioaccumulation three times higher in the shallow permanently mixed Southern North Sea setup than in the deeper seasonally mixed

Northern North Sea setup. In our model, this is mostly caused because the megabenthos in the shallow Southern North Sea can feed directly from the phyto-and zooplankton bloom. This gives them greater access to protein-rich food that strongly binds to MeHg. In the Northern North Sea, the ecosystem revolves around the sinking of detritus. Since detritus binds less MeHg than living material, there is a reduction in overall Hg bioaccumulation in the Northern North Sea compared to the Southern North Sea, but especially for MeHg. This means two things. First of all, in the well-mixed Southern North Sea, filter feeders have a competitive advantage as they can filter out fresh food and feed on relatively high trophic level zooplankton. Filter feeders have the highest MeHg values at the base of the benthic food web, and therefore a higher concentration of filter feeders will lead to a higher fraction of filter feeders in the predator diet and thus more MeHg. Additionally, since the filter feeders feed on living pelagic material with higher MeHg values, the filter feeders themselves also have higher MeHg. Thus, predators and, consequently, the top predators have higher MeHg values in the Southern North Sea compared to the Northern North Sea as a result of the increased water column mixing. In Fig. 5.10 we show the correlation between the natural logarithm of bioaccumulated Hg and the trophic level in the Northern North Sea. Interestingly, the trophic level of megabenthos is higher in the Northern North Sea, while the bioaccumulation level is lower. This is because the detritus is cycled more often in the pelagic before it is consumed by megabenthos, because the detritus is in constant equilibrium with the water column for its partitioning of Hg and MeHg, this does not translate to higher bioaccumulation. This lower bioaccumulation results in lower concentrations of MeHg in high trophic levels of fish.

5.4 Comparing model and observations

First, we compare the values for iHg. The probability that the model is within 2 standard deviations of the observation is $>$0.95 in all cases. In most cases, the LR10 is $<$ 0.1, which provides strong evidence in favor of the null hypotheses, indicating that the distribution of the model output closely matches the distribution of the observations and suggests that the model accurately reproduces the properties of the observations. The only instance where the LR10 $>$0.1 for iHg is for suspension feeders. This comparison yields several interesting results. Our model estimates that suspension feeders have the highest iHg values, but comparing our model with field observations shows that the observed values are even higher. In our model, the high iHg values are caused by the very efficient Hg scavenging of small DOM particles. These small particles have the highest Hg/C ratio (as was shown in Fig. 5.7) and can only be consumed by suspension feeders. This leads to very high iHg and low MeHg in suspension feeders. The result that our model partially replicates the high iHg values in the suspension feeders indicates that we underestimated this effect or that additional factors were contributing to the high iHg levels found. In Orani et al. (2020), it is demonstrated that the extremely low MeHg/Hg ratio in suspension-feeding sponges may be caused by the demethylation of MeHg by symbiotic bacteria. Our study expands on this by showing that the high

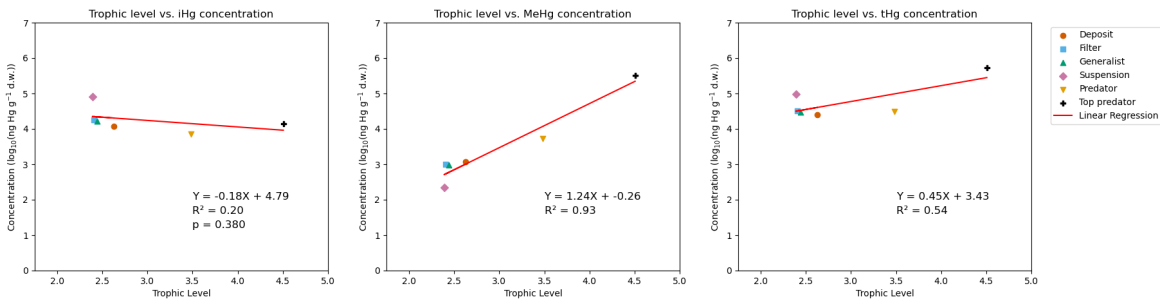

Figure 5.9: The natural logarithm of the modeled bioaccumulation of iHg, MeHg and tHg in the permanently mixed Southern North Sea using the allometric scaling model is shown against the trophic level. Notably is the stronger slope (1.24) in bioaccumulation of MeHg, which is notably higher than the slope in the default setup (0.66). The slope in the allometric scaling model overlaps much better with the observed relationship of 1.14.

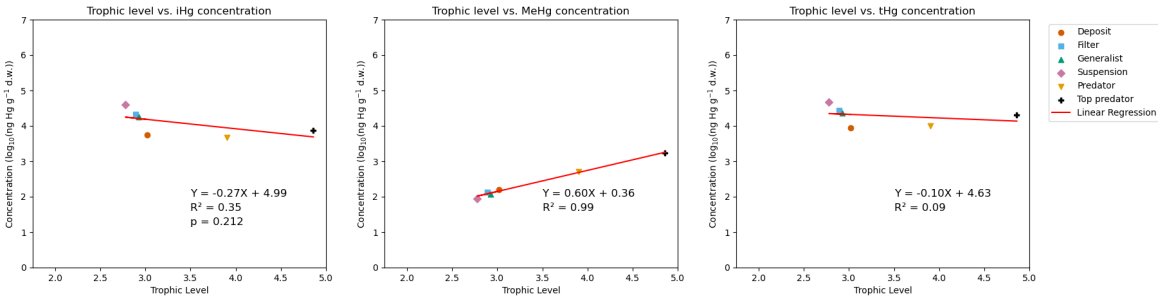

Figure 5.10: The natural logarithm of the modeled bioaccumulation of iHg and MeHg in the permanently mixed Northern North Sea setup. While the slope is somewhat similar (0.60 vs 0.66) the overall bioaccumulation of MeHg is notably lower than in the permanently mixed Southern North Sea.

iHg and low MeHg values can partially be explained by the consumption of DOM by suspension feeders, but the proposed demethylation could explain why we cannot fully replicate the observations. Based on this, it is likely that the unique bioaccumulation values in suspension feeders are caused by a combination of their ability to feed on DOM, together with biochemical processes that occur in their symbiotic bacteria. Notably, while not statistically significant, our model overestimates the mean iHg values with a normalized bias of 0.61 and 0.77 for filter feeders and 0.60 and 0.60 for generalist feeders in the Southern North Sea and Northern North Sea, respectively. In Fig 5.7 we see that the majority of this iHg originates from bioconcentration. This discrepancy is described in more detail later in the paper.

Our base model fails to reproduce the high values in the top predators, but this is improved in the allometric scaling model. The normalized bias is reduced from -0.84 to -0.32, but the LR10 is reduced only from 0.53 to 0.37. This shows that while the modeled mean is closer to the observed mean, there is no strong indication that the modeled values are from the same distribution as the observations. In the allometric scaling model, we get a linear relationship of 1.24x-0.26 (R^2=0.93), which is very similar to the 1.14x+0.389 found in the field observations. The drastic improvement in the allometric scaling model compared to the base model indicates that the lower MeHg release rates in high-trophic-level animals should be taken into account. We tried to run the model with the lower MeHg release rate in all megabenthos, but this resulted in unrealistically high values in both the base and top of the food web, so we cannot just use the lower MeHg release rate at every trophic level. Because of this, we conclude that the difference in the release rate of MeHg-related body size, metabolic rate, or activity likely has a significant contribution to the high MeHg values in high-trophic-level animals.

The last difference between our model and observations is that our model deposit feeders have considerably higher MeHg bioaccumulation compared to generalist feeders, filter feeders, and suspension feeders. This is not the case in the field observations where deposit feeders are similar to filter feeders and generalist feeders in MeHg. Interestingly, we already gave deposit feeders a lower assimilation efficiency compared to other functional groups. Since we do not model actual organisms, this difference can be caused by other differences in the organisms, such as their metabolic rate, or the assimilation efficiency of deposit feeders should be even lower. A final option is that the MERCY v2.0 model is mainly focused and verified on pelagic Hg cycling, so we potentially overestimate the sediment MeHg content or the AE of sediment-bound MeHg.

5.5 Bioconcentration of iHg

The largest bias in our model, which remains uncorrected in the allometric scaling model, is the overestimation of iHg in the filter, deposit, and generalist feeders. Although the modeled iHg values are not out of the observed range, the consistently high normalized bias indicates that the model overestimates the bioaccummulation of iHg. In Fig. 5.7 we can see that the vast majority of iHg in filter, deposit, and generalist feeders originates from bioconcentration. The most important driver of bioconcentration is the ratio between uptake and release rate, or the uptake-release ratio. Our model has an uptake-release ratio

of 210 l g^{-1} d.w. This is derived from Tsui and Wang (2004), as it represents the lowest ratio found in the literature. The exact rate was obtained by withdrawing the modeled carbon excretion rate and deducting this from the measured iHg release rate to have an iHg specific release rate, this rate was found to be 0.04 d^{-1}, as presented in Chapter 3. Other studies such as Pan and Wang (2011) found higher uptake-release ratios between 424 and 781 l g^{-1} d.w.

To address this uncertainty, we tested an alternative scenario in which we doubled the bioconcentrated iHg release rate, 0.04 d^{-1} to 0.08 d^{-1}, thus lowering the uptake-release ratio to 105 l g^{-1} dw. This adjustment resulted in a normalized bias in the Southern North Sea of -0.09, 0.15 and 0.15 for the deposit, filter, and generalist feeders, respectively. This shows how the uptake and release rates of iHg can impact the iHg content of megabenthos, and that the uptake-release ratio used in the model is likely overestimated.

The discrepancy between the modeled and observed iHg can be caused by several factors. First, iHg concentrations in North Sea megabenthos could be higher than those reported in other coastal zones. However, there are no empirical data to support or invalidate this conclusion at the moment. Secondly, translating experimentally obtained uptake and release rates to observations of iHg might depend on the drivers that are not captured in the model. In either case, it is hard to verify the root of this high normalized bias, as the bioaccumulation of iHg is comparatively understudied compared to the bioaccumulation of MeHg, both in models and empirical studies.

5.6 Model limitations

Our model is designed to have the same rates for all megabenthos groups. This allows us to isolate the effect of the feeding strategy, but it should be taken into account that this also means that the model is limited in its ability to predict bioaccumulation of iHg or MeHg in specific animals. Furthermore, when our model is compared to the data in the literature, it should be noted that field studies measuring Hg at the base of the food web are rare. Our model is run in the North Sea, while most of the field observations are from different regions. This is somewhat mitigated by aggregating large amounts of data and comparing it to our idealized water column scenarios to identify general trends, but it must be noted that comparison can always be improved by having more data to compare it to. The first and most notable limitation is that some field studies that analyzed megabenthos benthos did not differentiate between iHg and MeHg and that most studies did not estimate the trophic level of the animals. This is especially problematic when comparing Hg levels with our model.

The difference in bioaccumulation between the permanently mixed Southern North Sea setup and the seasonally mixed Northern North Sea setup is caused by several assumptions in the model. Notably, instant partitioning between dissolved Hg and Hg associated with detritus. The complication with this is that the partitioning coefficients are based on the $\log(k)^{ow}$ values of Hg, while it has been demonstrated that the binding of Hg to organic material also depends on its sulfate content (Seelen et al. 2023). Since the ECOSMO E2E model is a Redfield ratio-based model, we did not take the freshness of the organic material into account, but this might play a role and should be investigated in further studies.

A final interaction that we did not take into account is *in vivo* Hg speciation. This is not taken into account because at the moment there is too much uncertainty about the role this plays in Hg bioaccumulation. However, the earlier mentioned demethylation in sponges by Orani et al. (2020) and additional studies that demonstrate Hg speciation in cuttlefish by Gentè et al. (2023) and Hg methylating bacteria in copepods by Gorokhova et al. (2020) indicate that the bioaccumulation of iHg and MeHg may not be fully independent processes. These could be important interactions, and especially *in vivo*, methylation could be a driver of high MeHg values, but more empirical studies must be performed on the rates of this before this can be incorporated in models in a meaningful way.

5.7 Summary and conclusion

In this study, we analyze the role of the trophic level and the feeding strategy on the bioaccumulation of iHg and MeHg. We did this by performing a literature study and running a fully coupled 1D model in two idealized setups representing two different hydrodynamics regimes in which macrobenthic communities

can live. Our study estimates that the trophic level predicts up to 32% of the variability MeHg in the benthic food web. If we include both the feeding strategy and the trophic level, this increases to 72%. We show that several feeding strategies have significant differences.

We show that there are notable differences between feeding strategies. iHg is higher in suspension feeders and MeHg is low in suspension feeders and grazers, while filter feeders have the highest MeHg followed by deposit feeders. Our model expands on this by demonstrating that we can accurately model the bioaccumulation of iHg and MeHg at the base of the food web by only taking the feeding strategy into account. Because our base model agrees well with both observed iHg (R^2=0.86) and MeHg (R^2=0.91) in the Southern North Sea setup, we conclude that you can accurately model the bioaccumulation of both iHg and MeHg at the base of the food web based on the feeding strategy. However, this strong performance is mostly because 4 out of our 6 megabenthos groups are low trophic level non-predators, and our base model starts to underperform considerably in its ability to model MeHg bioaccumulation in higher trophic levels. This problem is solved by taking into account the allometric scaling law and assuming that MeHg removal from the organism is not linked to the total but rather to the base metabolic rate. Because of this, we accept our hypothesis that the feeding strategy is an essential driver of the bioaccumulation of iHg and MeHg in low-trophic-level animals, but other differences in the organisms between high- and low-trophic-level animals should also be taken into account when predicting MeHg values in high-trophic-level fish. Our model and observation focus on lower-trophic-level benthic invertebrates, with some high-trophic-level animals added to create context. The importance of this for the bioaccumulation of MeHg in animals of high trophic levels is that all biomagnification is an exponential function starting at the base of the food web. Therefore, a change in MeHg at the base of the food web will correspond to a similar relative increase at the top of the food chain. Because the feeding strategy has such a large impact on the base of the food web, high trophic-level animals would have considerably different MeHg values depending on the species composition of the base of the food web.

Interestingly, despite the lower biomagnification potential of iHg, its high abundance in certain low-trophic-level animals can lead to higher tHg in low trophic level animals than in higher-trophic-level animals. This discrepancy can distort risk perception, as safety assessments often rely on tHg measurements that do not distinguish between iHg and MeHg. Such animals may have high Hg values while remaining safe for human consumption. Our findings demonstrate the importance of Hg speciation data in marine organisms to help improve food safety guidelines and inform regulatory policies.

5.7.1 Societal relevance & future work

Our study highlights the critical role of benthic diversity in driving MeHg bioaccumulation. Both trophic interactions and the feeding strategy significantly influence MeHg bioaccumulation, which has important implications for seafood safety and fisheries management. Understanding these processes can help explain the spatial and temporal variability in the MeHg content of fish, which is crucial for policymakers to develop effective regulations that safeguard human health and marine ecosystems.

Our findings suggest that fish from food webs dominated by filter feeders would have the highest MeHg content, since filter feeders have the highest MeHg content in both our model and observations. It also creates an indication that the introduction of bivalve communities in the form of mussel or oyster farming could increase MeHg levels in higher food chains. However, such changes in the ecosystem would inevitably change other factors in the ecosystem, including biomass and trophic interactions that are also essential drivers for MeHg bioaccumulation. This means that case-by-case studies are needed to fully understand how changes in the base of the food web will affect the concentration of MeHg in high trophic level fish.

We strongly recommend targeted field studies that systematically measure iHg, MeHg, and trophic levels in diverse marine communities to assess how the structure of the food web influences the bioaccumulation of MeHg in seafood.

5.8 Acknowledgments

Readability suggestions for this paper were generated using rAI tools such as ChatGPT (OpenAI), while AI-based spell checks such as Grammarly and Writefull were used to correct spelling. In addition, AI

tools helped optimize the R and Python scripts and provide coding suggestions. All suggestions were implemented only after critical manual evaluation. Finally, Google Scholar and Perplexity were used to find sources for literature research, which were consequently manually read, verified, and cited.

Author contributions

The contributions per author are listed in Table 5.4.

Table 5.4: Contributions per Author. Authors are: David Johannes Amptmeijer (DA), Andrea Padilla (AP), Sofia Modesti (SM), Prof. Dr. Corinna Schrum (CS), and Dr. Johannes Bieser (JB).

Contributor role	**Role definition**	**Authors**
Conceptualisation	Conceptualized the study	DA, JB, CS
	Developed the research objectives	DA, JB, CS
Methodology	Implementation of the model into FABM	DA
	Compiled the database of megabenthos iHg and MeHg observations	DA, AP
Evaluation	Evaluated the model performance against observations	JB, DA, AP, SM
	Performed statistical tests on the observations	DA, AP, SM
Writing	Writing of the original draft	DA
	Review of the original draft and quality control	AP, SM, JB, DA
Supervision	Supervised the development of the work	CS, JB, DA
Funding acquisition	Acquired funding via the GMOS-Train ITN	JB

Conflict of interest

None of the authors declare any conflict of interest.

Funding

This research has been funded by the European Union's Horizon 2020 research and innovation programme under the Marie Skłodowska-Curie grant agreement no. 860497.

5.9 Annex 1

The table with all observations used for this study is shown in Table 5.5.

Table 5.5: Data used for the literature study. tHg and Mehg values are in ng Hg g^{-1} d.w.

Species	Common name	Trophic level	feeding strategy	tHg	MeHg	Location	Reference
Stronglyocentrotus droebachiensis	Sea urchin	1,87	Deposit	24	2	Svalbard	Korejwo et al. (2022)
Ophiopholis aculeata	Brittle star	2,70	Filter	47	2	Svalbard	Korejwo et al. (2022)
Baccinum glaciale	Glacial whelk	3,71	Deposit	49	12	Svalbard	Korejwo et al. (2022)
Henricia sp	starfish	3,17	Predator	348	19	Svalbard	Korejwo et al. (2022)
Astarte borealis	Northern Astarte	2,90	Suspension	44	10	Chukchi Sea	Fox et al. (2013)
Ampelisca macrocephala	Amphipod	2,70	Deposit	70	32	Chukchi Sea	Fox et al. (2013)
Chinoecetes opilio	Snow crab	4,10	Predator	131	102	Chukchi Sea	Fox et al. (2013)
Neptunea heros	Northern neptune	4,30	Predator	195	171	Chukchi Sea	Fox et al. (2013)
Buccinum spp	Whelk	4,10	Predator	269	171	Chukchi Sea	Fox et al. (2013)
Gammarellus sp.	Gammarid	2,37	Predator	39	15	Gulf of St. Lawrence	Lavoie et al. (2010)
Littorina littorea	Common periwinkle	2,29	Grazer	51	13	Gulf of St. Lawrence	Lavoie et al. (2010)
Buccinum undatum	Waved whelk	2,83	Predator	127	85	Gulf of St. Lawrence	Lavoie et al. (2010)
Tectura testudinalis	Common tortoise limpet	2,00	Grazer	51	9	Gulf of St. Lawrence	Lavoie et al. (2010)
Strongylocentrotus droebachiensis	Green sea urchin	1,69	Deposit	42	5	Gulf of St. Lawrence	Lavoie et al. (2010)
Hippoglossoides platessoides	American plaice	4,22	Benthic fish	146	77	Gulf of St. Lawrence	Lavoie et al. (2010)
Glyptocephalus cynoglossus	Witch flounder	4,22	Benthic fish	179	100	Gulf of St. Lawrence	Lavoie et al. (2010)
Somateria mollissima	Common eider	3,47	Seabird	640	565	Gulf of St. Lawrence	Lavoie et al. (2010)
Anguilla anguilla	European eel		Benthic fish	1161	895	Baltic Sea	Polak-Juszczak (2018)
Gadus morhua	Atlantic cod		Benthic fish	346	269	Baltic Sea	Polak-Juszczak (2018)
Platichtys flesus	European flounder		Benthic fish	77		Baltic Sea	Polak-Juszczak (2014)
Platichtys flesus	European flounder		Benthic fish	58		Baltic Sea	Polak-Juszczak (2014)
Pleuronectes platessa	European plaice		Benthic fish	51		Baltic Sea	Polak-Juszczak (2014)
Pleuronectes platessa	European plaice		Benthic fish	40		Baltic Sea	Polak-Juszczak (2014)
Scophthalmus maximus	Turbot		Benthic fish	114		Baltic Sea	Polak-Juszczak (2014)
sScophthalmus maximus	Turbot		Benthic fish	85		Baltic Sea	Polak-Juszczak (2014)
Macoma balthica	Baltic macoma		Deposit	53		Baltic Sea	Polak-Juszczak (2014)
Macoma balthica	Baltic macoma		Deposit	25		Baltic Sea	Polak-Juszczak (2014)
Saduria entomon	Isopod		Predator	21		Baltic Sea	Polak-Juszczak (2014)
Saduria entomon	Isopod		Predator	14		Baltic Sea	Polak-Juszczak (2014)
Acanthella acuta	Cactus sponge		Suspension	115	6	Mediterranean Sea	Orani et al. (2020)
Acanthella acuta	Cactus sponge		Suspension	66	7	Mediterranean Sea	Orani et al. (2020)
Acanthella acuta	Cactus sponge		Suspension	107	11	Mediterranean Sea	Orani et al. (2020)
Acanthella acuta	Cactus sponge		Suspension	95	9	Mediterranean Sea	Orani et al. (2020)
Axinella damicornis	Crumpled dustor sponge		Suspension	97	2	Mediterranean Sea	Orani et al. (2020)
Axinella damicornis	Crumpled dustor sponge		Suspension	212	9	Mediterranean Sea	Orani et al. (2020)
Axinella damicornis	Crumpled dustor sponge		Suspension	252	7	Mediterranean Sea	Orani et al. (2020)
Chondrilla nucula	Caribbean chicken-liver sponge		Suspension	149	2	Mediterranean Sea	Orani et al. (2020)
Chondrilla nucula	Caribbean chicken-liver sponge		Suspension	233	1	Mediterranean Sea	Orani et al. (2020)
Chondrilla nucula	Caribbean chicken-liver sponge		Suspension	519	4	Mediterranean Sea	Orani et al. (2020)
Chondrilla nucula	Caribbean chicken-liver sponge		Suspension	317	4	Mediterranean Sea	Orani et al. (2020)
Haliclona fulva	Orange encrusting sponge		Suspension	80	3	Mediterranean Sea	Orani et al. (2020)
Haliclona fulva	Orange encrusting sponge		Suspension	76	2	Mediterranean Sea	Orani et al. (2020)
Haliclona fulva	Orange encrusting sponge		Suspension	107	6	Mediterranean Sea	Orani et al. (2020)
Haliclona fulva	Orange encrusting sponge		Suspension	146	6	Mediterranean Sea	Orani et al. (2020)
Halichondria panicea	Breadcrumb sponge		Suspension	81	23	Killkieran Bay	Orani et al. (2020)
Halichondria panicea	Breadcrumb sponge		Suspension	122	9	Killkieran Bay	Orani et al. (2020)
Hymeniacidon perlevis	Breadcrumb sponge		Suspension	107	20	Killkieran Bay	Orani et al. (2020)
Hymeniacidon perlevis	Breadcrumb sponge		Suspension	170	26	Killkieran Bay	Orani et al. (2020)
Chlamys nobilis	Noble scallop		Filter	60	19	Dapeng Bay	Pan and Wang (2011)
Ruditapes philippinarum	Manilla clam		Filter	47	17	Tolo Harbo	Pan and Wang (2011)
Saccostrea cucullata	Hooded oyster		Filter	70	15	Clear Water Bay	Pan and Wang (2011)
Perna viridis	Green mussel		Filter	30	9	Tolo Harbo	Pan and Wang (2011)
Septifer virgatus	Black mussel		Filter	92	10	Clear Water Bay	Pan and Wang (2011)
Ilyanassa obsoleta	Eastern mudsnail		Deposit	60		Gulf of Maine	Chen et al. (2009)
Amphipod spp.	Amphipod		Deposit	12		Gulf of Maine	Chen et al. (2009)
Mytilidae spp	Mussel		Filter	142	79	Eastern U.S.	Chen et al. (2014)
Carcinus maenas	Green Crab		Predator	57	42	Eastern U.S.	Chen et al. (2014)
Mytilidae spp	Mussel		Filter	173		Gulf of St. Lawrence	Cossa and Tabard (2020)
Maldanidae spp.	Bamboo Worm		Deposit	101	70	Minas Basin, Bay of Fundy	Sizmur et al. (2013)
Corophium volutator	Mud scud		Deposit	43	11	Minas Basin, Bay of Fundy	Sizmur et al. (2013)
Glyceridae spp.	Bloodworm		Predator	37	9	Minas Basin, Bay of Fundy	Sizmur et al. (2013)
Mytilidae spp	Mussel		Filter	95		Narragansett Bay, RI/MA U.S.	Taylor et al. (2012)
Nereidae spp.	Ragworm		Deposit	139		Narragansett Bay, RI/MA U.S.	Taylor et al. (2019)
Amphipod spp.	Amphipod		Deposit	93		Narragansett Bay, RI/MA U.S.	Taylor et al. (2019)
Carcinus maenas	Green Crab		Predator	126		Narragansett Bay, RI/MA U.S.	Taylor et al. (2019)
Carcinus maenas	Green Crab		Predator		80	Eastern U.S.	Taylor et al. (2019)
Mytilidae spp	Mussel		Filter		83	Eastern U.S.	Taylor et al. (2019)
Ilyanassa obsoleta	Eastern mudsnail		Deposit	177		Narragansett Bay, RI/MA U.S.	Taylor et al. (2019)
Litorrina littorea	Common periwinkle		Grazer	90		Narragansett Bay, RI/MA U.S.	Taylor et al. (2019)
Litorrina littorea	Common periwinkle		Grazer		30	Eastern U.S.	Taylor et al. (2019)
Corophium volutator	Mud scud		Deposit	10		Bay of Fundy, Nova Scotia	English et al. (2015)
Macoma balthica	Baltic macoma		Deposit	10		Bay of Fundy, Nova Scotia	English et al. (2015)
Ilyanassa obsoleta	Eastern mudsnail		Deposit	40		Bay of Fundy, Nova Scotia	English et al. (2015)
Litorrina littorea	Common periwinkle		Grazer	20		Bay of Fundy, Nova Scotia	English et al. (2015)
Nereidae spp.	Ragworm		Deposit	10		Bay of Fundy, Nova Scotia	English et al. (2015)
Maldanidae spp.	Bamboo Worm		Deposit	20		Bay of Fundy, Nova Scotia	English et al. (2015)
Balanus balanus	Acorn barnacle	2,32	Filter	10	3	Minas Basin, Bay of Fundy	Bradford et al. (2023)
Carcinus maenas	Green Crab	2,91	Predator	32	23	Minas Basin, Bay of Fundy	Bradford et al. (2023)
Corophium volutator	Mud scud	2,00	Deposit	22	11	Minas Basin, Bay of Fundy	Bradford et al. (2023)
Glyceridae spp.	Bloodworm	4,15	Predator	29	18	Minas Basin, Bay of Fundy	Bradford et al. (2023)
Goniadidae spp.	Goniadidae	4,18	Predator	69	37	Minas Basin, Bay of Fundy	Bradford et al. (2023)
Ilyanassa obsoleta	Eastern mudsnail	2,59	Deposit	139	26	Minas Basin, Bay of Fundy	Bradford et al. (2023)
Lineidae spp.	Ribbon worm	2,99	Deposit	31	13	Minas Basin, Bay of Fundy	Bradford et al. (2023)
Litorrina littorea	Common periwinkle	2,34	Grazer	60	8	Minas Basin, Bay of Fundy	Bradford et al. (2023)
Macoma balthica	Baltic macoma	2,32	Deposit	76	11	Minas Basin, Bay of Fundy	Bradford et al. (2023)
Maldanidae spp.	Bamboo Worm	2,37	Deposit	45	23	Minas Basin, Bay of Fundy	Bradford et al. (2023)
Mytilus edulis	Blue mussel	2,10	Filter	59	10	Minas Basin, Bay of Fundy	Bradford et al. (2023)
Nereidae spp.	Ragworm	2,21	Deposit	80	6	Minas Basin, Bay of Fundy	Bradford et al. (2023)
Pagurus acadiarnus	Acadian hermit crab	2,90	Predator	17	7	Minas Basin, Bay of Fundy	Bradford et al. (2023)
Phyllodocidae spp.	Paddle worm	2,94	Predator	67	18	Minas Basin, Bay of Fundy	Bradford et al. (2023)

Figure 5.11: Hermit crab (*Pagurus bernhardus*). Picture taken by Dr. Eric Wurtz.

Bridging chapter

In the previous study, I demonstrated that suspension feeders are unique in their very low MeHg/Hg ratio and that this can partially be explained by their ability to consume DOM. The model is deliberately designed to isolate the effect of the feeding strategy; this means that we can make conclusions about the importance of the feeding strategy, but it also means that we cannot necessarily explain the low MeHg/Hg ratio as other drivers might play a role. This is because several interactions that could influence this ratio are not accounted for. Most importantly, there is limited importance of suspension feeders in the North Sea. As mentioned in the previous chapter, the important category of DOM-consuming suspension feeders that had extremely high inorganic and low MeHg values were sponges found in the bay of Villefranche la Mer. Because of this, I updated the model in 2 ways. Using the newly developed hGOTM tool developed by my supervisor Dr. Johannes Bieser, I could generate a physical setup to resemble the bay of Villefranche in which I could simulate HMA sponges in circumstances where they were sampled. Secondly, I updated the model to have more realistic rates and lifestyles for both HMA sponges and the other modeled macrobenthos. This included making several changes to the ECOSMO E2E model, notably including both semi-labile DOM and terrestrial DOM so that the HMA sponges have a consistent supply of DOM to consume. This allowed me to use this model to first perform a sensitivity study on the demethylation in HMA sponges suggested by Orani et al. 2020 and estimate a demethylation rate of MeHg in HMA sponges. This allowed me to quantify how *in vivo* MeHg demethylation in HMA sponges influences the bioaccumulation of MeHg in HMA sponges and subsequently the bioaccumulation in higher trophic levels.

Figure 5.12: Breadcrumb sponge (*Halichondria panicea*). Picture taken by Dr. Eric Wurtz.

CHAPTER 6

DOM Uptake and Demethylation in HMA Sponges: Drivers of Low MeHg in Benthic Food Webs

David J. Amptmeijer[1],Ulrike Hanz[3],, Johannes Bieser[1], Corinna Schrum[1,2]

[1]Matter Transport and Ecosystem Dynamics, Helmholtz-Zentrum Hereon, Geesthacht, Germany
[2]Universität Hamburg, Institute for Marine Sciences, Mittelweg 177, 20146 Hamburg, Germany
[3]Benthic Ecology, Alfred Wegener Institute, Am Alten Hafen 26, 27568 Bremerhaven, Germany

Mercury (Hg), particularly methylmercury (MeHg), is a bioaccumulative neurotoxins that threaten human health through seafood consumption. Remediation of MeHg in the marine environment is limited, and effective clean-up solutions are scarce. Sponges have been proposed as natural bioremediators due to their ability to efficiently filter out large amounts of Hg from the water column, and they may demethylate MeHg into the less toxic inorganic Hg (iHg). We used a one-dimensional (1D) water column model to explore drivers of MeHg bioaccumulation in sponges, focusing on Dissolved Organic Matter (DOM) uptake and *in vivo* demethylation. The model is based on field observations from the Bay of Villefranche, where sponges show high levels off iHg in both Low Microbial Abundance (LMA) and High Microbial Abundance (HMA) groups while having low levels of the more toxic MeHg, especially in HMA sponges. Model results indicate that DOM uptake by LMA sponges explains their low MeHg levels, while uptake of refractory DOM in HMA sponges can account for their even lower MeHg concentrations. Active demethylation is not required to reproduce observed MeHg levels, although microbial demethylation remains possible. A rate of $\sim$1% d^{-1} could explain the 58% lower concentration of MeHg in HMA sponges compared to LMA sponges, though rates up to 16% d^{-1} are plausible. Elevated iHg concentrations suggest strong retention, possibly due to limited release or binding to cellular components such as sulfated polysaccharides. These mechanisms could reduce MeHg concentrations in benthic fish by up to 45% through trophic transfer of low MeHg organic matter. Our results highlight the potential of sponge-based bioremediation.

Keywords: Mercury (Hg), Methylmercury (MeHg), Bioaccumulation, Ecosystem modeling

Publication Status

This chapter is based on a to be submitted paper. It is submitted to be presented at the World Sponge Conference.

Graphical abstract

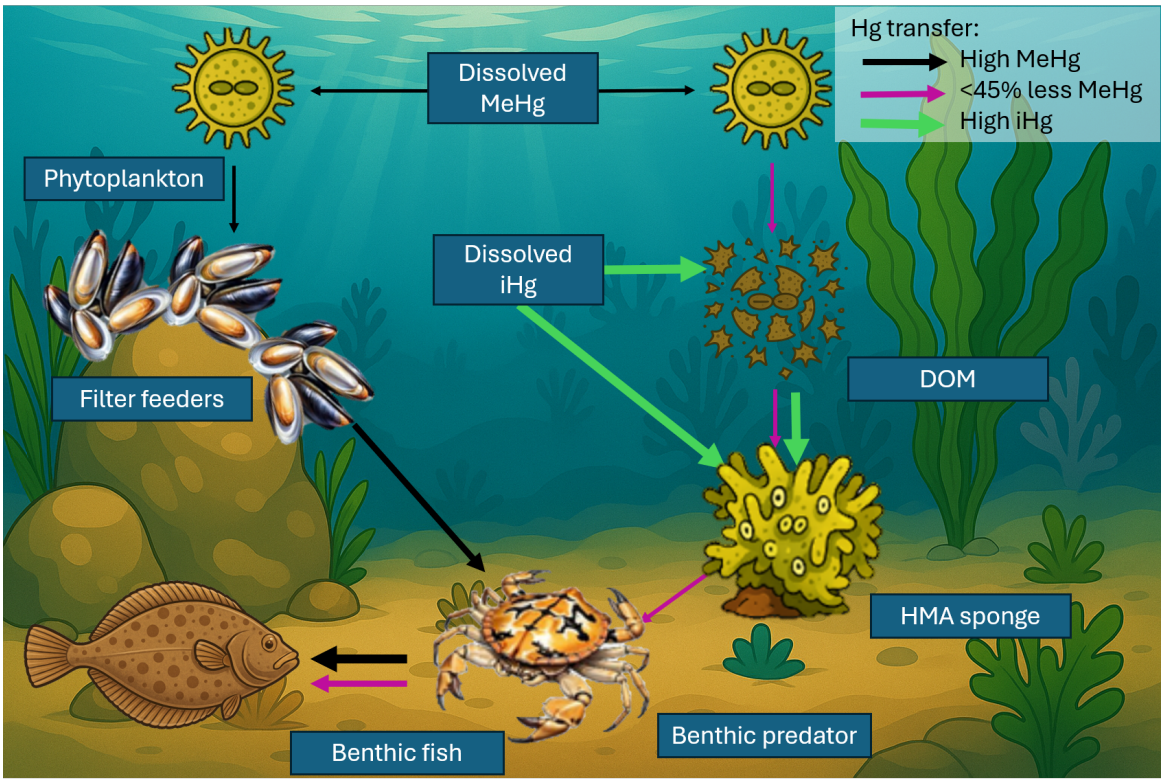

Figure 6.1: Our model shows that megabenthic animals that directly consume phytoplankton accumulate considerably higher MeHg concentrations than suspension feeders, such as sponges, which feed on dissolved organic matter (DOM). When high microbial abundance (HMA) sponges dominate the base of the benthic food web and consume large amounts of DOM, the bioaccumulation of MeHg in high trophic level fish can be up to 45% lower. At the same time sponge taken up a very high amount of iHg, which can partially be explained by high partitioning of iHg to DOM. The image is composed of several sub-images that are generated using openART and GPT 4.1.

.

6.1 Introduction

Mercury (Hg) and methylmercury (MeHg), are both toxic pollutants that can bioaccumulate throughout the food chain (Mason et al. 1995). Although both Hg and MeHg can bioaccumulate, MeHg has a much higher bioaccumulation potential and greater toxicity (Jeong et al. 2024). MeHg bioaccumulates especially in high-trophic-level fish, which poses health risks to humans when consumed. In commercially important species such as Mediterranean bluefin tuna (*Thunnus thynnus*), Hg concentrations can increase by up to 8 orders of magnitude compared to seawater levels (Storelli et al. 2002; Tseng et al. 2021). Consumption of MeHg-polluted fish causes adverse health effects in humans and is estimated to cost the European Union up to €8-9 billion per annum, mostly due to the loss of intelligence in children (Bellanger et al. 2013). Furthermore, Hg pollution leads to reduced fish stocks and restrictions on fishing practices, which can decrease supply and profitability in the fishing sector (Pacyna et al. 2006). Hg is present in the marine ecosystem in several distinct chemical species that form a dynamic equilibrium. Important species for marine Hg cycling are elemental Hg (Hg^0), dissolved Hg (Hg^{2+}), monomethyl mercury ($MMHg^+$), dimethylmercury (DMHg), and cinnabar (HgS). Hg0 and DMHg are both dissolved gaseous Hg that can evaporate from the surface ocean. Hg^{2+} and $MMHg^+$ are the only Hg species known to bioaccumulate (Morel et al. 1998). HgS can be precipitated and is considered the most important sink of Hg out of the biosphere. In this paper, all species together are referred to as Hg, the sum of both $MMHg^+$ and DMHg is referred to as MeHg, and all non-methylated Hg is referred to as inorganic Hg (iHg). As only $MMHg^+$ and Hg^{2+} have been shown to bioaccumulate, we will model the bioaccumulation of these two Hg species, as was done in Chapter 3. A

table with commonly abbreviations in this study including the different Hg species is shown in Table 6.1.

The primary pathway for MeHg bioaccumulation in aquatic ecosystems begins with direct uptake of MeHg from the water column by respiration, absorption, or swallowing. When this uptake results in higher concentrations within the organism than in the surrounding water, it is called bioconcentration. This occurs because MeHg binds strongly to organic material, especially selenol groups (-SH) groups, which are common in proteins (Lavoie et al. 2015). This process can increase MeHg concentrations within organisms by up to 100,000 times compared to concentrations in surrounding water (Lee and Fisher 2016). This process is dependent on the surface area of organic membranes with water, and is therefore especially efficient in small animals (Mason et al. 1995). Because of this, this process is especially important at the base of the food web, in organisms such as phytoplankton (Mason et al. 1995). Bioconcentration however, does significantly influence the bioaccumulation of MeHg in higher trophic levels, as is discussed in Chapter 4. When predators consume phytoplankton, these predators can take up MeHg that is bioconcentrated in phytoplankton very efficiently, leading to a higher concentration of MeHg in predators compared to their prey (Mason et al. 1996). This process of increasing MeHg with increasing trophic positions is called biomagnification and can lead to extremely high concentrations of MeHg in high trophic level animals, including species that are often consumed by humans (Lavoie et al. 2013).

The importance of this route of bioaccumulation is supported by strong evidence from models (Schartup et al. 2018; Rosati et al. 2022; Bieser et al. 2023), field studies (Lavoie et al. 2010), and laboratory experiments (Mason et al. 1995; Tsui and Wang 2004; Wang and Wong 2003).

6.1.1 The role of DOM in MeHg bioaccumulation

Dissolved Organic Matter (DOM) plays a crucial role in the bioaccumulation process. DOM can bind to MeHg and these DOM-MeHg complexes can be transported to phytoplankton through transport channels (Garcia-Arevalo et al. 2024). The bioavailability of MeHg is significantly influenced by the characteristics of DOM, particularly the presence of specific functional groups within the DOM, such as thiol groups (DOM-RSH) (Seelen et al. 2023).

Although phytoplankton forms the base of most marine food webs, not all trophic chains start with living phytoplankton. While most aquatic animals can only feed on material that is large enough to be filtered from the water, sponges, in particular, can consume DOM (De Goeij et al. 2013). Due to their pumping activity, sponges and their associated microbes can process and filter up to 24,000 liters of seawater per day (Vogel 1974). Sponges can utilize symbiotic bacteria, but there is a strong distinction between High-Microbial-Assemblage (HMA) sponges and Low-Microbial-Assemblage (LMA) sponges. HMA sponges can have 10^8 to 10^{10} bacteria g^{-1} sponge, whereas LMA sponges have 10^5 to 10^6 bacteria g^{-1} sponge, which is roughly equivalent to the concentration of bacteria in seawater (Hentschel et al. 2012). Symbiotic bacteria can extract DOM out of the water for consumption, giving sponges the rare ability among marine animals to utilize DOM as a food source. This difference in the size of the microbiome also means that HMA sponges have a higher assimilation efficiency of DOM compared to LMA sponges (Bart et al. 2020). LMA sponges, on the other hand, compensate for the decreased size of their microbiome and their ability to utilize DOM as a food source by relying on pumping large water concentrations and filtering more particulate organic material (Hentschel et al. 2006). While in HMA sponges, the high abundance of associated microbes can account for **up to 35% to 40%** of the total biomass of sponges (Vacelet and Donadey 1977). This high microbial biomass is crucial for the sponge's nutrition and overall health, as these microbes play essential roles in nutrient cycling and processing DOM within the sponge's ecosystem. Furthermore, bacterial symbionts from HMA sponges possess a wide variety of genes that confer unique biogeochemical attributes not commonly found in other animals (Webster and Thomas 2016). The unique ability of sponges to consume DOM can have a ripple effect throughout the food chain since HMA sponges utilize organic matter that is not available to other organisms and transfer it to higher trophic levels (Hanz et al. 2022). In this way, they play an important ecological role as pseudo-autotrophic producers and they facilitate the indirect transfer of DOM via sponges to higher trophic level predators, such as fish, starfish, or sea urchins, which feed on sponges. Additionally, DOM assimilated into larger organic material by sponges can be excreted as detritus, which can be consumed by other animals in a process known as the sponge loop (De Goeij et al. 2013).

6.1.2 Hg in sponges

Studies analyzing iHg and MeHg in sponges found extreme variability in the Hg and MeHg content. Orani et al. (2020) found that in the Mediterranean Sea sponges generally have extremely low MeHg and a low MeHg/Hg ratio of 4%, while sponges in the intertidal area of the Celtic Sea have very high MeHg concentrations and high MeHg / Hg ratios of between 7 and 28%. Recent efforts in sponge identification suggest that of the 4 sponges sampled from Orani et al. (2020) from the Mediterranean Sea, 3 species are classified as LMA sponges; *Acanthella acuta* (Gloeckner et al. 2014), *Cymbaxinella damicornis*, recently reclassified under the genus *Axinella* (Erwin et al. 2015), and *Haliclona fulva* (García-Bonilla et al. 2019), while 1 sponge, *Chondrilla nucula*, is classified as HMA (Thiel et al. 2007). Remarkably, all sampled sponges have an extremely low MeHg concentration and a low MeHg/Hg ratio, but the HMA sponges have both lower MeHg and higher iHg compared to the sampled LMA sponges.
The low MeHg content in sponges in the Mediterranean Sea is proposed to be caused by active *in vivo* MeHg demethylation by Orani et al. (2020). HMA sponges have been found to contain bacterial symbionts that possess the MerA and MerB genes (Santos-Gandelman et al. 2014a). The merA gene transcribes the mercuric reductase protein that converts Hg^{2+} to volatile Hg^0 and merB transcribes for organomercurial lyase, which catalyzes the breakdown of carbon Hg through protonolyses and can demethylate toxic MeHg into less toxic Hg^{2+} (Mathema et al. 2011), but this does not explain the low concentration of MeHg in LMA sponges. An alternative proposal for the low MeHg concentration of HMA sponges is that this is low due to the consumption of DOM. This is proposed in Chapter 5. This is a modeling study in which the effect of feeding strategy of iHg and MeHg is modeled. In this study, the binding of iHg and MeHg to DOM and detritus is based on Batrakova et al. (2014), which finds a higher affinity of DOM to bind iHg rather than MeHg, whereas detritus has a stronger affinity for MeHg. In Chapter 5, the feeding on DOM is shown to be a driver of high iHg and low MeHg in suspension feeders. In that study, the feeding strategy was isolated and their model does not consider other biological factors that might impact bioaccumulation, such as *in vivo* demethylation, the extended lifespan of sponges, and their low metabolic rate. Additionally, the model is simulated in conditions representing the North Sea, where HMA sponges are not present. In this study, we expand on the model presented in Chapter 3 by creating a more realistic model of sponges. We focus on incorporating the life cycles and feeding behaviors of megabenthos groups to enhance the understanding of iHg and MeHg bioaccumulation in Mediterranean Sea sponges, while running the simulation under hydrodynamic and climatological conditions typical of the Western Mediterranean Sea, where HMA sponges are common.

6.1.3 The hypotheses

Based on the previous literature, we have 3 hypotheses.

- The low MeHg concentrations in LMA sponges can be attributed to their consumption of DOM, while the even lower levels observed in HMA sponges are likely due to both DOM consumption and active demethylation.
- The elevated iHg concentrations in both LMA and HMA sponges can be explained by their uptake of inorganic mercury from DOM.
- Sponges can reduce the MeHg concentration in benthic fish by having a low MeHg concentration and forming the base of the food web

To test these hypotheses, we constructed a model to trace the bioaccumulation of MeHg within the Mediterranean Sea food web in the Bay of Villefranche, a region of notable concern with respect to Hg contamination (Claisse 1989), using a state-of-the-art food web model. This enables us to initially assess the levels of iHg and MeHg accumulating in LMA sponges and determine if our model can accurately replicate the observed data. Subsequently, we can estimate the demethylation rate necessary to account for the observed differences between LMA and HMA sponges. Finally, we can use this model to assess the differences in MeHg bioaccumulation in fish in a setup with and without sponges to see if sponges influence the MeHg bioaccumulation in fish.

Table 6.1: Definitions of Hg abbreviations.

Abbreviation	Meaning
Hg	Refers to Hg in general
Hg^{2+}	Dissolved Hg (Bioaccumulates)
Hg^{0}	Elemental Hg (Volatile)
$MMHg^{+}$	Monomethylmercury (Bioaccumulates, extremely toxic)
DMHg	Dimethylmercury (Volatile, extremely toxic)
MeHg	$MMHg^{+}$ + DMHg
iHg	Sum of all Hg that is not MeHg
DGM	Dissolved Hg^{0} and DMHg
HMA sponge	High microbial assemblage sponge
LMA sponge	Low microbial assemblage sponge
DOM	Dissolved organic matter
lDOM	Labile dissolved organic matter
sDOM	Semi-labile dissolved organic matter
rDOM	Refractory dissolved organic matter
SPs	sulfated polysaccharides

6.2 Materials and methods

6.2.1 The model domain; The Bay of Villefranche

The Bay of Villefranche is a natural bay located just west of the French-Italian border, near the French town of Villefranche-sur-Mer. The Bay is known for its deep oligotrophic waters with steep underwater topography, rocky inlets, and sandy bottoms. The nearby Villefranche Canyon creates diverse habitats that support different benthic communities. Monitoring programs within the Bay were mainly focused on planktonic research of coastal waters (Dolan 2014). This is the reason why similar and abundantly available long-term benthic community data from nearby areas of the Gulf of Lyon were used to evaluate our model.

6.2.2 The hydrodynamic model; GOTM

The one-dimensional (1D) Generalized Ocean Turbulence Model (GOTM) is used as the hydrodynamic model, which calculates the turbulence of a vertical 1D water column setup by computing the solutions to the one-dimensional version of the transport equation of momentum, salinity, and temperature (Bolding et al. 2021). The model is nudged to observational data sets for temperature and salinity. The setups are designed using the hGOTM tool, which is driven by gridded bathymetry data for water depth (1/240°) (GEBCO Bathymetric Compilation Group 2020), the ECMWF ERA5 dataset for meteorological data (Wouters et al. 2021), the World Ocean Atlas for salinity and temperature profiles (Garcia H.E. et al. 2019) and TPOX-9 atlas for tides (Egbert and Erofeeva 2002).

6.2.3 Coupling GOTM to the biogeochemical models using FABM

The MERCY v2.0 model and the ECOSMO E2E model are coupled to the GOTM model using the Framework for Aquatic Biogeochemical Modeling (FABM) (Bruggeman and Bolding 2014). The biogeochemical models are coded into FABM. The FABM interfaces communicate the state variables between the GOTM model and the biogeochemical models. Physics is modeled with a vertical grid resolution of 0.71 grid cell m^{-1}. The model's state variables are updated every 120 seconds using the forward Euler method to solve the ordinary differential equation.

Hg cycling and speciation; the MERCY v2.0 model

Hg speciation and cycling are modeled using the MERCY v2.0 model (Bieser et al. 2023). The MERCY v2.0 model is an Hg cycling and speciation model that simulates the cycling and speciation of Hg, Hg^0, $MMHg^+$, DMHg, and HgS, its partition to detritus and DOM, and the bioaccumulation of $MMHg^+$ and Hg^{2+} while taking into account biomagnification and bioconcentration at every trophic level.

Carbon cycling and ecosystem dynamics; the ECOSMO E2E model

The ecosystem in which Hg bioaccumulates is simulated using an altered version of the ECOSMO E2E model. The original ECOSMO model presented by Daewel and Schrum (2013) is expanded in the ECOSMO E2E model to incorporate higher trophic levels while preserving consistency in lower trophic levels (Daewel et al. 2019). Several adjustments to this model are presented in Chapter 3 to make sure that the model, which is originally developed for carbon cycling, is also suitable for bioaccumulation. In this paper, the ECOSMO E2E model is further altered by expanding the megabenthos by splitting it into 6 megabenthos groups separated by their feeding strategies. For every group, a model organism is selected based on which group is parameterized. The megabenthos groups and model organisms are filter feeders (mussel; *Mytilus sp*), deposit feeders (lugworm; *Arenicula marina*), generalist feeders (brown shrimp; *Crangon crangon*), suspension feeders (LMA sponge; *Mycale hentscheli*), suspension feeders with bacterial symbionts (HMA sponge; *Chondrilla nucula*), benthic predators (crab; *Carcinus maenas*), and benthic fish (European plaice; *Pleuronectes platessa*). Furthermore, the 2 pelagic species of fish representing herring and cod are removed to better represent the 17m deep shallow water of the Bay of Villefranche, as these species would not be present in the Bay of Villefranche. The specific species used for this model are not always the main species in these ecosystems since biological rate measurements are not available for most species. However, we assume that biological rates are representative of broader functional groups and still represent the expected ecosystem functioning.

6.2.4 Nutrient fluxes in the 1D model

Nutrient cycling is normally dependent on lateral fluxes that are not present in a 1D water column model. To compensate for this, an atmospheric deposition of 0.13 NO_3 µmol d^{-1}, 0.13 NH_4 µmol d^{-1}, 3.93E-4 PO_4 µmol d^{-1}, and 6.28E-2 SiO_4 µmol d^{-1} is introduced to compensate for the burial of organic material. This approach of using atmospheric deposition as a tuning parameter follows the methodology applied in the 1D GOTM-ECOSMO-MERCY setups for the North and Baltic Seas used in Chapter 3. The deposition values are chosen to produce realistic wintertime nutrient concentrations and support chlorophyll levels in line with observed data. This is further evaluated in the model evaluation section.

6.2.5 The megabenthos model

The physiological parameters of megabenthos within our model are derived from rates observed in laboratory conditions or through field studies. Given the inherent variability present in biological data, definitive rates are not always available and have been inferred from the referenced studies. The deposit feeders, generalist feeders, benthic predators, and benthic fish all feed based on a feeding rate and half saturation. Feeding and respiration rates are presented here as daily rates. Therefore, a feeding or respiration rate of 0.1 d^{-1} would mean that the animal consumes or respires 10% of its body weight per day. This modeling approach is based on the macrobenthos functional group in the original ECOSMO E2E model (Daewel et al. 2019). The feeding of mussels, HMA, and LMA sponges is based on their filtration rate within the bottom grid cells of the model. They consume a fraction of all food in the bottom grid cell, calculated as their filtration rate [m^3 d^{-1}] divided by the volume of the bottom grid cell [m^3], giving us the uptake [d^{-1}]. There is a maximum consumption rate beyond which a higher concentration of food in the water column will not lead to a higher intake rate. It should be noted that while we estimate the feeding, respiration, and mortality rates of megabenthos based on empirical studies, the modeled animal still represents functional groups.

The uptake rates of the **deposit feeder** are taken from ex-situ studies performed on a sand-eating lugworm (*Arenicula marina*), whereas this also represents other deposit feeders such as gastropods in the model. The respiration rate based on this study is 0.013 d^{-1}, and the mortality rate is 0.0005 d^{-1}. The respiration rate is estimated based on the measured oxygen consumption and converted to carbon respiration, assuming a respiratory quotient of 0.85 (Rodil et al. 2019). The mortality rate is based on the observed life expectancy of 5 years. The grazing rate is 0.12, based on the measured maximum carbon consumption rate (Rijsgard and Banta 1998; Rodil et al. 2019).

The **filter feeders** in our model are modeled after mussels (*Mytilus sp.*). They are parameterized to have a filtration rate of 9.60E-4 m^3 m^{-3} d^{-1}, a maximum feeding rate of 0.21 d^{-1}, a respiration rate of 0.00867 d^{-1}, and a mortality rate of 0.0063 d^{-1} (Koopmans and Wijffels 2008). The high filtration rate means that mussels can grow the fastest of all megabenthos groups in our model when food is abundant, but their high respiration rate means that they are competitively disadvantageous when food is limited.

The model organism for the **generalist feeder** in our set-up is the brown shrimp (*Crangon crangon*). They eat microzooplankton, mesozooplankton, detritus, and sediment organic carbon. They are estimated to have a lifespan of 3 years, or a mortality rate of 0.0083 d^{-1}, and a maximum feeding rate of 0.12 d^{-1} (Perger and Temming 2012). Regnault (1981) found a respiration rate of per 51μl O^2 h^{-1} in a 91 mg^{-1} d.w. shrimp, or 0.55 mg O_2 g^{-1} d.w. This can be translated into a respiration rate of 0.00752 d^{-1} based on a respiratory quotient of 0.85 (Rodil et al. 2019). As a generalist, they thrive in highly variable circumstances where their ability to use different food sources gives them a competitive advantage.

Benthic predator

The benthic predator is the mid-level trophic animal that couples Hg bioaccumulation from the base of the food web to higher trophic levels. As such, this is arguably the functional group that represents the largest number of species in our model. Rates are estimated after the shore crab (*Carcinus maenas*), but the functional group of benthic predators would also include other animals. This is because there is not one animal that feeds on all the included megabenthos groups. Notable predators of HMA sponges are, for example, white seabream (*Diplodus sargus*), the nudibranch *Hypselodoris cantabrica*, and the purple sea urchin (*Paracentrotus lividus*) (Bertolino et al. 2024; Cruz et al. 2012; Maldonado and Uriz 1998). The benthic predator is modeled based on laboratory studies of Wallace (1973). They found a feeding rate of 0.065 d^{-1} at 10 °C and 0.13 d^{-1} at 24 °C and observed that the investigated shore crabs were not active below 5 °C. In addition, they found respiration rates between 0.0277 and 0.133 d^{-1}. Based on this, we assume that benthic predators below 5 °C do not hunt; above 24 °C they have their optimum grazing rate of 0.13 d^{-1}. We used this information to approximate the temperature-dependent respiration ($R_{BP}(T)$) and grazing ($P_{BP}(T)$) rates for the benthic predator as follows:

$$R_{BP}(T) = \begin{cases} 0.00277 & \text{if } T \leq 5 \\ 0.00055 \cdot T & \text{if } 5 < T \leq 24 \\ 0.0133 & \text{if } T > 24 \end{cases}$$

$$P_{BP}(T) = \begin{cases} 0 & \text{if } T \leq 5 \\ 0.0054 \cdot T & \text{if } 5 < T \leq 24 \\ 0.13 & \text{if } T > 24 \end{cases}$$

For this benthic predator, we assume a life expectancy of 3 years or a mortality rate of 0.008 d^{-1}.

Benthic fish

The benthic fish is modeled after common species such as the common sole (*Solea solea*), gilthead seabream (*Sparus aurata*), and European flounder (*Platichthys flesus*) which are often found near the seabed among vegetation or sandy substrates. They have a strong temperature-dependent grazing rate and respiration rate. Based on the work by Fonds et al. (1992) on European plaice (*Pleuronectes platessa*) we approximate the temperature-dependent respiration ($R_{BF}(T)$) and grazing ($P_{BF}(T)$) for the benthic fish as follows:

$$R_{BF}(T) = \begin{cases} 0.005 & \text{if } T \leq 2 \\ 0.005 + 0.002 \cdot (T - 2) & \text{if } 2 < T \leq 18 \\ 0.037 & \text{if } T > 18 \end{cases}$$

Max feeding rate

$$P_{BF}(T) = \begin{cases} 0.0135 & \text{if } T \leq 2 \\ 0.0135 + 0.008 \cdot (T - 2) & \text{if } 2 < T \leq 19 \\ 0.129 & \text{if } T > 18 \end{cases}$$

We assume a lifespan of 5 years, which results in a mortality rate of 0.0048 d^{-1}.
A schematic overview of all functional groups of megabenthos and how they are incorporated into the ECOSMO E2E model is shown in figure 6.2.

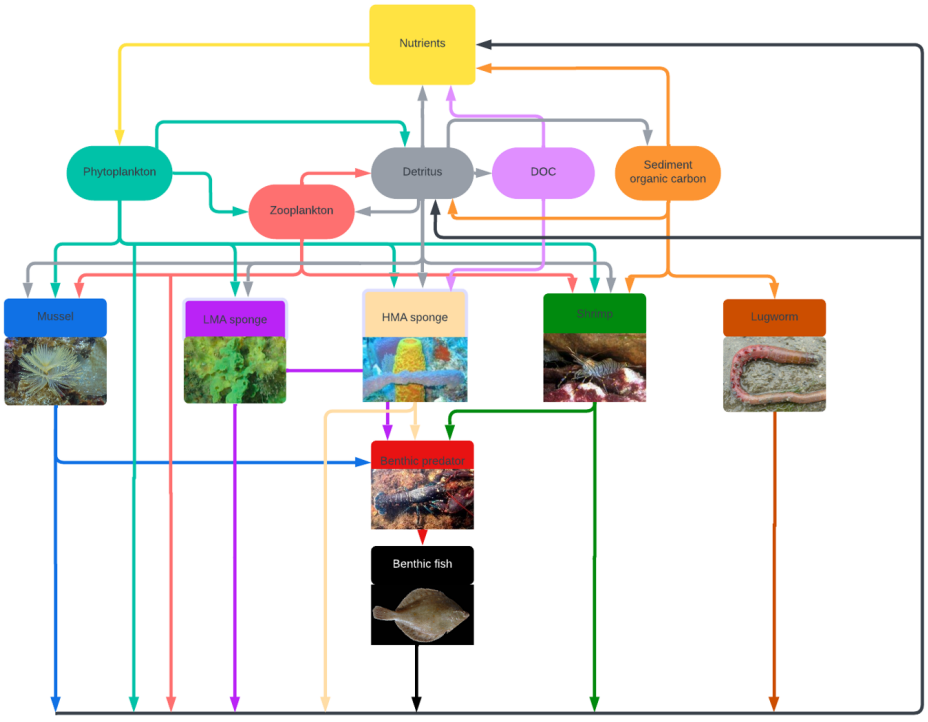

Figure 6.2: Schematic overview of the implemented megabenthos model. Sources of the images are: filter feeder: `https://en.wikipedia.org/wiki/Sabella_spallanzanii`, HMA sponge: `https://www.flickr.com/photos/noaaphotolib/5015046804/`, generalist feeder: `https://en.wikipedia.org/wiki/Shrimp`, deposit feeder: `https://fr.wikipedia.org/wiki/Arenicolidae`, benthic predator: `https://en.wikipedia.org/wiki/Lobster`, and top predator: `https://en.wikipedia.org/wiki/Plaice`. The photo of the LMA sponge is taken by Dr. Eric Wurtz and shared for the use in this publication.

6.2.6 semi-labile DOM

ECOSMO E2E has two forms of pelagic aquatic organic carbon, detritus, and labile DOM (lDOM) (Daewel et al. 2019). Since DOM is a key driver in giving sponges their competitive advantage over other suspension feeders, we also added semi-labile DOM (sDOM). sDOM does not have a sinking speed; both HMA and LMA sponges can consume it with the same efficiency as lDOM, and bacteria degrade it at the same rate as detritus. When organic material is formed in the model, it is formed as 40% lDOM, 12% sDOM, and 48% detritus. There is an additional rate of sDOM formation from detritus of 0.001 d^{-1}. These formation ratios and rates are chosen to have a realistic sDOM value of 0-50 mgC m^{-3}, based on (Lønborg et al. 2024), rather than on established rates of sDOM formation. This is described in more detail in Chapter 5.

6.2.7 Refractory DOM

In addition to the sDOM added to the model, we also added refractory DOM (rDOM). This DOM is estimated to represent 97% of the global DOM pool (Baltar et al. 2021; Lønborg et al. 2024). Estimates of rDOM in the Bay of Villefranche are not available, but measurements from a bay on Medes Island estimate the concentration of total DOM at 2.56 gC m^{-3} (Ribes et al. 1999). Since our model has 0-50 mgC m^{-3} sDOM we estimate that an additional 2.5 gC rDOM gC m^{-3} could be present in our modeled domain. Given the uncertainty surrounding the extent to which sponges utilize rDOM when lDOM, sDOM, and detritus are available, and the substantial uncertainty of rDOM's binding to Hg compared to sDOM and lDOM, we run the model simulations both with and without 2.5 gC rDOM m^{-3}. When rDOM is added, it is implemented as a fixed background concentration that is not consumed by bacteria or catabolized into nutrients. This rDOM reacts within the model in 2 ways. First, HMA sponges can take up rDOM. Since rDOM is represented as constant background concentrations, it is unaffected by sponge uptake. To address this, and considering its low energy value as a food source for sponges, its uptake is limited to 10% efficiency compared to fresh DOM. Therefore, for HMA sponges, 2.5 gC rDOM m^{-3} corresponds to an equivalent of 0.25 gC m^{-3} lDOM, sDOM, or detritus in terms of its food availability. The difference in efficiency between the consumption of rDOM and other food sources is not based on a known value, but it is a necessary estimation, since if HMA sponges could feed on rDOM as efficiently as on other food fractions, they would overgrow everything, which is not what is observed in the Mediterranean Sea benthic food web. Because of this, it is used as a tuning parameter to increase the sponge biomass in a somewhat natural way, so we can evaluate the importance of the HMA sponges under different possible circumstances, and can evaluate the influence of sponges on fish MeHg bioaccumulation under a scenario with a high sponge biomass. rDOM is assumed to be mostly organic carbon with no other nutrients. The original ECOSMO E2E model assumes a Redfield Ratio in all consumers, but we deviate from this when HMA sponges consume rDOM to account for the low C:N and C:P ratio in rDOM. When HMA consumes rDOM, the biomass originating from rDOM is tracked, and when they release carbon due to respiration or mortality, the consumed rDOM is not released as labile nutrients for phytoplankton. The same is true when predators and top predators consume HMA sponges directly or indirectly. It is traced how much of the organic carbon originates from rDOM, and when this rDOM-originating organic carbon is released, it is not transferred to dissolved nutrients that are usable by phytoplankton. It is possible that in real life sponges consume rDOM that contains micronutrients, and these nutrients later may be bioavailable; this is however not studied and out of the scope of this model. To summarize, the rDOM approach offers an approximation that allows HMA sponges and their predators to achieve greater biomass without violating the mass conservation principles of the rest of the model, and rDOM does not react directly with any biota, except HMA sponges in the model.

The second way in which rDOM interacts in our model is through partitioning to iHg and MeHg. In the MERCY v2.0 model, the binding partitioning between lDOM and iHg and MeHg is assumed to be based on the K_{ow}. We use the same partitioning coefficient for lDOM, sDOM, and rDOM. A partitioning coefficient of $\log(K_{ow})$=6.4 for iHg and a coefficient of $\log(K_{ow})$=5.9 for MeHg is used. This value is the same as is used in Bieser et al. (2023) and is based on Tesán Onrubia et al. (2020).

6.2.8 LMA and HMA sponges

LMA and HMA sponges were modeled separately. It must be stated that sponges are an incredibly diverse group, and comprehensive studies analyzing rates in sponges are rare. Because of this, we take the published rates of sponges and evaluate them as well as possible. LMA sponges have a maximum consumption rate of 0.01 d^{-1}, a filtration rate of 4.80E-4 m^{-3} d^{-1}, and a combined respiration and mortality rate of 0.00257, based on the LMA sponge *Halichondira panicea* (Thomassen and Riisgadrd 1995). LMA sponges feed on phytoplankton, detritus, lDOM, and sDOM.

To distinguish the LMA and HMA sponges, we make two adjustments. First, the microbiome of HMA sponges gives them the ability to consume rDOM. However, this comes at a cost. HMA sponges are denser and filter water 52%-94% slower, due to their investment in maintaining bacterial symbionts (Weisz et al. 2008). However, their uptake efficiency is higher because of the uptake of additional DOM through their symbionts. Because of this, we give HMA sponges a filtration rate of 3.60E-4 m^{-3} d^{-1}, which is 25% lower than the LMA sponges. In our model, HMA sponges feed on detritus, lDOM, sDOM, and rDOM. When sponges are compared to observations we assume a carbon to dry weight ratio of 1:5, based on Bart et al. (2021). It is worth mentioning that while the 1:5 ratio was measured in Atlantic Deep Sea sponges rather than Mediterranean Sea sponges, it originates from the demosponges *Geodia atlantica* which should resemble the demosponges sampled in Orani et al. (2020).

6.2.9 Bioaccumulation of Hg and MeHg

The parameters and interactions with respect to bioaccumulation are based on the 1D model presented in Chapter 5. Importantly, our model models both the biomagnification and bioconcentration of both iHg and MeHg at every trophic level. In Chapter 5 it is shown that this model can accurately model MeHg bioaccumulation at the base of the food web without tuning. The bioconcentration in phytoplankton depends on the size-dependent bioaccumulation and the release rate for both iHg and MeHg. The bioconcentration in all megabenthos is based on the macrobenthos functional group from Chapter 3 and they have an uptake rate of 1.68E-5 m^3 mgC^{-1} d^{-1} and 2.22E-5 m^3 mgC^{-1} d^{-1} for iHg and MeHg, respectively. All megabenthos have a release rate of 0.04 d^{-1} for iHg while there is no additional release rate for MeHg. Additionally, both MeHg and iHg are released with respiration and mortality. For biomagnification, an iHg assimilation efficiency (AE) of 0.31 is used and a MeHg AE of 0.95, when biota or detritus is consumed. When sediment is consumed, the AE of iHg is 0.07 and 0.43 for MeHg, based on Dutton and Fisher (2012). When DOM is consumed, the AE is 0.95 for both iHg and MeHg. This is based on the work of Garcia-Arevalo et al. (2024) in phytoplankton, which shows that DOM can play an essential role in facilitating iHg transfer into cells. The assumption is that the DOM molecules are absorbed as a whole, and therefore the iHg associated with this would have a high assimilation efficiency for both iHg and MeHg.

6.2.10 Scenarios

We suggest that there are 2 pathways leading to HMA sponges having a lower MeHg content than LMA sponges; the consumption of DOM and *in vivo* demethylation. To assess the relative importance of both pathways we first model the bioaccumulation in HMA sponges under base conditions, where there is no rDOM for the sponges to feed on and the sponges do not demethylate. Afterwards, we simulate sponge bioaccumulation in a scenario where 2.5 gC rDOM m^{-3} is present. This allows us to quantify the effect of rDOM consumption on the bioaccumulation of MeHg in HMA sponges. We then perform a sensitivity analysis by varying demethylation rates in HMA sponges to identify the demethylation required to explain the observed MeHg bioaccumulation in LMA and HMA sponges.

Finally, we assess MeHg bioaccumulation in benthic fish by comparing the base case to the scenarios with 2.5 gC rDOM m^{-3}. This allows us to estimate the potential impact of HMA sponges on MeHg concentrations in fish. We focus on the 2.5 gC rDOM m^{-3} scenario because it represents a high HMA sponge biomass resembling a sponge reef. The goal is to evaluate whether this effect is plausible, rather than to quantify its real-world magnitude, as the 1D water column model used here is not suitable for capturing spatial complexity.

6.2.11 Statistical interpretation of the results

The evaluation of MeHg bioaccumulation in LMA and HMA sponges involves assessing the Mean Percentage Bias (MPB), of which the equation is shown in Table 6.7 in annex 1. This metric was chosen because typically in assessing models the bias is used, which is the average difference between model and observations; however, we could not use this due to the uneven amount of data between the model output and observations. Therefore, we first take the mean of the model output, and then estimate the percentile bias between the modeled and observed mean. This is further supported by performing a Kolmogorov–Smirnov (KS) and Wilcoxon signed-rank (W) tests. These non-parametric tests are selected because the small sample sizes (n = 4 for HMA and n = 6 for LMA) are insufficient to reliably test for normality in the observed data. The KS test is conducted using the `ks.test()` function, and the Wilcoxon signed-rank test is performed with the `wilcox.test()` function in R (version 4.1.2, "Bird Hippie"). The evaluation considers the D-statistic, the Kolmogorov–Smirnov p-value (KS-p), and the Wilcoxon p-value (W-p). All tests are based on comparisons between the average daily model outputs from the last decade of the simulation and the observations reported by Orani et al. (2020).

The D-statistic measures the maximum deviation between the cumulative distributions of the model and observations, thus measuring the maximum differences in the distribution. A D value below 0.1 suggests very similar distributions, values between 0.1 and 0.5 indicate minor to moderate differences, and a D value greater than 0.5 shows a large difference. The KS-p value calculates whether a significant difference between the modeled and observed distributions exists, while the W-p value estimates the significance of the difference between their medians. P-values below 0.05 for either KS-p or W-p are considered significant.

There is a large difference in sample sizes, with 3652 model data points compared to only 4 and 6 observed data points for HMA and LMA sponges, respectively. This imbalance can influence the D, KS-p and W-p values. Therefore, the KS and W test results are interpreted to compare the setups, rather than definitive indicators of model fit or mismatch. Especially for the KS test, analyzing the distribution of 4 or 6 points should not be used to come to definitive conclusions. Despite these constraints, the D, KS-p, and W-p results still provide valuable insights into the overall agreement between modeled and observed MeHg bioaccumulation patterns in HMA and LMA sponges and can help to compare the different model scenarios.

6.3 Model evaluation

6.3.1 Evaluation of Nutrient cycling

As mentioned in the methods section, the nutrient deposition is selected to create a realistic phytoplankton community to drive our megabenthos model. In our model, the wintertime nutrient concentrations are 0.12 µmol l^{-1} NH_4^+, 5.0 µmol l^{-1} NO_3^-, 0.3 µmol l^{-1} PO_4^{3-}, and 1.6 µmol l^{-1} $Si(OH)_4$. These values are on the higher end of observations in the Western Mediterranean Sea but align with elevated nutrient concentrations found in the Gulf of Lion, where surface nitrate and phosphate concentrations reach up to 3.58 ± 1.16 µmol l^{-1} and 0.2–0.3 µmol l^{-1}, respectively . While the modeled silicate concentration is on the lower end of the observed range (1.6–5.8 µmol l^{-1}), based on the World Ocean Atlas 2018, silicate is not typically a limiting factor for phytoplankton growth in the Western Mediterranean, making this value acceptable for our modeling purposes (Belgacem et al. 2021). Based on this, we conclude that the modeled nutrient concentrations are in line with observations and can be used to simulate phytoplankton in our model.

6.3.2 Evaluation of primary production

We evaluate the modeled chlorophyll a concentrations against NASA MODIS-A satellite chlorophyll time series, for the same geographic location (https://oceancolor.gsfc.nasa.gov/). The observational chlorophyll time series was sourced from the COPEPOD project (REPHY 2020). The NASA combined-satellite chlorophyll data presents monthly mean values, allowing for a comprehensive comparison. To evaluate whether

the model captures the general chlorophyll a dynamics of the region, we focused on monthly means. Specifically, we averaged modeled chlorophyll values for each calendar month over the last decade of the simulation (e.g., the mean of all Januarys, all Februarys, etc.), and compared these to the corresponding monthly means from the NASA dataset.

While this approach smooths over interannual variability, it offers a way to assess whether the model captures the typical seasonal cycle and magnitude of phytoplankton. Given our focus on bioaccumulation processes, this comparison helps ensure that the modeled phytoplankton concentrations are within a realistic range and appropriate for driving biogeochemical dynamics in the Bay of Villefranche.

The results of the chlorophyll comparison between the model and the observations are shown in Fig. 6.3a, and the corresponding Taylor diagram is shown in Fig. 6.3b. The equations from which the metrics are derived are shown in Table 6.7. The modeled and observed chlorophyll concentrations exhibit a Pearson correlation of 0.59. The root mean square error (RMSE), is 0.127 mg m^{-3}. The maximum observed chlorophyll is 0.54 mg m^{-3} and modeled is 0.55 mg m^{-3}, while the observed mean is 0.31 mg m^{-3} and the modeled mean is 0.28 mg m^{-3}, resulting in a mean bias of -0.028 mg m^{-3}. Overall, the comparison reveals a low bias and relatively high correlation, indicating that the modeled phytoplankton dynamics are consistent with expectations for the Bay of Villefranche and provide a suitable basis for the biogeochemical processes explored in this study.

6.3.3 Evaluation of the megabenthic biomass

The benthic communities in this area have high specialization and display a patchy distribution, complicating the evaluation of our 1D model. According to Rosenberg et al. (2003), biomass values in the shallow Bay of Lyon vary widely, between 0 and 40 g ash-free dry weight m^{-2}, showing notable regional differences. Despite this, our modeled benthic biomass at 17 m ranges between 3.5 and 5 gC m^{-2}, as shown Table 6.2 and visualized in Fig. 6.4. This is in good agreement with the observed biomass of 2.1 g ash-free dry weight m^{-2} (equating to approximately 4.2 gC m^{-2} using a carbon-to-weight ratio of 1:2) at 25 m depth, as reported by Rosenberg et al. (2003). In the Gulf of Lyon, distinct benthic communities dominated by filter feeders (e.g., Spisula subtruncata, Venus ovata), deposit feeders (Scoloplos armiger), and generalist predators (Nephtys hombergii) have been identified (Labrune et al. 2007; Fromentin et al. 1997; Rosenberg et al. 2003). Although our one-dimensional model cannot resolve these complex spatial differences, our model does support stable populations of all megabenthic functional groups, making it a reasonable representation of the general benthic community structure in the area.

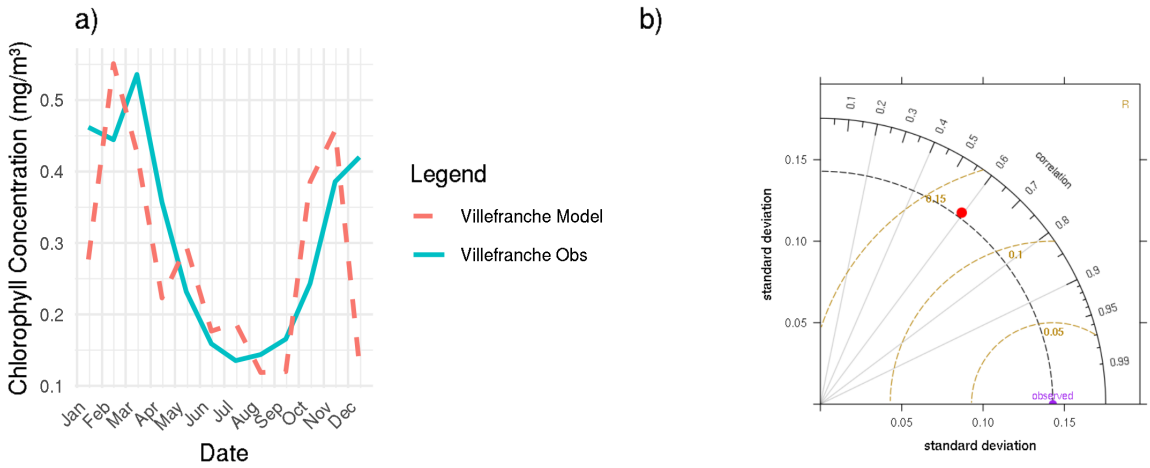

Figure 6.3: Validation of modeled chlorophyll concentrations. a) Monthly means over the last 10 years from the model and NASA MODIS-A satellite chlorophyll time series. b) Taylor diagram comparing the model and observations, showing a Pearson correlation coefficient of 0.59 and a root mean square error (RMSE) of 0.13 mg m^{-3}, based on monthly means of the 10-year averages.

Table 6.2: Model results for the biomass and bioaccumulation in the Bay of Villefranche. Biomass is shown in mgC m^{-2} and bioaccumulation in ng Hg gC^{-1}, so pelagic biomass was integrated over the watercolumn depth.

Category	**Biomass**		**iHg**		**MeHg**	
Functional group	Mean	SD	Mean	SD	Mean	SD
Generalist feeders	256	177	67	8	22	5
Deposit feeders	1741	614	64	7	18	3
Filter feeders	158	118	62	9	29	9
HMA sponges	252	82	168	42	27	5
LMA sponges	1375	692	116	20	26	8
Benthic predators	382	425	61	5	36	7
Benthic fish	226	231	61	10	61	10
Microzooplankton	16	26	37	21	12	4
Mesozooplankton	25	23	55	13	12	3
Phytoplankton	41	32	1	3	2	4
Detritus	5	4	453	32	3	1
DOM	168	108	729	49	4	2

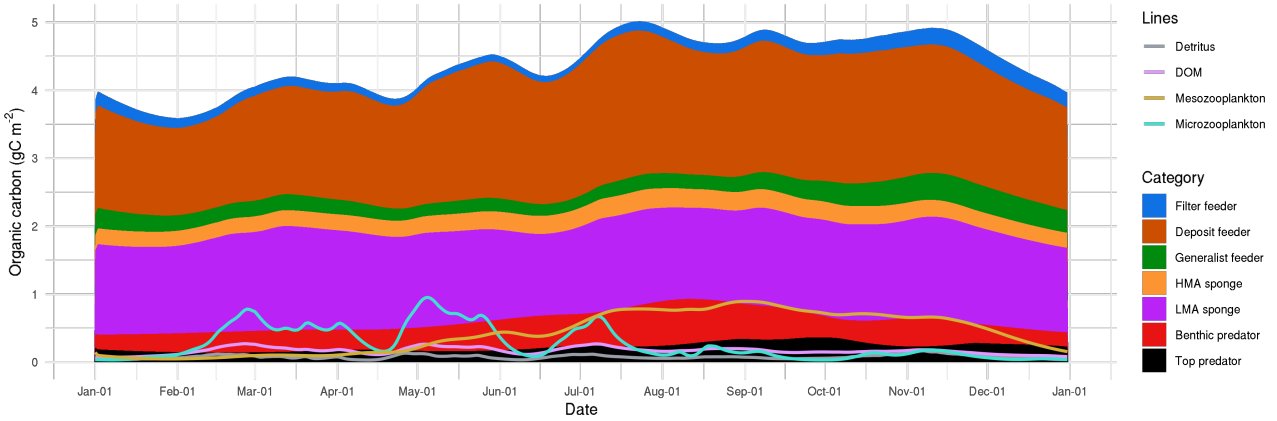

Figure 6.4: The 10-year average consumer biomass.

6.3.4 Evaluation of Hg and MeHg concentrations

Bioaccumulation starts with the dissolved concentration of the pollutants. Therefore, it is essential to assess that the MERCY v2.0 model generates concentrations of Hg and MeHg that are in line with observations. The modeled and observed aquatic concentrations of iHg and MeHg are shown in Table 6.3. Our model estimates Hg and MeHg concentrations in the Bay of Villefranche of 1.00±0.071 and 0.019±0.005 pM respectively. Observations in shallow coastal stations in the Gulf of Lion by Cossa et al. (2017) found mean Hg concentrations of 1.52±1.00 pM and MeHg concentrations of 0.026±0.024 pM, though some MeHg concentrations were below the detection limit, introducing uncertainty. This means that our modeled Hg and MeHg concentrations are well within the observed range and within 1 standard deviation, with a MPB of -34% for Hg and -26% for MeHg compared to the observed mean. Based on these results, we conclude that our model reproduces observed Hg and MeHg concentrations in the water, making it suitable to be used in our bioaccumulation modelling framework.

6.3.5 Evaluation of the MeHg bioaccumulation

The bioaccumulated iHg and MeHg per functional group are shown in Table 6.2. Observations distinguishing MeHg bioaccumulation in megabenthic organisms to compare our model results to are are. We found measurements for MeHg bioaccumulation in phytoplankton, microzooplankton, and mesozooplankton by

Table 6.3: Comparison of modeled MeHg bioaccumulation against available observations. Bioaccumulation is shown in ng Hg mgC^{-1} and the concentration of aquatic Hg and MeHg in pM. The phyto-and-zooplankton data is compared to samples from Tesán Onrubia et al. (2020), while the benthic fish data is compared to samples of European hake *(Merluccius merluccius)* and common sole *(Solea solea)* presented by Llull et al. (2017). All values are reported as the mean±SD, except for the observations in fish, where the SD was not available and is instead shown as the mean (min–max) of the observations.

	Modeled MeHg	Observed MeHg
Aquatic Hg	1.00 ± 0.071	1.52 ± 1.00
Aquatic MeHg	0.019±0.005	0.026 ± 0.024
Phytoplankton	0.6±2	0.8±1
Microzooplankton	6±2	3±2
Mesozooplankton	6±2	6±3
Benthic fish	61±10	60 (33–120)

Tesán-Onrubia et al. (2023), and mesozooplankton, whereas Llull et al. (2017) reported measurements in fish. Assessing fish is challenging because our functional group encompasses several benthopelagic predators with varying MeHg levels. Thus, we present the range of observed MeHg content for the most common benthopelagic predators in the region, namely, the European hake *(Merluccius merluccius)* and the common sole *(Solea solea)*, as illustrated in Table 6.3. We assumed a carbon-to-weight ratio of 1:2 for fish and zooplankton based on Ricciardi and Bourget (1998), and for phytoplankton, a 1:3 ratio based on Cushing (1958). Fish bioaccumulation data were reported in wet weight; we converted this to dry weight, assuming a dry weight-to-wet weight ratio of 1:5 based on Cresson et al. (2017). Since the SD was not available for the comparison to fish, we calculated the mean based on the weighted average. Although the data are insufficient for robust statistical analysis, the average MeHg content is 46 ng Hg mgC^{-1} for European hake and 69 ng Hg mgC^{-1} for common sole while the weighted average of both species together is 60 ng Hg mgC^{-1}, as recorded by Llull et al. (2017). Consequently, our model value of 61 ng Hg mgC^{-1} falls within the observed range for the benthopelagic predatory fish considered in our model.

6.4 Results

6.4.1 Expected demethylation rate of HMA sponges

Figure 6.5 shows the bioaccumulation of MeHg in HMA sponges. Without demethylation, the average bioaccumulation of MeHg is higher than the observations in HMA sponges. Having a demethylation rate of 1% d^{-1} reduces the bioaccumulation of MeHg to 10 ng Hg gC^{-1}, which better aligns it with the average observed MeHg concentration of 13 ng Hg gC^{-1} in HMA sponges. Furthermore, increasing the demethylation rate to 2.5% per day aligns the MeHg content of the HMA sponges with the lowest observations in the HMA sponges. The statistical comparison of the base model and the scenario with 1% and 2.5% demethylation d^{-1} are shown in Table 6.4. In the base model, there is a positive MPB for the MeHg content of HMA sponges (+136%) and the KS-p of <0.001 and W-p of <0.001 show a significant variation between the observed and modeled data, both in their distribution and median values. In the scenario where HMA sponges have 1% demethylation, the HMA sponges have a smaller negative bias (-23%) while the D statistic of 0.45 shows a minor difference in the distribution of the modeled and observed bioaccumulation, while the KS-p of 0.39 shows that this difference is not statistically significant. Additionally, the W-p of 0.79 shows that there is also no statistically significant difference between the observed and modeled median MeHg bioaccumulation. In the 2.5% demethylation d^{-1} scenario, the KS-p and W-p values show no significant difference between this scenario and the observations, however their value of 0.0072 and 0.0019 is considerably lower compared to the 1% d^{-1} scenario. These reduced p-values, combined with the high D value of 0.84 and an increased negative MPB of /62% show that the 2.5% demethylation d^{-1} underestimates the MeHg content of HMA sponges and has lower agreement with the observations than the scenario with 1% demethylation d^{-1}.

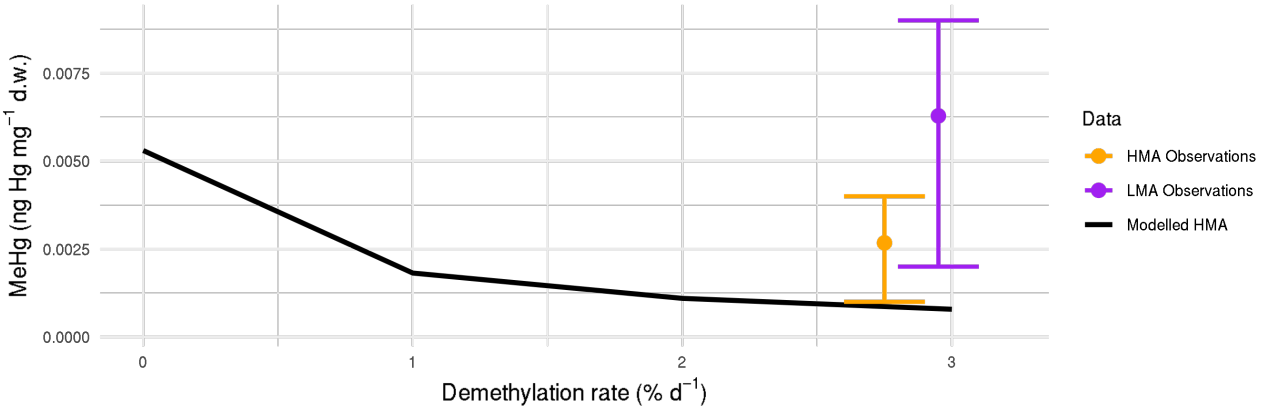

Figure 6.5: The modeled mean MeHg concentration in HMA sponges with different demethylation rates. Without demethylation, MeHg levels in HMA sponges align with those observed in LMA sponges, as indicated by the purple sidebar. A demethylation rate of 2.5% d^{-1} reproduces the minimum observed MeHg concentration in modeled HMA sponges, while a rate of 0.5% d^{-1} reproduces the maximum, as shown by the orange sidebar. A demethylation rate of 1% d^{-1} in HMA sponges provides the best agreement with the observed mean when rounded down to the nearest 0.5%.

6.4.2 Low MeHg due to DOM consumption in HMA sponges

We investigate the hypothesis that HMA sponges can have low MeHg due to their reliance on DOM as food. To investigate this we ran the model with 2.5 gC rDOM m^{-3}, which could be consumed by HMA sponges. Table 6.4 presents the results of MeHg bioaccumulation in LMA and HMA sponges alongside the outcomes of the KS-and-W tests, in comparison with the observations reported by Orani et al. (2020). In LMA sponges, a KS-p value of 0.32 and a D-statistic of 0.36 suggest no substantial difference in the modeled and observed distribution, while the MPB of -13% indicates a small bias between the modeled and observed mean. This is supported by a W-p of 0.23 which indicates no significant deviation between the modeled and observed median. For HMA sponges, there is no significant discrepancy between the observed and modeled distributions as signified by a KS-p value of 0.35. Additionally, the D-statistic of 0.46 indicates a moderate similarity between the modeled and observed distributions. The MBP of -23% along with a W-p value of 0.33 indicates a small bias in the mean, and no significant difference between the modeled and observed median. To summarize, in the scenario with 2.5 gC rDOM m^{-3} there is no significant difference in either the median or the distribution of MeHg bioaccumulation in both LMA and HMA sponges. Since the consumption of rDOM alone accounts for the low MeHg levels in HMA sponges, the model was not rerun with a demethylation rate and 2.5gC m^{-3}, as this was unnecessary to explain the observed low MeHg concentrations in HMA sponges.

Table 6.4: Observed and modeled bioaccumulation of MeHg in LMA and HMA sponges The mean, minimum, and maximum observed and modeled values are shown. Bioaccumulation values are shown in ng Hg mgC^{-1}. For the model scenarios, the mean percentile bias (MBP), the Kolmogorov–Smirnov p-values (KS-p) and D-statistic (D) are shown, as well as the Wilcoxon p-value (W-p). A * marks a significant difference at the 95% confidence level between the model and observations.

	LMA							HMA						
	Mean	MPB (%)	Min	Max	KS-p	D	W-p	Mean	MPB (%)	Min	Max	KS-p	D	W-p
Observations	31	–	10	45	–			13	–	5	20	–		
Base model	30	-3	18	72	0.12	0.45	0.26	31	+138	22	52	<0.001*	1.0	<0.001*
2.5 gC rDOM	27	-13	9	69	0.32	0.36	0.23	10	-23	3	39	0.35	0.46	0.33
1% Demethylation	29	-6	18	71	0.12	0.45	0.24	10	-23	7	30	0.39	0.45	0.79
2.5% Demethylation	25	-19	14	50	0.014	0.59	0.078	5	-62	3	16	0.0072	0.84	0.019

* indicates signicant deviations between the model and observations at the 95% confidence interval.

6.4.3 Low MeHg bioaccumulation in fish due to rDOM consumption in HMA sponges

In our model, consumption of rDOM can influence MeHg bioaccumulation in three ways. First, in our current parameterization, rDOM binds dissolved MeHg, with the same strength as lDOM and sDOM. If we include rDOM, the MeHg concentration per DOM can be reduced due to biomass dilution. This will result in lower concentration of MeHg in suspension feeders consuming DOM, and consequently in predators consuming these suspension feeder. Secondly, the consumption of rDOM by HMA sponges allows the consumption of carbon that is otherwise not bioavailable. This increases the biomass of HMA sponges, and consequently, it increases the biomass of the benthic predator and benthic fish. The shift in biomass causes a shift in the diet of the benthic predator; in the base model, the majority of their diet would consist of deposit feeders and LMA sponges, whereas in the 2.5 gC rDOM setup, their diet would mostly consist of HMA sponges followed by deposit feeders. Since HMA sponges have an extremely low MeHg concentration, this results in low MeHg in benthic predators and, consequently, in benthic fish. The concentration of MeHg in benthic fish is 68 ng Hg g^{-1} in the base model and only 61 ng Hg g^{-1} in the setup with 2.5 gC $rDOM^{-3}$. If we run the model with 2.5 gC rDOM $^{-3}$, but without HMA sponges, the bioaccumulation of MeHg in fish is 124 ng Hg mgC^{-1}. This means that the HMA sponges in this setup reduce the MeHg content of the fish by 45%. This effect is not present in the base model, nor in the setup with 1% demethylation d^{-1}, which can be explained by the low biomass of HMA sponges in the base setup compared to the 2.5 gC rDOM m^{-1} setup. This shows that the 45% reduction is an upper bound of the reduction that can be expected in benthic fish in ecosystems that are dominated by HMA sponges at the base of the food web compared to ecosystems without sponges.

6.4.4 The maximum and minimum demethylation rates

Since we can replicate the low MeHg content of both LMA and HMA sponges in the 2.5 gC rDOM scenario, we conclude that *in vivo* MeHg demethylation is not necessary to explain the observed iHg and MeHg content of either LMA or HMA sponges. However, it must be noted that the bioconcentration rates of iHg and MeHg in HMA sponges in the model are very uncertain. Because of this, it is also possible that the uptake rate is higher, which would mean a higher demethylation rate is necessary to explain the observed values. The iHg concentration in LMA and HMA sponges can be assessed by simulating a tenfold rise in LMA sponge uptake rates and a twentyfold rise for HMA sponges. This results in uptake rates of 1.68E-4 and 3.35E-4 in m^3 mgC d^{-1} for iHg in LMA and HMA sponges, respectively, and uptake rates of 2.20e-4 and 4.41e-4 m^3 mgC d^{-1} for MeHg. The modeled iHg and MeHg concentrations under these circumstances are shown in Table 6.5. Under these circumstances, a demethylation rate of 16% in HMA sponges gives the best agreement with observations, rounded to the nearest full percent point.

Table 6.5: Observed and modeled concentrations of iHg and MeHg in LMA and HMA sponges. The High Uptake (HU) models has uptake rates of 1.68E-4 and 3.35E-4 in m^3 mgC^{-1} d^{-1} for iHg in LMA and HMA sponges, respectively, and uptake rates of 2.20e-4 and 4.41e-4 m^3 mgC^{-1} d^{-1} for MeHg in LMA and HMA sponges respectively. In the low Release Rate (LR) model the release rate of iHg is reduced and this is equal to the respiration rate. In the LR model the earlier estimated 1% d^{-1} *in vivo* demethylation rate is used while in the HU model the *in vivo* demethylation rate required to reproduce observels MeHg levels is estimated to be 16% d^{-1}. Additonally the mean percent bias (MPB) between the modeled and observed concentration is shown. All bioaccumulation values are in ng Hg mgC^{-1}.

	iHg					MeHg				
	Observed	Model (HU)	MPB (%)	Model (LR)	MPB (%)	Observed	Model (HU)	MPB (%)	Model (LR)	MPB (%)
LMA	696	659	6	592	18	31	122	−75	28	11
HMA	1523	1476	3	1448	5	13	13	0	10	30

6.4.5 The high iHg of LMA and HMA sponges.

An additional method for the model to reproduce the high iHg content of sponges is to reduce the release rate. As shown in Table 6.5, the model also reproduces the high iHg content of both LMA and HMA if we assume that iHg is strongly retained in sponges and only released equal to the respiration rate of sponges. This model is referred to as the Low Release (LR) rate model. In this parameterization, there is no additional release rate of iHg in sponges. This parameterization can reproduce both the iHg and MeHg bioaccumulation in both LMA and HMA sponges with an MPB of 30% or lower.

6.5 Discussion

A summary of the results is shown in Fig. 6.6. Here we see that the model can produce the observed MeHg concentration in both LMA and HMA sponges if we assume either rDOM consumption or *in vivo* MeHg demethylation in HMA sponges of 1%. Additionally, it shows that if we assume a reduced release rate of sponges, the model can replicate the high iHg and low MeHg concentration in both LMA and HMA sponges. In this study, we tested several different scenarios for the bioaccumulation of iHg and MeHg in sponges; here we discuss the differences between these scenarios and how the results of this study can help us better understand the bioaccumulation of Hg in sponges.

6.5.1 With or without rDOM; what is the most realistic scenario

As mentioned in the model development segment, an rDOM concentration of 2.5 mgC m^{-3} is observed. However, as the name suggests, this rDOM is refractory and generally unresponsive. This raises the question as to what degree it should be incorporated in the model. There are 2 key questions;

- To what degree do sponges feed on rDOM compared to lDOM and sDOM
- Does Hg bind with equal preference to rDOM, sDOM and lDOM, and is this different for iHg and MeHg.

An argument for focusing solely on lDOM and sDOM is presented by Seelen et al. (2023). They show that the thiol content of DOM is lower in marine environments than in rivers and that DOM of terrestrial origin has a stronger affinity to bind MeHg as it is richer in thiol groups. If terrestrial DOM that is non-refractory has a considerably higher affinity to bind DOM, it is likely that this transfers MeHg to sponges upon consumption. If this is the case, having lDOM and sDOM in our model to bind and transfer MeHg, while excluding rDOM, might replicate real-world circumstances. Where labile fractions of DOM dominate MeHg binding and transfer.

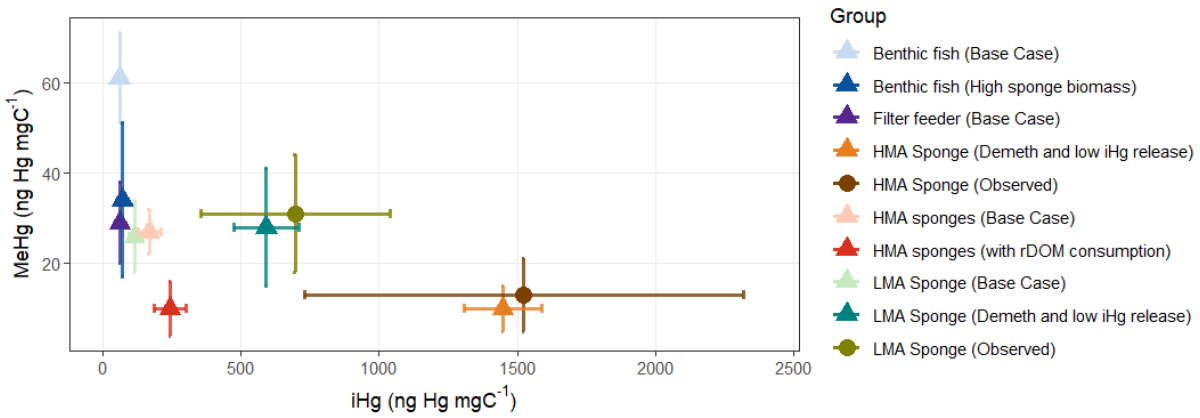

Figure 6.6: Summary visualising the important results. The triangles represent model values and the circles observations of LMA and HMA sponges. The scenario with a demethylation rate of 1% d^{-1} and reduced Hg release rate has a strong overlap with the observed LMA and HMA sponges. The MeHg concentration in fish (Blue) is reduced by 45% in the scenario where sponges have high biomass.

Additionally, while it is currently understood that HMA sponges can consume DOM, including rDOM, the degree to which they do this is poorly understood. In shallow Mediterranean Sea water, other food sources are available. Because of this, HMA sponges might predominantly feed on the more labile fractions of DOM, and rDOM could play a minor or insignificant role, both in carbon cycling and in MeHg bioaccumulation.

Arguments in favor of including rDOM are that we know it is present in large concentrations and there is only limited evidence to suggest it does not play a major role in both Hg and carbon cycling. This is also supported by our model. Our model shows good agreement (% MPB < 26) with no significant difference (ks-P > 0.28) between the modeled and observed MeHg concentrations in both LMA and HMA sponges when we incorporate rDOM in the model.

Additionally, it is established knowledge that DOM plays an important role in Hg bioaccumulation, as demonstrated by Schartup et al. (2015), and that different DOM fractions can affect Hg bioaccumulation in distinct ways, as shown by Seelen et al. (2023). Therefore, improving the representation of DOM and detritus cycling, particularly by including distinct fractions such as rDOM, represents a logical step forward to increase Hg cycling and bioaccumulation models, even in models that do not incorporate HMA sponges. To improve the model in this regard, more empirical data is needed to link rDOM to concentrations and composition to bioaccumulation. Improved knowledge of which fractions of DOM are consumed by LMA and HMA sponges and to which degree, coupled with a better understanding of the MeHg binding strength of this DOM fraction, could greatly improve our understanding of what drives these low MeHg concentrations in HMA sponges.

6.5.2 The important role of HMA sponges in lowering MeHg content of fish

While demethylation and DOM consumption can both play a role in causing the low MeHg content of sponges, especially HMA sponges, they certainly have an extremely low MeHg content. In addition, HMA sponges can have large biomass and be the main part of low-trophic-level biomass. Our model shows that this can dramatically reduce the MeHg content of higher benthic fish; in our model, this is a reduction of 45%. This percentage is, of course, highly dependent on the MeHg concentration of sponges, the MeHg concentration of other megabenthos, and the degree to which sponges are consumed. While the role of sponges in the ecosystem is understudied, as discussed in the model development section, it is clear that sponges are both directly and indirectly consumed by important commercial species of fish.

6.5.3 The iHg content of sponges

The model mainly focuses on explaining the low MeHg content of the sponges and the observed difference between LMA and HMA sponges. However, investigating the unusually high iHg content of HMA sponges is an essential part of the Hg sponge biochemistry and should be taken into account. We demonstrate that we can explain both the iHg and MeHg concentrations found in HMA sponges by assuming an iHg and MeHg uptake rate of 3.88E-9 for iHg and 5.10E-9 for MeHg. The issue with this parameterization is that we can offer no explanation for the low MeHg content of LMA sponges. An additional way we can reproduce the observed iHg content of sponges is if we alter the release rate. We can reproduce the high iHg content of both HMA and LMA sponges if we assume that the release rate of iHg is equal to the carbon respiration rate of the sponge, which is much lower than what has been observed for other animals such as small crustaceans and bivalves (Tsui and Wang 2004; Pan and Wang 2011). While this is speculative at the moment, a potential explanation can be found in the unique structure of sponges. A study on the glass sponge *Euplectella aspergillum* found that they have elevated Hg levels in the spicules. *C. nucula* is a demosponge, not a glass sponge, but it still has glass spicules. But a similar buildup of iHg in structural components of the sponge might be happening in other components of the sponge. Demosponges rely on a protein called spongin and sulfated polysaccharides (SPs) to bind the sponge together. A possible explanation for the reduced release rate of iHg in sponges could be that iHg remains bound to the SPs in sponges.

We propose this for three reasons.

- SPs in *C. nucula* have a very high sulfate to sugar ratio of 1:5 (Vilanova et al. 2007).
- SPs with high sulfate content have been found to bind 50 mg of Hg g^{-1} SPs (Cruz et al. 2017).
- Sponges contain up to 3% SPs, providing abundant bindings sites for iHg (Esteves et al. 2011).

Combining these observations, we can estimate that sponges with 3% dry weight SPs would be able to bind 1500 ng Hg mg^{-1} dry weight, or 7500 ng Hg mgC^{-1} assuming a 1:5 carbon to weight dry weight ratio. This is higher than observed and shows that the SPs in *C. nucula* would be able to store the observed Hg concentrations. Note that this is a rough estimation and, for example, the iHg binding data of the SPs are based on bacterially produced linear SPs rather than branched SPs produced by demosponges. It does, however, indicate that the high SPs content of the sponge could explain its high iHg content. Given that our model predicts elevated iHg concentrations in sponges due to DOM consumption, but it cannot fully reproduce the observed iHg levels, it seems the high iHg content in sponges results from a combination of both drivers.

6.5.4 Low MeHg in HMA sponges; Demethylation, DOM consumption or both

The fact that our model can reproduce MeHg concentrations without demethylation in both HMA and LMA sponges shows that demethylation may not be necessary to describe the observed patterns. This does not mean that demethylation cannot play a role, but since LMA sponges do not contain large amounts of sulfate-reducing bacteria that can demethylate MeHg, a compelling argument can be made based on our model that the low MeHg concentration in LMA sponges is caused by the consumption of DOM and detritus, which make up a substantial part of their diet. The even lower MeHg content of HMA sponges can then be explained by an increased dependence on DOM by HMA sponges, *in vivo* MeHg demethylation, or a combination of both.

The expected demethylation rate is linked to the uptake rate of MeHg, which is uncertain. Because of this, we see two potential pathways that lead to the observed bioaccumulation of iHg and MeHg in LMA and HMA sponges.

The scenario with no *in vivo* MeHg demethylation, as is explored in the 2.5 gC rDOM scenario, and low *in vivo* MeHg demethylation, as is explored in the 1% demethylation scenario, can both reproduce the observed MeHg concentration in MeHg sponges, but lack a full explanation for the elevated iHg concentration in sponges. Because of this, we conclude that both no or low *in vivo* MeHg demethylation in HMA sponges is possible, and we supplement this paper with a proposed explanation on why sponges could have high iHg based on their chemical composition.

An alternative explanation for the observations presented in this paper is that sponges may bioconcentrate Hg at an accelerated pace, accounting for the elevated iHg levels, coupled with a rapid demethylation rate reaching up to 16%, which accounts for the low observed MeHg. The challenge with this explanation is the lack of compelling evidence for a rapid *in vivo* demethylation rate in LMA sponges, and consequently, this model fails to reproduce the low MeHg levels observed in LMA sponges.

Consequently, we consider it most likely that the high iHg content of sponges results from their increased ability to concentrate iHg due to their substantial SPs content. The low MeHg levels in LMA sponges are attributed to the consumption of DOM, while the reduced MeHg levels in HMA sponges arise from DOM consumption, possibly accompanied by an *in vivo* demethylation rate of 1%.

6.5.5 Limitations of the rDOM implementation

A major simplification in our model lies in the implementation of rDOM. In our setup, rDOM serves as a proxy for organic material that can be consumed by HMA sponges but is not dissimilated by non-sponge-associated microbes on timescales relevant to our model. This approach is particularly suited to a 1D configuration, where a constant flow of rDOM can be assumed throughout the system. The current implementation was chosen to ensure consistency in nutrient availability for phytoplankton growth, to preserve mass balance across the model, and to enable HMA sponges to use rDOM for growth; as such, it serves

as a useful proof of concept to explore whether rDOM could play a meaningful role in ecosystem functioning. However, this implementation is limited in scope. In a 3D model or in stratified water columns where vertical mixing is reduced, rDOM transport may significantly influence the distribution and cycling of Hg. Furthermore, potential effects of rDOM, such as its role in light attenuation, are not incorporated in the model. To fully assess the role of rDOM in both HMA sponge ecology and Hg biogeochemistry, cycling, and bioaccumulation, a more realistic representation will be necessary.

6.5.6 A potential role of sponges in bioremediation

Sponges are unique in their ability to bioaccumulate Hg, as they both have extremely high levels of iHg while maintaining very low levels of MeHg. This characteristic makes them a prime candidate for bioremediation studies. If the model is accurate for sponge grounds, they could be advantageous for Hg remediation. On the one hand, in Hg-polluted regions, sponges could bioaccumulate the less toxic iHg, which could then be extracted for bioremediation, with a diminished risk of MeHg since the majority of the Hg remains in its unmethylated form. Furthermore, the low MeHg content in HMA sponges means that organisms feeding on them would accumulate less MeHg, ultimately resulting in lower MeHg levels in higher trophic levels, as demonstrated in our model. These findings suggest that actively managing sponge grounds could both mitigate MeHg accumulation in fish and provide a sustainable method for extracting Hg from the marine environment.

6.6 Evaluate the hypotheses

We accept the hypothesis that **the consumption of DOM can explain the low MeHg content of LMA sponges, while a combination of consumption of DOM and demethylation explains the even lower concentration in HMA sponges**. We expand this by showing that while demethylation can play a role, DOM consumption can explain both the low MeHg concentration in LMA sponges, while the even lower concentration in HMA sponges can be explained by rDOM consumption or a demethylation rate of 1% d^{-1}.
We reject the hypothesis that **the consumption of DOM can explain the high iHg values of LMA and HMA sponges**. Even with an assimilation of 0.95 for iHg when DOM was consumed, our modeled iHg bioaccumulation was still an order of magnitude lower than observed. We demonstrate that the consumption of DOM can increase the iHg content in sponges, but to reproduce the iHg bioaccumulation, we need to assume that iHg is only released with respiration and not through an additional turnover or respiration rate, or that sponges have an elevated iHg uptake rate. We expand by providing an explanation of how we think that the binding of iHg to SPs in sponges can reduce the iHg from sponges.
We accept the final hypothesis that **sponges can lower the concentration of MeHg in fish**. We supplement this by showing a reduction of 45% in our model.

6.7 Summary and Conclusion

In this study, we modeled the benthic ecosystem of the Bay of Villefranche using the 1D GOTM-ECOSMO-MERCY coupled system. The simulated chlorophyll concentrations align with the NASA MODIS-A satellite time series. Pelagic iHg and MeHg concentrations are consistent with observations by Cossa et al. (2017), and MeHg bioaccumulation falls within the range reported by Llull et al. (2017) and Tesán Onrubia et al. (2020). We ran the simulations assuming both that rDOM influences the ecosystem and Hg cycling, and assuming that rDOM is unreactive and does not play a key role. Comparison of our model results with the observations by Orani et al. (2020) demonstrates the following.

- The consumption of DOM in sponges can explain the low MeHg content in LMA sponges.
- The difference between MeHg bioaccumulation in LMA and HMA sponges can be explained by (1) the consumption of rDOM by HMA sponges, or (2) an *in vivo* demethylation rate of 1% d^{-1} in HMA sponges.
- If *in vivo* demethylation occurs in HMA sponges, it is likely 1% d^{-1} and unlikely faster than 16% d^{-1}.
- The consumption of DOM by sponges contributes to elevated iHg levels, but this mechanism alone is insufficient to explain the extremely high iHg concentrations observed in both LMA and HMA sponges. This suggest that sponges either have an icnreases uptake or a reduced release rate of iHg. We present evidence to support the further hypotheses that the high iHg concentration in sponges is caused by a reduced release rate of iHg.

Conflict of interest

None of the authors declare any competing interests.

Funding

This research has been funded by the European Union's Horizon 2020 research and innovation programme under the Marie Skłodowska-Curie grant agreement no. 860497.

6.8 Acknowledgments

Readability suggestions for this paper were generated using gAI tools such as ChatGPT (OpenAI), while AI-based spell checks such as Grammarly and Writefull were used to correct spelling. In addition, AI tools helped optimize the R and Python scripts and provide coding suggestions. All suggestions were implemented only after critical manual evaluation. Finally, Google Scholar and Perplexity were used to find sources for literature research, which were consequently manually read, verified, and cited. Several sub-images were generated that together compose the graphical abstract; these were generated using openART and GPT-4.1.

Author contributions

The contributions per author are listed in Table 6.6.

Annex 1

The table of equations used to evaluate the model are shown in Table 6.7.

Table 6.6: Contributions per Author. Authors are: David Johannes Amptmeijer (DA), Dr. Ulrike Hanz (UH), Prof. Dr. Corinna Schrum (CS), and Dr. Johannes Bieser (JB).

Contributor role	**Role definition**	**Authors**
Conceptualisation	Conceptualized the study	DA, JB, UH, CS
	Developed the research objectives	DA, JB, UH, CS
Methodology	Implementation of the model into FABM	DA
	Identified the LMA or HMA sponges in the observational dataset	UH
	Developed the hGOTM tool required to build the physical setup of the model	JB
	Built the physical GOTM setup for the Bay of Villefranche	DA
Evaluation	Evaluated the model performance against observations	DA
	Performed statistical tests on the observations	DA
Writing	Writing of the original draft	DA
	Review of the original draft and quality control	UH, JB, DA
Funding acquisition	Acquired funding via the GMOS-Train ITN	JB

Table 6.7: Formulas for statistical metrics used to evaluate model. x_i and y_i are the modeled and observed values, respectively, n is the number of data points, and $\bar{x}$ is the modeled mean and $\bar{y}$ the observed mean.

Metric	**Formula**
Root Mean Square Error (RMSE)	$\text{RMSE} = \sqrt{\frac{1}{n}\sum_{i=1}^{n}(x_i - y_i)^2}$
Pearson correlation coefficient r	$r = \frac{\sum_{i=1}^{n}(x_i-\bar{x})(y_i-\bar{y})}{\sqrt{\sum_{i=1}^{n}(x_i-\bar{x})^2}\sqrt{\sum_{i=1}^{n}(y_i-\bar{y})^2}}$
Standard deviation σ	$\sigma = \sqrt{\frac{1}{n}\sum_{i=1}^{n}(x_i - \bar{x})^2}$
Bias	$\text{Bias} = \frac{1}{n}\sum_{i=1}^{n}(x_i - y_i)$
Mean Percent Bias (MPB)	$\text{MPB} = 100 \times \frac{\bar{x}-\bar{y}}{\bar{y}}$

CHAPTER 7

Summary and conclusions; What are the key biological drivers of MeHg bioaccumulation in the marine food web

In order to evaluate the main research question; "What are the key biological drivers of methylmercury(MeHg) bioaccumulation in the marine food web?", I will first summarize the previous chapters, then I will evaluate the 5 sub research questions. After this I will combine these results into a comprehensive overview to summarize my contributions to our understanding of biological drivers of MeHg bioaccumulation. The main research question is then evaluated in the next discussion, which is the next chapter.

7.1 Summary of the chapters

Chapter 1; Introduction

Chapter 1 is the introduction to this thesis. Here I present a brief history of mercury (Hg) pollution and bioaccumulation research. I briefly explain why Hg is a pollutant of global concern and what knowledge gap complicates Hg management. Here I also introduce the basis of numerical modeling, and why this tool is used in this thesis to investigate Hg bioaccumulation in the marine environment. Finally, I present how the research presented in this thesis was conceptualized and how this should contribute to the management of Hg.

Chapter 2; How can the bioaccumulation of inorganic mercury (iHg) and methylmercury (MeHg) be parameterized in a biogeochemical model?

This chapter explains how I incorporated bioaccumulation into the MERCY v2.0 model. This is the first model to couple atmospheric Hg concentrations with the bioaccumulation of methylmercury (MeHg) in fish. Furthermore, it is the only coupled Hg bioaccumulation model that resolves both the bioaccumulation of inorganic Hg (iHg) and the bioconcentration of iHg and MeHg at every trophic level while including high trophic level biota. Finally, we show in the validation of this model that all plankton bioaccumulation is

within the range of observations and that there is good agreement between the modeled and observed concentrations of MeHg in fish.

Chapter 3; How does ecosystem structure and function influence mercury cycling in marine environments?

In this chapter, I analyze three idealized 1D water column setups representing coastal dynamics common in the North and Baltic Seas to quantify the effect of bioaccumulation, biogenic reduction, and the partitioning of Hg into detritus and Dissolved Organic Matter (DOM). Furthermore, I analyze the 3D ECOSMO-HAMSOM-MERCY coupled system to quantify the effect of bioaccumulation on the Hg budget of the North and Baltic Seas. In this chapter, I present the following results.

1. Bioaccumulation can increase marine total MeHg by 44%.
2. Biogenic reduction by cyanobacteria can decrease marine average tHg by 9% through evasion to the atmopshere.
3. Bioaccumulation reduces total Hg burial in the North and Baltic seas by 14 kg y^{-1}.

These results demonstrate that the ecosystem can play an important role in Hg cycling.

Chapter 4; What are the dominant drivers of MeHg bioaccumulation in high-trophic-level fish?

In the second chapter, I analyze the effect of iHg bioaccumulation and MeHg bioconcentration at higher trophic levels on MeHg bioaccumulation. I analyzed this by running the three idealized 1D water column setups used in paper 1 with and without these interactions. This showed that:

1. The fraction of MeHg bioaccumulation that is caused by the bioconcentration of MeHg at higher trophic levels depends on the trophic level and increases on average 15% per trophic level.
2. The reduction in dissolved Hg^{2+} due to bioaccumulation does not result in a lower bioaccumulation of MeHg.

Chapter 5; How does the feeding strategy of low-trophic-level biota affect the bioaccumulation of iHg and MeHg?

In the third chapter, I updated megabenthos and fish in the ECOSMO E2E ecosystem model to represent a more diverse megabenthic community. This was used to investigate the large variability that is observed in Hg bioaccumulation at the base of the food web. I run this model in two 1D water column models of the North Sea. This chapter shows that:

1. The feeding strategy is a key driver of the bioaccumulation of iHg.
2. The trophic level is the main driver of tHg concentrations in animals with a high trophic level.
3. The feeding strategy is the main driver of high tHg variability in low trophic level animals.
4. The high observed levels of tHg in low-trophic-level animals are probably due to less toxic iHg rather than MeHg.

Chapter 6; What explains the low MeHg concentrations observed in high microbial abundance (HMA) sponges, and how does this influence MeHg exposure in higher trophic levels?

In chapter 6 and the final chapter, I updated the model used in Chapter 3 so that the animals not only have different dietary preferences but resemble their counterparts more closely in the real world. Additionally, I overhauled the DOM cycle in the model and added DOM-consuming sponges as a functioning megabenthos group. I run this model in one 17-m deep-water column setup that resembles the hydrodynamic conditions in the Bay of Villefranche. This was done to compare it with observations about Hg and MeHg in sponges. In this chapter, I show that:

1. The high iHg and low MeHg content of Low Microbial Assemblage (LMA) sponges can be explained by their consumption of DOM.
2. An *in vivo* demethylation rate of 1%, or the consumption of rDOM in HMA sponges is sufficient to cause the observed difference between HMA and LMA sponges
3. The consumption of DOM in sponges contributes to their high iHg content, but it is not enough to fully explain the high observed iHg content in either LMA or HMA sponges
4. The MeHg content of high-trophic level fish can be reduced by up to 45% in ecosystems where the base of the foodweb is dominated by HMA sponges

7.2 Short evaluation of the research questions

All the sub-research questions are evaluated in their respective chapters, but here I provide a small answer to all the sub-research questions.

> *"How can the bioaccumulation of inorganic mercury (iHg) and methylmercury (MeHg) be parameter- ized in a biogeochemical model?"*

Bioaccumulation can be achieved accurately in a fully coupled model by simulating marine Hg cycling and incorporating bioconcentration and biomagnification.

> *"How does ecosystem structure and function influence mercury cycling in marine environments?"*

The ecosystem influences Hg cycling by removing aquatic MeHg during the phytoplankton bloom and releasing it after the bloom. MeHg is unusual as a pollutant because MeHg is readily replaced by new methylated Hg. This process increases total MeHg.

> *"What are the dominant drivers of MeHg bioaccumulation in high-trophic-level fish?"*

Bioaccumulation at high trophic levels is primarily driven by bioconcentration of MeHg into primary producers and consequent biomagnification, but bioconcentration of MeHg in consumers has an important role.

> *"How does the feeding strategy of low-trophic-level biota affect the bioaccumulation of iHg and MeHg?"*

The feeding strategy of the low trophic level megafauna has a very strong influence on the bioaccumulation of Hg. In particular, DOM consumption by suspension feeders leads to high iHg content, while filter feeding results in the highest MeHg content.

> *"What explains the low MeHg concentrations observed in high microbial abundance (HMA) sponges, and how does this influence MeHg exposure in higher trophic levels?"*

The low MeHg content in LMA sponges can be attributed to their consumption of DOM. The even lower concentration in HMA can either be caused by a 1% *in vivo* demethylation d^{-1} or the consumption of rDOM. Additionally, the low concentration of MeHg in HMA sponges can cause a reduction of MeHg in benthic fish of up to 45% in an ecosystem dominated by HMA sponges compared to an ecosystem without sponges.

7.3 Conclusion

Based on the 5 sub-research questions, we can now answer the main research question:

"What are the key biological drivers of MeHg bioaccumulation in the marine food web?"

The bioaccumulation of MeHg is typically modeled on the basis of the bioconcentration of MeHg into primary producers and consequent biomagnification. Based on the work in this thesis, I expand on this and conclude that the bioaccumulation of MeHg in the marine food chain is also influenced by:

1. Feedback mechanism of the ecoystem on marine Hg cycling.
2. The bioconcentration of MeHg in consumers.
3. The feeding strategy of low trophic level biota and consequently the species composition.
4. The bentho-pelagic coupling, and ecosystem structures influencing this coupling.
5. *In vivo* MeHg demethylation rates, which strongly affect bioaccumulation of MeHg but remain understudied.

In addition to this qualitative evaluation, the results are summarized in Fig. 7.1. This figure illustrates that Hg is a unique pollutant whose marine cycle is strongly influenced by the ecosystem. To predict the MeHg content of seafood, both ecosystem characteristics and bioaccumulation processes must be considered. The established understanding that bioconcentration in primary producers and subsequent biomagnification drives MeHg concentrations in high trophic level fish is expanded by our finding that bioconcentration in consumers and feeding strategy at the base of the food web also play an essential role in MeHg bioaccumulation. Additionally, I demonstrate that the low MeHg content of LMA sponges can be explained by their consumption of DOM, while the even lower MeHg bioaccumulation in HMA sponges is driven either by the consumption of rDOM or by an *in vivo* MeHg demethylation rate of 1% d^{-1}. We demonstrate that the low MeHg content in HMA sponges can lead to a 45% reduction in MeHg concentrations in high trophic level fish when HMA sponges dominate the base of the food web. The ability of HMA sponges to accumulate large amounts of Hg while storing it in the less toxic iHg form makes them an important target for future research on their potential role in bioremediation.

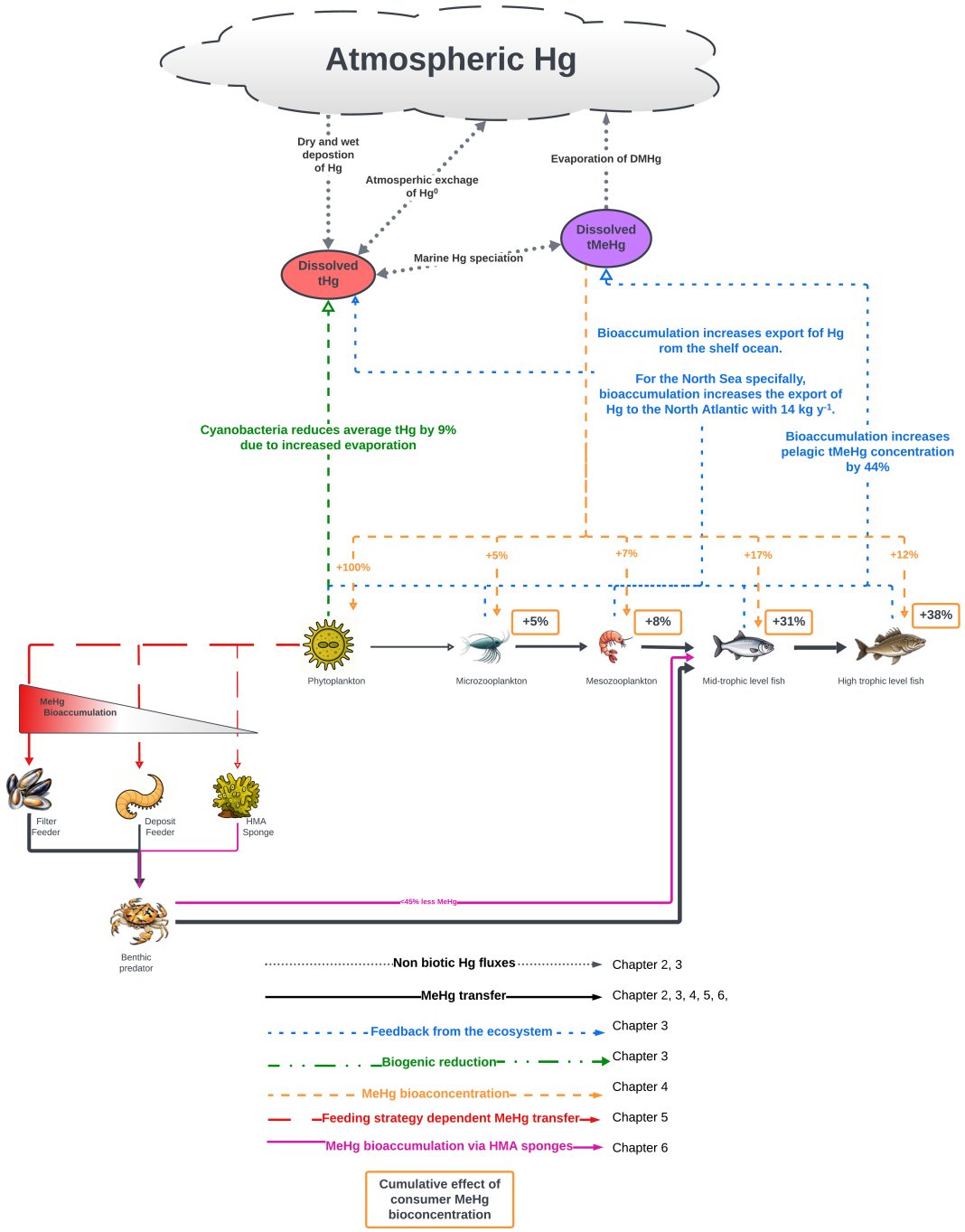

Figure 7.1: Schematic overview of the contributions of this thesis to our understanding of the bioaccumulation of MeHg. The feedback from the ecosystem on Hg cycling and MeHg concentrations (blue lines) is discussed in chapter 3. How bioconcentration in consumers (orange lines) increases the bioaccumulation of MeHg is discussed in Chapter 4. On the left of the plots is visualised how different benthic feeding strategies can influence MeHg bioaccumulation (red lines), which is discussed in Chapter 5. Finally, it is shown that the low MeHg concentration in HMA sponges can reduce the MeHg bioaccumulation in higher trophic levels (purple lines), as is discussed in Chapter 6. Thicker lines indicate more MeHg transfer, but line thickness is is just a visual indicator and their is no direct relationship between line thickness and MeHg transfer.

Figure 7.2: White Sea-squirt (*Phallusia mammillata*), a tunicate. Picture taken by Dr. Eric Wurtz.

CHAPTER 8
Discussion

The field of Hg research is relevant and fast-evolving. In this chapter, the noval contributions of this thesis to Hg research are first reiterated. Then the apparent paradox in the results about the significance of iHg bioaccumulation for MeHg bioaccumulation. Chapters 3 and 4 suggest minimal iHg impact, whereas Chapter 6 shows that iHg can crucially influence the MeHg bioaccumulation via *in vivo* Hg speciation. Subsequently, I will examine how factors such as the carbon content, the trophic levels of organisms, and the type of observations influence my ability to evaluate the model against observations. I will then address the model's inherent limitations, discussing the necessity of aggregating various biological groups into functional categories as a simplification and how these choices might challenge bioaccumulation modeling related to carbon dynamics. Following this, I will consider how models can assist the Minamata Convention on Mercury. I propose that while comprehensive models are not yet practical, they can nonetheless highlight critical knowledge gaps needed for effective policy-making. I will then delve into the policy ramifications of this thesis, noting how standardized iHg and MeHg measurements can improve model validations and how ecosystem structure might affect MeHg bioaccumulation in top-level predators. Finally, I will outline my views on the future of marine bioaccumulation research and its potential to aid the Minamata Convention on Mercury.

8.1 Novel contributions of this thesis

This thesis advances the field of Hg biogeochemistry by quantifying biological drivers of MeHg bioaccumulation that have previously been underrepresented or absent in models. The novel contribution of this thesis comes in several steps: the design and implementation of the first Hg model linking atmospheric Hg concentration to MeHg in fish, as presented in Chapter 2, the quantification of several pre-identified, yet understudied drivers, as presented in Chapter 3, 4, and 5, and the identification of new Hg bioaccumulation mechanisms, as is presented in Chapter 6. I demonstrate that bioaccumulation has an integral role in Hg cycling, quantify the importance of bioconcentration in consumers, and establish that feeding strategy is a key driver of Hg bioaccumulation in lower trophic level biota. Most notably, it is the first study that identifies DOM consumption as a critical driver of low MeHg bioaccumulation in suspension feeders and identifies this as a potential mitigator of MeHg bioaccumulation in fish. However, model results must always be interpreted with a degree of skepticism, and it is important to identify and evaluate what results of this thesis conflict with established literature, what uncertainties might be present in our results, and how these results can be utilized to further advance the field of Hg bioaccumulation modeling.

8.2 Conflicting results in this thesis

A conflict in the results of this thesis is the impact of iHg bioaccumulation on MeHg bioaccumulation. Initially, in Chapter 4, I show that iHg bioaccumulation does not have a significant effect on MeHg bioaccumulation. In contrast, Chapter 6 investigates the link between iHg bioaccumulation and MeHg through

in vivo Hg speciation. This apparent contradiction suggests that the role of iHg in the bioaccumulation of MeHg depends on the significance of *in vivo* Hg speciation. In the case of the HMA sponges, enough high-quality data were available, and the sponges are at the base of the food web, so the uptake of iHg and MeHg could reasonably be assessed.

To determine whether the importance of *in vivo* Hg speciation is HMA sponge specific or common throughout the marine food web requires further investigation. This can be achieved by laboratory studies that investigate the interaction directly, or by collecting data that include iHg, MeHg, and trophic levels. Ideally, both laboratory studies are used to assess speciation rates, and field studies are performed to obtain data so that these rates can be verified using models. If *in vivo* Hg speciation occurs at significant rates, the bioaccumulation of iHg would provide a substrate for *in vivo* iHg methylation, thereby increasing the bioaccumulation of MeHg. Although this hypothesis is speculative at the moment, it provides a fascinating direction for future research. This highlights the ecosystem-specific nature of Hg dynamics, and understanding how different ecosystems impact Hg speciation and bioaccumulation is an essential step in further developing the predictive capacity of Hg bioaccumulation models. This complexity also demonstrates the unique attributes of Hg as a pollutant. A major distinction between MeHg and other persistent pollutants, such as persistent organic pollutants (POPs), is that MeHg is actively formed in marine environments through microbial methylation of inorganic mercury, whereas POPs are synthetic and highly resistant to degradation (Ramlal et al. 1986). Because conventional POPs are anthropogenic compounds not naturally synthesized, an increase in biomass can cause these pollutants to be diluted across the higher biomass, thereby reducing their concentration in other biota and in the water (Dachs et al. 2000). This is not the case for MeHg, as it is actively formed in nature; an increase in biomass may initially reduce MeHg concentrations through a process called growth dilution, where biomass growth temporarily outpaces the production of new MeHg, but the dissolved MeHg concentration will re-equilibrate over time, as shown in Chapter 3. This is supported by observations of this effect in eutrophic estuaries in Northern Taiwan, where increased phytoplankton biomass led to decreased MeHg concentrations (biomass dilution) Fang and Chang (2024), and by laboratory studies demonstrating that rapid zooplankton growth can reduce MeHg bioaccumulation in fish (growth dilution) Karimi et al. (2007). Thus, while phytoplankton growth can temporarily lower MeHg concentrations, this effect is typically temporary due to ongoing in situ MeHg production.

8.3 Limitations in model validation

Validating bioaccumulation models against field observations is essential for ensuring model quality. However, several challenges complicate this process in the case of Hg. Primarily due to:

- The uncertainty of the carbon content of biota
- Variability of the trophic level of biota
- Quantity and quality of the data

8.3.1 The uncertainty of the carbon content of biota

The ECOSMO E2E model is extensively used in this thesis to model an ecosystem in which bioaccumulation occurs. This model assumes a Redfield ratio to simulate ecosystem dynamics (Daewel and Schrum 2013). Although this implication allows for efficient tracking of nutrients in the ecosystem, it introduces uncertainties. Some animals deviate from the Redfield ratio (Sicko-Goad et al. 1984). Our model simulates biomass in carbon per volume and bioaccumulation in bioaccumulated Hg per volume, so we model bioaccumulation in Hg C^{-1}. However, most measurements, including those used in Chapter 2, 3, 5, and 6, are made in wet weight or dry weight, which can introduce a large uncertainty when the exact carbon and water content of the animals is not known. Although this inaccuracy is consistent, its overall effect remains limited. While there are variations in the carbon content of biota within the same functional group. Especially in high trophic level animals such as fish, the carbon content was found to vary between 42.8 and 48.4% in Lake Superior (Tanner et al. 2000). This is an 11.6% deviation, which is not insignificant, but manageable.

8.3.2 Variability of the trophic level of biota

In Chapters 3, 4, and 5 I investigated the trophic level as a driving force of the bioaccumulation of MeHg. Models and measurements do not always estimate the trophic level. Although often an estimation of the trophic level can be assessed, knowing the exact trophic level under different circumstances provides great insight. While in this thesis I show that MeHg bioaccumulation is not solely determined by bioconcentration at the base of the food web and consequent biomagnification, this is still the main pathway for MeHg bioaccumulation, and bioconcentration at the base of the food web combined with the trophic level is the most important determinant for MeHg bioaccumulation (Wu et al. 2019). Several interactions, such as cannibalism within the functional group (Fraser et al. 2005), parasites (Lafferty et al. 2006), and consumption of detritus or DOM (Albeny-Simões et al. 2015), can influence the trophic level of animals and consequently their trophic level, but these interactions are not necessarily included in the functional approach used by most models (Daewel et al. 2019). Estimating the trophic level in bioaccumulation models should be seen as a near-essential tool to take into account when comparing model data with field observations. Since biomagnification is exponentially related to trophic level, the bioaccumulation in high trophic levels is extremely sensitive to the modeled trophic level. The upside is that the trophic level is often measured in observational studies and it can be modeled for a fair comparison. This is discussed in more detail later in the discussion when recommendations for future Hg bioaccumulation are discussed.

8.3.3 Quantity and quality of the data

Proper model validation would best be performed using datasets in which key parameters, including iHg, MeHg, trophic level, and carbon content, are measured simultaneously in the same samples. This is because there is a significant increase in statistical power and a reduction of type II errors when matched samples are used rather than unmatched samples, as extensively discussed in textbooks such as *Experimental Design and Data Analysis for Biologists* (Quinn and Keough 2002). This can be more critical than increasing the number of samples. Some samples in which both iHg, MeHg, the trophic level, and the carbon content are estimated would be perfect. Of course, enough samples should be taken to estimate whether the values are representative of the larger population or an outlier. Not knowing the MeHg content, trophic level, or carbon content of the samples introduces additional uncertainties in the comparison between models and observations. For example, Chapter 5 uses a large dataset for model validation, but many samples lack the trophic level or MeHg content. Samples missing one or more key parameters could not be used in every analysis, weakening both the statistical analyses and the robustness of the model validation. I understand the limitations that empirical scientists face, but if the trophic level of 10 fish is estimated and the Hg content of 10 different fish is estimated in a different study, it is hard to merge those values into a robust dataset, which would not be the case if the Hg content and trophic level were assessed in the same 10 fish. In this scenario, extensive sampling is performed; aligning key parameters within the same sample could greatly enhance the utility and reduce the number of samples required. In addition, often only the mean and standard deviation of the data are published rather than the full dataset. When validating models, raw data can often be a very valuable addition to the paper. The sharing of raw datasets according to the FAIR principle could significantly improve the validation of the model and the reproducibility of the research findings (Wilkinson et al. 2016). In addition to this, sharing metadata such as sampling conditions, depth, or other noteworthy circumstances, even those that are seemingly unimportant, can help modelers contextualize the observed data, making it more useful for validation and further research. An observational study supporting this is that of Hammerschmidt and Fitzgerald (2006), which found a significant increase in MeHg concentrations in longer-lived fish, even when their trophic level was unchanged. Including measurements that estimate the age of fish species could therefore improve model validation by accounting for factors beyond trophic position. Another example of this is the study by Chen et al. (2004), who discusses the complexity of comparing observations of Hg bioaccumulation in different aquatic environments and shows better conclusions can be derived when data is published that facilitates the comparison between observational studies.

8.4 Model limitations

The models used in this thesis are designed to replicate Hg bioaccumulation in line with observations and allow us to study Hg bioaccumulation. That does, however, not mean there are no limitations to what the models presented in this thesis can be used for. Here I would like to discuss the main limitations of the models by discussing the limitations of the employed models, and evaluate the choice of predominantly using 1D models in this thesis, by discussing the benefits and limitations of using 1D models.

8.4.1 Diversity between organisms within a functional group

A challenge in modeling bioaccumulation is the diversity between organisms. When assessing the rate of chemical or physical processes, several key drivers can often be identified. For example, in the Hg cycling, several processes are influenced by photochemistry and the partitioning of Hg and MeHg to DOM is influenced by the chemical composition of the DOM (Seelen et al. 2023). While these interactions can be complicated to quantify in the lab, and even harder to assess their influence in nature, they depend on several key interactions that can be estimated because they depend on well-defined interactions.
However, when considering biota the situation becomes far more complicated. There are approximately 35,600 species of fish (Fishbase 2024), not to mention the vast invertebrate and microbial diversity that is essential in Hg cycling. A key complication in modeling ecosystems is the existence of stable sub-optimal equilibria in biodiversity. By this I mean that ecosystems are often shaped by the species that are already present and use the available resources, preventing other species from settling (Folke et al. 2004). This means that the species living in a certain area at a moment in time are very dependent on which species were already there. For carbon models, this complexity is often addressed by the earlier discussed functional group approach, where species are grouped under the assumption that their average traits represent the group as a whole (Zakharova et al. 2019). While this approach effectively models average carbon fluxes, it creates a problem when dealing with specific hard-to-assess reactions such as *in vivo* Hg speciation, as can be seen in Chapter 6 and is discussed in Li et al. (2022). Both studies show that bioaccumulation is extremely sensitive to an *in vivo* demethylation rate, and it shows that organisms with similar carbon cycling can have drastically different effects on MeHg bioaccumulation. If different similar trophic level animals have small differences in their size, mobility, respiration rate, or chemical compositions, there might be differences in how much MeHg they bioconcentrate, and thus how much MeHg eventually reaches top predators, as is discussed in Chapter 5 and 6. Examples of this would be sea stars, crabs, and small fish. They are all typically seen as middle trophic level benthic animals, but their MeHg and iHg levels are very different, as shown in the literature study component of Chapter 5. However, in the ECOSMO E2E model, they would all be categorized as macrobenthos Daewel et al. (2019). Even when animals are classified by feeding strategy, significant variability in internal chemistry can influence Hg and MeHg uptake. An example of this is the microbiome of HMA sponges, which is studied in this thesis in Chapter 6. However, while HMA sponges are unique for having such a large microbiome both in size and variability, there is evidence that smaller microbiomes of other animals also influence Hg speciation (Gentè et al. 2023; Gorokhova et al. 2020). The relevance of this is demonstrated in Chapter 6, where I demonstrate that even a very low demethylation rate of 1% d^{-1} still can explain the observed difference between LMA and HMA sponges, a difference of 57% in MeHg concentrations. For basic carbon cycling models HMA sponges can be seen as just another suspension feeder, but for Hg cycling they are very unique, and essential to understand. This highlights that biological groups critical to carbon cycling are not necessarily the same as those driving Hg speciation and bioaccumulation, and how sensitive MeHg bioaccumulation can be to *in vivo* Hg speciation rates. If we use a functional group-based carbon model that is optimized for carbon we might miss these types of organisms.
Despite these limitations, a functional group approach is still a necessary simplification. Even if we know all the *in vivo* Hg speciation and bioaccumulation rates, accurately modeling the bioaccumulation and speciation of iHg and MeHg of 2000 animals in the North Sea alone would require 4000 state variables to run, making it computationally unfeasible. In addition to this, the amount of laboratory work to obtain unique rates for each animal would be enormous. Nonetheless, existing data reveal several general patterns in *in vivo* Hg speciation. To evaluate whether these patterns are trivial or indicative of significant

interactions, it is essential to measure rates in a sufficient number of animals so that we understand the interaction enough to identify key groups to undergo Hg *in vivo* Hg speciation. This will help determine the significance of the reaction and allow the estimation of *in vivo* Hg speciation rates for all functional groups. The sponge study also exemplifies a practical application of a model, in which rates are estimated based on the available data. Although there is a substantial amount of data, some influencing factors remain unknown. This underscores the necessity for additional measurements, experimental research, and modeling to close the gaps in our comprehension.

8.4.2 Model Complexity vs. Realism; the choice of using 1D models

Most studies in this thesis were performed using the 1D Generalized Ocean Turbulence Model (GOTM) (Burchard et al. 1999b). Setups were designed to either represent a variety of hydrodynamical circumstances expected in coastal oceans, as was the case in Chapter 3, 4, and 5, or to represent a specific scenario, as was the case in 6. Here I will discuss more about why modeling in 1D was a deliberate choice and what advantages and limitations this approach has. Following the rule that a model should be as simple as possible but not simpler, we chose the appropriate model based on the requirements of each research question . Generally, models of low complexity are more suitable for process understanding, while models of high complexity are more suitable for projections and predictions (O'Neill and Rust 1979; Hasselmann 1976; Jakeman et al. 2006).

Advantages of 1D:

The main benefit of using a 1D model is its straightforwardness in terms of implementation, validation, and cost-effectiveness in computational resources Bruggeman et al. (2024). While not every configuration was used, several versions of the 1D model were often run simultaneously to test different hypotheses and determine which interactions warranted further research. This method is impractical for complex 3D models, as executing the model with even a few hundred configurations would require an excessive amount of computational power. Therefore, I believe that 1D models serve as an ideal tool for the current stage of marine Hg modeling. They allow for a rapid evaluation of existing knowledge on a topic, identification of knowledge gaps, and assessment of uncertainty in drivers under various simplified scenarios. This comes with an additional benefit that using 1D simulations isolates the effect of the study. By removing variable drivers such as horizontal transport, a 1D model can reduce its internal variability compared to a 3D model. This reduced internal variability means that the processes of interest can be better studied under varying circumstances. This allows the 1D model to make generalized observations about key interactions.

Limitations of 1D:

However, this improved efficiency comes at the cost of reduced applicability to real-world scenarios. The 1D water column models are very good at identifying key factors under controlled conditions but are of limited use in predicting actual outcomes or estimating a budget, as is shown by Hwong et al. (2022) and discussed in Chapter 3. As illustrated in Chapter 6, HMA sponges can lower MeHg levels in fish by up to 45%. However, the 1D model used in this study doesn't serve as a comprehensive representation of the Mediterranean Sea ecosystem, as it does not contain a validated spatial HMA sponge biomass component which could influence organic carbon transfer from HMA sponges to benthic predators. Therefore, although 1D models excel in pinpointing potentially influential drivers, their ability to predict their impact on real-world systems is limited. To address this issue, the method used in Chapter 3 can be used. In this chapter, I first evaluate the hypothesis that the ecosystem considerably influences the marine Hg cycle across three 1D setups, simulating idealized scenarios of permanently mixed, seasonally mixed, and permanently stratified water columns. Subsequently, the influence on the Hg budget in the North and Baltic Seas was assessed via an already validated 3D model. The limitation here is the dependency on existing 3D models that accurately represent marine carbon and Hg fluxes. In the context of Chapter 6, such a model was unavailable, limiting our ability to estimate the impact of HMA sponges on Mediterranean Sea fish until model improvements are made.

To summarize: 3D models provide a more realistic representation of the natural environment because they account for spatial variability in three dimensions. As a result, they have a better capacity to reproduce and predict real-world conditions. Whereas 1D models simplify the system by focusing on vertical processes at a single location. This makes them well-suited for isolating and understanding key mechanisms through controlled *in silico experiments*.It is generally advisable to choose a model that is sufficiently complex to address the research question without being unnecessarily complicated (Höge et al. 2018). This approach suggests that, for analyzing knowledge gaps and pinpointing essential drivers, simpler 1D models are the best choice. These models provide the flexibility needed to test hypotheses, and their simplicity offers an in-depth comprehension of the model dynamics and the influences driving the outcomes.

Future Directions:

As the research gaps in Hg bioaccumulation modeling are reduced, research questions are increasingly likely to focus on assessing complex policy scenarios, for example, via the Multi-Compartment Hg Modeling and Analysis Project (MCHgMAP) (Dastoor et al. 2024). Because of Hg's nature as a global pollutant, understanding how different policy scenarios can shape anthropogenic Hg emissions, and how this would influence the MeHg exposure to humans can only be fully understood using a 3D fully coupled global ocean-atmosphere model (Sunderland and Selin 2013). Because of this, it makes sense that as knowledge gaps are reduced and lessons are learned from simpler models, these lessons can be implemented in more complex models to investigate more complex research questions.

8.5 Using models to assist the Minamata convention

It is important to keep the previously discussed topic of model complexity into account when considering how models should be used in support of the Minamata Convention. While there are multiple ways in which models can serve as useful tools, when modeling MeHg bioaccumulation, the first and perhaps the most obvious is using models to predict real-world scenarios. Notably, models such as the study by Zhou et al. (2025) attempt to estimate the predicted MeHg content of fish. An ideal for this would be a full-earth digital twin, such as Destination Earth, that can estimate food safety under different emission scenarios (Attinger et al. 2024). However, it is crucial to ensure the quality of the models before important policy decisions are made based on an overestimated performance of the models. Currently, several key drivers of Hg bioaccumulation are still highly uncertain, as is both discussed in this thesis and by (Kotalik et al. 2025), and these predictions should be viewed with a high degree of skepticism. The use case for models that is primarily used in this thesis is to identify gaps in our current understanding. A model can be seen as an in-silico experiment, in which assumptions about a problem are tested and it is observed whether the model's predictions align with observations. If the model successfully replicates the observations, we can be more confident in our understanding of the problem. If this isn't the case, or the model needs to be heavily tuned or constrained, it indicates that crucial drivers are missing or wrongly parameterized. In this case, models can be used to identify these gaps and determine the empirical data needed to improve the model Rykiel (1996).

8.6 My recommendation for the the Multi-Compartment Hg Modeling and Analysis Project in terms of bioaccumulation parametisation

In this thesis, several drivers are identified that are key biological drivers of MeHg bioaccumulation. In investigating this, several drivers are also identified that appear to be of little significance. The next logical step in Hg bioaccumulation modeling is to implement the drivers that are identified in this thesis in global models. In this thesis, there are several lessons that are easy to translate into the parameterization of bioaccumulation that could help the modeling efforts of the MCHgMAP (Dastoor et al. 2024).

Results in this thesis support the need for the MCHgMAP

The need for the MCHgMAP is demonstrated by several studies, for example the study by Zhang et al. (2023b), which demonstrates that an updated global Hg model that incorporates vegetation uptake, seawater sources, riverine discharge, and atmospheric Hg redox chemistry estimates 40% higher Hg re-emission than previous models, mostly due to higher ocean re-emissions. Studies such as this demonstrate that in order to fully understand Hg fluxes, all compartments of the Hg cycle should be accounted for. The results of Chapter 3 expand on this by showing that the ecosystem is an integral part of the Hg cycle as well. This further demonstrates the importance of a large modeling framework by demonstrating that Hg cycling cannot be accurately estimated without an ecosystem model. Naturally, fully coupled end-to-end models that simulate bioaccumulation would account for bioaccumulation. However, several other ecosystem drivers of Hg cycling, such as cyanobacterially induced biogenic reduction, can only be properly accounted for in a model that takes both ecosystem dynamics, marine Hg cycling, and atmospheric Hg dynamics into account. And drivers such as this can have a major influence over regional and global Hg dynamics.

8.6.1 What I recommend doing

Based on the results of my thesis and the lessons I learned during my project, there are several biological drivers of MeHg bioaccumulation that I think should be incorporated in any large-scale end-to-end model. While I recognize that elements added to such a model incur a considerable cost, there are factors of MeHg bioaccumulation that, in my opinion, are important enough to justify the trade-off. My recommendations are visualized in Fig. 8.1 and discussed in more detail in the paragraph below.

Model bioaccumulation when Hg speciation should be resolved

One of the main contributions of this paper is the evaluation and quantification of the feedback between bioaccumulation of iHg and MeHg and marine Hg cycling. This builds on the work of Kuss et al. (2015), which demonstrates the important role of biota in Hg cycling in the Baltic Sea, by demonstrating the control of cyanobacteria on the air-sea exchange of Hg. I expand on this in Chapter 3 by showing that biota can have an influence on the seasonal cycling of MeHg and increase total MeHg by taking up MeHg from the water column in spring, and protecting it from photodemethylation while light intensity is highest and releasing it in winter when the light intensity is lower. On the other hand, this paper demonstrates that the effects of bioaccumulation on tHg are much less pronounced. Because of this, I would recommend that any models that do not solely focus on tHg fluxes, but attempt to understand Hg speciation as well, should include bioaccumulation.

Modeling the trophic level

It is recommended to model the trophic level of all modeled biota in order to ensure a valid validation of the model performance. This is essential, and it is worth it. It is a useful simplification to combine different animals into functional groups, but this does mean that it can be hard to evaluate exactly which real-world animals represent your modeled organism for validation. Because of this, the trophic level is an essential parameter to evaluate for each modeled functional group before bioaccumulation can be accurately validated.

The importance of modeling the trophic level two-fold. First of all, as shown in Chapter 3 there was a consistent negative bias in the used ecosystem model vs. the observed trophic level. This is caused by the functional group approach of models, in which ecosystem complexity is reduced to increase model viability. This is an important step in model development, but the reduced ecosystem complexity can reduce the amount of trophic interactions (Haller-Bull and Rovenskaya 2019). This means that the modeled trophic level can be consistently lower than the observed, which would result in reduced bioaccumulation. This can be compensated for in the model by increasing the uptake or trophic transfer efficiency of Hg. However, in doing so, the model does not reproduce the right results for the right reason. By adjusting parameters to fit observed data despite structural inaccuracies, the model may lose its ability to predict outcomes in different scenarios, as the adjustments are not grounded in reality (Gygi et al. 2023).

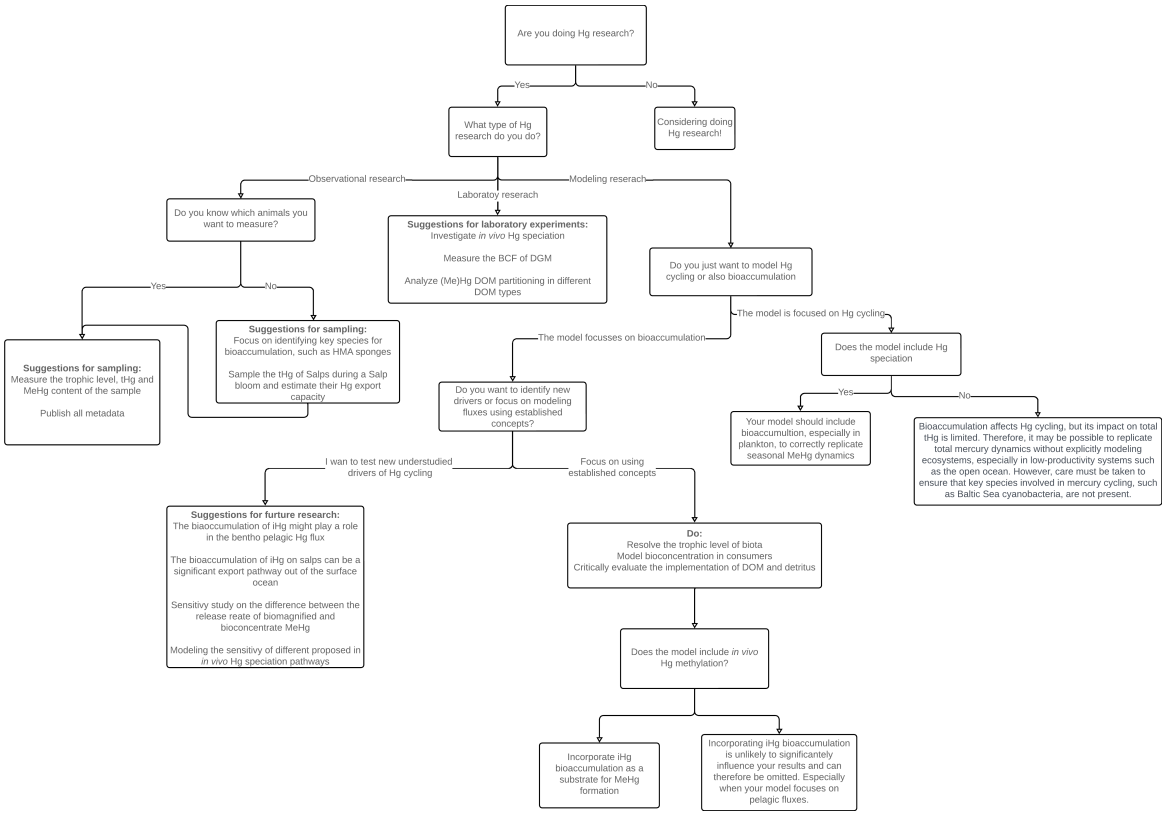

Figure 8.1: My recommendation for future work on Hg science based on my experience writing this doctoral thesis.

The second reason is that bioaccumulation is extremely sensitive to the trophic level, as is shown in Chapter 3. Here the BMF is modeled in line with observations, but because the model underestimates the trophic level of cod, by 0.5-0.7, the bioaccumulation of MeHg is underestimated by 64-79%. Because biomagnification is exponentially related to the trophic level, a small difference in trophic position can have a dramatic effect on the modeled bioaccumulation. Should a model predicts a change in MeHg bioaccumulation, it might relate to shifts in trophic positions owing to food web reorganization or to variations in Hg dynamics.

The trophic level implementation in this thesis

The way the trophic level was estimated in Chapters 3, 4, and 5 was by incorporating one additional state variable for each ecosystem functional group. Whenever carbon fluxes occur, this tracer variable is updated simultaneously with the state variables. The rate of change is calculated as:

$$\frac{dTracer_g}{dt} = \sum_{s=1}^{n_z} \left(F_{pred(g,s)} \cdot (TL_s + 1)\right) - \sum_{l=1}^{n_l} F_{ex(g,l)} \cdot TL_g \tag{8.1}$$

Where:

$Tracer_g$ – tracer variable of functional group g [$mgC^{-1}m^3$]

t – time [s]

$F_{pred(g,s)}$ – total flux of tracer due to predation by group g on group s [m^3 mgC^{-1} s^{-1}]

TL_s – trophic level of functional group s [unitless]

TL_g – trophic level of functional group g [unitless]

$F_{ex(g,l)}$ – total flux of tracer lost by excretion from group g due to loss process l [m^3 mgC^{-1} s^{-1}]

n_z – number of functional groups that group g predates on [unitless]

n_l – number of loss terms for functional group g [unitless]

This means that the TL_g can be calculated as:

$$TL_g = \frac{Tracer_g}{OC_g} \tag{8.2}$$

OC_g- the organic carbon of functional group g [mgC m^{-3}]

The benefit of this approach is that it resolves every trophic level on both a spatial and temporal scale; this means that it can be evaluated how the trophic dynamics change with depth, if there is a seasonal effect on the trophic level or the bentho-pelagic coupling. The downside of this approach is its computational cost, as it requires adding one state variable per biological functional group.

The cost of calculating the trophic level

In my 1D setup, the expense of including additional state variables was not a concern. However, in a global 3D model, the computational cost of introducing extra state variables can be substantial (Kern et al. 2024). There are several methods for estimating trophic level, each with distinct advantages and limitations. For example, the EcoTrop model (Gascuel and Pauly 2009) employs a dynamic ecosystem approach, representing marine ecosystems as a continuous flow of biomass across trophic levels rather than focusing on individual species. While this method is efficient for estimating system-level trophic structure, it does not resolve gross carbon fluxes and is therefore limited in its ability to assess bioaccumulation. Ultimately, the choice of method involves balancing computational efficiency with ecological realism. Given the importance of trophic level in bioaccumulation modeling, explicit implementation, despite its higher computational cost, may often be the most robust approach.

Be very critical about the role of detritus DOM in Hg cycling, and its link to bioaccumulation

The results of Chapter 5 and 6 are largely driven by the consumption of detritus and DOM and its effect on the bioaccumulation of iHg and MeHg. This is in line with studies such as the ones from that demonstrate the importance of detritus and DOM on Hg bioaccumulation (Seelen et al. 2023; Schartup et al. 2015). Especially the partitioning behaviour of DOM to iHg and MeHg can be radically different for DOM of different origin, and the fate of this DOM can heavily be influenced by the ecosystem, for example due to microbial degradation of DOM (Graham et al. 2012), a change in photochemical processes due to light shading of phytoplankton (Fleck et al. 2013), and the direct consumption of DOM by sponges (De Goeij et al. 2013). Additionally, sometimes the consumption of detritus in higher trophic level animals is included in models, as is the case in the ECOSMO E2E model. The complication is that if detritus is only modeled as one state variable, there is likely a very significant difference between the partitioning behavior of iHg and MeHg with microscopic detritus fractions and large detritus particles. High trophic level fish would consume large detritus particles such as deceased animals, while they would not hunt for microscopic particles that are more efficient in Hg scavenging. While this is no issue for carbon fluxes, the parameterization that is, for example, used in the ECOSMO E2E model, can affect bioaccumulation.

Challenges in DOM modeling

Improving the representation of detritus and DOM cycling in models is challenging for several reasons. The first is a large knowledge gap, both in DOM cycling and in the interactions between Hg and DOM. DOM is typically operationally defined as which carbon can pass through a filter with a pore size between 0.2 to 0.7 μm (Lønborg et al. 2024). However, this distinction between DOM and detritus is somewhat arbitrary, especially regarding Hg partitioning. There might be more overlap in Hg partitioning between DOM and barely-particulate organic carbon fractions than between smaller and larger fractions of detritus, as detritus captures such a large range of particle sizes. Additionally, the chemical composition, particularly the thiol content of DOM, plays a key role in the partitioning between Hg and DOM. (Seelen et al. 2023; Schartup et al. 2018).

An additional point of complication is that DOM is often clustered by its turnover rate, and especially refractory DOM (rDOM) has some hard-to-model properties. The definition of rDOM is reviewed by Baltar

et al. (2021) which discusses the lack of a clear definition of the term. In a model, I would refer to rDOM as DOM with such a long residence time that its degradation would be out of the scope of the biogeochemical model used, but this lack of a clear definition complicates the intercomparison between studies, as something that could be classified as rDOM in an incubation experiment lasting days might not be considered rDOM in a model that simulates decades. In Chapter 6 I solved this by making rDOM a fixed parameter. This approach works in a 1D setup as there would be a constant flux of terrestrial DOM, and the uptake from our local ecosystem would be unlikely to dramatically lower the rDOM concentration. In a 3D model, however, that does not work, because even if we assume that rDOM is not dissimilated into nutrients, it can still be transported, and when it is transported, it could affect the transport of Hg bound to this rDOM.

Coupling DOM and detritus to marine Hg cycling

The coupling to detritus and DOM is a key, understudied parameter in Hg cycling. This involves understanding the dynamics of marine DOM, its interactions with Hg, and the most effective ways to represent these processes in models. Multiple implementations are feasible, but based on my experience, care must be taken to ensure internal consistency in how detritus is represented. For example, it would be inconsistent to implement Hg binding to detritus as if it involves only small particles, while simultaneously modeling high trophic level fish feeding on detritus assumed to be large carcasses. To my knowledge, this specific issue has not been widely addressed in the literature, but I consider it an important point for future model development. This issue arises because separating detritus into different fractions might not be necessary for carbon cycling, and bioaccumulation models, such as those used in this thesis, often rely on models developed for carbon cycling. Some level of particle clustering will always be necessary, but splitting detritus into several sub-fractions may be essential to accurately capture both bioaccumulation and carbon fluxes.

It is crucial in a Hg cycling model to ensure that when DOM and detritus are grouped, each group has a partitioning coefficient with iHg and MeHg that mimics natural partitioning. While extensive studies on partitioning coefficients between organic carbon and different Hg species have been performed, there are variations in the observed partition coefficients (Tesán Onrubia et al. 2020; Allison et al. 2005; Batrakova et al. 2014). This variability is also evident in nature, where a study by Cui et al. (2021) found significant differences in partitioning between detritus, DOM, and Hg across the Arctic, Atlantic, and Pacific Oceans. Combined with the observations of Seelen et al. (2023) that partitioning between DOM and MeHg can vary due to small-scale differences in DOM composition, it becomes clear that correctly parameterizing the partitioning of detritus and DOM to Hg in a global Hg model is both essential and complex.

Model the bioconcentration of consumers

This recommendation is straightforward and forms the main conclusion of Chapter 4. This thesis demonstrates that the relevance of bioconcentration in consumers increases with food chain length. Especially when analyzing bioaccumulation in seafood, which is often of a high trophic level, the uptake of MeHg from the water column should be incorporated at every trophic level. Parameterizing a bioaccumulation model for high trophic level animals without accounting for bioconcentration in consumers likely results in one of three issues: underestimation of bioaccumulation, overtuning the model to exaggerate biomagnification, or overestimating bioaccumulation at the base of the food web. In all cases, this leads to an overfitted model, which can, as discussed before, reduce its predictive capabilities.

8.6.2 What I think might be good

There are several interactions that my thesis suggests are important, though the evidence is less conclusive than for the previously discussed points. I believe these drivers should be considered for inclusion in every model, but they can be omitted depending on the circumstances.

Evaluate the role of *in vivo* Hg speciation

I think there is currently not enough information to accurately incorporate *in vivo* Hg speciation into models. However, both the results of Chapter 6 and the modeling study by Li et al. (2022) demonstrate the very

high sensitivity of bioaccumulation to *in vivo* Hg speciation. When combined with observations that confirm the existence of *in vivo* Hg speciation in at least some animals (Gorokhova et al. 2020; Gentè et al. 2023; Wang et al. 2017), it seems likely that this could be a major biological driver of MeHg bioaccumulation. Nevertheless, the rates of these processes remain highly uncertain, and caution should be taken when incorporating processes to which the model is highly sensitive, especially when there is limited knowledge of the underlying interactions and few means to validate the assumed rates due to the broader uncertainties in the system. Given these uncertainties, I recommend that dedicated studies be conducted to investigate *in vivo* Hg speciation, but I advise caution when incorporating this process into general Hg bioaccumulation or cycling models.

Incorporate the role of different ecological regimes on bioaccumulation

An interaction potentially valuable for inclusion in global models, despite possible drawbacks, is the investigation of how various biological regimes influence bioaccumulation at the base of the food web. In many ecosystems, similar physical conditions can support different biological communities, but the presence of one community may prevent the establishment of another. For example, both filter-feeding mussels, deposit-feeding lugworms, and seagrasses can exist under comparable conditions in the Wadden Sea, but these species exist as ecosystem engineers, modifying their surroundings in ways that favor their own persistence while inhibiting the establishment of other species (Rehlmeyer et al. 2024; Meadows et al. 2012; Volkenborn et al. 2007). Since MeHg concentrations at the base of the food web drive overall bioaccumulation, and our results in Chapter 5 demonstrate differences in bioaccumulation between feeding strategies, it follows that similar physical environments could produce different MeHg levels in high trophic level fish depending on the community composition at the food web's base. This recommendation aligns with recent observations that ecological drivers are essential for predicting Hg bioaccumulation, as shown in studies of North American dragonflies Kotalik et al. (2025). Even if the biological regime differences are not explicitly incorporated, they may be implicitly accounted for if animals are modeled as consuming the most abundant food sources, thus reflecting real feeding dynamics. I suggest that if a large model predicts a patchy distribution of bioaccumulation, evaluating the causes of this patchiness can be a worthwhile endeavor, rather than focusing solely on comparing modeled and observed means.

8.6.3 What I think is not worth it

Several interactions I examined are not significant enough and remain insufficiently researched to be incorporated into the models. As such, I would not recommend them to be included at this time. That does not mean that these interactions should never be included in a model, but that their implementation should be very critically evaluated.

Model bioconcentratated and biomagnified iHg and MeHg as seperate state variables

In my model, I incorporated the bioconcentrated and biomagnified iHg and MeHg as separate state variables so that they could have different release rates. I came to the conclusion that this might not be worth it. Having 2 extra state variables in a global 3D model is extremely computationally expensive, and the certainty about different release rates based on the origin of the Hg bioaccumulation is very uncertain. I would not say that it can never be worth it to keep these variables separate. Maybe our understanding of rates improves, or it can be helpful to troubleshoot if certain bioaccumulation originates from certain interactions. But overall, I think the effect on the bioaccumulation of MeHg is limited.

Model the bioconcentration of iHg, as long as *in vivo* Hg speciation is not incorporated

The relevance of iHg in MeHg bioaccumulation is nuanced. Based on the results of Chapter 3 I would think that the ecosystem has no significant impact on iHg levels, while the results of Chapter 4 verify this and demonstrate that the bioaccumulation of iHg has no significant impact on the bioaccumulation of MeHg. But, as discussed above, the system is highly sensitive to *in vivo* Hg speciation. Because of this, I would not recommend incorporating the bioaccumulation of iHg into a large 3D end-to-end model, unless

sufficient evidence emerges that demonstrates that the *in vivo* methylation of iHg is a significant contributor to MeHg bioaccumulation.

8.7 Broader policy implications

My results demonstrate several points that are potentially relevant for policy in support of the Minamata convention. Although Chapters 3 and 4 focus mainly on quantifying the importance of various drivers in Hg modeling, Chapters 5 and 6 identify drivers that are directly relevant to Hg management.
In Chapter 5 I demonstrate ecosystem community structure has a strong effect on the bioaccumulation of MeHg in seafood. This is important as it ties together several key points in environmental management, demonstrating how biodiversity influences bioaccumulation. While the model results should be verified in experimental settings, it is evident that the filter feeder bioaccumulates more Hg than comparable trophic-level animals. This is of relevance since filter feeders, known for their rapid growth and edibility, are extensively cultivated as seafood in many coastal regions. Our model indicates that if filter feeders were the majority of the base of the benthic food web, the MeHg content of animals of high trophic level would increase.

8.7.1 Sponge based Hg remediation in aquaculture

Furthermore, the potential for demethylation and Hg scavenging by HMA sponges, as demonstrated in Chapter 6, suggests a promising avenue for mercury management. HMA sponges are capable of filtering substantial amounts of Hg from the water column and can either demethylate MeHg into the less toxic iHg or efficiently scavenge iHg. While the large-scale application of sponges for bioremediation in natural environments may be challenging, sponges are shown to be extremely resilient to Hg and they have been shown to grow in areas with heavy Hg pollution due to artisanal mining (Santos-Gandelman et al. 2014b; Cardona et al. 2022). Their usage as a nature-based filtration system in aquaculture settings could be both practical and cost-effective. Additionally, given that HMA sponges consume DOM, it is plausible that they could also remove organic pollutants that bind to organic matter via hydrophobic interactions. The usage of sponges for bioremediation is suggested and reviewed in other scientific literature, such as the review by Amato et al. (2023). But for Hg, the benefits of using sponges could prove to be even more significant than for other pollutants, as not only do the sponges filter out Hg from the water column, they also store Hg as the less toxic iHg, reducing the risk of direct or indirect trophic transfer via either the direct consumption of sponges, or the excretion of detritus by sponges. Although further research is needed, these findings highlight the potential multifunctional role of HMA sponges in contaminant management.
A final potential component of the Hg remediation in aquaculture that warrants further research is the combination that the partitioning between Hg and DOM is heavily influenced by the thiol content of DOM and the ability of sponges to consume non-labile DOM (Seelen et al. 2023; De Goeij et al. 2013). This is pure speculation at this point, but in closed aquaculture settings, you could potentially introduce non-labile thiol-rich DOM into the system. This DOM would bind Hg extremely resistant, resist microbial degradation, but would be able to be consumed by sponges. This might make sponges even more efficient at filtering out Hg. Greatly increasing the Hg scavenging potential of DOM.

8.7.2 Policy to support the use of Hg remedation by sponges

Using sponges for Hg remediation in natural environments presents additional challenges, as it is not feasible to control entire ecosystems to manage Hg bioaccumulation. However, these results indicate that certain vulnerable ecosystem components, such as HMA sponges, could provide significant benefits and should be protected. Based on these findings, I recommend:

- Supporting empirical validation of the link between MeHg bioaccumulation in seafood and the feeding strategies of low trophic level animals.
- Promoting biodiversity in coastal areas, with particular emphasis on protecting HMA sponge communities, to help reduce the risk of MeHg bioaccumulation.

- Investigating the potential role of HMA sponges as a nature-based solution for MeHg management in aquaculture and/or coastal zones.
- Incorporating standardized measurements of iHg, MeHg, trophic level, and carbon content in the same samples as part of the Minamata Convention effectiveness evaluation, to improve our understanding of Hg transfer through food webs.

If empirical studies confirm these model results, I would also recommend investigating whether DOM consumption by HMA sponges increases their uptake of other pollutants, such as POPs. Care must be taken not to over-extrapolate model results; nevertheless, these findings have the potential to inform and support the objectives of the Minamata Convention. Finally, I would like to note that the GMOS-TRAIN ITN framework was designed to foster interdisciplinary collaboration, and it has been very successful in facilitating significant discussion and exchange between specialists from different disciplines. However, ongoing collaboration between modelers and empirical scientists remains essential for producing reliable, high-quality models, and there is always room for improvement. I hope such collaboration will be further strengthened in the future.

8.8 Final Outlook: The Future of Hg Modeling in Support of the Minamata Convention

As discussed above, I believe that Hg (and pollution) modeling has a clear and critical goal: to enable the generation of models that can estimate the spread, levels, and toxicity of pollutants under different emissions scenarios. Ideally, such models would allow policymakers to assess the impact of specific emissions on Hg pollution across temporal and spatial scales. While varying degrees of accuracy are inevitable, the ultimate goal is to reach a point where models can provide actionable estimates.
This thesis contributes to this by identifying key drivers of MeHg bioaccumulation that are critical to ensuring the quality of the predictive capacity of such a model. Understanding the key drivers of marine Hg speciation and MeHg bioaccumulation in seafood is crucial to making such a global model. In fields such as marine pollution research, data collection is extremely challenging and expensive, so ensuring that every data point collected contributes effectively to making such a model is essential. Whether we design such a digital twin around traditional differential models or the Bayesian probability distribution of modern machine learning techniques, the challenge of predicting 100% of outcomes based on a limited amount of data is daunting.
I encourage empirical scientists to read this work and critically evaluate the results of my model so that collaboration can be a two-way street. On the one hand, I would like empirical scientists to validate or disprove the conclusions I draw in this thesis. On the other hand, I hope empirical scientists read this thesis and critically evaluate their own measurement techniques or data-sharing practices and consider taking my recommendations into account. Hopefully, this way we can increase our understanding of Hg pollution and better manage it as a collaborative effort.
In conclusion, this thesis not only advances our fundamental understanding of the biological drivers of Hg bioaccumulation, but also outlines critical directions for future research and offers practical guidance for both policy development and the refinement of modeling approaches. In the following chapter, I will expand on these proposed research directions and discuss what I believe should be the next steps for Hg science.

Figure 8.2: The SA agulhas II during the SCALE-WIN22 crusie in which we samples Hg in the Southern Ocean. Picture taken by David Amptmeijer.

CHAPTER 9

Future research

This chapter discusses key interactions that potentially influence Hg bioaccumulation but could not be incorporated into the model. These are interactions that I believe to be important, but their significance is based on unknown key drivers. After extensive work on modeling MeHg bioaccumulation in the marine food chain, I identify three main directions for future research: the role of ecosystem complexity, *in vivo* Hg speciation, and the bioaccumulation of gaseous Hg species.

9.1 The role of ecosystem complexity

I discuss the importance of capturing ecosystem complexity in Chapter 3 and Chapter 5, where I compare the trophic levels that are modeled and measured in the North and Baltic Seas. The trophic level remains an important contributor to the MeHg content of consumers, and I strongly advise both modelers and empirical scientists to assess the trophic level to ensure a fair comparison of MeHg content. In Chapter 8, I discuss these findings and explain why it is crucial to consider this in a comprehensive modeling framework like the MCHgMAP project. Here, I wish to discuss the specific future efforts that I believe are necessary to better encapsulate ecosystem complexity in the context of bioaccumulation modeling.

I think future work to increase our understanding of the effect of ecosystem complexity on bioaccumulation modeling is necessary, as the complexity in marine ecosystems is more than just the number of trophic interactions. Marine animals typically consume a diverse range of prey items. I demonstrate the importance of this in Chapters 5 and 6, where I discuss the role of the feeding strategy and the importance of DOM as a food source. Since DOM and phytoplankton have different inorganic Hg (iHg) and methylmercury (MeHg) values, a trophic chain with DOM as part of the base will have different iHg and MeHg values than a food chain that starts exclusively with phytoplankton. It is important to identify which animals will likely have a large effect on the bioaccumulation of iHg and MeHg. During my presentation on HMA sponges at the GMOS-Train annual meeting, my colleague Jan Gačnik wondered if sponges are unique, or are the models so sensitive that the inclusion of another animal group affects everything? This is a valid question, but the evidence suggests that HMA sponges are unique. Most animals exhibit relatively similar behaviors. Hence, I doubt that the bioaccumulation in Atlantic cod would be significantly affected by the presence of more mussels or oysters in an area. The main focus should not be on adding as many species as possible, but rather on identifying key interactions that could drive bioaccumulation and are currently being overlooked. Some interactions that I believe are often overlooked but that might significantly influence bioaccumulation are;

- Salp blooms and consequent Hg sedimentation
- Benthic diversity
- Biogenic Anoxia and its role in MeHg production

A potential role for salps in global Hg cycling

Salps, cnidarians, and ctenophores are fast-growing pelagic animals that I believe could significantly impact global Hg cycling. Especially salps, for example, can grow incredibly fast, and during salp blooms, they may account for up to 82% of the total particulate organic carbon generated by all epipelagic zooplankton. Upon their death, this organic material is effectively transported to the deep sea. It is estimated that salps and other tunicates contribute to the downward export of 2.7 billion tonnes of carbon each year (Steinberg et al. 2022). If this exported carbon contains a high concentration of Hg, it could represent a crucial Hg sink.

Future research into these interactions would, in my opinion, come in 2 steps. First, reliable measurements and bioaccumulation factors for salps should be measured in nature. Since the carbon cycling effect of salps is already understood to a degree, this would allow the formation of a non-spatial model in which we estimate the Hg export based on the concentration in salps and the estimated carbon export. This in itself is already very useful as it verifies or rejects the hypothesis that salps have a significant effect on Hg cycling. If this predicts an important role, I believe that a fast-growing fast-sinking zooplankton functional group should be included in the MCHgMAP.

While I looked at the benthic food web in chapter 5 and 6, I think there might be interactions that can play key roles. This is particularly important, as coastal areas that are rich in benthos are often important areas for fisheries, and megabenthos is also eaten as seafood.

9.1.1 Improving bentho-pelagic coupling in models

I believe a driver that might cause inaccuracy in the models is the bentho-pelagic coupling. It is often underestimated how big the benthic food web is. The highest trophic levels of benthic invertebrates are typically megafaunal predatory seastars, with a trophic level of 4.2-5.0, which gives them a similar trophic level as tuna and higher than cod (Amiraux et al. 2023). These sea stars, however, are not consumed by pelagic fish and are therefore not likely to influence MeHg concentrations in seafood. There are, however, plenty of high trophic level invertebrates such as the red king crab and the Atlantic blue crab with high trophic levels of 3.0-3.5 that are consumed by predatory fish (Fuhrmann et al. 2017; Baird and Ulanowicz 1989). If a benthic predatory fish, such as cod, eats a benthic invertebrate with a trophic level of 2.0 or a benthic invertebrate with a trophic level of 3.5 we would expect the MeHg content of this fish to be 10-15x higher, even though megabenthos is often seen as the same functional group. Because of this, I believe further modeling efforts are needed to ensure a proper bentho-pelagic coupling in the model. An example from my own work is the consumption of the macrobenthos functional group by both functional group fish 1 and functional group fish 2 in the ECOSMO E2E model. While there may not be a difference in carbon fluxes, when fish 1 resembling herring would eat macrobenthos, it would eat lower trophic level small invertebrates, whereas fish 2, which would resemble cod, would prey on large megabenthos, such as crabs and benthic fish. If macrobenthos is only 1 functional group, the high difference in MeHg concentration between the low trophic level animals consumed by herring and the high trophic level animals consumed by cod cannot easily be accounted for. In coastal waters, I believe expanding the benthic food web is necessary in order to fully capture bioaccumulation. I don't think this needs to be overly complex; a first-order benthic consumer feeding on pelagic plankton and a second-order consumer preying on the first-order consumer, as well as potentially on mesozooplankton and fish 1, should suffice. In this setup, fish 1 can feed on the first-order benthic consumers, while fish 2 would prey on the second-order benthic consumers. Then the modeled trophic level of both benthic groups can be assessed and they can individually be compared to field observations.

9.1.2 Biogenic Anoxia and its role in MeHg production

Another potentially important interaction of the megabenthos is biologically induced anoxia. Several regions, such as the Baltic and the Mediterranean Sea, can have anoxic conditions (Diaz 2001). While anoxia can occur naturally, it is greatly increased by eutrophication, as more eutrophication means larger production in the surface water, which leads to more sinking of organic material that is consumed by biota. When this is consumed, oxygen is used and anoxia can be formed (Dai et al. 2023). In well-mixed water,

such as the North Sea, this does not lead to anoxia, as oxygen is remixed from the surface water. In stratified water, this can create persistent anoxia. Anoxic conditions increase MeHg production and can therefore greatly increase the MeHg content of biota (Jensen and Jernelov 1969; Compeau and Bartha 1985). Even if megabenthos does not survive during long periods of anoxia, the MeHg can be mixed towards shallow water, or mobile animals can feed on scavenged detritus in the anoxic zone (Ramalhosa et al. 2006; Riedel et al. 2010). This aspect is already recognized, and I am not claiming that it is a novel contribution of my thesis. However, I want to mention it, as it is crucial to acknowledge that biota can impact anoxia, and accurately understanding this relationship is vital for precise predictions of marine MeHg concentrations, and consequently, MeHg bioaccumulation.

I would expand on this by theorizing that HMA sponges could play a role in anoxia-induced Hg methylation. I believe this might be the case for several reasons. First of all, when HMA sponges consume DOM, they consume food that is otherwise not available and in doing so respirate oxygen that would otherwise not be respirated (De Goeij et al. 2013). Additionally, it is shown that HMA sponges are resilient against anoxic conditions, meaning that they can sustain themselves longer when anoxia occurs (Hanz et al. 2019). Finally, as shown by (Hoffmann et al. 2006) and discussed in chapter 6, HMA sponges have sulfate-reducing bacteria. Sulfate-reducing bacteria are known to anaerobically respirate by producing sulfide. When the area is oxygenated again, this sulfide will first react with oxygen before oxygen becomes available, strengthening the anoxia even further. While anoxia is known in the Mediterranean Sea, the link between HMA sponges and anoxia is, to my knowledge, not investigated. This remains purely speculative, as too many key drivers are currently unknown to model the interaction. However, HMA sponges may contribute to anoxia in the Mediterranean Sea, potentially influencing MeHg production.

A final role for HMA sponges that I identified in my model is the potential for phytoplankton fertilization by HMA sponges. It must again be noted that this is extremely speculative, as this is an observation in a model focused on Hg dynamics, rather than in a model focused on understanding sponge dynamics. Phytoplankton growth is typically controlled by Liebig's law of the minimum (Baar 1994). This states that phytoplankton grows until one of the essential drivers of growth is limiting. This is typically light, carbon, nitrogen, or phosphorus. The requirement for phytoplankton growth is controlled by the Redfield Ratio, which states that phytoplankton grows with a C:N:P ratio of 106:16:1 (Redfield 1934). In the bay of Villefranche, phytoplankton is limited by light in winter, but when light is sufficient during spring, summer, and autumn, the size of the phytoplankton bloom is limited by phosphorus. One of the drivers of phosphorus limitations for phytoplankton is that a large portion of the phosphorus is in the form of (refractory) Dissolved Organic Phosphorus (DOP) (Thingstad and Rassoulzadegan n.d.). While the Redfield ratio is 106:16:1, the ratio of DOC:DON:DOP in the Mediterranean Sea is very similar in non-refractory DOM with a ratio of 160:15:1, but it is higher in refractory DOM with a ratio of 950:55:1 (Aminot and Kérouel 2004). This means that if refractory DOM is respirated, and the nutrients are released and made available for phytoplankton, the system will remain phosphorus limited, as the amount of phosphorus in the DOM is below the Redfield ratio. However, it is still phosphorus that is being made bioavailable while it would otherwise not be, which could facilitate increased phytoplankton growth.

9.2 *In vivo* Hg speciation

A key component that I mention in the discussion in Chapter 8 is the potential role of *in vivo* Hg speciation. This is mostly because it is demonstrated both in Chapter 6 and Li et al. (2022) how sensitive bioaccumulation is to *in vivo* Hg speciation. In chapter 6 I demonstrate the relevance of *in vivo* Hg speciation in the form of demethylation of MeHg in Mediterranean HMA sponges and how this can lead to a reduction of MeHg in benthic fish. HMA sponges are unique in many ways that are often poorly understood, but they are also unlikely to be the only animals that influence the bioaccumulation of Hg due to the process of *in vivo* Hg speciation.

Biogenic Hg speciation has been shown to be very important in the case of biogenic reduction of Hg^{2+} to Hg^0 by cyanobacteria. This is discussed in great detail by Kuss et al. (2015) and quantified in Chapter 3. Less is known about potential Hg speciation in other primary producers. However, it has been proposed that phytoplankton can contribute to the MeHg demethylation or the transfer of Hg to cinnabar (HgS). A

recent review paper by (Cossart et al. 2022) describes this as overlooked. I agree with this conclusion, as there is neither understanding nor rates to implement these interactions in the current models; it could, however, play an important role in controlling Hg speciation. The effect of Hg methylation in invertebrates is being further investigated; the problem is that invertebrates are such an incredibly diverse group that it is hard to transfer data of individual species to a fair representation in a functional-based ecosystem model. However, research on cuttlefish and copepods shows these animals can methylate Hg (Gentè et al. 2023; Gorokhova et al. 2020). The issue is that the proof of concept and the quantified interaction that can be used in the models are not the same. That being said, studies such as the one in chapter 6 can be performed to estimate the rates of interactions that would be required to produce the data we observe. However, this was only possible because there was a lot of data on Hg concentration and speciation in HMA sponges. Performing a similar study on copepods or cuttlefish would require a lot of data on both Hg, MeHg in both copepods and their food. The issue is that there is currently such a range in observations that the model already produces results that are within the observed range, but we don't understand the drivers of the large variation in iHg and MeHg concentrations sufficiently to narrow estimate the rates of potential missing drivers. This means that I could not do a sensitivity study on these rates and validate it the same way as the study in Chapter 6.

In vivo Hg speciation from a modeler's perspective is an interesting problem. The only coupled models that include this interaction are the model presented in Chapter 6 and the model published by Li et al. (2022). However, both models only include *in vivo* MeHg demethylation. Having a low uptake and low demethylation rate and a high uptake and high demethylation rate leads to similar concentrations of MeHg higher in the food chain, as long as the assimilation efficiency and grazing pressure remain constant. The main driver of the MeHg content that is transferred in trophic interactions is the MeHg content of the prey. It does not matter whether this MeHg content is low due to a low bioconcentration rate, a low uptake due to trophic interactions, or a high demethylation rate. In this regard, even if *in vivo* Hg demethylation is poorly understood, measurements of Hg release rates combined with observed MeHg can give modelers an estimated MeHg loss term, which would implicitly include all loss terms of MeHg, be it direct excretion or demethylation. However, there are strong benefits in understanding *in vivo* Hg speciations. The first is that the demethylation rates of MeHg could not be directly correlated with other drivers of MeHg release for biota. Understanding the individual drivers of MeHg release will lead to a better understanding of which animals release MeHg at which rate under which circumstances. This information can be used to help modelers estimate MeHg loss rates or inform empirical scientists of the animals that might be worth studying. The second reason why understanding *in vivo* Hg speciation is essential for Hg modeling is its significance in determining whether MeHg can be formed via *in vivo* Hg methylation of iHg. In such a case, the impact of *in vivo* Hg speciation could not be covered by a single general term but would instead rely on the bioaccumulation and *in vivo* methylation rates of iHg. This implies that to fully understand MeHg bioaccumulation, a comprehensive understanding of iHg bioaccumulation is necessary. Research by Gorokhova et al. (2020) and Gentè et al. (2023) provides substantial evidence that *in vivo* methylation of iHg into MeHg is possible, but estimating if this is a significant driver of MeHg bioaccumulation is an area that needs further study. At this time, the inclusion of *in vivo* Hg speciation would benefit greatly from more laboratory studies that study and quantify this interaction in key species. If consistent patterns emerge this can be translated to a rate estimation for specific functional groups, however, at this time I believe there is so much uncertainty that an attempt to model this in anything else than a highly constrained setting would likely just be an exercise in model overfitting. When enough empirical knowledge is established models can be used to estimate the sensitivity of the systems to *in vivo* Hg speciation, and quantify the effect of this in nature. In Chapter 6 *in vivo* Hg speciation is implemented using the modular Framework for Aquatic Biogeochemical Modeling (FABM). It must be noted that the FABM implementation used in this model would be highly suitable to model *in vivo* Hg speciation. The modularity of the FABM framework allows to quickly add or remove bioccumulation of different Hg species and can easily include methylation and demethylation rates to couple the different state variables.

Another possible route for *in vivo* MeHg formation is the demethylation of dimethylmercury (DMHg) into $MMHg^{+}$. At present, this is not included in any model, as there is no evidence for the bioaccumulation of Dissolved Gaseous Hg (DGM) (Morel et al. 1998), which includes DMHg, but as discussed below, this interaction may also prove important; however, evidence is lacking to verify or reject this hypothesis.

9.3 The role of DGM in Hg bioaccumulation

DGM is the sum of Hg^0 and DMHg. The bioaccumulation of DGM is a complicated topic and, as argued, an understudied one. New evidence suggests DMHg plays a key role in MeHg cycling (Kleindienst et al. 2023). It is impossible to accurately model the bioaccumulation of DGM without more laboratory data, but it might be an important driver of Hg bioaccumulation. I think this is important following a discussion I had with Prof. Dr. Milena Horvat. She pointed out that from a cell biological point of view, there is no reason why DGM would not easily penetrate through cells. I would expand on this by noting that fish gills are optimized to absorb large amounts of gaseous compounds from water. If DGM comes into contact with the gills or other organic membranes, there is no biochemical explanation why this would not be taken up at a fast rate. The essential question is what happens after Hg enters the organism? I will first discuss what I think will happen with DGM when it is absorbed in plankton and then discuss how I think this is different in fish. Note that this is pure speculation as no data on the topic exists.

9.3.1 DGM in phytoplankton

For phytoplankton, DGM is generally assumed to enter and exit cells with relative ease due to the nonpolar nature of the compounds (Morel et al. 1998). Although this is a common belief, I propose that within phytoplankton, DMHg may remain inside the cells. Given that DMHg is susceptible to photodegradation and that phytoplankton cells are permeable to light. This means that DMHg could be photodegraded into $MMHg^+$ within these cells. I hypothesize that some portion of DMHg entering the cells will convert to $MMHg^+$, which will bind organic material, thereby promoting bioaccumulation.

9.3.2 DGM in invertebrates

I believe the logic applies to zooplankton as phytoplankton, at least in the case of microzooplankton. Microzooplankton such as copepods are permeable to light, and since they take up oxygen they would likely also absorb DGM, meaning that the non-polar DMHg could be photoreduced to the polar $MMHg^+$, facilitating bioaccumulation. I think this is different in the case of large invertebrates, such as mesozooplankton or megabenthos. While I think they would still take up DGM via respiration, larger animals are impermeable to light, and if photodegradation does not occur the stability of DGM might increase, meaning its subsequent fate is even less clear. Invertebrates may expel it during respiration. The lack of photodegradation does, however, not guarantee the stability of DMHg. Studies have demonstrated the presence of methylating and demethylating bacteria in invertebrates like cuttlefish, copepods, and sponges (Gentè et al. 2023; Orani et al. 2020; Gorokhova et al. 2020). Consequently, it is conceivable that DGM could be converted to Hg^{2+} or $MMHg^+$ after being absorbed by invertebrates; however, this process remains largely unknown and under-researched.

9.3.3 DGM in fish

In fish, there is more evidence to suspect the importance of DGM bioaccumulation and formation of $MMHg^+$, although much is still unclear. The gills of fish are optimized organs to facilitate the transfer of gases from water to the blood of fish (Park et al. 2014), so the gills of the fish will likely filter out DGM as a gaseous compound . When DGM is taken through the gills into the bloodstream, it is transported to the liver and intestines. While there is no direct evidence to support that DMHg will be transformed to MeHg in fish, MeHg can be demethylated into iHg in the liver and intestine of fish (Wang et al. 2017). This would indicate to me that the liver can potentially transfer DMHg to MeHg. The importance of DMHg for Hg cycling is an evolving topic, but DMHg is shown to be dominant Hg species in some areas, such as the deep Atlantic and the Mediterranean Sea. Because of this, I think DMHg can be taken up through the fish gills and converted to MeHg in the liver, which can then bioaccumulate. However, how important this interaction is currently is unknown.

Although all modeling takes educated guesses to a greater or lesser degree, there is a line between uncertain numbers and random numbers. However, if a relatively small number of studies are performed

to estimate *in vivo* Hg speciation rates, especially DMHg demethylation rates, models can be used to estimate the importance of this interaction in nature.

9.4 Summary

To use predictive models coupling Hg emissions with MeHg in fish at higher trophic levels, three steps must still be taken.

- Specific high-quality ecosystem models must be designed with bioaccumulation in mind. Then their quality in bioaccumulation modeling needs to be evaluated on a regional and global scale.
- The bioconcentration of DMHg and Hg^0 and their fate in the organism after bioaccumulation need to be evaluated and, if it is shown to be important, implemented.
- The *in vivo* Hg speciation rates need to be estimated, at least on the functional group level, so that an estimation of these rates can be implemented.

9.5 Final outlook

An observant reader might have noticed in the paragraph above that I believe from all the directions of future work the potential for *in vivo* Hg speciation should be prioritized as I discuss the importance of this interaction on the relevance of ecosystem complexity and the bioaccumulation of DGM. I believe that *in vivo* Hg speciation is potentially a core component of the bioaccumulation of MeHg that is currently extremely understudied and poorly understood. It is entirely possible that laboratory studies will show these rates are too low to be significant, but both Chapter 6 and Li et al. (2022) demonstrate the strong sensitivity of bioaccumulation to demethylation rates, and here I discuss how these demethylation rates could further influence the bioaccumulation of MeHg. Once *in vivo* Hg speciation is better understood, model ecosystems can be adjusted accordingly. Only then can the importance of DGM bioaccumulation be reliably understood and quantified, and its current assumed insignificance be confirmed or challenged. With these steps, I believe that modeling of the bioaccumulation of MeHg can be drastically improved.

CHAPTER 10

List of Publications

1. Bieser, J., Amptmeijer, D. J., Daewel, U., Kuss, J., Soerensen, A. L., and Schrum, C.: The 3D biogeochemical marine mercury cycling model MERCY v2.0 – linking atmospheric Hg to methylmercury in fish, *Geosci. Model Dev.*, 16, 2649–2688, https://doi.org/10.5194/gmd-16-2649-2023, 2023.

2. Amptmeijer, D. J., Mikhavee, E., Daewel, U., Bieser, J., and Schrum, C.: Bioaccumulation as a driver of high MeHg in the North and Baltic Seas, *EGUsphere* [preprint], https://doi.org/10.5194/egusphere-2025-1486, 2025.

3. Amptmeijer, D. and Bieser, J.: Bioconcentration as a key driver of Hg bioaccumulation in high trophic level fish, *EGUsphere* [preprint], https://doi.org/10.5194/egusphere-2025-312, 2025.

4. Amptmeijer, D. J., Padilla, A., Modesti, S., Schrum, C., and Bieser, J.: Feeding strategy as a key driver of the bioaccumulation of MeHg in megabenthos, *EGUsphere* [preprint], https://doi.org/10.5194/egusphere-2025-1494, 2025.

5. Amptmeijer, D. J., Hanz, U., Bieser, J., and Schrum, C.: DOM Uptake and Demethylation in HMA Sponges: Drivers of Low MeHg in Benthic Food Webs, *in preparation*.

Figure 10.1: Pancake ice in the Southern Ocean. Picture taken by David Amptmeijer.

Bibliography

Akçay, Miğraç, H. Mustafa Özkan, Charlie J. Moon, and Baruch Spiro (July 2006). “Geology, mineralogy and geochemistry of the gold-bearing stibnite and cinnabar deposits in the Emirli and Halıköy areas (Ödemiş, İzmir, West Turkey)”. In: *Ore Geology Reviews* 29.1, pp. 19–51.

Albeny-Simões, Daniel, Ebony G. Murrell, Evaldo F. Vilela, and Steven A. Juliano (Mar. 2015). “A multifaceted trophic cascade in a detritus-based system: density-, trait-, or processing-chain-mediated effects?” In: *Ecosphere (Washington, D.C)* 6.3, p. 32.

Allison, Jerry D, Terry L Allison, and Robert B Ambrose (2005). *ALLISON, J. D. AND T. L. ALLISON. PARTITION COEFFICIENTS FOR METALS IN SURFACE WATER, SOIL, AND WASTE. U.S. Environmental Protection Agency, Washington, DC*. Tech. rep.

Amato, Amalia et al. (Jan. 2023). “Marine sponges as promising candidates for integrated aquaculture combining biomass increase and bioremediation: an updated review”. In: *Frontiers in Marine Science* 10, p. 1234225.

Aminot, Alain and Roger Kérouel (Dec. 2004). “Dissolved organic carbon, nitrogen and phosphorus in the N-E Atlantic and the N-W Mediterranean with particular reference to non-refractory fractions and degradation”. In: *Deep-Sea Research Part I: Oceanographic Research Papers* 51.12, pp. 1975–1999.

Amiraux, Rémi, David J. Yurkowski, Philippe Archambault, Marie Pierrejean, and C. J. Mundy (Jan. 2023). “Top predator sea stars are the benthic equivalent to polar bears of the pelagic realm”. In: *Proceedings of the National Academy of Sciences of the United States of America* 120.1, e2216701120.

Andersson, M. E., J. Sommar, K. Gårdfeldt, and O. Lindqvist (June 2008). “Enhanced concentrations of dissolved gaseous mercury in the surface waters of the Arctic Ocean”. In: *Marine Chemistry* 110.3-4, pp. 190–194.

Arrhenius, F and S Hansson (1996). “Growth and seasonal changes in energy content of young Baltic Sea herring”. In: *Clupea harengus L.).-ICES Journal of Marine Science* 53, pp. 792–801.

Asare, Michael Opare and Jerry Owusu Afriyie (June 2021). “Ancient Mining and Metallurgy as the Origin of Cu, Ag, Pb, Hg, and Zn Contamination in Soils: A Review”. In: *Water, Air, & Soil Pollution 2021 232:6* 232.6, pp. 1–22.

Attinger, Sabine et al. (2024). “Digital Twins of Planet Earth. Synthesis Paper”. In: *Helmholtz Earth & Environment.*

Baar, H. J.W. de (Jan. 1994). “von Liebig’s law of the minimum and plankton ecology (1899–1991)”. In: *Progress in Oceanography* 33.4, pp. 347–386.

Backhaus, Jan O. (Sept. 1983). “A semi-implicit scheme for the shallow water equations for application to shelf sea modelling”. In: *Continental Shelf Research* 2.4, pp. 243–254.

Baeyens, W., M. Leermakers, T. Papina, A. Saprykin, N. Brion, J. Noyen, M. De Gieter, M. Elskens, and L. Goeyens (Nov. 2003). “Bioconcentration and Biomagnification of Mercury and Methylmercury in North Sea and Scheldt Estuary Fish”. In: *Archives of Environmental Contamination and Toxicology* 45.4, pp. 498–508.

Baird, Daniel and Robert E Ulanowicz (1989). “The Seasonal Dynamics of The Chesapeake Bay”. In: *Ecological Monographs* 59.4, pp. 329–364.

Baltar, Federico, Xosé A. Alvarez-Salgado, Javier Arístegui, Ronald Benner, Dennis A. Hansell, Gerhard J. Herndl, and Christian Lønborg (Apr. 2021). “What Is Refractory Organic Matter in the Ocean?” In: *Frontiers in Marine Science* 8.

Bart, Martijn C., Anna de Kluijver, Sean Hoetjes, Samira Absalah, Benjamin Mueller, Ellen Kenchington, Hans Tore Rapp, and Jasper M. de Goeij (Oct. 2020). "Differential processing of dissolved and particulate organic matter by deep-sea sponges and their microbial symbionts". In: *Scientific Reports 2020 10:1* 10.1, pp. 1–13.

Bart, Martijn C. et al. (Mar. 2021). "Dissolved organic carbon (DOC) is essential to balance the metabolic demands of four dominant North-Atlantic deep-sea sponges". In: *Limnology and Oceanography* 66.3, pp. 925–938.

Bartnik, Agnieszka (Dec. 2023). "Feeding pigs in ancient Rome". In: *Zeszyty Wiejskie* 29, pp. 139–153.

Batrakova, N., O. Travnikov, and O. Rozovskaya (Dec. 2014). "Chemical and physical transformations of mercury in the ocean: A review". In: *Ocean Science* 10.6, pp. 1047–1063.

Belgacem, Malek, Katrin Schroeder, Alexander Barth, Charles Troupin, Bruno Pavoni, Patrick Raimbault, Nicole Garcia, Mireno Borghini, and Jacopo Chiggiato (Dec. 2021). "Climatological distribution of dissolved inorganic nutrients in the western Mediterranean Sea (1981-2017)". In: *Earth System Science Data* 13.12, pp. 5915–5949.

Bellanger, Martine et al. (2013). "Economic benefits of methylmercury exposure control in Europe: monetary value of neurotoxicity prevention". In: *Environmental health : a global access science source* 12.1.

Bergan, Torbjörn and Henning Rodhe (2001). "Oxidation of Elemental Mercury in the Atmosphere; Constraints Imposed by Global Scale Modelling". In: *Journal of Atmospheric Chemistry* 40, pp. 191–212.

Bertolino, M., A. Reboa, C. Armenio, M. Castellano, S. Felline, A. Terlizzi, and G. Bavestrello (July 2024). "Sponges as feeding resource for the white seabream Diplodus sargus (Linnaeus, 1758) from the Mediterranean Sea". In: *The European Zoological Journal* 91.2, pp. 1192–1198.

Bieser, Johannes, David Amptmeijer, Ute Daewel, Joachim Kuss, Anne L Soerenson, and Corinna Schrum (Oct. 2023). "The 3D biogeochemical marine mercury cycling model MERCY v2.0; linking atmospheric Hg to methyl mercury in fish". In: *Geoscientific Model Development Discussions*, pp. 1–59.

Bieser, Johannes and Corinna Schrum (2016). "Impact of marine mercury cycling on coastal atmospheric mercury concentrations in the North- and Baltic Sea region". In: *Elementa* 2016.

Black, Frank J., Brett A. Poulin, and A. Russell Flegal (May 2012). "Factors controlling the abiotic photodegradation of monomethylmercury in surface waters". In: *Geochimica et Cosmochimica Acta* 84, pp. 492–507.

Bogosavljević Petrović, Vera, Divna Jovanović, Milica Marić Stojanović, and Velibor Andrić (Jan. 2017). "The origin, production and use of quartz crystals in the Neolithic of Serbia: Vinča-Belo Brdo". In: *Quaternary International* 429, pp. 24–34.

Bohr, N (1913). "On the Constitution of Atoms and Molecules". In: *Philos. Mag* 26, p. 476.

Bolding, Karsten, Jorn Bruggeman, Hans Burchard, and Lars Umlauf (June 2021). "General Ocean Turbulence Model - GOTM". In.

Borgå, Katrine, Aaron T Fisk, Paul F Hoekstra, and Derek C G Muir (2004). "Biological and chemical factors of importance in the bioaccumulation and trophic transfer of persistent organochlorine contaminants in Arctic marine food webs". In: *Environmental Toxicology and Chemistry; Special Issue Honoring Don Mackay* 23.10.

Bowman, Katlin L., Chad R. Hammerschmidt, Carl H. Lamborg, and Gretchen Swarr (June 2015). "Mercury in the North Atlantic Ocean: The U.S. GEOTRACES zonal and meridional sections". In: *Deep-Sea Research Part II: Topical Studies in Oceanography* 116, pp. 251–261.

Bowman, Katlin L., Carl H. Lamborg, and Alison M. Agather (Mar. 2020). "A global perspective on mercury cycling in the ocean". In: *Science of The Total Environment* 710, p. 136166.

Box, George E P (1976). "Science and Statistics". In: *Journal of the American Statistical Association* 71.356, pp. 791–799.

Boyd, Claude E., Aaron A. McNevin, and Robert P. Davis (June 2022). "The contribution of fisheries and aquaculture to the global protein supply". In: *Food Security* 14.3, pp. 805–827.

Bradford, Molly A., Mark L. Mallory, and Nelson J. O'Driscoll (Mar. 2023). "Mercury bioaccumulation and speciation in coastal invertebrates: Implications for trophic magnification in a marine food web". In: *Marine Pollution Bulletin* 188, p. 114647.

Bresnan, E., S. Hay, S. L. Hughes, S. Fraser, J. Rasmussen, L. Webster, G. Slesser, J. Dunn, and M. R. Heath (Jan. 2009). “Seasonal and interannual variation in the phytoplankton community in the north east of Scotland”. In: *Journal of Sea Research* 61.1-2, pp. 17–25.

Bridges, Christy C. and Rudolfs K. Zalups (July 2010). *Transport of inorganic mercury and methylmercury in target tissues and organs*.

Bruggeman, Jorn and Karsten Bolding (Nov. 2014). “A general framework for aquatic biogeochemical models”. In: *Environmental Modelling & Software* 61, pp. 249–265.

Bruggeman, Jorn, Karsten Bolding, Lars Nerger, Anna Teruzzi, Simone Spada, Jozef Skákala, and Stefano Ciavatta (2024). “EAT v1.0.0: a 1D test bed for physical-biogeochemical data assimilation in natural waters”. In: *Geosci. Model Dev* 17, pp. 5619–5639.

Bryan, G. W. (1979). “Bioaccumulation of Marine Pollutants”. In: *Philosophical Transactions of the Royal Society of London. Series B, Biological Sciences* 286.1015, pp. 483–505.

Bullock, O. Russell and Katherine A. Brehme (2002). “Atmospheric mercury simulation using the CMAQ model: Formulation description and analysis of wet deposition results”. In: *Atmospheric Environment* 36.13, pp. 2135–2146.

Bullock, O. Russell, Katherine A. Brehme, and George R. Mapp (June 1998). “Lagrangian modeling of mercury air emission, transport and deposition: An analysis of model sensitivity to emissions uncertainty”. In: *Science of The Total Environment* 213.1-3, pp. 1–12.

Burchard, Hans, Karsten Bolding, and Manuel Ruiz-Villarreal (Dec. 1999a). *GOTM, a general ocean turbulence model. Theory, implementation and test cases*.

Burchard, Hans, Karsten Bolding, and Manuel R Villarreal (1999b). *GOTM, a General Ocean Turbulence Model. Theory, implementation and test cases*. Tech. rep.

Burger, Joanna and Michael Gochfeld (Mar. 2011). “Mercury and selenium levels in 19 species of saltwater fish from New Jersey as a function of species, size, and season”. In: *Science of The Total Environment* 409.8, pp. 1418–1429.

Burson, Amanda, Maayke Stomp, Larissa Akil, Corina P.D. Brussaard, and Jef Huisman (May 2016). “Unbalanced reduction of nutrient loads has created an offshore gradient from phosphorus to nitrogen limitation in the North Sea”. In: *Limnology and Oceanography* 61.3, pp. 869–888.

Butenschön, Momme et al. (Apr. 2016). “ERSEM 15.06: A generic model for marine biogeochemistry and the ecosystem dynamics of the lower trophic levels”. In: *Geoscientific Model Development* 9.4, pp. 1293–1339.

Calvo, Florent, Elke Pahl, Michael Wormit, and Peter Schwerdtfeger (July 2013). “Evidence for low-temperature melting of mercury owing to relativity”. In: *Angewandte Chemie - International Edition* 52.29, pp. 7583–7585.

Campanella Id, Fabio, Peter J Auster, J Christopher Taylor, and Roldan C Muñoz (Feb. 2019). “Dynamics of predator-prey habitat use and behavioral interactions over diel periods at sub-tropical reefs”. In: *PLOS ONE* 2.14.

Cardona, Gladys Inés, María Camila Escobar, Alejandro Acosta-González, Patricia Marín, and Silvia Marqués (Apr. 2022). “Highly mercury-resistant strains from different Colombian Amazon ecosystems affected by artisanal gold mining activities”. In: *Applied microbiology and biotechnology* 106.7, pp. 2775–2793.

Carson, Rachel (1962). *Silent Spring*.

Carvalho, Cristina M L, Eng-Hui Chew, Isaac Hashemy, Jun Lu, and Arne Holmgren (2008). “Inhibition of the Human Thioredoxin System, a molecular mechanism of mercury toxicity”. In.

Casas, Stellio and Cédric Bacher (Aug. 2006). “Modelling trace metal (Hg and Pb) bioaccumulation in the Mediterranean mussel, Mytilus galloprovincialis, applied to environmental monitoring”. In: *Journal of Sea Research* 56.2, pp. 168–181.

Chakravarti, L J and P A Cotton (2014). “The Effects of a Competitor on the Foraging Behaviour of the Shore Crab Carcinus maenas”. In: *PLoS ONE* 9.4, p. 93546.

Chaudret, Robin, Julia Contreras-Garcia, Mickaël Delcey, Olivier Parisel, Weitao Yang, and Jean Philip Piquemal (May 2014). “Revisiting H2O nucleation around Au+ and Hg 2+: The peculiar ”pseudo-soft” character of the gold cation”. In: *Journal of Chemical Theory and Computation* 10.5, pp. 1900–1909.

Chen, Celia Y, Richard S Stemberger, Neil C Kamman, Brandon M Mayes, and Carol L Folt (2004). "Patterns of Hg Bioaccumulation and Transfer in Aquatic Food Webs Across Multi-lake Studies in the Northeast US". In: *Ecotoxicology* 14, pp. 135–147.

Chen, Celia Y., Mark E. Borsuk, Deenie M. Bugge, Terill Hollweg, Prentiss H. Balcom, Darren M. Ward, Jason Williams, and Robert P. Mason (Feb. 2014). "Benthic and Pelagic Pathways of Methylmercury Bioaccumulation in Estuarine Food Webs of the Northeast United States". In: *PLOS ONE* 9.2, e89305.

Chen, Celia Y., Michelle Dionne, Brandon M. Mayes, M. Ward Darron, Sturup Stefan, and Jackson P. Brian (2009). "Mercury Bioavailability and Bioaccumulation in Estuarine Food Webs in the Gulf of Maine". In: *Environ. Sci. Technol.* 43, pp. 1804–1810.

Chen, Long et al. (2019). "Trans-provincial health impacts of atmospheric mercury emissions in China". In.

Christy, S.B. (1879). "On the genesis of cinnabar deposits". In: *American Journal of Science* 3, pp. 453–463.

Cibic, Tamara, Laura Baldassarre, Federica Cerino, Cinzia Comici, Daniela Fornasaro, Martina Kralj, and Michele Giani (June 2022). "Benthic and Pelagic Contributions to Primary Production: Experimental Insights From the Gulf of Trieste (Northern Adriatic Sea)". In: *Frontiers in Marine Science* 9.

Claisse, D (1989). "Chemical Contamination of French Coasts The Results of a Ten Years Mussel Watch". In: *Marine Pollution Bulletin*.

Clark, J. S. (2005). "Why environmental scientists are becoming". In: *Ecology Letters* 8, pp. 2–4.

Compeau, G C and R Bartha (1985). *Sulfate-Reducing Bacteria: Principal Methylators of Mercury in Anoxic Estuarine Sedimentt*. Tech. rep. 2, pp. 498–502.

Conley, Daniel J. et al. (May 2009). "Hypoxia-related processes in the Baltic Sea". In: *Environmental Science and Technology* 43.10, pp. 3412–3420.

Copping, Matthew (2009). "Death in the beer-glass: the Manchester arsenic-in-beer epidemic of 1900-1 and the long-term poisoning of beer". In: *Brewery History* 132.132, pp. 31–57.

Cossa, Daniel, Xavier Durrieu de Madron, Jörg Schäfer, Laurent Lanceleur, Stéphane Guédron, Roselyne Buscail, Bastien Thomas, Sabine Castelle, and Jean Jacques Naudin (Feb. 2017). "The open sea as the main source of methylmercury in the water column of the Gulf of Lions (Northwestern Mediterranean margin)". In: *Geochimica et Cosmochimica Acta* 199, pp. 222–237.

Cossa, Daniel and Anne-Marie Tabard (2020). "Mercury in Marine Mussels from the St. Lawrence Estuary and Gulf (Canada): A Mussel Watch Survey Revisited after 40 Years". In: *Applied science* 10, p. 7556.

Cossa, Daniel et al. (2022). "Mediterranean Mercury Assessment 2022: An Updated Budget, Health Consequences". In: *Cite This: Environ. Sci. Technol* 56, p. 3862.

Cossa, Daniel et al. (Oct. 2023). "Mercury deposition in the Eastern Mediterranean: Modern fluxes in the water column and Holocene accumulation rates in abyssal sediment". In: *Chemical Geology* 636, p. 121652.

Cossart, Thibaut, Javier Garcia-Calleja, João Santos, and Lotfi Kalahroodi (2022). "Role of phytoplankton in aquatic mercury speciation and transformations". In: *Environmental chemistry*.

Counter, S Allen and Leo H Buchanan (2004). "Mercury exposure in children: a review". In.

Cresson, Pierre, Morgane Travers-Trolet, Manuel Rouquette, Charles André Timmerman, Carolina Giraldo, Sébastien Lefebvre, and Bruno Ernande (Oct. 2017). "Underestimation of chemical contamination in marine fish muscle tissue can be reduced by considering variable wet:dry weight ratios". In: *Marine Pollution Bulletin* 123.1-2, pp. 279–285.

Cruz, João Filipe da, Helena Gaspar, and Gonçalo Calado (Mar. 2012). "Turning the game around: Toxicity in a nudibranch-sponge predator-prey association". In: *Chemoecology* 22.1, pp. 47–53.

Cruz, Kimberly, Jean Guézennec, and Tamar Barkay (July 2017). "Binding of Hg by bacterial extracellular polysaccharide: a possible role in Hg tolerance". In: *Applied Microbiology and Biotechnology* 101.13, pp. 5493–5503.

Cruz, Mariana Hill, Iris Kriest, Yonss Saranga José, Rainer Kiko, Helena Hauss, and Andreas Oschlies (May 2021). "Zooplankton mortality effects on the plankton community of the northern Humboldt Current System: Sensitivity of a regional biogeochemical model". In: *Biogeosciences* 18.9, pp. 2891–2916.

Cui, Xinyun, Carl H. Lamborg, Chad R. Hammerschmidt, Yang Xiang, and Phoebe J. Lam (May 2021). "The Effect of Particle Composition and Concentration on the Partitioning Coefficient for Mercury in Three Ocean Basins". In: *Frontiers in Environmental Chemistry* 2, p. 660267.

Cushing, D H (1958). “The estimation of carbon in phytoplankton”. In: *Rappt. Proces-Verbaux Reunions, Conseil Perm. Intern. Exploration Mer* 144, pp. 32–33.

Daan, R and M Mulder (2001). “The macrobenthic fauna in the Dutch sector of the North Sea in 2003 and a comparison with previous data”. In: *NIOZ-RAPPORT* 2001-2, p. 97.

Dachs, Jordi, Steven J. Eisenreich, and Raymond M. Hoff (Mar. 2000). “Influence of Eutrophication on Air-Water Exchange, Vertical Fluxes, and Phytoplankton Concentrations of Persistent Organic Pollutants”. In: *Environmental Science and Technology* 34.6, pp. 1095–1102.

Daewel, Ute and Corinna Schrum (June 2013). “Simulating long-term dynamics of the coupled North Sea and Baltic Sea ecosystem with ECOSMO II: Model description and validation”. In: *Journal of Marine Systems* 119-120, pp. 30–49.

— (Sept. 2017). “Low-frequency variability in North Sea and Baltic Sea identified through simulations with the 3-D coupled physical-biogeochemical model ECOSMO”. In: *Earth System Dynamics* 8.3, pp. 801–815.

Daewel, Ute, Corinna Schrum, and Jed I. MacDonald (May 2019). “Towards end-to-end (E2E) modelling in a consistent NPZD-F modelling framework (ECOSMO E2E-v1.0): Application to the North Sea and Baltic Sea”. In: *Geoscientific Model Development* 12.5, pp. 1765–1789.

Dai, Minhan et al. (2023). “Persistent eutrophication and hypoxia in the coastal ocean”. In: *Cambridge Prisms: Coastal Futures* 1.

Dastoor, Ashu, Andrew Ryzhkov, Dorothy Durnford, Igor Lehnherr, Alexandra Steffen, and Heather Morrison (Mar. 2015). “Atmospheric mercury in the Canadian Arctic. Part II: Insight from modeling”. In: *Science of The Total Environment* 509-510, pp. 16–27.

Dastoor, Ashu et al. (2024). “The Multi-Compartment Hg Modeling and Analysis Project (MCHgMAP): Mercury modeling to support international environmental policy”. In: *Geoscientific Model Development-Discussions* preprint.

De Goeij, Jasper M., Dick Van Oevelen, Mark J.A. Vermeij, Ronald Osinga, Jack J. Middelburg, Anton F.P.M. De Goeij, and Wim Admiraal (Oct. 2013). “Surviving in a marine desert: The sponge loop retains resources within coral reefs”. In: *Science* 342.6154, pp. 108–110.

Diaz, Robert J. (Mar. 2001). “Overview of Hypoxia around the World”. In: *Journal of Environmental Quality* 30.2, pp. 275–281.

Dibble, T. S., M. J. Zelie, and H. Mao (2012). “Thermodynamics of reactions of ClHg and BrHg radicals with atmospherically abundant free radicals”. In: *Atmospheric Chemistry and Physics* 12.21, pp. 10271–10279.

Dijkstra, Jennifer A., Kate L. Buckman, Darren Ward, David W. Evans, Michele Dionne, and Celia Y. Chen (Mar. 2013). “Experimental and Natural Warming Elevates Mercury Concentrations in Estuarine Fish”. In: *PLOS ONE* 8.3, e58401.

Dolan, John R. (Sept. 2014). “The History of Biological Exploration of the Bay of Villefranche”. In: *Protist* 165.5, pp. 636–644.

Dommergue, A, F Sprovieri, N Pirrone, R Ebinghaus, S Brooks, J Courteaud, and C P Ferrari (2010). “Overview of mercury measurements in the Antarctic troposphere”. In: *Atmos. Chem. Phys* 10, pp. 3309–3319.

Dou, Bozheng et al. (2023). “Machine Learning Methods for Small Data Challenges in Molecular Science”. In: *Chem. Rev* 123.

Driscoll, Charles T, Robert P Mason, Hing Man Chan, Daniel J Jacob, and Nicola Pirrone (2013). “Mercury as a Global Pollutant: Sources, Pathways, and Effects Terms of Use”. In: *Environ. Sci. Technol* 47.

Dufour, Suzanne C. (2018). “Bivalve Chemosymbioses on Mudflats”. In: *Mudflat Ecology*, pp. 169–184.

Durnford, D, A Dastoor, D Figueras-Nieto, and A Ryjkov (2010). “Long range transport of mercury to the Arctic and across Canada”. In: *Atmos. Chem. Phys* 10, pp. 6063–6086.

Dutton, Jessica and Nicholas S. Fisher (2012). “Bioavailability of sediment-bound and algal metalsto killifish Fundulus heteroclitus”. In: *Aquatic biology* 16, pp. 85–96.

Dyer, Peter (2009). “The 1900 arsenic poisoning epidemic”. In: *Brewery History* 130.130, pp. 65–85.

Ebinghaus, R., C. Temme, S. E. Lindberg, and K. J. Scott (2004). “Springtime accumulation of atmospheric mercury in polar ecosystems”. In: *Journal De Physique. IV : JP* 121, pp. 195–208.

Egbert, Gary D. and Svetlana Y. Erofeeva (Feb. 2002). “Efficient Inverse Modeling of Barotropic Ocean Tides”. In: *Journal of Atmospheric and Oceanic Technology* 19.2, pp. 183–204.

Ekino, Shigeo, Mari Susa, Tadashi Ninomiya, Keiko Imamura, and Toshinori Kitamura (Nov. 2007). “Minamata disease revisited: An update on the acute and chronic manifestations of methyl mercury poisoning”. In: *Journal of the Neurological Sciences* 262.1-2, pp. 131–144.

Emeis, Kay Christian et al. (Jan. 2015). “The North Sea — A shelf sea in the Anthropocene”. In: *Journal of Marine Systems* 141, pp. 18–33.

English, Matthew D., Gregory J. Robertson, and Mark L. Mallory (Dec. 2015). “Trace element and stable isotope analysis of fourteen species of marine invertebrates from the Bay of Fundy, Canada”. In: *Marine Pollution Bulletin* 101.1, pp. 466–472.

Erwin, Patrick M, Rafel Coma, Eduard Serrano, and Marta Ribes (2015). “Stable symbionts across the HMA-LMA dichotomy: low seasonal and interannual variation in sponge-associated bacteria from taxonomically diverse hosts”. In: *FEMS Microbiology Ecology* 91.10.

Esteves, Ana I.S., Marisa Nicolai, Madalena Humanes, and Joao Goncalves (2011). “Sulfated polysaccharides in marine sponges: Extraction methods and anti-HIV activity”. In: *Marine Drugs* 9.1, pp. 139–153.

Euler, L. (1768). *Institutiones calculi integralis (Foundations of integral calculus)*.

Evers, David C, Susan Egan Keane, Niladri Basu, and David Buck (2016). “Evaluating the effectiveness of the Minamata Convention on Mercury: Principles and recommendations for next steps”. In.

Fan, Song-Miao and Daniel J. Jacob (1992). “Surface ozone depletion in the Arctic spring sustained by bromine reactions on aerosols”. In: *Letters to nature* 359, pp. 522–524.

Fang, Tien Hsi and Fu Wei Chang (Aug. 2024). “Temporal variation of mercury and methyl mercury in water and accumulation by phytoplankton in the eutrophic estuary, northern Taiwan”. In: *Marine pollution bulletin* 205.

FAO (2020). “The State of World Fisheries and Aquaculture 2020”. In: *Food and Agriculture Organization of the United Nations*.

FAO/WHO (2012). *GENERAL STANDARD FOR CONTAMINANTS AND TOXINS IN FOOD AND FEED*. Tech. rep., pp. 65–66.

Farina, Marcelo, Michael Aschner, and João B.T. Rocha (Nov. 2011). “Oxidative stress in MeHg-induced neurotoxicity”. In: *Toxicology and Applied Pharmacology* 256.3, pp. 405–417.

Feinberg, Aryeh, Thandolwethu Dlamini, Martin Jiskra, Viral Shah, and Noelle E. Selin (Apr. 2022). “Evaluating atmospheric mercury (Hg) uptake by vegetation in a chemistry-transport model”. In: *Environmental Science. Processes & Impacts* 24.9, p. 1303.

Fennel, W. and T Neumann (2015). *Introduction to the Modelling of Marine Ecosystems - second edition*.

Fishbase (2024). *Search FishBase*.

Fitzgerald, William F, Carl H Lamborg, and Chad R Hammerschmidt (2007). “Marine Biogeochemical Cycling of Mercury”. In.

Fleck, Jacob A, Gary Gill, Brian A Bergamaschi, Tamara E C Kraus, Bryan D Downing, and Charles N Alpers (2013). “Concurrent photolytic degradation of aqueous methylmercury and dissolved organic matter”. In.

Folke, Carl, Steve Carpenter, Brian Walker, Marten Scheffer, Thomas Elmqvist, Lance Gunderson, and C. S. Holling (2004). *Regime shifts, resilience, and biodiversity in ecosystem management*.

Fonds, M., R. Cronie, A. D. Vethaak, and P. Van Der Puyl (June 1992). “Metabolism, food consumption and growth of plaice (Pleuronectes platessa) and flounder (Platichthys flesus) in relation to fish size and temperature”. In: *Netherlands Journal of Sea Research* 29.1-3, pp. 127–143.

Fox, Austin L, Emily A Hughes, Robert P Trocine, John H Trefry, Susan V Schonberg, Nathan D Mctigue, Brenda K Lasorsa, Brenda Konar, and Lee W Cooper (2013). “Mercury in the northeastern Chukchi Sea: Distribution patterns in seawater and sediments and biomagnification in the benthic food web”. In.

Fraser, Alison J., Thomas M. Cahill, David C. Lasenby, Donald Mackay, and Lynne Milford (Apr. 2005). “The role of cannibalism and contaminant source on bioaccumulation in aquatic food webs”. In: *Environmental toxicology and chemistry* 24.4, pp. 909–915.

Fromentin, Jean-Marc, Jean-Claude Dauvin, Frédéric Ibanez, Jean-Marie Dewarumez, and Bernard Elkaim (1997). *Long-term variations Macrobenthos Community structure*. Tech. rep., pp. 43–53.

Fuhrmann, Mona M., Torstein Pedersen, and Einar M. Nilssen (Feb. 2017). "Trophic niche of the invasive red king crab Paralithodes camtschaticus in a benthic food web". In: *Marine Ecology Progress Series* 565, pp. 113–129.

Garcia H.E. et al. (2019). "World Ocean Atlas 2018: Product Documentation. A. Mishonov, Technical Editor." In.

Garcia-Arevalo, Isabel, Jean-Baptiste Berard, Johannes Bieser, Severine Le Faucheur, Clarisse Hubert, Thomas Lacour, Bastien Thomas, Daniel Cossa, and Joël Knoery (2024). "Mercury Accumulation Pathways in a Model Marine Microalgae: Sorption, Uptake, and Partition Kinetics". In.

García-Bonilla, Erika, Pedro F B Brandão, Thierry Pérez, and Howard Junca (2019). "Stable and Enriched Cenarchaeum symbiosum and Uncultured Betaproteobacteria HF1 in the Microbiome of the Mediterranean Sponge Haliclona fulva (Demospongiae: Haplosclerida)". In: *ENVIRONMENTAL MICROBIOLOGY* 77, pp. 25–36.

Gascuel, Didier and Daniel Pauly (Nov. 2009). "EcoTroph: Modelling marine ecosystem functioning and impact of fishing". In: *Ecological Modelling* 220.21, pp. 2885–2898.

GEBCO Bathymetric Compilation Group (2020). *The GEBCO_2020 Grid - a continuous terrain model of the global oceans and land.* Tech. rep.

Geider, Richard J., Hugh L. MacIntyre, and Todd M. Kana (1998). "A dynamic regulatory model of phytoplanktonic acclimation to light, nutrients, and temperature". In: *Limnology and Oceanography* 43.4, pp. 679–694.

Gentè, Sophie et al. (2023). "In Vivo Mercury (De)Methylation Metabolism in Cephalopods under Different pCO 2 Scenarios". In: *Cite This: Environ. Sci. Technol* 57, p. 5770.

Ghodrati Shojaei, Mehdi, Lars Gutow, Jennifer Dannheim, Eike Rachor, Alexander Schröder, and Thomas Brey (Jan. 2016). "Common trends in German Bight benthic macrofaunal communities: Assessing temporal variability and the relative importance of environmental variables". In: *Journal of Sea Research* 107, pp. 25–33.

Gizem Bacaksızlar, N and Nisa Önsel (2013). "MODELING THE DYNAMICS OF METHYLMERCURY BIOMAGNIFICATION". In: *International System Dynamics Conferences*.

Gloeckner, Volker et al. (2014). *The HMA-LMA Dichotomy Revisited: an Electron Microscopical Survey of 56 Sponge Species*. Tech. rep.

Gorokhova, Elena, Anne L. Soerensen, and Nisha H. Motwani (2020). "Mercury-methylating bacteria are associated with copepods: A proof-of-principle survey in the Baltic Sea". In: *PLoS ONE* 15.3.

Gosnell, Kathleen J. and Robert P. Mason (Dec. 2015). "Mercury and methylmercury incidence and bioaccumulation in plankton from the central Pacific Ocean". In: *Marine Chemistry* 177, pp. 772–780.

Graham, Andrew M, George R Aiken, and Cynthia C Gilmour (2012). "Dissolved Organic Matter Enhances Microbial Mercury Methylation Under Sulfidic Conditions". In: *Environ. Sci. Technol* 46, p. 29.

Griffies, Stephen M (2003). "Fundamentals of ocean climate models Contents". In.

Gygi, Jeremy P., Steven H. Kleinstein, and Leying Guan (2023). "Predictive overfitting in immunological applications: Pitfalls and solutions". In: *Human Vaccines & Immunotherapeutics* 19.2, p. 2251830.

Haitzer, Markus, George R. Aiken, and Joseph N. Ryan (Aug. 2002). "Binding of mercury(II) to dissolved organic matter: the role of the mercury-to-DOM concentration ratio". In: *Environmental science & technology* 36.16, pp. 3564–3570.

Hall, B. D., R. A. Bodaly, R. J.P. Fudge, J. W.M. Rudd, and D. M. Rosenberg (Nov. 1997). "Food as the dominant pathway of methylmercury uptake by fish". In: *Water, Air, and Soil Pollution* 100.1-2, pp. 13–24.

Haller-Bull, Vanessa and Elena Rovenskaya (Nov. 2019). "Optimizing functional groups in ecosystem models: Case study of the Great Barrier Reef". In: *Ecological Modelling* 411, p. 108806.

Hamelink, J. L. (1977). "Current Bioconcentration Test Methods and Theory". In: *ASTM Special Technical Publication* STP 634, pp. 149–161.

Hammerschmidt, Chad R and William F Fitzgerald (2006). "Bioaccumulation and Trophic Transfer of Methylmercury in Long Island Sound". In: *Arch. Environ. Contam. Toxicol* 51, pp. 416–424.

Hanz, Ulrike et al. (Nov. 2019). “Environmental factors influencing benthic communities in the oxygen minimum zones on the Angolan and Namibian margins”. In: *Biogeosciences* 16.22, pp. 4337–4356.

Hanz, Ulrike et al. (2022). “The important role of sponges in carbon and nitrogen cycling in a deep-sea biological hotspot”. In.

Harada, Masazumi (1995). “Minamata Disease: Methylmercury Poisoning in Japan Caused by Environmental Pollution”. In: *Critical Reviews in Toxicology* 25.1, pp. 1–24.

Harding, Gareth, John Dalziel, and Peter Vass (July 2018). “Bioaccumulation of methylmercury within the marine food web of the outer Bay of Fundy, Gulf of Maine”. In: *PLoS ONE* 13.7.

Hasselmann, K. (Jan. 1976). “Stochastic climate models: Part I. Theory”. In: *Tellus A: Dynamic Meteorology and Oceanography* 28.6, p. 473.

Hedgecock, Ian Michael, Francesco De Simone, Francesco Carbone, and Nicola Pirrone (Apr. 2024). “Modelling the Fate of Mercury Emissions from Artisanal and Small Scale Gold Mining”. In: *EGUsphere* preprint.

Heip, C et al. (1992). “Trends in biomass, density and diversity of North Sea macrofauna”. In: *ICESJ. mar. Sci* 49, pp. 13–22.

Hentschel, Ute, Jörn Piel, Sandie M. Degnan, and Michael W. Taylor (Sept. 2012). “Genomic insights into the marine sponge microbiome”. In: *Nature Reviews Microbiology* 10.9, pp. 641–654.

Hentschel, Ute, Kayley M Usher, and Michael W Taylor (2006). “Marine sponges as microbial fermenters”. In: *FEMS Microbiol Ecol* 55, pp. 167–177.

Hjerne, Olle, Susanna Hajdu, Ulf Larsson, Andrea S. Downing, and Monika Winder (2019). “Climate Driven Changes in Timing, Composition and Magnitude of the Baltic Sea Phytoplankton Spring Bloom”. In.

Hoffmann, Friederike, Hans Tore Rapp, and Joachim Reitner (Aug. 2006). “Monitoring microbial community composition by fluorescence in situ hybridization during cultivation of the marine cold-water sponge Geodia barretti”. In: *Marine Biotechnology* 8.4, pp. 373–379.

Höge, Marvin, Thomas Wöhling, and Wolfgang Nowak (Mar. 2018). “A Primer for Model Selection: The Decisive Role of Model Complexity”. In: *Water Resources Research* 54.3, pp. 1688–1715.

Horowitz, Hannah M. et al. (May 2017). “A new mechanism for atmospheric mercury redox chemistry: Implications for the global mercury budget”. In: *Atmospheric Chemistry and Physics* 17.10, pp. 6353–6371.

Hsi, Hsing-Cheng, You-Wen Hsu, Tien-Chin Chang, and Ling-Chu Chien (2016). “Methylmercury Concentration in Fish and Risk-Benefit Assessment of Fish Intake among Pregnant versus Infertile Women in Taiwan”. In.

Hughes, Michael F., Barbara D. Beck, Yu Chen, Ari S. Lewis, and David J. Thomas (Oct. 2011). “Arsenic Exposure and Toxicology: A Historical Perspective”. In: *Toxicological Sciences* 123.2, p. 305.

Hwong, I.Y, S.C. Sherwood, and D. Fuchs (2022). “Can We Use 1D Models to Predict 3D Model Response to Forcing in an Idealized Framework”. In: *Journal of advances in modeling earth systems*.

ICES (2020). “Mercury data (biota) from the ICES DOME database (Contaminants and biological effects of contaminants in biota)”. In: *Data Outputs*.

— (Nov. 2022). “Greater North Sea ecoregion – fisheries overview”. In.

Jackson, Togwell A and Ta Jackson (1997). “Long-range atmospheric transport of mercury to ecosystems, and the importance of anthropogenic emissions-A critical review and evaluation of the published evidence”. In: *Environ. Rev* 5, pp. 99–120.

Jakeman, A. J., R. A. Letcher, and J. P. Norton (May 2006). “Ten iterative steps in development and evaluation of environmental models”. In: *Environmental Modelling & Software* 21.5, pp. 602–614.

Jennings, Simon and Johan Van Der Molen (Oct. 2015). “Trophic levels of marine consumers from nitrogen stable isotope analysis: estimation and uncertainty”. In: *ICES Journal of Marine Science* 72.8, pp. 2289–2300.

Jensen, S and A Jernelov (1969). “Biological Methylation of Mercury in Aquatic Organisms”. In: *Nature* 223.5205, pp. 753–754.

Jeong, Haksoo, Wajid Ali, Philippe Zinck, Sami Souissi, and Jae Seong Lee (Sept. 2024). “Toxicity of methylmercury in aquatic organisms and interaction with environmental factors and coexisting pollutants: A review”. In: *Science of the Total Environment* 943.

Jermilova, Una et al. (Mar. 2025). “Assessing mercury exposure to water and fish of the Mackenzie watershed using a Bayesian network analysis”. In: *Integrated Environmental Assessment and Management* 21.2, pp. 396–413.

Jiskra, Martin et al. (Apr. 2018). “A vegetation control on seasonal variations in global atmospheric mercury concentrations”. In: *Nature Geoscience 2018 11:4* 11.4, pp. 244–250.

Johansson, Carolina, Anna F. Castoldi, Natalia Onishchenko, Luigi Manzo, Marie Vahter, and Sandra Ceccatelli (2007). “Neurobehavioural and molecular changes induced by methylmercury exposure during development”. In: *Neurotoxicity Research* 11.3-4, pp. 241–260.

Judd, Nancy, Lucinda Tear, and John Toll (Jan. 2014). “From sediment to tissue and tissue to sediment: An evaluation of statistical bioaccumulation models”. In: *Integrated Environmental Assessment and Management* 10.1, pp. 102–113.

Jung, G, I M Hedgecock, and N Pirrone (2009). “Geoscientific Model Development ECHMERIT V1.0-a new global fully coupled mercury-chemistry and transport model”. In: *Geosci. Model Dev* 2, pp. 175–195.

Kahru, M and R Elmgren (2014). “Multidecadal time series of satellite-detected accumulations of cyanobacteria in the Baltic Sea”. In: *Biogeosciences* 11, pp. 3619–3633.

Karimi, Roxanne, Celia Y. Chen, Paul C. Pickhardt, Nicholas S. Fisher, and Carol L. Folt (May 2007). “Stoichiometric controls of mercury dilution by growth”. In: *Proceedings of the National Academy of Sciences of the United States of America* 104.18, pp. 7477–7482.

Kawarazuka, Nozomi and Christophe Béné (2011). “The potential role of small fish species in improving micronutrient deficiencies in developing countries: building evidence”. In: *Public Health Nutrition* 11, pp. 1927–1938.

Kehris, Brands (2022). “Right to healthy environment”. In: *Expert Seminar on “UN recognition of the right to a clean, healthy, and sustainable environment: past developments and future prospects”*.

Kendzierska, Halina and Urszula Janas (Dec. 2024). “Functional diversity of macrozoobenthos under adverse oxygen conditions in the southern Baltic Sea”. In: *Scientific Reports* 14.1.

Kern, Skyler, Mary E. McGuinn, Katherine M. Smith, Nadia Pinardi, Kyle E. Niemeyer, Nicole S. Lovenduski, and Peter E. Hamlington (Jan. 2024). “Computationally efficient parameter estimation for high-dimensional ocean biogeochemical models”. In: *Geoscientific Model Development* 17.2, pp. 621–649.

Kessler, Rebecca (Oct. 2013). “The Minamata Convention on Mercury: A First Step toward Protecting Future Generations”. In: *Environmental Health Perspectives* 121.10, A304.

Khakzad, Sorna, Marnix Pieters, and Koenraad Van Balen (Dec. 2015). “Coastal cultural heritage: A resource to be included in integrated coastal zone management”. In: *Ocean & Coastal Management* 118, pp. 110–128.

Kim, Eunhee, Robert P. Mason, and Christine M. Bergeron (Nov. 2008). “A modeling study on methylmercury bioaccumulation and its controlling factors”. In: *Ecological Modelling* 218.3-4, pp. 267–289.

Kleindienst, Alina, Igor Živković, Emmanuel Tessier, Alkuin Koenig, Lars Eric Heimbürger-Boavida, Milena Horvat, and David Amouroux (Oct. 2023). “Assessing comparability and uncertainty of analytical methods for methylated mercury species in seawater”. In: *Analytica Chimica Acta* 1278, p. 341735.

Koopmans, Marieke and René H. Wijffels (Sept. 2008). “Seasonal Growth Rate of the Sponge Haliclona oculata (Demospongiae: Haplosclerida)”. In: *Marine Biotechnology (New York, N.y.)* 10.5, p. 502.

Korejwo, Ewa, Dominika Saniewska, Jacek Bełdowski, Piotr Balazy, and Michał Saniewski (Nov. 2022). “Mercury concentration and speciation in benthic organisms from Isfjorden, Svalbard”. In: *Marine Pollution Bulletin* 184, p. 114115.

Korn, Peter (June 2017). “Formulation of an unstructured grid model for global ocean dynamics”. In: *Journal of Computational Physics* 339, pp. 525–552.

Kotalik, Christopher J., James J. Willacker, Jeff S. Wesner, Branden L. Johnson, Colleen M. Flanagan Pritz, Sarah J. Nelson, David M. Walters, and Collin A. Eagles-Smith (Jan. 2025). “Ecosystem Drivers of Freshwater Mercury Bioaccumulation Are Context-Dependent: Insights from Continental-Scale Modeling”. In: *Environmental Science and Technology* 59.3, pp. 1780–1789.

Krause-Jensen, Dorte, Stiig Markager, and Tage Dalsgaard (Mar. 2012). “Benthic and Pelagic Primary Production in Different Nutrient Regimes”. In: *Estuaries and Coasts* 35.2, pp. 527–545.

Kuss, Joachim (2014). “Water-air gas exchange of elemental mercury: An experimentally determined mercury diffusion coefficient for Hg0 water-air flux calculations”. In: *Limnology and Oceanography* 59.5, pp. 1461–1467.

Kuss, Joachim, Florian Cordes, Volker Mohrholz, nther Nausch, Michael Naumann, Siegfried Kru, and Detlef E Schulz-Bull (2017). “The Impact of the Major Baltic Inflow of December 2014 on the Mercury Species Distribution in the Baltic Sea”. In.

Kuss, Joachim, Siegfried Krüger, Johann Ruickoldt, and Klaus Peter Wlost (Mar. 2018). “High-resolution measurements of elemental mercury in surface water for an improved quantitative understanding of the Baltic Sea as a source of atmospheric mercury”. In: *Atmospheric Chemistry and Physics* 18.6, pp. 4361–4376.

Kuss, Joachim, Norbert Wasmund, nther Nausch, and Matthias Labrenz (2015). “Mercury Emission by the Baltic Sea: A Consequence of Cyanobacterial Activity, Photochemistry, And Low-Light Mercury Transformation”. In: *Environ. Sci. Technol* 2022.20, p. 16.

Kutta, Wilhelm (1901). “Beitrag zur näherungsweisen Integration totaler Differentialgleichungen”. In: *Zeitschrift für Mathematik und Physik*.

Kwasigroch, Urszula, Magdalena Bełdowska, Agnieszka Jdruch, and Katarzyna Łukawska-Matuszewska (Mar. 2021). “Distribution and bioavailability of mercury in the surface sediments of the Baltic Sea”. In: *Environmental Science and Pollution Research 2021 28:27* 28.27, pp. 35690–35708.

Kwaśniak, Justyna, Lucyna Falkowska, and Magdalena Kwaśniak (May 2012). “The assessment of organic mercury in Baltic fish by use of an in vitro digestion model”. In: *Food Chemistry* 132.2, pp. 752–758.

Kyodo news (2024). *Japan court orders compensation to 26 unrecognized Minamata victims*.

Laacouri, Aicam, Edward A. Nater, and Randall K. Kolka (Sept. 2013). “Distribution and uptake dynamics of mercury in leaves of common deciduous tree species in Minnesota, U.S.A.” In: *Environmental Science and Technology* 47.18, pp. 10462–10470.

Labrune, Céline, Antoine Grémare, Jean Michel Amouroux, Rafael Sardá, João Gil, and Sergi Taboada (Jan. 2007). “Assessment of soft-bottom polychaete assemblages in the Gulf of Lions (NW Mediterranean) based on a mesoscale survey”. In: *Estuarine, Coastal and Shelf Science* 71.1-2, pp. 133–147.

Lafferty, Kevin D., Andrew P. Dobson, and Armand M. Kuris (July 2006). “Parasites dominate food web links”. In: *Proceedings of the National Academy of Sciences of the United States of America* 103.30, pp. 11211–11216.

Lamborg, Citation, Katilin Bowman, Chad Hammerschmidt, Cindy Gilmour, Kathleen Munson, Noelle Selin, and Chun-Mao Tseng (2014). “Mercury in the Anthropocene Ocean”. In: *Oceanography* 27.1, pp. 76–87.

Lavoie, Raphael A, Craig E Hebert, Jean-François Rail, Birgit M Braune, Emmanuel Yumvihoze, Laura G Hill, and David R S Lean (2010). “Trophic structure and mercury distribution in a Gulf of St. Lawrence (Canada) food web using stable isotope analysis”. In.

Lavoie, Raphael A, Timothy D Jardine, Matthew M Chumchal, Karen A Kidd, and Linda M Campbell (2013). “Biomagnification of Mercury in Aquatic Food Webs: A Worldwide Meta-Analysis”. In.

Lavoie, Stephen P., Daphne T. Mapolelo, Darin M. Cowart, Benjamin J. Polacco, Michael K. Johnson, Robert A. Scott, Susan M. Miller, and Anne O. Summers (Dec. 2015). “Organic and inorganic mercurials have distinct effects on cellular thiols, metal homeostasis, and Fe-binding proteins in Escherichia coli”. In: *Journal of Biological Inorganic Chemistry* 20.8, pp. 1239–1251.

Lee, Cheng Shiuan and Nicholas S. Fisher (Sept. 2016). “Methylmercury uptake by diverse marine phytoplankton”. In: *Limnology and Oceanography* 61.5, pp. 1626–1639.

Lehmann, Andreas et al. (2021). “Salinity dynamics of the Baltic Sea”. In: *Earth System Dynamics* 13.1, pp. 373–392.

Li, Mi Ling, Emma J. Gillies, Renea Briner, Carie A. Hoover, Kristen J. Sora, Lisa L. Loseto, William J. Walters, William W.L. Cheung, and Amanda Giang (July 2022). “Investigating the dynamics of methylmercury bioaccumulation in the Beaufort Sea shelf food web: a modeling perspective”. In: *Environmental Science: Processes & Impacts* 24.7, pp. 1010–1025.

Li, Mi Ling, Colin P. Thackray, Vicky W.Y. Lam, William W.L. Cheung, and Elsie M. Sunderland (Oct. 2024). "Global fishing patterns amplify human exposures to methylmercury". In: *Proceedings of the National Academy of Sciences of the United States of America* 121.40, e2405898121.

Lin, Heyu et al. (2021). "Mercury methylation by metabolically versatile and cosmopolitan marine bacteria". In: *The ISME Journal* 15, pp. 1810–1825.

Lindqvist, Oliver and Henning Rodhe (2017). "Atmospheric mercury-a review". In.

Liu, Maodian, Qianru Zhang, Taylor Maavara, Shaoda Liu, Xuejun Wang, and Peter A Raymond (2021). "Rivers as the largest source of mercury to coastal oceans worldwide". In: *nature geoscience* 14, pp. 672–677.

Llull, Rosa Maria, Mercè Garí, Miquel Canals, Teresa Rey-Maquieira, and Joan O. Grimalt (Oct. 2017). "Mercury concentrations in lean fish from the Western Mediterranean Sea: Dietary exposure and risk assessment in the population of the Balearic Islands". In: *Environmental Research* 158, pp. 16–23.

Logemann, Kai, Leonidas Linardakis, Peter Korn, and Corinna Schrum (2021). "Global tide simulations with ICON-O: testing the model performance on highly irregular meshes". In: *Ocean Dynamics* 71, pp. 43–57.

Lønborg, Christian et al. (Feb. 2024). "A global database of dissolved organic matter (DOM) concentration measurements in coastal waters (CoastDOM v1)". In: *Earth System Science Data* 16.2, pp. 1107–1119.

Mackay, D and A Fraser (2000). "Bioaccumulation of persistent organic chemicals: mechanisms and models". In: *Environmental Pollution* 110, pp. 375–391.

Mackay, Donald (1991). *Multimedia Environmental Models: The Fugacity Approach*.

Madgett, Alethea S., Kyari Yates, Lynda Webster, Craig McKenzie, and Colin F. Moffat (Dec. 2021). "The concentration and biomagnification of trace metals and metalloids across four trophic levels in a marine food web". In: *Marine Pollution Bulletin* 173, p. 112929.

Maldonado, Manuel and Maria J Uriz (1998). "Microrefuge exploitation by subtidal encrusting sponges: patterns of settlement and post-settlement survival". In: *MARINE ECOLOGY PROGRESS SERIES Mar Ecol Prog Ser* 174, pp. 141–150.

Mason, R. P., Anna L Choi, William F Fitzgerald, Chad R Hammerschmidt, Carl H Lamborg, Anne L Soerensen, and Elsie M Sunderland (2012). "Mercury biogeochemical cycling in the ocean and policy implications $". In.

Mason, R. P., J. R. Reinfelder, and F. M.M. Morel (Feb. 1995). "Bioaccumulation of mercury and methylmercury". In: *Water, Air, and Soil Pollution 1995 80:1* 80.1, pp. 915–921.

Mason, R. P., John R. Reinfelder, and François M.M. Morel (1996). "Uptake, toxicity, and trophic transfer of mercury in a coastal diatom". In: *Environmental Science and Technology* 30.6, pp. 1835–1845.

Mathema, Vivek Bhakta, Balkrishna Chand Thakuri, and Mika Sillanpää (Dec. 2011). *Bacterial mer operon-mediated detoxification of mercurial compounds: A short review*.

Meadows, Peter S., Azra Meadows, and John M.H. Murray (July 2012). "Biological modifiers of marine benthic seascapes: Their role as ecosystem engineers". In: *Geomorphology* 157-158, pp. 31–48.

Menden-Deuer, Susanne, and Evelyn J. Lessard (2000). "Carbon to volume relationships for dinoflagellates, diatoms, and other protist plankton". In: *Limnology and Oceanography* 45.3, pp. 569–579.

Metian, Marc, Simon Pouil, Christine Dupuy, Jean-Louis Teyssié, Michel Warnau, and Paco Bustamante (2020). "Influence of food (ciliate and phytoplankton) on the trophic transfer of inorganic and methylmercury in the Pacific cupped oyster Crassostrea gigas". In: *Environmental Pollution* 257.

Mikolajewicz, Uwe and Ernst Maier-Reimer (1994). "Mixed boundary conditions in ocean general circulation models and their influence on the stability of the model's conveyor belt". In: *JOURNAL OF GEOPHYSICAL RESEARCH* 99, pp. 633–655.

Ministry of the Environment-Government of Japan (2002). *Minamata Disease The History and Measures - Chapter 4*.

Montagnes, David J S and Andy Fenton (2012). "Prey-abundance affects zooplankton assimilation efficiency and the outcome of biogeochemical models". In: *Ecological Modelling* 243, pp. 1–7.

Moore, Gordon (1965). "Cramming more components onto integrated systems". In: *Electronics* 38.

Morel, François M M, Anne M L Kraepiel, and Marc Amyot (1998). "The Chemical Cycle and Bioaccumulation of Mercury". In: *Source: Annual Review of Ecology and Systematics* 29, pp. 543–566.

Muhaya, B B M, M Leermakers, and W Baeyens (1997). “Total mercury and methylmercury in sediments and in the polychaete nereis diversicolor at groot buitenschoor (scheldt estuary, belgium)”. In: *Water, Air, and Soil Pollution* 94, pp. 109–123.

Nausch, Gunther, Wolfgang Mattheus, and Rainer Feistel (2003). “Hydrographic and hydrochemical conditions in the Gotland Deep area between 1992 and 2003”. In: *OCEANOLOGIA* 45.4, pp. 557–569.

Neely, W. Brock. (1980). “Chemicals in the environment : distribution, transport, fate, analysis”. In: p. 245.

Newton Lewis, Gilbert and By Gilbert Newton Lewis (1901). “The Law of Physico-Chemical Change”. In: *American Academy of Arts & Sciences* 37.3, pp. 49–69.

Nfon, Erick, Ian T Cousins, Olli Järvinen, Arun B Mukherjee, Matti Verta, and Dag Broman (2009). “Trophodynamics of mercury and other trace elements in a pelagic food chain from the Baltic Sea”. In.

Nilsen, Marianne, Torstein Pedersen, Einar Magnus Nilssen, and Stein Fredriksen (Dec. 2008). “Trophic studies in a high-latitude fjord ecosystem — a comparison of stable isotope analyses (δ13C and δ15N) and trophic-level estimates from a mass-balance model”. In: *https://doi.org/10.1139/F08-180* 65.12, pp. 2791–2806.

Nordhaus, William D, Ernst Berndt, Tim Bresnahan, Paul Chwelos, Iain Cockburn, Robert Gordon, Steve Landefeld, Phil Long, and Chuck Powell Eric Weese (2006). “An Economic History of Computing 1”. In.

Norn, Svend, Henrik Permin, Edith Kruse, and Poul R. Kruse (2008). “[Mercury–a major agent in the history of medicine and alchemy]”. In: *Dansk medicinhistorisk arbog* 36, pp. 21–40.

Norrby, Lars J (1991). “Why Is Mercury Liquid? Or, Why Do Relativistic Effects Not Get into Chemistry Textbooks?” In: *Journal of Chemical Education* 68.2, pp. 110–113.

Nriagu, Jerome O (1994). “Mercury pollution from the past mining of gold and silver in the Americas”. In: *The science of the the total environment* 149, pp. 167–181.

O’Neill, R. V. and B. Rust (July 1979). “Aggregation error in ecological models”. In: *Ecological Modelling* 7.2, pp. 91–105.

Obrist, Daniel, Jane L Kirk, Lei Zhang, Elsie M Sunderland, Martin Jiskra, and Noelle E Selin (2018). “A review of global environmental mercury processes in response to human and natural perturbations: Changes of emissions, climate, and land use”. In: *Ambio* 47.2, pp. 116–140.

Olenina, Irina et al. (2003). “Biovolumes and size-classes of phytoplankton in the Baltic Sea”. In: *HELCOM Balt.Sea Environ. Proc. No. 106, 144pp.* 607, pp. 110–114.

Olinger, Lauren K., Wendy K. Strangman, Steven E. McMurray, and Joseph R. Pawlik (May 2021). “Sponges With Microbial Symbionts Transform Dissolved Organic Matter and Take Up Organohalides”. In: *Frontiers in Marine Science* 8, p. 665789.

Oliveri, Elvira, Daniela Salvagio Manta, Maria Bonsignore, Simone Cappello, Giorgio Tranchida, Emanuela Bagnato, Nadia Sabatino, Santina Santisi, and Mario Sprovieri (Nov. 2016). “Mobility of mercury in contaminated marine sediments: Biogeochemical pathways”. In: *Marine Chemistry* 186, pp. 1–10.

Orani, Anna Maria, Emilia Vassileva, Sabine Azemard, and Olivier P. Thomas (Dec. 2020). “Comparative study on Hg bioaccumulation and biotransformation in Mediterranean and Atlantic sponge species”. In: *Chemosphere* 260, p. 127515.

Outridge, P. M., R. P. Mason, F. Wang, S. Guerrero, and L. E. Heimbürger-Boavida (Oct. 2018). *Updated Global and Oceanic Mercury Budgets for the United Nations Global Mercury Assessment 2018*.

Pacyna, Elisabeth G., Jozef M. Pacyna, Frits Steenhuisen, and Simon Wilson (July 2006). “Global anthropogenic mercury emission inventory for 2000”. In: *Atmospheric Environment* 40.22, pp. 4048–4063.

Pan, Ke and Wen Xiong Wang (Oct. 2011). “Mercury accumulation in marine bivalves: Influences of biodynamics and feeding niche”. In: *Environmental Pollution* 159.10, pp. 2500–2506.

Park, Keunhwan, Wonjung Kim, and Ho Young Kim (June 2014). “Optimal lamellar arrangement in fish gills”. In: *Proceedings of the National Academy of Sciences of the United States of America* 111.22, pp. 8067–8070.

Peeters, J C H, H Haas, L Peperzak, and L P M J Wetsteyn (1991). *Limiting factors for phytoplankton in the North Sea*. Tech. rep. 10, pp. 261–267.

Perger, R. and A. Temming (June 2012). “A new method to determine in situ growth rates of decapod shrimp: A case study with brown shrimp Crangon crangon”. In: *Marine Biology* 159.6, pp. 1209–1222.

Pickhardt, Paul C. and Nicholas S. Fisher (Jan. 2007). “Accumulation of inorganic and methylmercury by freshwater phytoplankton in two contrasting water bodies”. In: *Environmental Science and Technology* 41.1, pp. 125–131.

Pickhardt, Paul C., Maria Stepanova, and Nicholas S. Fisher (2006). “Contrasting uptake routes and tissue distributions of inorganic and methylmercury in mosquitofish (Gambusia affinis) and redear sunfish (Lepomis microlophus)”. In: *Environmental Toxicology and Chemistry* 25.8, pp. 2132–2142.

Pirrone, N. et al. (2010). “Global mercury emissions to the atmosphere from anthropogenic and natural sources”. In: *Atmospheric Chemistry and Physics* 10.13, pp. 5951–5964.

Pliny the Elder (77). *”Naturalis Historia” (Natural History)*.

Polak-Juszczak, Lucyna (2012). “Bioaccumulation of mercury in the trophic chain of flatfish from the Baltic Sea”. In: *Chemosphere* 89.5, pp. 585–591.

— (2014). “Selenium and mercury molar ratios in commercial fish from the Baltic Sea: Additional risk assessment criterion for mercury exposure”. In.

— (2018). “Distribution of organic and inorganic mercury in the tissues and organs of fish from the southern Baltic Sea”. In: *Environmental Science and Pollution Research* 25, pp. 34181–34189.

Prohaska, Thomas et al. (May 2022). “Standard atomic weights of the elements 2021 (IUPAC Technical Report)”. In: *Pure and Applied Chemistry* 94.5, pp. 573–600.

Qu, Zan, Naiqiang Yan, Ping Liu, Yao Chi, and Jinping Jia (Nov. 2009). “Bromine Chloride as an Oxidant to Improve Elemental Mercury Removal from Coal-Fired Flue Gas”. In: *Environmental Science and Technology* 43.22, pp. 8610–8615.

Quinn, Gerry P. and Michael J. Keough (Mar. 2002). “Experimental Design and Data Analysis for Biologists”. In: *Readings in Economic Sociology*, pp. 1–9.

Radivojević, Miljana, Thilo Rehren, Ernst Pernicka, Dušan Šljivar, Michael Brauns, and Dušan Borić (2010). “On the origins of extractive metallurgy: New evidence from Europe”. In: *Journal of Archaeological Science* 37.11, pp. 2775–2787.

Ramalhosa, Elsa, Susana Río Segade, Eduarda Pereira, Carlos Vale, and Armando Duarte (2006). “Mercury cycling between the water column and surface sediments in a contaminated area”. In: *Water Research* 40.15, pp. 2893–2900.

Ramlal, Patricia S, John W M Rudd, Robert E Hecky, and Agassiz North Associates (1986). “Methods for Measuring Specific Rates of Mercury Methylation and Degradation and Their Use in Determining Factors Controlling Net Rates of Mercury Methylation”. In: *APPLIED AND ENVIRONMENTAL MICROBIOLOGY* 51.1, pp. 110–114.

Ravichandran, Mahalingam (2004). “Interactions between mercury and dissolved organic matter - A review”. In: *Chemosphere* 55.3, pp. 319–331.

Redfield, Alfred (1934). “On the proportions of organic derivatives in sea water and their relation to the composition of plankton.” In: *James Johnstone Memorial Volume*, pp. 176–192.

Regnault, Michele (1981). “Journal of Comparative Physiology. B Respiration and Ammonia Excretion of the Shrimp Crangon crangon L.: Metabolic Response to Prolonged Starvation”. In: *J. Comp. Physiol* 141, pp. 549–555.

Rehlmeyer, Katrin et al. (2024). “Reintroduction of self-facilitating feedbacks could advance subtidal eelgrass (Zostera marina) restoration in the Dutch Wadden Sea OPEN ACCESS EDITED BY Katrin Rehlmeyer k.rehlmeyer@rug.nl † PRESENT ADDRESS”. In: *Frotiers in Marine Science*.

Reichstein, Markus, Gustau Camps-Valls, Bjorn Stevens, Martin Jung, Joachim Denzler, and Nuno Carvalhais (2019). “Deep learning and process understanding for data-driven Earth system science”. In: *Nature*.

Reinhart, Bethany, Karen A Kidd, R Allen Curry, and Nelson J O’driscoll (2018). “Mercury bioaccumulation in aquatic biota along a salinity gradient in the Saint John River estuary Quantitative modeling of existing and future fish habitats in the Saint John River View project Emerging contaminants View project”. In: *Article in Journal of Environmental Sciences*.

REPHY (2020). “Time Series: REPHY Villefranche”. In: *https://www.st.nmfs.noaa.gov/copepod/time-series/fr-50114/*.

Ribes, M, R Coma, JM Gili - Journal of Plankton Research, and undefined 1999 (1999). “Seasonal variation of particulate organic carbon, dissolved organic carbon and the contribution of microbial communities

to the live particulate organic carbon in a shallow near-bottom ecosystem at the Northwestern Mediterranean Sea". In: *Journal of Plankton Research* 21.6, pp. 1077–1100.

Ricciardi, Anthony and Edwin Bourget (1998). "Weight-to-weight conversion factors for marine benthic macroinvertebrates". In: *Marine ecology progress series* 163, pp. 245–251.

Richardson, Katherine, Flemming Bo, Pedersen Richardson, Bo Pedersen, and K Richardson (1998). *Estimation of new production in the North Sea: consequences for temporal and spatial variability of phytoplankton*. Tech. rep., pp. 574–580.

Riedel, B, M Stachowitsch, M Zuschin, and Bettina Riedel (2010). *Low dissolved oxygen impacts in the orthern Adriatic: critical thresholds for benthic assemblages*. Tech. rep. ICES CM 2010/H:09 Theme Session H.

Rijsgard, H.U. and G.T. Banta (1998). "Irrigation and deposit feeding by the lugworm Arenicula marina, characteristics and secondary effects on the environment. A review of current knowledge." In: *Vie et Milieu / Life & Environment* 4.$(, pp. 243–257.

Riva, Michele Augusto, Alessandra Lafranconi, Marco Italo D'Orso, and Giancarlo Cesana (2012). "Lead Poisoning: Historical Aspects of a Paradigmatic "Occupational and Environmental Disease"". In: *Safety and Health at Work* 3.1, p. 11.

Robson, Greg (2005). *Gold*.

Robson, Greg and Pumbaa (2006). *Mercury*.

Rodil, I F, K M Attard, J Norkko, R N Glud, and A Norkko (2019). "Estimating Respiration Rates and Secondary Production of Macrobenthic Communities Across Coastal Habitats with Contrasting Structural Biodiversity". In.

Rosati, G. et al. (Apr. 2018). "Mercury in the Black Sea: New Insights From Measurements and Numerical Modeling". In: *Global Biogeochemical Cycles* 32.4, pp. 529–550.

Rosati, Ginevra, Donata Canu, Paolo Lazzari, and Cosimo Solidoro (2022). "Assessing the spatial and temporal variability of methylmercury biogeochemistry and bioaccumulation in the Mediterranean Sea with a coupled 3D model". In: *Biogeosciences* 19, pp. 3663–3682.

Rosenberg, Rutger, Antoine Gre´maregre´mare, Jean-Michel Amouroux, and Hans C Nilsson (2003). "Benthic habitats in the northwest Mediterranean characterised by sedimentary organics, benthic macrofauna and sediment profile images". In: *Estuarine, Coastal and Shelf Science* 57, pp. 297–311.

Rykiel, Edward J (1996). "momme Testing ecological models: the meaning of validation". In: *Ecological Modelling* 90, pp. 229–244.

Sanei, Hamed, Peter M Outridge, Kazumasa Oguri, Gary A Stern, Bo Thamdrup, Frank Wenzhöfer, and Feiyue Wang (2021). "High mercury accumulation in deep-ocean hadal sediments". In: *Scientific Reports* 11.1, pp. 1–8.

Santos-Gandelman, Juliana F, Marcia Giambiagi-Demarval •, Guilherme Muricy, Tamar Barkay, and Marinella S Laport (2014a). "Mercury and methylmercury detoxification potential by sponge-associated bacteria". In: *Antonie van Leeuwenhoek* 106, pp. 585–590.

— (2014b). "Mercury and methylmercury detoxification potential by sponge-associated bacteria". In: *Antonie van Leeuwenhoek* 106, pp. 585–590.

Sarà, G. and R. Sarà (Apr. 2007). "Feeding habits and trophic levels of bluefin tuna Thunnus thynnus of different size classes in the Mediterranean Sea". In: *Journal of Applied Ichthyology* 23.2, pp. 122–127.

Savage, Candida, Peter R. Leavitt, and Ragnar Elmgren (May 2010). "Effects of land use, urbanization, and climate variability on coastal eutrophication in the Baltic Sea". In: *Limnology and Oceanography* 55.3, pp. 1033–1046.

Schartup, Amina T, Udonna Ndu, Prentiss H Balcom, Robert P Mason, and Elsie M Sunderland (2015). "Contrasting Effects of Marine and Terrestrially Derived Dissolved Organic Matter on Mercury Speciation and Bioavailability in Seawater". In.

Schartup, Amina T, Asif Qureshi, Clifton Dassuncao, Colin P Thackray, Gareth Harding, Elsie M Sunderland, † Harvard, and John A Paulson (2018). "A Model for Methylmercury Uptake and Trophic Transfer by Marine Plankton". In: *Environ. Sci. Technol* 52, p. 18.

Schippmann, Bianca and Hans Burchard (Jan. 2011). "Rosenbrock methods in biogeochemical modelling – A comparison to Runge–Kutta methods and modified Patankar schemes". In: *Ocean Modelling* 37.3-4, pp. 112–121.

Schmidbaur, Hubert, Wilhelm Graf, and Gerhard Müller (Mar. 1988). “Weak Intramolecular Bonding Relationships: The Conformation-Determining Attractive Interaction between Gold(I) Centers”. In: *Angewandte Chemie International Edition in English* 27.3, pp. 417–419.

Scholz, Patrick et al. (Nov. 2019). “Assessment of the Finite-volumE Sea ice-Ocean Model (FESOM2.0) - Part 1: Description of selected key model elements and comparison to its predecessor version”. In: *Geoscientific Model Development* 12.11, pp. 4875–4899.

Schroeder, W. H., K. G. Anlauf, L. A. Barrie, J. Y. Lu, A. Steffen, D. R. Schneeberger, and T. Berg (July 1998). “Arctic springtime depletion of mercury”. In: *Nature 1998 394:6691* 394.6691, pp. 331–332.

Schrum, Corinna, Irina Alekseeva, and Mike St. John (June 2006). “Development of a coupled physical–biological ecosystem model ECOSMO: Part I: Model description and validation for the North Sea”. In: *Journal of Marine Systems* 61.1-2, pp. 79–99.

Schrum, Corinna and Jan O. Backhaus (Aug. 1999). “Sensitivity of atmosphere–ocean heat exchange and heat content in the North Sea and the Baltic Sea”. In: *Tellus A* 51.4, pp. 526–549.

Schuster, Paul F. et al. (Feb. 2018). “Permafrost Stores a Globally Significant Amount of Mercury”. In: *Geophysical Research Letters* 45.3, pp. 1463–1471.

Seelen, Emily, Van Liem-Nguyen, Urban Wünsch, Zofia Baumann, Robert Mason, Ulf Skyllberg, and Erik Björn (2023). “Dissolved organic matter thiol concentrations determine methylmercury bioavailability across the terrestrial-marine aquatic continuum”. In: *Nature Communications* 14.

Seigneur, Christian, Krish Vijayaraghavan, Kristen Lohman, Prakash Karamchandani, and Courtney Scott (Jan. 2004). “Global Source Attribution for Mercury Deposition in the United States”. In: *Environmental Science and Technology* 38.2, pp. 555–569.

Seixas, Tércia G., Isabel Moreira, Salvatore Siciliano, Olaf Malm, and Helena A. Kehrig (Mar. 2014). “Differences in methylmercury and inorganic mercury biomagnification in a tropical marine food web”. In: *Bulletin of Environmental Contamination and Toxicology* 92.3, pp. 274–278.

Selin, Noelle E. (2009). “Global biogeochemical cycling of mercury: A review”. In: *Annual Review of Environment and Resources* 34, pp. 43–63.

Selin, Noelle E., Daniel J. Jacob, Robert M. Yantosca, Sarah Strode, Lyatt Jaeglé, and Elsie M. Sunderland (June 2008). “Global 3-D land-ocean-atmosphere model for mercury: Present-day versus preindustrial cycles and anthropogenic enrichment factors for deposition”. In: *Global Biogeochemical Cycles* 22.2.

Sellers, P., C.A. Kelly, J.W.M. Rudd, and A.R. MacHutton (1996). “Photodegradation of methylmercury in lakes ”. In: *Letters to nature* 380, pp. 694–696.

Shah, Viral et al. (Nov. 2021). “Improved mechanistic model of the atmospheric redox chemistry of mercury”. In: *Environmental Science and Technology* 55.21, pp. 14445–14456.

Sheehan, Mary C, Thomas A Burke, Ana Navas-Acien, Patrick N Breysse, John Mcgready, and Mary A Fox (2014). “Systematic reviews Global methylmercury exposure from seafood consumption and risk of developmental neurotoxicity: a systematic review”. In: *Bull World Health Organ* 92, pp. 254–269.

Si, Lin and Parisa A. Ariya (Feb. 2018). “Recent advances in atmospheric chemistry of mercury”. In: *Atmosphere* 9.2.

Sicko-Goad, Linda M, Claire L Schelske, and Eugene F Stoermer (1984). “Estimation of intracellular carbon and silica content of diatoms from natural assemblages using morphometric techniques’”. In: *Limnol. Oceanogr* 29.6, pp. 1170–178.

Silberberger, Marc J., Paul E. Renaud, Ingrid Kröncke, and Henning Reiss (Apr. 2018). “Food-web structure in four locations along the European shelf indicates spatial differences in ecosystem functioning”. In: *Frontiers in Marine Science* 5.APR, p. 300569.

Silva, Jafferson Kamphorst Leal da, Guilherme J.M. Garcia, and Lauro A. Barbosa (Dec. 2006). “Allometric scaling laws of metabolism”. In: *Physics of Life Reviews* 3.4, pp. 229–261.

Simpson, W R et al. (2007). “Atmospheric Chemistry and Physics Halogens and their role in polar boundary-layer ozone depletion”. In: *Atmos. Chem. Phys* 7, pp. 4375–4418.

Singh, Tarkeshwar, François Counillon, Jerry Tjiputra, Yiguo Wang, and Mohamad El Gharamti (Feb. 2022). “Estimation of Ocean Biogeochemical Parameters in an Earth System Model Using the Dual One Step Ahead Smoother: A Twin Experiment”. In: *Frontiers in Marine Science* 9, p. 775394.

Sisma-Ventura, Guy, Jacob Silverman, Yael Segal, Hagar Hauzer, Maria Abu Khadra, Nir Stern, Tamar Guy-Haim, and Barak Herut (May 2024). “Exceptionally high levels of total mercury in deep-sea sharks of the Southeastern Mediterranean sea over the last 40 years”. In: *Environment international* 187.

Sizmur, Tom, João Canário, Travis G. Gerwing, Mark L. Mallory, and Nelson J. O’Driscoll (May 2013). “Mercury and methylmercury bioaccumulation by polychaete worms is governed by both feeding ecology and mercury bioavailability in coastal mudflats”. In: *Environmental Pollution* 176, pp. 18–25.

Slemr, Franz et al. (Aug. 2018). “Mercury distribution in the upper troposphere and lowermost stratosphere according to measurements by the IAGOS-CARIBIC observatory: 2014-2016”. In: *Atmospheric Chemistry and Physics* 18.16, pp. 12329–12343.

Soerensen, Anne L., Elsie M. Sunderland, Christopher D. Holmes, Daniel J. Jacob, Robert M. Yantosca, Henrik Skov, Jesper H. Christensen, Sarah A. Strode, and Robert P. Mason (Nov. 2010). “An improved global model for air-sea exchange of mercury: High concentrations over the North Atlantic”. In: *Environmental Science and Technology* 44.22, pp. 8574–8580.

Soerensen, Anne L. et al. (Apr. 2016). “A mass budget for mercury and methylmercury in the Arctic Ocean”. In: *Global Biogeochemical Cycles* 30.4, pp. 560–575.

Soetaert, Karline and Peter M.J. Herman (2009). *A practical guide to ecological modelling: Using R as a simulation platform*. Springer Netherlands, pp. 1–372.

Sommar, Jonas, Stefan Osterwalder, and Wei Zhu (June 2020). “Recent advances in understanding and measurement of Hg in the environment: Surface-atmosphere exchange of gaseous elemental mercury (Hg0)”. In: *Science of The Total Environment* 721, p. 137648.

Stamenkovic, Jelena and Mae S. Gustin (Mar. 2009). “Nonstomatal versus stomatal uptake of atmospheric mercury”. In: *Environmental Science and Technology* 43.5, pp. 1367–1372.

Steger, Jan, Hendrik Pehlke, Benoit Lebreton, Thomas Brey, and Jennifer Dannheim (Oct. 2019). “Benthic trophic networks of the southern North Sea: Contrasting soft-sediment communities share high food web similarity”. In: *Marine Ecology Progress Series* 628, pp. 17–36.

Steinberg, Deborah K. et al. (Jan. 2022). “The Outsized Role of Salps in Carbon Export in the Subarctic Northeast Pacific Ocean”. In: *Global Biogeochemical Cycles* 37.1, e2022GB007523.

Stelmakh, Lyudmyla and Nelya Kovrigina (2021). “Phytoplankton Growth Rate and Microzooplankton Grazing under Conditions of Climatic Changes and Anthropogenic Pollution in the Coastal Waters of the Black Sea (Sevastopol Region)”. In.

Storelli, M. M., R. G. Stuffler, and G. O. Marcotrigiano (Aug. 2002). “Total and methylmercury residues in tuna-fish from the Mediterranean sea”. In: *Food Additives and Contaminants* 19.8, pp. 715–720.

Streets, David G., Hannah M. Horowitz, Zifeng Lu, Leonard Levin, Colin P. Thackray, and Elsie M. Sunderland (July 2019). “Five hundred years of anthropogenic mercury: Spatial and temporal release profiles”. In: *Environmental Research Letters* 14.8.

Sunderland, Elsie M and Noelle E Selin (2013). “Future trends in environmental mercury concentrations: implications for prevention strategies”. In.

Tacon, Albert G.J. and Marc Metian (Sept. 2009). “Fishing for feed or fishing for food: Increasing global competition for small pelagic forage fish”. In: *Ambio* 38.6, pp. 294–302.

Takanezawa, Yasukazu, Kouhei Ishikawa, Shunsuke Nakayama, Ryosuke Nakamura, Yuka Ohshiro, Shimpei Uraguchi, and Masako Kiyono (Dec. 2023). “Conversion of methylmercury into inorganic mercury via organomercurial lyase (MerB) activates autophagy and aggresome formation”. In: *Scientific Reports* 13.1.

Tanner, Danny K., John C. Brazner, and Valerie J. Brady (2000). “Factors influencing carbon, nitrogen, and phosphorus content of fish from a Lake Superior coastal wetland”. In: *Canadian Journal of Fisheries and Aquatic Sciences* 57.6, pp. 1243–1251.

Taylor, David L., Jennifer C. Linehan, David W. Murray, and Warren L. Prell (Apr. 2012). “Indicators of sediment and biotic mercury contamination in a southern New England estuary”. In: *Marine Pollution Bulletin* 64.4, pp. 807–819.

Taylor, V. F., K. L. Buckman, E. A. Seelen, N. M. Mazrui, P. H. Balcom, R. P. Mason, and C. Y. Chen (Mar. 2019). “Organic carbon content drives methylmercury levels in the water column and in estuarine food webs across latitudes in the Northeast United States”. In: *Environmental Pollution* 246, pp. 639–649.

Tesán Onrubia, Javier A. et al. (May 2020). “Mercury Export Flux in the Arctic Ocean Estimated from 234Th/238U Disequilibria”. In: *ACS Earth and Space Chemistry* 4.5, pp. 795–801.

Tesán-Onrubia, Javier Angel et al. (Sept. 2023). “Bioconcentration, bioaccumulation and biomagnification of mercury in plankton of the Mediterranean Sea”. In: *Marine Pollution Bulletin* 194, p. 115439.

The Mainichi (2023). *Editorial: Minamata disease ruling stresses Japan gov't relief must match reality (Englisch version)*.

Thewes, Daniel, Emil V. Stanev, and Oliver Zielinski (May 2022). “Steps Toward Modelling the Past and Future North Sea Ecosystem With a Focus on Light Climate”. In: *Frontiers in Marine Science* 9, p. 818383.

Thiel, Vera, Sven Leininger, Rolf Schmaljohann, Franz Brümmer, and Johannes F Imhoff (2007). “Sponge-specific Bacterial Associations of the Mediterranean Sponge Chondrilla nucula (Demospongiae, Tetractinomorpha)”. In: *Microbial Ecology* 54, pp. 101–111.

Thingstad, Frede and Fereidoun Rassoulzadegan (n.d.). *Nutrient limitations, microbial food webs, and 'biological C-pumps': suggested interactions in a P-limited Mediterranean*. Tech. rep.

Thomassen, Ssren and Hans Ulrik Riisgadrd (1995). “Growth and energetics of the sponge Halichondria panicea”. In: 128, pp. 239–246.

Trevors, J. T. (Jan. 1986). *Mercury methylation by bacteria*.

Troost, T. A., M. Blaas, and F. J. Los (Sept. 2013). “The role of atmospheric deposition in the eutrophication of the North Sea: A model analysis”. In: *Journal of Marine Systems* 125, pp. 101–112.

Trudel, Marc and Joseph B. Rasmussen (June 1997). “Modeling the elimination of mercury by fish”. In: *Environmental Science and Technology* 31.6, pp. 1716–1722.

Tseng, Chun-Mao, Shin-Jing Ang, Yi-Sheng Chen, Jen-Chieh Shiao, Carl H Lamborg, Xiaoshuai He, and John R Reinfelder (2021). “Bluefin tuna reveal global patterns of mercury pollution and bioavailability in the world's oceans”. In: *PNAS* 118.38.

Tsui, Martin T.K. and Wen Xiong Wang (2004). “Uptake and Elimination Routes of Inorganic Mercury and Methylmercury in Daphnia magna”. In: *Environmental Science and Technology* 38.3, pp. 808–816.

UNEP (2021). “Guidance on monitoring of mercury and mercury compounds to support evaluation of the effectiveness of the Minamata Convention”. In: *United Nations Environment (UNEP), Geneva, Switzerland* UNEP/MC/COP.4/INF/12.

Vacelet, Jean and Claude Donadey (1977). “Electron microscope study of the association between some sponges and bacteria”. In: *Journal of Experimental Marine Biology and Ecology* 30.3, pp. 301–314.

Van Leeuwen, Sonja, Paul Tett, David Mills, and Johan Van Der Molen (2015). “Stratified and nonstratified areas in the North Sea: Long-term variability and biological and policy implications”. In: *Journal of Geophysical Research: Oceans* 120.7, pp. 4670–4686.

Van Veen, H W et al. (2002). “Mechanisms of mercury bioremediation Related papers A New Approach t o t he Remediat ion of Heavy Met al Liquid Wast es via Off-Gases Produced by... Mechanisms of mercury bioremediation”. In: *Biochemical Society Transactions* 30, pp. 743–746.

Vandal, Grace M., William. F Fitzgerald, Claude F. Boutron, and Jean-Pierre Candelone (1993). “Variations in mercury deposition to Antarctica over the past 34,000 years”. In: *LETTERS TO NATURE* 362, pp. 621–623.

Vermaat, Jan E., Abigail McQuatters-Gollop, Marieke A. Eleveld, and Alison J. Gilbert (Oct. 2008). “Past, present and future nutrient loads of the North Sea: Causes and consequences”. In: *Estuarine, Coastal and Shelf Science* 80.1, pp. 53–59.

Vilanova, Eduardo, Carla Zilberberg, Michele Kochem, Marcia R. Custodio, and Paulo A. S. Mourão (2007). “A novel biochemical method to distinguish cryptic species of Chondrilla (Chondrosida, Demospongiae) based on its sulfated polysaccharides”. In: *Porifera research : Biodiversity , innovation and sustainaBility*, pp. 653–659.

Vogel, Steven (1974). *Current-induced flow through the sponge, Halichondria.* Tech. rep., pp. 443–456.

Volkenborn, N., S. I.C. Hedtkamp, J. E.E. van Beusekom, and K. Reise (Aug. 2007). “Effects of bioturbation and bioirrigation by lugworms (Arenicola marina) on physical and chemical sediment properties and implications for intertidal habitat succession”. In: *Estuarine, Coastal and Shelf Science* 74.1-2, pp. 331–343.

Wallace, J C (1973). “Feeding, Starvation and Metabolic Rate in the Shore Crab Carcinus maenas”. In: *Marine Biology* 20, pp. 227–281.

Walve, Jakob and Ulf Larsson (1999). “Carbon, nitrogen and phosphorus stoichiometry of crustacean zooplankton in the Baltic Sea: implications for nutrient recycling”. In.

Wang, WX and RSK Wong (2003). “Bioaccumulation kinetics and exposure pathways of inorganic mercury and methylmercury in a marine fish, the sweetlips Plectorhinchus gibbosus”. In: *Marine Ecology Progress Series* 261.

Wang, Xun, Zhengduo Bao, Che Jen Lin, Wei Yuan, and Xinbin Feng (Aug. 2016). “Assessment of Global Mercury Deposition through Litterfall”. In: *Environmental Science and Technology* 50.16, pp. 8548–8557.

Wang, Xun, Fengchang Wu, and Wen Xiong Wang (June 2017). “In Vivo Mercury Demethylation in a Marine Fish (Acanthopagrus schlegeli)”. In: *Environmental Science and Technology* 51.11, pp. 6441–6451.

Webster, Nicole S. and Torsten Thomas (Apr. 2016). “The sponge hologenome”. In: *mBio* 7.2, pp. 135–151.

Weisz, Jeremy B., Niels Lindquist, and Christopher S. Martens (Mar. 2008). “Do associated microbial abundances impact marine demosponge pumping rates and tissue densities?” In: *Oecologia* 155.2, pp. 367–376.

West, Johannes, Sonja Gindorf, and Sofi Jonsson (May 2022). “Photochemical Degradation of Dimethylmercury in Natural Waters”. In: *Environmental Science and Technology* 56.9, pp. 5920–5928.

Whalin, Lindsay, Eun Hee Kim, and Robert Mason (Dec. 2007). “Factors influencing the oxidation, reduction, methylation and demethylation of mercury species in coastal waters”. In: *Marine Chemistry* 107.3, pp. 278–294.

WHO (2020). *10 chemicals of public health concern*.

Wilkinson, Mark D. et al. (Mar. 2016). “The FAIR Guiding Principles for scientific data management and stewardship”. In: *Scientific Data 2016 3:1* 3.1, pp. 1–9.

Wouters, H., J. Berckmans, R. Maes, E. Vanuytrecht, and K. De Ridder (2021). “Global bioclimatic indicators from 1979 to 2018 derived from reanalysis, version 1.0, Copernicus Climate Change Service (C3S) Climate Data Store (CDS), DOI: 10.24381/cds.bce175f0”. In.

Wu, Pianpian, Martin J. Kainz, Andrea G. Bravo, Staffan Åkerblom, Lars Sonesten, and Kevin Bishop (2019). “The importance of bioconcentration into the pelagic food web base for methylmercury biomagnification: A meta-analysis”. In: *Science of the Total Environment* 646, pp. 357–367.

Yamaguchi, Mari (2023). “Japan’s court recognizes more victims of Minamata mercury poisoning and awards them compensation”. In: *Independent*.

Zaferani, Sara and Harald Biester (Sept. 2021). “Mercury Accumulation in Marine Sediments – A Comparison of an Upwelling Area and Two Large River Mouths”. In: *Frontiers in Marine Science* 8, p. 732720.

Zagar, Dusan, Elena Romano, and Marco Barra (2006). “Mass balance of mercury in the Mediterranean Sea”. In.

Zakharova, L, K M Meyer, and M Seifan (2019). “Trait-based modelling in ecology: A review of two decades of research”. In.

Zhang, Hua, Wenxiong Wang, Chejen Lin, Xinbin Feng, Jianbo Shi, Guibin Jiang, and Thorjørn Larssen (Mar. 2022). “Decreasing mercury levels in consumer fish over the three decades of increasing mercury emissions in China”. In: *Eco-Environment & Health* 1.1, pp. 46–52.

Zhang, Y. Joseph, Tomas Fernandez-Montblanc, William Pringle, Hao Cheng Yu, Linlin Cui, and Saeed Moghimi (May 2023a). “Global seamless tidal simulation using a 3D unstructured-grid model (SCHISM v5.10.0)”. In: *Geoscientific Model Development* 16.9, pp. 2565–2581.

Zhang, Yanxu, Anne L Soerensen, Amina T Schartup, Elsie M Sunderland, and Harvard John A Paulson (2020). “A Global Model for Methylmercury Formation and Uptake at the Base of Marine Food Webs”. In: *Biogeochemical Cycles* 34.2.

Zhang, Yanxu et al. (May 2021). “Global health effects of future atmospheric mercury emissions”. In: *Nature Communications 2021 12:1* 12.1, pp. 1–10.

Zhang, Yanxu et al. (Mar. 2023b). “An updated global mercury budget from a coupled atmosphere-land-ocean model: 40% more re-emissions buffer the effect of primary emission reductions”. In: *One Earth* 6.3, pp. 316–325.

Zhao, Changjin, Ute Daewel, and Corinna Schrum (Apr. 2019). “Tidal impacts on primary production in the North Sea”. In: *Earth System Dynamics* 10.2, pp. 287–317.

Zhong, Huan and Wen-Xiong Wang (2009). “Controls of Dissolved Organic Matter and Chloride on Mercury Uptake by a Marine Diatom”. In: *Environ. Sci. Technol.* 43.23, pp. 8993–9003.

Zhou, Haifeng, Yumeng Li, Qiumeng Zhong, Xiaohui Wu, and Sai Liang (Feb. 2025). “Global mercury dataset with predicted methylmercury concentrations in seafoods during 1995–2022”. In: *Scientific Data 2025 12:1* 12.1, pp. 1–8.

Zhou, Jun and Daniel Obrist (Oct. 2021). “Global Mercury Assimilation by Vegetation”. In: *Environmental Science and Technology* 55.20, pp. 14245–14257.

Zhu, Senlin, Zhonglong Zhang, and Xiaobo Liu (Aug. 2017). “Enhanced Two Dimensional Hydrodynamic and Water Quality Model (CE-QUAL-W2) for Simulating Mercury Transport and Cycling in Water Bodies”. In: *Water 2017, Vol. 9, Page 643* 9.9, p. 643.

Zhu, Siyu, Peipei Wu, Siyi Zhang, Oliver Jahn, Shu Li, and Yanxu Zhang (Oct. 2023). “A high-resolution marine mercury model MITgcm-ECCO2-Hg with online biogeochemistry”. In: *Geoscientific Model Development* 16.20, pp. 5915–5929.

Acknowledgements

I would first like to thank my wonderful family. When I began my PhD, I never expected that by the end of it, I would have bought a house and had two wonderful children. My partner, Ulrike, was an invaluable discussion partner throughout this journey. Her PhD thesis inspired me to investigate the link between Hg bioaccumulation and HMA sponges, which I explored in Chapter 6, where she is also a much-valued co-author. Her advice as a co-author really improved my skills in academic writing and also translated to improvements in other chapters of this thesis.

My first child, Vivi (or Vivienne) was born at the beginning of the COVID-19 pandemic, just as I was starting my PhD. Although lockdown was a challenging period for many, I enjoyed the opportunity to spend so much time at home with my family. It was a very nice experience to combine working on my PhD with watching Vivi grow up. Later, with Bo's birth and the purchase of our home, I was lucky to experience the flexibility of academic research together with the joy of seeing our children grow.

I would like to thank my parents and sisters, Mieke, Wim, Sara, and Rosa, who were always supportive and eager to help, whether with childcare or assisting with renovations. On that note, I extend my thanks to Pieter, Gerard, Manuel, Gisela, Dagmar, Alfred, Tim, Chef, Bram, Mick, Martijn, Alkuin, Silvana, Stan, Tommy, Hamit, Felix, Vincent, Pascal, Elena, Fabian, Liam, Deborah, Annelore, Dieter, and everyone else who helped with moving, renovating, and childcare. Although these tasks might seem unrelated to my PhD, the support was very helpful in creating the stable home environment I needed to complete this work.

I also thank my supervisor, Johannes, for his support and guidance, even when I may have bitten off more than I could chew in my personal life. I am grateful for the understanding and flexibility I received at Hereon, which allowed me to balance my work and family life. I know this is not always possible. This was especially true under the supervision of my professor, Corinna, who greatly encouraged me to finish this thesis while also being understanding of my commitment as a parent.

I would also like to acknowledge and thank the students I supervised, Andrea Padilla and Sofia Modesti. Not only for their valuable contributions to Chapter 5, but also for helping me see how it is to supervise students and learn as a supervisor. To this extent, I would also like to thank all my other co-authors, Dr. Johannes Bieser, Prof. Dr. Corinna Schrum, Dr. Ute Daewel, Dr. Elena Mikheeva, Prof. Dr. Corinna Schrum, and Dr. Ulrike Hanz for their contributions to the chapters they contributed to.

This PhD thesis was not completed in isolation, but as part of the GMOS-TRAIN ITN network. I greatly benefited from the shared expertise and networking opportunities the network provided. I had the opportunity to attend two ICMGP conferences in person, as well as several other conferences, summer schools, and meetings. These experiences significantly improved my understanding of Hg, not only in its role in bioaccumulation but also as a global pollutant. I am especially grateful to my supervisor in Nantes, Dr. Joël Knoery, as well as the Project Coordinator, Milena Horvat, and the Administrative Coordinator, Vanja Usenik, for their invaluable support.

Through GMOS-TRAIN, I also had the unique opportunity to participate in a research cruise aboard the SA Agulhas II. This was an incredible experience, and I would like to thank both the crew and the South African government for facilitating the expedition. I also thank Suzanne, Casper, Jared, Liam, Kayla, Lide, Sonja, Lynwill, Nathalia, and Lars for their advice, insights, and support during the expedition, both on the ship and ashore.

I especially thank Johannes and Joel for their thorough proofreading of this doctoral work and their invaluable suggestions to both improve this text and future writings. After Joel suggested that the text should be readable for people outside of science, I also thank Mieke and Alfred for advising that the thesis introduction and discussion be accessible to those outside my field, and for their reflective reading on the text's clarity.

Finally, I want to thank everyone who contributes to open-source software. In particular, the GOTM and FABM software, developed and maintained by the Bolding Bruggeman company. This played a fundamental role in my PhD research. Attending the GOTM-FABM course organized by Karsten Bolding and Jörn Bruggeman at the start of my PhD gave me critical knowledge that underpins every first-author publication in this thesis. I am especially grateful for the responsiveness and support offered by the team whenever I had questions, which sets the gold standard for open-source software.

I also thank Henri De Plaen from KU Leuven, whose LaTeX thesis template served as the basis for my

own. Additionally, I used images from Wikipedia and academic papers for model overview graphics and the introductory sections of this thesis. I am immensely grateful to all contributors to open-access materials who made it possible to find and use these resources.

As declared in the declaration of oath, all work presented in this thesis is my own and I take full responsibility for its content. However, given the growing role of AI in academic workflows, I find it necessary to elaborate. In this thesis, OpenArt.ai was used to generate schematic illustrations of animals featured in graphical abstracts, which were then assembled in Lucidchart. Perplexity and ChatGPT (versions 3.0–4.0) were used for brainstorming, refining R and Python code, formatting LaTeX, and grammar and spell checking. Grammarly and Writefull were employed to support spelling and grammar corrections. An exception where initial text was produced using AI was for the translation of the abstract. I read and verified the translated abstracts, and the German abstract was additionally proofread by Dr. Johannes Bieser and Dr. Ulrike Hanz and the Dutch version by Mieke Spronk, but the initial translation was made using GPT 4.1. All outputs were critically reviewed, and the final decisions reflect my own judgment.

I think the acknowledgment of AI tools is essential, as these tools, like any tool or source, can influence outcomes, particularly when they have an inherent bias. While specific outputs from generative models are not replicable, specifying the model and version used may aid transparency if certain biases or issues are later identified. I also recognize that AI poses unique challenges: its summaries are not peer-reviewed, nor are they reproducible, and should therefore be treated as unverified opinions until validated by primary sources.

Of course, scientists should never over-rely on AI, and AI can never replace rigorous evaluation of the underlying literature. However, this does not mean such tools should be excluded from academic workflows. I think perplexity offers a valuable alternative to the near-monopoly of Google in academic search, while ChatGPT excels at identifying spelling errors and improving sentence clarity, enhancing the readability of texts. For example, Perplexity helped me discover a German-language report by the Bundesanstalt für Gewässerkunde (BfG) that I may not have otherwise found, but it also produced inaccurate summaries on occasion, highlighting once again the necessity of critical reading.

To conclude, I support the responsible use of AI to improve research efficiency and inclusivity. Taxpayer-funded science must balance tradition with innovation, and AI tools can offer substantial workflow benefits without compromising academic rigor, especially for non-native English speakers navigating scientific writing. Nevertheless, these tools must be used with caution, transparency, and with a focus on a commitment to truth.

Figure 10.2: Visiting the Hg mines in Idrija with GMOS-TRAIN. Picture Dr. Radojko Jačimović (JSI)

With penguins during field work in Rothera. Picture by Gerrit van der Goot.

About the Author

I was born in the Netherlands in 1993 and quickly discovered my passion for Biology and Chemistry. This interest led me to move to Groningen to pursue a BSc in Molecular Biology at the Rijksuniversiteit Groningen. During the introduction week, I spoke with representatives from the biological dive organization G.B.D. Calamari and decided to join. This turned out to be a turning point in my career, and diving sparked my interest in the marine environment. Around that time, a debate in the Netherlands surrounding the use of steel slugs in coastal protection occurred. Steel slugs were used as an affordable way to reinforce dikes, but evidence suggested that heavy metals could leach out of these slugs into the marine environment. My interest in this debate pushed me further into marine chemistry, and especially heavy metal pollution. I chose to follow up my bachelor's with an MSc in Marine Biology. During my master's, I completed two major projects. The first, at the Royal Netherlands Institute for Sea Research (NIOZ), focused on iron-binding ligands in the Transpolar Drift Stream. This project helped me appreciate the complex dynamics between marine ecology and chemistry. For my second project, I had the opportunity to travel to the British Antarctic Survey research station at Rothera, where I spent six months sampling persistent organic pollutants (POPs) in Ryder Bay. It was in Antarctica that I further developed my interest in pollution research. I find the combination of fundamental science and direct societal relevance very interesting. While at Rothera, thick sea ice initially prevented fieldwork. With limited internet access, I began building a model of pollutant cycling in Ryder Bay, learning modeling the old-fashioned way, from books. After graduating, I was offered a PhD position at the Helmholtz-Zentrum Hereon. During my PhD, I developed both as a modeler and a scientist. I participated in the SCALE-WIN22 cruise, gaining firsthand experience in the complexities of Hg sampling in the Southern Ocean. I also had the opportunity to supervise two master's students which taught me a great deal about mentoring and collaborative research.

(a) Diving in Longyearbyen.

(b) NIOZ summer course, Picture by Manuel Pecino Barrios.

(c) Field work in Svalbard. Picture taken by Dr. Luke Storrie.

(d) Sampling POPs in the Antarctic. Picture taken by Dr. Artem Kransobeav.

(e) Sunday dress up while sampling Hg in the Southern Ocean.

(f) Discussing Hg cycling with Johannes on our way to Abisko. Picture taken by Chariklea Gournia.

(g) Traveling to the annual meeting in Abisko. By Dr. Johannes Bieser.

(h) Thinking of Hg in our way to Abisko. Picture by Dr. Johannes Bieser.

Figure 10.3: Fieldwork impressions during the author's scientific journey

Declaration on Oath

I hereby declare and affirm that this doctoral dissertation is my own work and that I have not used any aids and sources other than those indicated.
If electronic resources based on generative artificial intelligence (gAI) were used in the course of writing this dissertation, I confirm that my own work was the main and value-adding contribution and that complete documentation of all resources used is available in accordance with good scientific practice. I am responsible for any erroneous or distorted content, incorrect references, violations of data protection and copyright law, or plagiarism that may have been generated by the gAI.

Ort, Datum Unterschrift

05.05.2026 David Johannes Amptmeijer

Eidesstattliche Versicherung

Hiermit erkläre ich an Eides statt, dass ich die vorliegende Dissertationsschrift selbst verfasst und keine anderen als die angegebenen Quellen und Hilfsmittel benutzt habe.
Sofern im Zuge der Erstellung der vorliegenden Dissertationsschrift generative Künstliche Intelligenz (gKI) basierte elektronische Hilfsmittel verwendet wurden, versichere ich, dass meine eigene Leistung im Vordergrund stand und dass eine vollständige Dokumentation aller verwendeten Hilfsmittel gemäß der Guten wissenschaftlichen Praxis vorliegt. Ich trage die Verantwortung für eventuell durch die gKI generierte fehlerhafte oder verzerrte Inhalte, fehlerhafte Referenzen, Verstöße gegen das Datenschutz- und Urheberrecht oder Plagiate.

Ort, Datum Unterschrift

05.05.2026 David Johannes Amptmeijer